

**THEORETICAL STUDY OF VARIABLE VISCOSITY NANOFLUIDS  
FLOW IN MICROCHANNELS**

by

**Ramotjaki Lucky Monaledi**

Dissertation presented for the degree

Doctor of Philosophy in the Faculty of Military Science

at

Stellenbosch University



**Supervisor: Prof Oluwole Daniel Makinde**

December 2020

Stellenbosch University



## ABSTRACT

The study of fluid flow and heat transfer through a microchannel is an important research area due to its wide applications in engineering and industrial processes. Some practical applications include problems dealing with cooling, lubrication of porous bearings, petroleum technology, ground water hydrology, drainage and purification processes. A nanofluid is the suspension of nanoparticles in a base fluid. Nanofluids are capable of heat transfer enhancement due to their high thermal conductivity. For practical applications of nanofluids, research in nanofluids convection is significant. Due to their enhanced properties, nanofluids can be used in the deficiency of technical and biomedical applications such as nanofluid coolant in electronics cooling, vehicle cooling and transformer cooling.

This study considered the detailed analysis of both single and two-phase Couette and Poiseuille flow behaviour and heat transfer using this innovative fluid as working fluid through a microchannel. Useful results for the velocity, temperature, nanoparticles concentration profiles, skin friction and Nusselt number were obtained and discussed quantitatively. The effects of important governing flow parameters on the entire flow structure were examined.

In this thesis, a more realistic modified Buongiorno's nanofluid model is proposed and utilized to examine the impact of nanoparticles' injection and distribution on inherent irreversibility in a microchannel Poiseuille flow of nanofluid with variable properties. The governing nonlinear differential equations are obtained and tackled numerically using the shooting method coupled with the Runge-Kutta-Fehlberg integration scheme. Graphical results showing the effects of the pertinent parameters on the nanofluid velocity, temperature, nanoparticles concentration, skin friction, Nusselt number, Sherwood number, entropy generation rate and Bejan number are presented and discussed quantitatively.

## DECLARATION AND COPYRIGHT

I, **Ramotjaki Lucky Monaledi**, do hereby declare to the Faculty of Military Science Stellenbosch University that this dissertation is my own original work and that it has neither been submitted nor being contemporarily submitted for a degree award in any other institution.

26<sup>th</sup> November, 2020.

---

**Ramotjaki Lucky Monaledi**, (Student)

Date

The above declaration is confirmed

26<sup>th</sup> November, 2020.

---

**Prof Oluwole Daniel Makinde**, (Supervisor)

Date

Copyright © 2020 Stellenbosch University

All rights reserved

## **CERTIFICATION**

The undersigned certify that they have read and found the dissertation titled,

**Theoretical study of Variable Viscosity Nanofluids Flow in Microchannels** to be in a form acceptable for examination by Faculty of Military Science Stellenbosch University, of the requirements for the degree of Doctor of Philosophy in Military Technology (Mathematics).

---

26<sup>th</sup> November, 2020.

**Prof Oluwole Daniel Makinde**, (Supervisor)

**Date**

## ACKNOWLEDGEMENT

I would like to thank the Almighty God since He is the source of my strength, faith and health that enabled me to complete this study successfully.

I would like to express my sincere gratitude to my supervisor Prof Oluwole Daniel Makinde for his patience, valuable guidance and encouragement throughout my research work. I have experienced an excellent level of supervision, important recommendations, support and opportunity to gain from his wealth of knowledge and had exposure to travel overseas using his research fund. His supervision has enhanced my knowledge in the field of computational fluid dynamics. Without him, this research would not have been a success.

I would like to express my deepest appreciation to my family for their support through their prayers, love and encouragement during my studies.

I would especially like to thank my lovely wife (Mary), my daughter (Mary-Ann), my sons (Morepi and David) and my mother (Dorah) for their love, constant support and most of all their patience during my absence.

I express my special thanks to S Lt K.S. Tshivhi for his valuable suggestions and fondness bestowed on me and providing the necessary help and support throughout the period of my doctoral research work.

A special thank you to the Faculty of Military Science Stellenbosch University for offering me the support and scholarship for paying my tuition fees. I want to extend a special thank you to Lt General L.K Mbatha, Chief of SA Army, for his outstanding leadership skills and valuable guidance.

Finally, I express my warm appreciation to everybody who has contributed in one way or another towards the success of my studies.

## **DEDICATION**

This thesis is dedicated to my gorgeous wife Mary, who is the pillar of my strength, and to my beautiful children Morepi, Mary-Ann and David.

I furthermore dedicate my thesis to my family members Dorah, Solomon, Nurse, Naomi, Ariel, Molefe, Madie, Ranka, Niklaas, Caleb, Sydie, Pelaetso, Lehlohonolo, and all my other family. Together they were the source of my happiness during all the challenges of my studies.

## TABLE OF CONTENTS

|   |       |
|---|-------|
| ABSTRACT.....                                 | i     |
| DECLARATION AND COPYRIGHT.....                | ii    |
| CERTIFICATION.....                            | iii   |
| ACKNOWLEDGEMENT.....                          | iv    |
| DEDICATION.....                               | v     |
| TABLE OF CONTENTS .....                       | vi    |
| LIST OF FIGURES .....                         | xi    |
| LIST OF TABLES .....                          | xv    |
| NOMENCLATURE .....                            | xvi   |
| LIST OF PUBLICATIONS .....                    | xviii |
| LIST OF CONFERENCES .....                     | xix   |
| CHAPTER 1.....                                | 1     |
| INTRODUCTION AND BASIC CONCEPTS .....         | 1     |
| 1.1    General Introduction .....             | 1     |
| 1.1.1    Channel Flow and Microchannels ..... | 1     |
| 1.2    Definition of Terms.....               | 3     |
| 1.2.1    Pressure .....                       | 3     |
| 1.2.2    Temperature .....                    | 3     |
| 1.2.3    Density .....                        | 3     |
| 1.2.4    Internal Energy .....                | 4     |
| 1.2.5    Specific Heat Capacity.....          | 4     |
| 1.2.6    Thermal Conductivity .....           | 4     |
| 1.2.7    Viscosity .....                      | 5     |
| 1.2.8    Temperature-Dependent Viscosity..... | 6     |
| 1.3    Heat Transfer Mechanisms.....          | 7     |
| 1.3.1    Conduction .....                     | 7     |
| 1.3.2    Convection .....                     | 7     |
| 1.3.3    Radiation .....                      | 9     |



|   |   |    |
|---|---|----|
| 1.4   | Mass Transfer.....                                | 10 |
| 1.5   | Nanofluids .....                                  | 11 |
| 1.5.1   | Synthesis of Nanofluids .....                     | 12 |
| 1.6   | Application of Nanofluids .....                   | 14 |
| 1.6.1   | Heat Transfer Applications.....                   | 15 |
| 1.6.2   | Space, Defense and Ships .....                    | 15 |
| 1.7   | Basic Equations Governing Nanofluids Flow.....    | 17 |
| 1.7.1   | Continuity Equation.....                          | 17 |
| 1.7.2   | Navier-Stoke's (Momentum) Equation .....          | 18 |
| 1.7.3   | Energy Equation .....                             | 18 |
| 1.7.4   | Nanoparticles Concentration Equation.....         | 19 |
| 1.7.5   | Entropy equation .....                            | 20 |
| 1.7.6   | Prandtl number .....                              | 20 |
| 1.7.7   | Eckert number .....                               | 21 |
| 1.7.8   | Skin friction coefficient.....                    | 21 |
| 1.7.9   | Sherwood number .....                             | 21 |
| 1.7.10  | Nusselt number .....                              | 22 |
| 1.8   | Literature Review.....                            | 22 |
| 1.9   | Statement Problem .....                           | 24 |
| 1.10  | Research Objectives.....                          | 24 |
| 1.11  | Significance of the Problem .....                 | 25 |
| 1.12  | Research Methodology/Computational Approach ..... | 26 |
| 1.12.1  | The Shooting Method .....                         | 26 |
| 1.12.2  | The Bisection Method .....                        | 28 |
| 1.12.3  | Newton-Raphson Method .....                       | 28 |
| 1.12.4  | The Runge-Kutta Method.....                       | 29 |
| 1.13  | Thesis Outline .....                              | 29 |
| CHAPTER 2.....  |   | 32 |
| INHERENT IRREVERSIBILITY IN CU-H <sub>2</sub> O NANOFLUID COUETTE FLOW WITH VARIABLE VISCOSITY AND NONLINEAR RADIATIVE HEAT TRANSFER..... |   | 32 |

|  |   |    |
|--|---|----|
| 2.1  | Introduction.....   | 32 |
| 2.2  | Problem Formulation .....   | 35 |
| 2.3  | Numerical Procedure .....   | 41 |
| 2.4  | Results and Discussion .....  | 42 |
| 2.4.1  | Effect of Parameter Variation on Velocity Profiles .....            | 44 |
| 2.4.2  | Effect of Parameter Variation on Temperature Profiles .....         | 47 |
| 2.4.3  | Skin Friction, Nusselt Number and Thermal Stability Conditions..... | 49 |
| 2.4.4  | Effect of Parameter Variation on Entropy Generation Rate .....      | 53 |
| 2.4.5  | Effect of Parameter Variation on Bejan Number .....                 | 55 |
| 2.5  | Conclusion.....   | 57 |
| CHAPTER 3.....   |   | 59 |
| ENTROPY ANALYSIS OF A RADIATING VARIABLE VISCOSITY EG/AG NANOFLUID FLOW<br>IN MICROCHANNELS WITH BUOYANCY FORCE AND CONVECTIVE COOLING ..... |   | 59 |
| 3.1  | Introduction.....   | 59 |
| 3.2  | Model Problem .....   | 62 |
| 3.3  | Numerical Procedure .....   | 66 |
| 3.4  | Results and Discussion .....  | 67 |
| 3.4.1  | Effect of Parameters Variation on Velocity Profiles .....           | 69 |
| 3.4.2  | Effect of Parameters Variation on Temperature Profiles .....        | 72 |
| 3.4.3  | Skin Friction, Nusselt Number and Thermal Stability Conditions..... | 74 |
| 3.4.4  | Effect of Parameters Variation on Entropy Generation Rate .....     | 77 |
| 3.4.5  | Effect of Parameters Variation on Bejan Number.....                 | 80 |
| 3.5  | Conclusion.....   | 83 |
| CHAPTER 4.....   |   | 84 |
| THERMOPHORESIS AND BROWNIAN MOTION EFFECTS ON A REACTIVE VARIABLE<br>VISCOSITY COUETTE FLOW IN A MICROCHANNEL.....                           |   | 84 |
| 4.1  | Introduction.....   | 84 |
| 4.2  | Model Problem .....   | 86 |
| 4.3  | Numerical Procedure .....   | 89 |
| 4.4  | Results and Discussion .....  | 90 |
| 4.4.1  | Velocity Profiles .....   | 91 |

|   |  |     |
|---|--|-----|
| 4.4.2   | Temperature Profiles .....   | 95  |
| 4.4.3   | Nanoparticles Concentration Profiles .....   | 99  |
| 4.4.4   | Skin Friction, Nusselt Number, Sherwood Number and Thermal Stability Criteria<br>103 |     |
| 4.4.5   | Entropy Generation Rate .....  | 106 |
| 4.4.6   | Bejan Number.....  | 110 |
| 4.5   | Conclusions .....  | 114 |
| CHAPTER 5.....  |  | 116 |
| MODELLING NANOPARTICLES DISTRIBUTION PATTERN IN A MICROCHANNEL FLOW OF<br>NANOFLUID FILLED WITH A POROUS MEDIUM.....                      |  | 116 |
| 5.1   | Introduction.....  | 116 |
| 5.2   | Model Problem .....  | 117 |
| 5.3   | Numerical Procedure .....  | 120 |
| 5.4   | Results and Discussion .....   | 120 |
| 5.5   | Conclusions .....  | 126 |
| CHAPTER 6.....  |  | 127 |
| ENTROPY GENERATION ANALYSIS IN A MICROCHANNEL POISEUILLE FLOWS OF<br>NANOFLUID WITH NANOPARTICLES INJECTION AND VARIABLE PROPERTIES ..... |  | 127 |
| 6.1   | Introduction.....  | 127 |
| 6.2   | Model Problem .....  | 129 |
| 6.3   | Numerical Procedure .....  | 134 |
| 6.4   | Results and Discussion .....   | 135 |
| 6.4.1   | Velocity Profiles .....  | 135 |
| 6.4.2   | Temperature Profiles .....   | 139 |
| 6.4.3   | Nanoparticles Concentration Profiles.....  | 143 |
| 6.4.4   | Skin Friction.....   | 147 |
| 6.4.5   | Nusselt Number and Sherwood Number.....  | 148 |
| 6.4.6   | Entropy Generation Rate .....  | 151 |
| 6.4.7   | Bejan Number.....  | 155 |
| 6.5.  | Conclusions .....  | 159 |

|  |     |
|--|-----|
| CHAPTER 7.....   | 161 |
| GENERAL DISCUSSION, CONCLUSION AND RECOMMENDATIONS ..... | 161 |
| 7.1. General Discussion.....                             | 161 |
| 7.2. Conclusions .....                                   | 161 |
| 7.3. Recommendations.....                                | 164 |
| 7.4. Future Research Work.....                           | 165 |
| LIST OF REFERENCES .....                                 | 166 |

## LIST OF FIGURES

|             |   |    |
|-------------|---|----|
| Figure 1.1  | Couette Flow and Poiseuille Flow Geometries.                            | 2  |
| Figure 1.2  | Schematic presentation of a microchannel reactor                        | 3  |
| Figure 1.3  | Illustration of conduction, convection and radiation heat transfer [23] | 7  |
| Figure 1.4  | Thermal Conductivity of Materials                                       | 12 |
| Figure 1.5  | Nanofluid Synthesis   | 13 |
| Figure 1.6  | Cu-water nanofluid  | 13 |
| Figure 1.7  | Al <sub>2</sub> O <sub>3</sub> -water nanofluid                         | 13 |
| Figure 1.8  | Applications of Nanofluids  | 15 |
| Figure 1.9  | Nanofluids being used to cooling military vehicle                       | 16 |
| Figure 1.10 | Waste heat transported by nanofluids to the hull of the ship            | 17 |
| Figure 2.1  | Problem Geometry  | 36 |
| Figure 2.2  | Velocity profiles with $\beta$  | 45 |
| Figure 2.3  | Velocity profiles with $\gamma$   | 45 |
| Figure 2.4  | Velocity profiles Nr  | 46 |
| Figure 2.5  | Velocity profiles Ec  | 46 |
| Figure 2.6  | Temperature profiles with $\beta$                                       | 47 |
| Figure 2.7  | Temperature profiles with Nr and $\phi$                                 | 48 |
| Figure 2.8  | Temperature profiles with Ec and $\gamma$                               | 48 |
| Figure 2.9  | Temperature profiles with m   | 49 |
| Figure 2.10 | Skin friction with $\phi$ , Ec and $\beta$                              | 50 |
| Figure 2.11 | Skin friction with Nr, m and $\gamma$                                   | 50 |
| Figure 2.12 | Nusselt number with $\phi$ , Ec and $\beta$                             | 51 |
| Figure 2.13 | Nusselt number with Nr, m and $\gamma$                                  | 51 |
| Figure 2.14 | Thermal stability criticality with $\phi$                               | 52 |
| Figure 2.15 | Thermal stability criticality with Nr                                   | 52 |
| Figure 2.16 | Entropy generation rate with $\beta$                                    | 53 |
| Figure 2.17 | Entropy generation rate with Nr and $\phi$                              | 54 |
| Figure 2.18 | Entropy generation rate with m  | 54 |
| Figure 2.19 | Entropy generation rate with Ec and $\gamma$                            | 55 |
| Figure 2.20 | Bejan number with $\beta$   | 56 |
| Figure 2.21 | Bejan number with Nr and $\phi$ .                                       | 56 |
| Figure 2.22 | Bejan number with Ec and $\gamma$                                       | 57 |
| Figure 3.1  | Problem geometry  | 62 |
| Figure 3.2  | Velocity profile with Ec and $\phi$                                     | 70 |
| Figure 3.3  | Velocity profile with Bi and Gr   | 70 |

|             |   |     |
|-------------|---|-----|
| Figure 3.4  | Velocity profile with $Nr$ and $\lambda$        | 71  |
| Figure 3.5  | Velocity profile with $m$                       | 71  |
| Figure 3.6  | Temperature profiles with $Ec$ and $\phi$       | 72  |
| Figure 3.7  | Temperature profiles with $Bi$ and $Gr$         | 73  |
| Figure 3.8  | Temperature profiles with $Nr$ and $\lambda$    | 73  |
| Figure 3.9  | Temperature profiles with $m$                   | 74  |
| Figure 3.10 | Skin friction with $Bi$ , $Nr$ and $Ec$         | 75  |
| Figure 3.11 | Skin friction with $\phi$ and $Ec$              | 75  |
| Figure 3.12 | Nusselt number with $\phi$ and $Ec^*$           | 76  |
| Figure 3.13 | Nusselt with $Bi$ , $Nr$ and $Ec$               | 76  |
| Figure 3.14 | Entropy generation rate with $Ec$ and $\phi$ .  | 78  |
| Figure 3.15 | Entropy generation rate with $Bi$ and $Gr$      | 78  |
| Figure 3.16 | Effects of $Nr$ and $\lambda$ on $Ns$ .         | 79  |
| Figure 3.17 | Effects of $m$ on $Ns$ .                        | 80  |
| Figure 3.18 | Bejan number with $Ec$ and $\phi$               | 81  |
| Figure 3.19 | Bejan number with $Bi$ and $Gr$                 | 81  |
| Figure 3.20 | Bejan number with $Nr$ and $\lambda$ .          | 82  |
| Figure 3.21 | Bejan number with $m$ .                         | 82  |
| Figure 4.1  | Problem Geometry                                | 86  |
| Figure 4.2  | Velocity profiles with increasing $\lambda$     | 92  |
| Figure 4.3  | Velocity profiles with increasing $\lambda_2$   | 93  |
| Figure 4.4  | Velocity profiles with increasing $Nt$          | 93  |
| Figure 4.5  | Velocity profiles with increasing $Ec$          | 94  |
| Figure 4.6  | Velocity profiles with increasing $Nb$          | 94  |
| Figure 4.7  | Effects of $\lambda_1$ on temperature profiles. | 95  |
| Figure 4.8  | Effects of $\lambda_2$ on temperature profiles  | 96  |
| Figure 4.9  | Temperature profiles with increasing $Nt$       | 96  |
| Figure 4.10 | Temperature profiles with increasing $Nb$       | 97  |
| Figure 4.11 | Temperature profiles with increasing $Ec$       | 97  |
| Figure 4.12 | Temperature profiles with increasing $m$        | 98  |
| Figure 4.13 | Temperature profiles with increasing $Sc$       | 98  |
| Figure 4.14 | Concentration profiles with $\lambda_1$ .       | 99  |
| Figure 4.15 | Concentration profiles with $\lambda_2$         | 100 |
| Figure 4.16 | Concentration profiles with $m$ .               | 100 |
| Figure 4.17 | Concentration profiles with $Nb$ .              | 101 |
| Figure 4.18 | Concentration profiles with $Sc$ .              | 101 |
| Figure 4.19 | Concentration profiles with $Ec$ .              | 102 |

|              |   |     |
|--------------|---|-----|
| Figure 4.20  | Concentration profiles with $Nt$ .                      | 102 |
| Figure 4.21  | Skin friction with $Ec$ , $\lambda_1$ and $\lambda_2$   | 103 |
| Figure 4.22  | Nusselt number with $Ec$ , $\lambda_1$ and $\lambda_2$  | 104 |
| Figure 4.23  | Sherwood number with $Ec$ , $\lambda_1$ and $\lambda_2$ | 104 |
| Figure 4.24  | Critical Eckert number $Ec^*$ with $Nb$                 | 105 |
| Figure 4.25  | Critical Eckert number $Ec^*$ with $Nt$                 | 105 |
| Figure 4.26  | Entropy generation rate with $\lambda_1$                | 106 |
| Figure 4.27  | Entropy generation rate with $\lambda_2$                | 107 |
| Figure 4.28  | Entropy generation rate with $Nb$                       | 107 |
| Figure 4.29  | Entropy generation rate with $Nt$                       | 108 |
| Figure 4.30  | Entropy generation rate with $Ec$                       | 108 |
| Figure 4.31  | Entropy generation rate with $m$                        | 109 |
| Figure 4.32  | Entropy generation rate with $Sc$                       | 109 |
| Figure 4.33  | Bejan number with increasing $\lambda_1$                | 110 |
| Figure 4.34  | Bejan number with increasing $\lambda_2$                | 111 |
| Figure 4.35  | Bejan number with increasing $Nt$                       | 111 |
| Figure 4.36  | Bejan number with increasing $Nb$                       | 112 |
| Figure 4.37  | Bejan number with increasing $Ec$                       | 112 |
| Figure 4.38  | Bejan number with increasing $m$                        | 113 |
| Figure 4.39: | Bejan number with increasing $Sc$                       | 113 |
| Figure 5.1   | Schematic diagram of the problem                        | 118 |
| Figure 5.2   | Effect of $Da$ on velocity profiles                     | 121 |
| Figure 5.3   | Effect of $Sc$ on velocity profiles                     | 122 |
| Figure 5.4   | Effect of $\lambda$ on velocity profiles                | 122 |
| Figure 5.5   | Nanoparticles concentration profiles with $Sc$          | 123 |
| Figure 5.6   | Nanoparticles concentration profiles with $\lambda$     | 124 |
| Figure 5.7   | Skin friction with $Sc$ and $\lambda$                   | 124 |
| Figure 5.8   | Skin friction with $A$ and $Da$                         | 125 |
| Figure 5.9   | Sherwood number with $Sc$ and $\lambda$                 | 125 |
| Figure 6.1   | Problem geometry  | 130 |
| Figure 6.2   | Velocity profiles with Cu-nanoparticles                 | 136 |
| Figure 6.3   | Velocity profiles with $\gamma$ .                       | 136 |
| Figure 6.4   | Velocity profiles with $Le$ .                           | 137 |
| Figure 6.5   | Velocity profiles with $Nb$                             | 137 |
| Figure 6.6   | Velocity profiles with $Nt$ .                           | 138 |
| Figure 6.7   | Velocity profiles with $\lambda$ .                      | 138 |
| Figure 6.8   | Velocity profiles with $Ec$ .                           | 139 |

|             |  |     |
|-------------|--|-----|
| Figure 6.9  | Temperature profiles with Cu-nanoparticles | 140 |
| Figure 6.10 | Temperature profiles with $\gamma$ .       | 140 |
| Figure 6.11 | Temperature profiles with Le.              | 141 |
| Figure 6.12 | Temperature profiles with Nb               | 141 |
| Figure 6.13 | Temperature profiles with $\lambda$ .      | 142 |
| Figure 6.14 | Temperature profiles with Nt.              | 142 |
| Figure 6.15 | Temperature profiles with Ec               | 143 |
| Figure 6.16 | Concentration profiles with $\gamma$ .     | 144 |
| Figure 6.17 | Concentration profiles with Le.            | 144 |
| Figure 6.18 | Concentration profiles with Nb.            | 145 |
| Figure 6.19 | Concentration profiles with $\lambda$ .    | 145 |
| Figure 6.20 | Concentration profiles with Nt.            | 146 |
| Figure 6.21 | Concentration profiles with Ec             | 146 |
| Figure 6.22 | Skin friction with increasing A            | 147 |
| Figure 6.23 | Nusselt number with Ec and $\lambda$       | 148 |
| Figure 6.24 | Nusselt number with Ec, Nb and $\gamma$ .  | 149 |
| Figure 6.25 | Nusselt number with Ec, Nt and Le.         | 149 |
| Figure 6.26 | Sherwood number with Ec, Nt and Le.        | 150 |
| Figure 6.27 | Sherwood number with Ec, Nb and $\gamma$ . | 150 |
| Figure 6.28 | Effects of Cu-nanoparticles on Ns          | 151 |
| Figure 6.29 | Entropy generation rate with $\gamma$ .    | 152 |
| Figure 6.30 | Entropy generation rate with Le            | 152 |
| Figure 6.31 | Entropy generation rate with $\lambda$ .   | 153 |
| Figure 6.32 | Entropy generation rate with Nb            | 153 |
| Figure 6.33 | Entropy generation rate with Ec.           | 154 |
| Figure 6.34 | Entropy generation rate with Nt.           | 154 |
| Figure 6.35 | Bejan number with Cu-nanoparticles         | 155 |
| Figure 6.36 | Bejan number with $\gamma$ .               | 156 |
| Figure 6.37 | Bejan number with Le.                      | 156 |
| Figure 6.38 | Bejan number with Nb.                      | 157 |
| Figure 6.39 | Bejan number with $\lambda$ .              | 157 |
| Figure 6.40 | Bejan number with Nt.                      | 158 |
| Figure 6.41 | Bejan number with Ec.                      | 158 |



## LIST OF TABLES

|           |   |     |
|-----------|---|-----|
| Table 1.1 | Viscosity-Temperature Equations as in the literatures ([11, 13, 18]).   | 6   |
| Table 1.2 | Typical values of convective heat transfer coefficients   | 8   |
| Table 1.3 | Thermophysical properties of water and nanoparticles [10-15]  | 14  |
| Table 2.1 | Nanoparticles and base fluid thermophysical properties [11, 83-84]  | 38  |
| Table 2.2 | The nanoparticles shape factors (m) [85, 99]  | 38  |
| Table 2.3 | Comparison between analytical and numerical results for Cu-Water  | 43  |
| Table 2.4 | Computations showing the effect of parameters variation on thermal stability critical Eckert number for Cu-water  | 44  |
| Table 3.1 | Nanoparticles and base fluid thermophysical properties [11, 58, 62, 86, 110-112]  | 64  |
| Table 3.2 | The nanoparticles shape factors (m) [11, 62]  | 64  |
| Table 3.3 | Computations showing the effect of parameters variation on thermal stability critical Eckert number ( $Ec^*$ ) for Silver-Ethylene Glycol nanofluid ( $A=1$ , $Pr = 137.48$ ) | 68  |
| Table 3.4 | Computations showing the effect of parameters variation on skin friction and Nusselt number ( $A=1$ , $Pr = 137.48$ )   | 68  |
| Table 4.1 | Computations showing the effect of parameters variation on thermal stability critical Eckert number $Pr = 6.2$  | 91  |
| Table 6.1 | Nanoparticles and base fluid thermophysical properties [101,137,140-141].   | 131 |

## NOMENCLATURE

|         |                                    |
|---------|------------------------------------|
| $(u,v)$ | Velocity components                |
| $(x,y)$ | coordinates                        |
| $C_p$   | Specific heat at constant pressure |
| $Nu$    | Local Nusselt number               |
| $Pr$    | Prandtl number                     |
| $Br$    | Brinkmann number                   |
| $Ec$    | Eckert number                      |
| $Gr$    | Grashof number                     |
| $Bi$    | Local Biot Number                  |
| $Ha$    | Hartmann Number                    |
| $q_w$   | Dimensional heat flux              |
| $Re_x$  | Local Reynolds number              |
| $T$     | temperature                        |
| $f_w$   | Suction/injection parameter        |
| $k$     | Thermal conductivity               |
| $h_f$   | Heat transfer coefficient          |

### Greek symbols

|          |                               |
|----------|-------------------------------|
| $\theta$ | Dimensionless temperature     |
| $\beta$  | Thermal expansion coefficient |
| $\alpha$ | Thermal diffusivity           |
| $\mu$    | Dynamic viscosity             |
| $\nu$    | Kinematic viscosity           |
| $\rho$   | Density                       |

$\tau_w$  Skin friction or shear stress

$\lambda$  Slip Coefficient

### **Subscripts**

$f$  Fluid

$s$  Solid

$nf$  Nanofluid

## LIST OF PUBLICATIONS

1. **R.L. Monaledi**, O.D. Makinde: Entropy Analysis of a Radiating Variable Viscosity EG/Ag Nanofluid Flow in Microchannels with Buoyancy Force and Convective Cooling. Defect and Diffusion Forum, Volume 387, 273–285, 2018.
2. **R.L. Monaledi**, O.D. Makinde: Inherent Irreversibility in Cu-H<sub>2</sub>O Nanofluid Couette Flow with variable Viscosity and Nonlinear Radiative Heat Transfer, International Journal of Fluid Mechanics Research, Volume 46(6), 525–543, 2019.
3. **R.L. Monaledi**, O.D. Makinde: Modelling Nanoparticles Distribution Pattern in a Microchannel Flow of Nanofluid Filled with a Porous Medium. Num. Com. Meth. Sci. Eng., Volume 1(3), 111- 116, 2019.
4. **R. L. Monaledi**, O. D. Makinde: Entropy Generation Analysis in a Microchannel Poiseuille Flows of Nanofluid with Nanoparticles Injection and Variable Properties. (Accepted & Published Online to Journal of Thermal Analysis and Calorimetry, 2020).
5. **R. L. Monaledi**, O. D. Makinde: Thermophoresis and Brownian Motion Effects on a Reactive Variable Viscosity Couette Flow in a Microchannel. (Submitted for Publication, 2020).

## LIST OF CONFERENCES

1. **R.L. Monaledi**, O.D. Makinde, presented a paper titled “*Entropy Analysis of Variable Viscosity Cu-H<sub>2</sub>O Nanofluid Couette flow in a Microchannel with Nonlinear Radiative Heat Transfer*” at 61<sup>st</sup> Annual Congress of the South African Mathematical Society on 1-3 December 2018, Rhodes University Grahamstown. (Awarded third Best Price for PhD presentations paper).
2. **R.L. Monaledi**, O.D. Makinde, presented a paper titled “*Analysis of Entropy Generation Rate and thermal Stability of Variable Viscosity Nanofluid in Couette Flow with Radiative Heat*” at International Congress of Mathematician (ICM) on 2-9 August 2018, Rio de Janeiro, Brazil.
3. **R.L. Monaledi**, O.D. Makinde, presented a paper titled “*Thermophoresis and Brownian Motion Effects on Entropy Generation in Couette flow of a reactive variable viscosity Nanofluid*” at International Conference on Emerging Trends in Computational Fluid Dynamics, 27-28 February 2019, CHRIST (Deemed to be University) Bangalore India.
4. **R.L. Monaledi**, O.D. Makinde, presented a paper titled: “*Modelling Heat Transfer Enhancement and Nanoparticles Distribution in Poiseuille Flow of a Reactive Nanofluid with Variable Properties*”. 62<sup>nd</sup> Annual Congress of the South African Mathematical Society, University of Cape Town, Cape Town, RSA. 1 – 4 December 2019.
5. **R.L. Monaledi**, O.D. Makinde presented a paper titled: “*Entropy Analysis of a Microchannel Poiseuille flow of Reactive Nanofluid with Thermophoresis and Brownian Motion Effects*”. 21<sup>st</sup> International Bangladesh Mathematics Conference, Department of Applied Mathematics, University of Dhaka, Dhaka, Bangladesh. 6 – 8 December 2019.



# CHAPTER 1

## INTRODUCTION AND BASIC CONCEPTS

### 1.1 General Introduction

Fluid Mechanics is the study of fluids either at rest (fluids static) or in motion (fluids dynamics and kinematics) and the subsequent effects of the fluids upon the boundaries which may be either solid surfaces or interfaces with other fluids. It is worth noting that both gases and liquids are classified as fluids according to Batchelor [8]. Fluids, unlike solids, cannot sustained resistance to a deforming force. Thus, a fluid is a substance that deforms continuously under the action of shearing forces, however small they may be. Deformation is caused by shearing forces - forces that act tangentially to the surfaces to which they are applied according to Douglas *et al.* [13]. Heat transfer fluids such as water, mineral oils and ethylene glycol play an important role in many industrial sectors including power generation, chemical production, air-conditioning, transportation an microelectronics. Although various techniques have been applied to enhance their heat transfer, they are performance enhancement and compactness of heat exchangers.

Outstanding high demands of modern technology for process intensification and device miniaturization, new types of fluids that are more effective in terms of heat exchange performance is of more importance to be introduced. To achieve this, it has been recently proposed to disperse small amounts of nanometre-sized particles and fibres in base fluids, resulting in what is commonly known as nanofluids.

#### 1.1.1 Channel Flow and Microchannels

Channel flow constitutes a very important class of flows in fluid mechanics due to its numerous applications in biological, industrial and engineering systems. As a result, it is important to study the characteristics of this flow and particular interest is how the effects of changing viscosity modify the flow pattern.

The viscosity of many fluids varies with temperature e.g. physiological fluids such as blood, various lubricants used in engineering systems like polymer solutions, mineral oils with polymer additives, etc. This variation in the fluid viscosity due to temperature is certainly going to affect the flow characteristics. In this respect, two types of channel flows, namely Poiseuille flow and Couette flow are considered. Poiseuille flow is the flow between two parallel stationary plates due to an imposed constant pressure gradient. Its general characteristic is a parabolic axial velocity profile. Couette flow is considered with the effect of viscosity due to temperature changes on the lubrication that occurs between two moving plates or between a fixed plate and a moving plate.

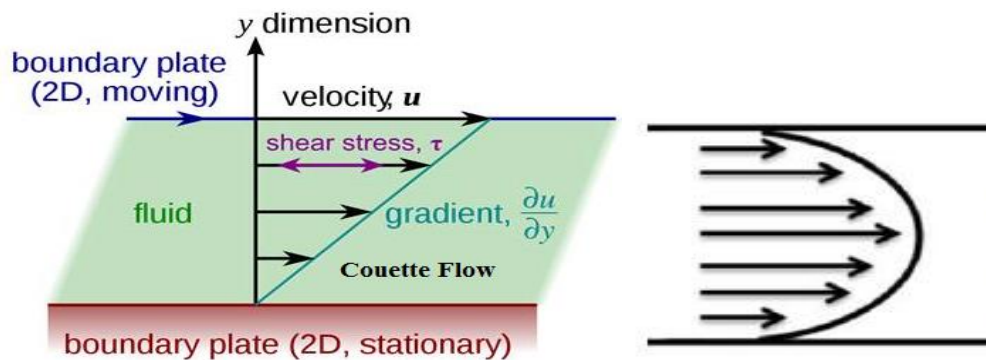


Figure 1.1 Couette flow and Poiseuille flow geometries. [142-143]

A microchannel in microtechnology is a channel with a hydraulic diameter below 1 millimetre (mm). They are increasingly used in fluid control and compact heat exchangers to achieve extremely high heat transfer rates under confined conditions. In this situation, condensation inside small-diameter channels can be found in heat pipes and compact heat exchangers for electronic equipment and spacecraft thermal control, automotive and residential air conditioning systems, and refrigeration systems. Microchannels are also used in a diversity of devices incorporating single-phase liquid flow. The prompt applications involved micromachined devices such as micropumps, microvalves, and microsensors.



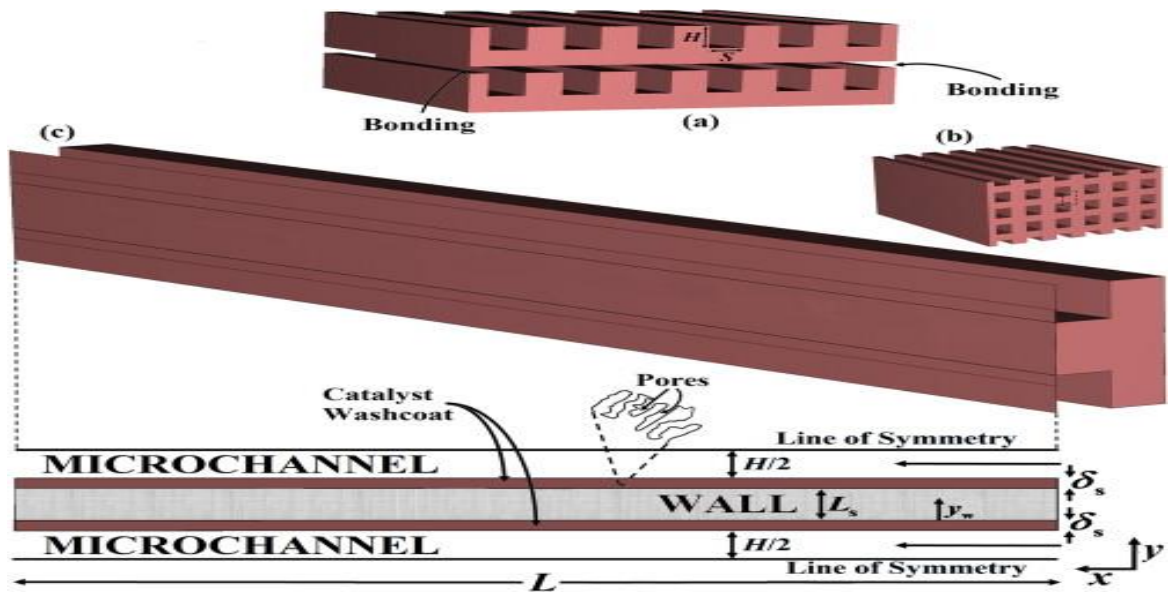


Figure 1.2 Schematic presentation of a microchannel reactor.[144]

## 1.2 Definition of Terms

### 1.2.1 Pressure

Pressure is the stress at a point in a static fluid. The gradient in pressure often drives a fluid flow, especially in ducts. The unit for pressure is  $\text{N m}^{-2}$ .

### 1.2.2 Temperature

This is the measure of the internal energy of a fluid. If the temperature differences are strong, heat transfer may be important. The unit for temperature is degree Celsius ( $^{\circ}\text{C}$ ).

### 1.2.3 Density

The density of a fluid is its mass per unit volume. Density in the liquid is nearly constant. This property aids the classification of fluids as either compressible or incompressible. A fluid is termed compressible if its density varies and increases nearly proportionally to the pressure level. Otherwise, it is termed incompressible according to White [14]. The unit of density is  $\text{kgm}^{-3}$ .

### 1.2.4 Internal Energy

In thermo-statics, the only energy in a substance is that which is stored in a system by molecular activity and molecular bonding forces. This is commonly denoted as internal energy. An identified mass of viscous fluid may be viewed as a thermodynamic system that stores various forms of energy.

Whenever any form of this fluid is being deformed, it results in an irreversible transformation of mechanical energy into internal or thermal energy. The internal energy of gas includes the energies of translation, rotation and vibration of the molecules as well as the energy of molecular dissociation and energy of electronic excitation of the molecules. The unit for internal energy is  $\text{J mol}^{-1}$ .

### 1.2.5 Specific Heat Capacity

This refers to the measure of the heat energy required to raise the temperature of one gram of a substance by one degree Celsius. Specific heat capacity is measured under two distinctly different experimental conditions. It is measured either under constant pressure condition or under constant volume condition. Typical values of the specific heat of gases are not much different from those of liquids. The unit for specific heat capacity is  $\text{J mol}^{-1} \text{K}^{-1}$ .

### 1.2.6 Thermal Conductivity

Thermal conductivity is the property of fluid that relates the vector rate of heat flow per unit area to the vector gradient of temperature. This proportionality that is observed experimentally for fluids and solids, is known as Fourier's law of heat conduction.

$$q = -k\nabla T \quad (1.1)$$

The minus sign satisfies the convection that heat flux is positive in the direction of decreasing temperature according to Kay and Crawford [18]. The unit for thermal conductivity is  $\text{W m}^{-1} \text{K}^{-1}$ .

### 1.2.7 Viscosity

A fluid at rest cannot resist shearing forces and if such forces act in a fluid which is in contact with a solid boundary, the fluid will flow over the boundary in such a way that the particles immediately in contact with the boundary have the same velocity as the boundary; while successive layers of fluid parallel to the boundary move with increasing velocity. Shear stresses opposing the relative motion of these layers are set up and their magnitude depends on the velocity gradient from layer to layer. For fluids, obeying Newton's law of viscosity, taking the direction of motion as the x-direction and  $U$  as the velocity of the fluid in the x-direction at a distance  $y$  from the boundary, the shear stress in the x-direction is given by [24]

$$\tau_x = \mu \frac{dU}{dy}, \quad (1.2)$$

where the constant  $\mu$  is called the coefficient of dynamic viscosity. The ratio of the coefficient of dynamic viscosity to mass density is called the kinematic viscosity,  $\nu$ .

$$\nu = \frac{\mu}{\rho}. \quad (1.3)$$

The viscosity property of fluids aids the classification of fluids into either Newtonian or non-Newtonian fluids. The unit of dynamic viscosity is  $kgm^{-1}s^{-1}$ . Viscosity is associated with collective currents that carry momentum from one region of the fluid to another. Consider a fluid where there is, in addition to thermal agitation of the molecules, a collective movement or current of the whole fluid for example, water running in a canal or pipe under a pressure difference. Traditionally viscosity is regarded as the most important material property and any practical study that requires the knowledge of fluid response would automatically turn to the basic understanding of viscosity. In general, the Newtonian model describes the rheological behaviour of fluids. The Newtonian model is simply a special case with a constant viscosity. However, constant viscosity is a strong deformation of fluids. It is the key factor in determining the amount of fluid flowing in channels. It also helps to determine whether the flow regime is laminar, transitional or turbulent. Accurate knowledge of viscosity is very useful for the computation of the pressure, velocity and temperature within the channels. Viscosity also helps to describe the flow behaviour of shear stress with respect to the rate of deformation of the fluid.

In general, the application of viscosity includes reservoir modelling, in which production rates and mobility for water flooding plays a major role.

### 1.2.8 Temperature-Dependent Viscosity

The effect of increasing the temperature of a fluid is to reduce the cohesive forces while simultaneously increasing the rate of molecular interchange. The former effect tends to cause a decrease of shear stress, while the latter causes it to increase.

The net result is that liquid shows a reduction in viscosity with increasing temperature. For instance most lubricants used in automobiles have a dynamic viscosity of 0.095Pas at 40°C and 0.0097Pas at 100°C, the operating oil viscosity being taken as 0.015Pas corresponding to an effective operating temperature of 81°C.

Table 1.1: Viscosity-temperature equations as in the literatures ([11, 13, 18])

| NAME                    | EQUATION   |
|-------------------------|--|
| Sutherland              | $\mu = \frac{(T/T_0)^{3/2}(T_0 + C)}{T + C}$                                   |
| Power Law               | $\mu = (T/T_0)^n$  |
| Reynolds                | $\mu = be^{-aT}$   |
| Slotte                  | $\mu = \frac{a}{(b+T)^c}$  |
| Walther                 | $\mu = \mu_0 + bd^{1/T^c}$   |
| Vogel                   | $\mu = ae^{\frac{b}{T-c}}$   |
| Arrhenius Type          | $\mu = \mu_0 \left( \frac{T}{T_0} \right)^n e^{\left( \frac{E}{RT} \right)}$   |
| Williams, Landel, Ferry | $\log \left( \frac{\mu}{\mu_0} \right) = - \frac{C_1(T - T_0)}{C_2 + T - T_0}$ |

### 1.3 Heat Transfer Mechanisms

Heat tends to move from a high-temperature region to a low-temperature region. This heat transfer may occur through the mechanisms of conduction and radiation. In engineering, the term convective heat transfer is used to describe the combined effects of conduction and fluid flow and is regarded as a third mechanism of heat transfer.

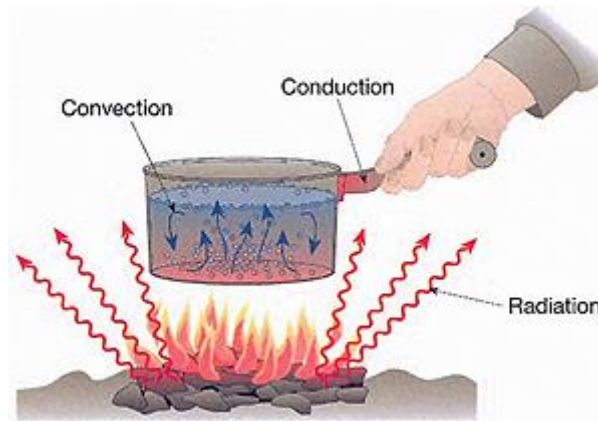


Figure 1.3 Illustration of conduction, convection and radiation heat transfer [145]

#### 1.3.1 Conduction

This is the most significant means of heat transfer in a solid. On a microscopic scale, conduction occurs as hot, rapidly moving or vibrating atoms and molecules interacting with neighbouring atoms and molecules, transferring some of their energy (heat) to these neighbouring atoms. In insulator, the heat flux is carried almost entirely by phonon vibrations. Electrons also conduct an electric current through conductive solids, and the thermal and electrical conductivities of most metals have about the same ratio. A good electrical conductor, such as copper, usually also conducts heat well. Thermoelectricity is caused by the relationship between electrons, heat fluxes and electrical currents.

#### 1.3.2 Convection

This is usually the dominant form of heat transfer in liquids and gases. This is a term used to characterize the combined effects of conduction and fluid flow. In convection, enthalpy transfer

occurs by the movement of hot or cold portions of the fluid together with heat transfer by conduction. Commonly an increase in temperature produces a reduction in density. Hence, when water is heated on a stove, hot water from the bottom of the pan rises, displacing the colder denser liquid that falls. Mixing and conduction result eventually in a nearly homogeneous density and even temperature. Three types of convection are commonly distinguished, they are free convection, forced convection and mixed convection.

Regardless of the particular nature of the convection heat transfer process, the rate of heat transfer is given by Newton's law of cooling as

$$q'' = h(T_w - T_\infty), \quad (1.4)$$

where  $h$  is the convective heat transfer coefficient,  $T_w$  is the geometry surface temperature and  $T_\infty$  is the free stream fluid temperature.

Table 1.2 Typical values of convective heat transfer coefficients

| Type of Convection         | $h(\text{W}/\text{m}^2\cdot\text{K})$ |
|----------------------------|---------------------------------------|
| Natural convection (air)   | 5 – 15                                |
| Natural convection (water) | 500 – 1000                            |
| Force convection (oil)     | 20 – 2000                             |
| Force convection (air)     | 10 – 200                              |
| Force convection (water)   | 300 – 20000                           |
| Water boiling              | 100000                                |
| Water condensing           | 5000- 10000                           |

### 1.3.2.1 Natural or Free Convection

Natural convection is caused by buoyancy forces due to density differences caused by temperature variations in the fluid. When heating, the density changes in the boundary layer and will cause the fluid to rise and be replaced by cooler fluid that will also heat and rise. This phenomenon is called free or natural convection. A common example of natural convection is the rise of smoke from a fire. It can be seen in a pot of boiling water in which the hot and less-

dense water on the bottom layer moves upwards in plumes, and the cool and denser water near the top of the pot sinks.

### **1.3.2.2 Forced Convection**

The fluid movement results from external surface forces such as a fan or pump i.e. pressure gradient. Forced convection is typically used to increase the rate of heat exchange.

Many types of mixing also utilize forced convection to distribute one substance within another. Forced convection also occurs as a by-product to other processes, such as the action of a propeller in fluid or aerodynamic heating. Fluid radiator systems, and also heating and cooling of parts of the body by blood circulation, are other familiar examples of forced convection.

### **1.3.2.3 Mixed Convection**

Mixed (combined) convection is a combination of forced and free convections which is the general case of convection when a flow is determined simultaneously by an outer forcing system (i.e., outer energy supply to the fluid-streamlined body system) and inner volumetric (mass) forces, viz., by the non-uniform density distribution of a fluid medium in a gravity field. The most vivid manifestation of mixed convection is the motion of the temperature stratified mass of air and water areas of the Earth that is traditionally studied in geophysics. However, mixed convection is found in the systems of much smaller scales, i.e., in many engineering devices.

## **1.3.3 Radiation**

This is the only form of heat transfer that can occur in the absence of any form of medium (i.e., through a vacuum). Thermal radiation is a direct result of the movements of atoms and molecules in a material. Since these atoms and molecules are composed of charged particles (protons and electrons), their movements result in the emission of electromagnetic radiation, which carries energy away from the surface. At the same time, the surface is constantly bounded by radiation from the surroundings, resulting in the transfer of energy to the surface.

Since the amount of emitted radiation increases with increasing temperature, it results in a net transfer of energy from higher temperatures to lower temperatures. The rate of radiation heat exchange between a small surface and large surrounding is given by the expression [6],

$$Q = \varepsilon \sigma^* A (T_s^4 - T_{sur}^4), \quad (1.5)$$

where  $\varepsilon$  is the surface emissivity,  $A$  is the surface area,  $\sigma^*$  is the Stefan-Boltzmann constant,  $T_s$  is the absolute temperature of the surface and  $T_{sur}$  is the absolute temperature of the surroundings. In differential form, the radiative heat flux within an optically dense medium can be expressed as [6],

$$Q = -\frac{4\sigma^*}{3k^*} \nabla T^4, \quad (1.6)$$

where  $k^*$  the mean absorption coefficient

#### 1.4 Mass Transfer

Mass transfer is mass in transit as the result of a species concentration difference in a mixture. Just as the temperature gradient constitutes the driving potential for heat transfer, the species concentration gradient in a mixture provides the driving potential for mass transfer. Mass transfer encompasses both mass diffusion on a molecular scale and the bulk mass transport from the convection process. Mass transfer may also result from a temperature gradient in a system that is known as thermal diffusion. Similarly, the concentration gradient can give rise to the temperature gradient and consequently heat transfer. These two effects are termed as coupled phenomena.

In industrial processes, mass transfer operations include separation of chemical components in distillation columns, absorbers such as scrubbers, absorbers such as activated carbon beds, and liquid-liquid extraction.

Mass transfer is often coupled to additional transport processes in industrial cooling towers. In many technical applications, heat transfer processes occur simultaneously with mass transfer processes.



## 1.5 Nanofluids

Fluid is a substance that deforms continuously under the application of shear stress (tangential force per unit area). Convectonal heat transfer fluids such as water, mineral oils and ethylene glycol play an important role in many industrial sectors including power generation, chemical production, air-conditioning, transportation and microelectronics. Although various techniques have been applied to enhance their heat transfer, their performance is often limited by their low thermal conductivities, which obstruct the performance enhancement and compactness of heat exchangers.

With the rising demands of modern technology for process intensification and device miniaturization, there is a need to develop new types of fluids that are more effective in terms of heat exchange performance. In order to achieve this, it has been recently proposed to disperse small amounts of nanometre-sized (10–50 nm) solid particles (nanoparticles) in base fluids, resulting into what is commonly known as nanofluids. The term “nanofluid” was coined by Choi [1] who was working with a group at the Argonne National Laboratory (ANL), USA, in 1995.

The nanoparticles used are ultrafine; therefore, nanofluids appear to behave more like a single-phase fluid than a solid–liquid mixture. The commonly used materials for nanoparticles are made of chemically stable metals (Al, Cu, Ag, Au, Fe), non-metals (graphite, carbon nanotubes), oxides ceramics ( $\text{Al}_2\text{O}_3$ , CuO,  $\text{TiO}_2$ ,  $\text{SiO}_2$ ), carbides (SiC), nitrides (AlN, SiN), layered (Al+  $\text{Al}_2\text{O}_3$ , Cu+C), PCM and functionalized nanoparticles. The base fluid is usually a conductive fluid, such as water, (or other coolants), oil (and other lubricants), polymer solutions, bio-fluids and other common fluids, such as paraffin. Investigations have shown that nanofluids possess enhanced thermophysical properties such as thermal conductivity, thermal diffusivity, viscosity and convective heat transfer coefficients compared to those of base fluids like oil or water [2–7].

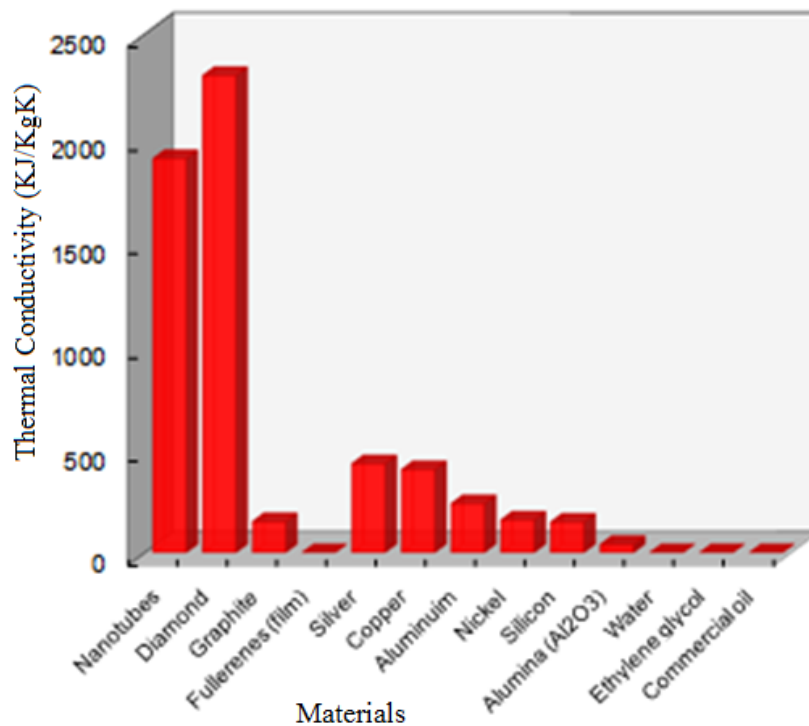


Figure 1.4 Thermal conductivity of materials [146]

### 1.5.1 Synthesis of Nanofluids

There are two techniques used in the production of nanofluids; the single-step method in which nanoparticles are evaporated directly into the base fluid and the two-step method in which nanoparticles are first prepared by either the inert gas-condensation technique or chemical vapour deposition method and then dispersed into the base fluid.

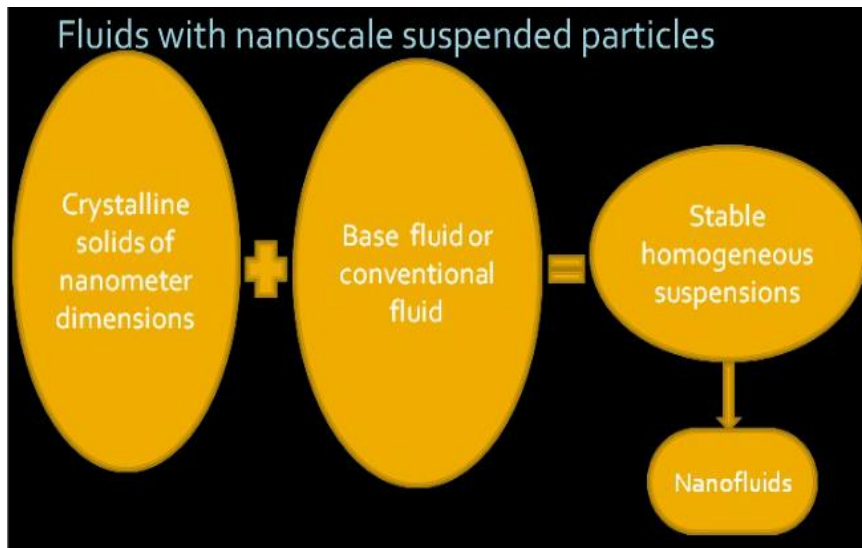


Figure 1.5 Nanofluid synthesis [147]

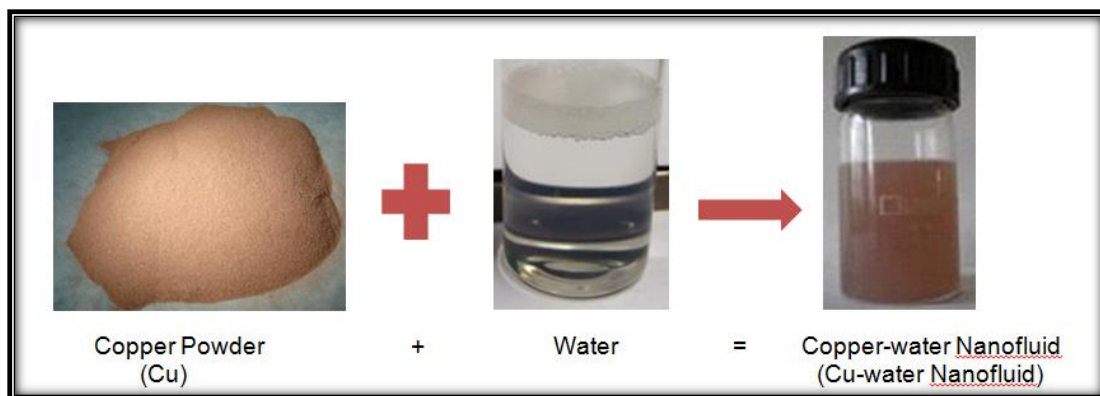


Figure 1.6 Cu-water nanofluid [148]

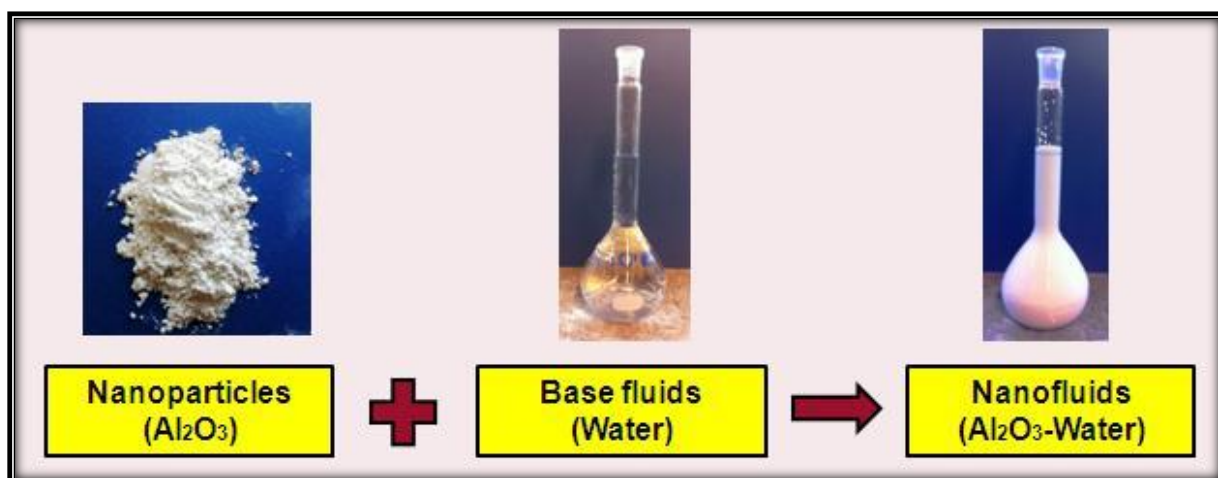


Figure 1.7 Al<sub>2</sub>O<sub>3</sub>-water nanofluid [149]

Table 1.3 Thermophysical properties of water and nanoparticles [10-15]

| <b>Material</b>                              | $\rho$ (kg/m <sup>3</sup> ) | $C_p$ (J/Kg K) | K(W/m K) | $\beta \times 10^{-5}$ (K <sup>-1</sup> ) |
|--|-----------------------------|----------------|----------|---|
| Pure Water                                   | 997.1                       | 4179           | 0.613    | 21  |
| Ethylene glycol                              | 1114                        | 2415           | 0.252    | 57  |
| Engine oil (EO)                              | 884                         | 1909           | 0.145    | 70  |
| Mineral Oil                                  | 920                         | 1670           | 0.138    | 64  |
| Blood  | 1063                        | 3594           | 0.492    | 0.18                                      |
| Silver (Ag)                                  | 10500                       | 235            | 429      | 1.89                                      |
| Copper (Cu)                                  | 8933                        | 385            | 401      | 1.67                                      |
| Iron   | 7870                        | 460            | 80       | 58  |
| Aluminium                                    | 2701                        | 902            | 237      | 2.31                                      |
| Copper Oxide (CuO)                           | 6510                        | 540            | 18       | 0.85                                      |
| Aluminium (Al <sub>2</sub> O <sub>3</sub> )  | 3970                        | 765            | 40       | 0.85                                      |
| Titanium Oxide (TiO <sub>2</sub> )           | 4250                        | 686.2          | 8.9538   | 0.9                                       |
| Silicon dioxide (SiO <sub>2</sub> )          | 3970                        | 765            | 36       | 0.63                                      |
| Iron Oxide (Fe <sub>3</sub> O <sub>4</sub> ) | 5180                        | 670            | 80.4     | 20.6                                      |

**Note:** SI units for electrical conductivity is Siemens per metre (Sm<sup>-1</sup>)

## 1.6 Application of Nanofluids

Nanofluids have an unprecedented combination of the four characteristic features desired in energy systems (fluid and thermal systems); increased thermal conductivity at low nanoparticle concentrations, strong temperature-dependent thermal conductivity, non-linear increase in thermal conductivity with nanoparticle concentration; and increase in boiling critical heat flux. These distinctive features enhance nanofluid's potential applications to improve heat transfer and energy efficiency in industrial and engineering areas including industrial coolants, smart fluids, nuclear reactors coolant, extraction of geothermal power nanofluids in automobile fuels, brake fluids, car radiator coolant, microelectronics cooling, bio and pharmaceutical industry [25-27].

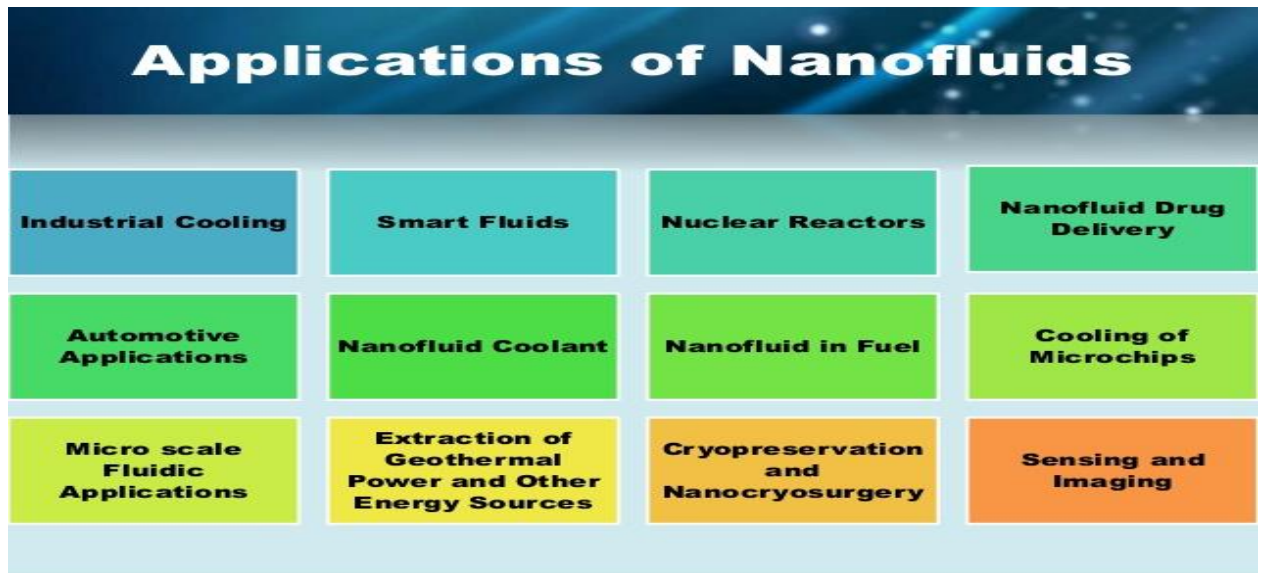


Figure 1.8 Applications of nanofluids [150]

### 1.6.1 Heat Transfer Applications

Since the introduction of nanofluids almost two decades ago, the potential of nanofluids in heat transfer applications has been highlighted in many publications [28-32]. These include industrial coolants, smart fluids, nuclear reactors, extraction of geothermal power electronic applications, etc.

### 1.6.2 Space, Defense and Ships

A number of military devices and systems require high heat flux cooling to the level of tens of ( $MW/m^2$ ). At this level, cooling with conventional fluids is challenging. Examples of military applications include cooling of power electronics and directed energy weapons involving high heat fluxes ( $500-1000W/cm^2$ ), and providing adequate cooling for them and the associated power electronics. Nanofluids have the potential to provide the required cooling in such applications as well as in other military systems, including military vehicles, submarines, and high-power laser diodes. In some cases, nanofluids research for defense applications includes multifunctional nanofluids with added thermal energy storage or energy harvesting through chemical reactions [9].



Figure 1.9 Nanofluids being used to cooling military vehicle [151-152]

The United States Department of Defense (US DOD) is developing new generations of pulsed power weapons, in electric warships with advanced electrical systems, all of which produce large amounts of heat. Waste heat from these systems may be of the order of megawatts, which can be transported by nanofluids to the hull of the ship. Therefore, the thermal management of weapons and hull heating can be accomplished simultaneously by circulating nanofluids to transport the heat from critical high heat flux components, in excess of  $1000\text{W}/\text{cm}^2$  and deliver it to the ship's hull. This heating of the ship's hull will reduce the drag of the ship and ultimately, save on fuel costs [22].





Figure 1.10 Waste heat transported by nanofluids to the hull of the ship [153]

## 1.7 Basic Equations Governing Nanofluids Flow

### 1.7.1 Continuity Equation

This equation is based on the law of conservation of mass, which states that “mass cannot be created or destroyed”. This implies that the rate of change of particle mass is zero. The equation of continuity is [63-75],

$$\frac{\partial \rho}{\partial t} + \nabla \cdot \rho \mathbf{V} = 0 \quad (1.7)$$

For an incompressible fluid (density is constant) then the equation becomes,

$$\nabla \cdot \mathbf{V} = 0, \quad (1.8)$$

In Cartesian coordinate, the above equation can be written as

$$\frac{\partial u}{\partial x} + \frac{\partial v}{\partial y} + \frac{\partial w}{\partial z} = 0. \quad (1.9)$$

### 1.7.2 Navier-Stoke's (Momentum) Equation

The equation of momentum is derived based on Newton's second law of motion

$\left( \sum F = ma = m \frac{du}{dt} \right)$ . This equation is also known as the Navier – stokes equation. Then, the

Navier-Stokes equation becomes [63-75],

$$\frac{\partial \mathbf{V}}{\partial t} + (\mathbf{V} \cdot \nabla) \mathbf{V} = -\frac{1}{\rho_{nf}} \nabla P + \frac{1}{\rho_{nf}} \nabla \cdot (\mu_{nf} \nabla \mathbf{V}) + F \quad (1.10)$$

where  $\mathbf{V}$  is the velocity vector , P is the pressure,  $\rho_{nf}$  is the nanofluid density,  $\mu_{nf}$  is the dynamic viscosity of the nanofluid, t is the time and F is the body force.

### 1.7.3 Energy Equation

This equation is derived from the first law of thermodynamics, which states that the amount of heat added to a system  $dQ$  equals to the change in internal energy  $dE$  plus the work done  $dW$  , that is  $dQ = dE + dW$  . In other words if a net energy transfer to a system occurs, the energy contained/stored in the system must increase by an amount equal to the energy transferred. The First Law of Thermodynamics requires that [33, 63-75],

$$(\rho C_p)_{nf} \left( \frac{\partial T}{\partial t} + (\mathbf{V} \cdot \nabla) T \right) = k_{nf} \nabla^2 T + \mu_{nf} \Phi + q''' \quad (1.11)$$



where  $(\rho C_p)_{nf}$  is the nanofluid heat capacity,  $\Phi$  is the viscous dissipation term,  $T$  is the nanofluid temperature,  $K_{nf}$  is nanofluid thermal conductivity and  $q'''$  is heat source term. The thermophysical properties of nanofluid are given in the following relations [6,16-21]:

$$\rho_{nf} = (1-\phi)\rho_f + \phi\rho_s, \quad \mu_{nf} = \frac{\mu_f(T)}{(1-\phi)^{2.5}}, \quad K_{nf} = K_f \left\{ \frac{K_s + 2K_f - 2\phi(K_f - K_s)}{K_s + 2K_f + 2\phi(K_f - K_s)} \right\} \quad (1.12)$$

$$(\rho C_p)_{nf} = (1-\phi)(\rho C_p)_f + \phi(\rho C_p)_s$$

where  $\rho_f$  density of the base fluid,  $\rho_s$  is density of the nanoparticle,  $\phi$  is the volume fraction of the nanoparticles,  $\mu_f$  is dynamic viscosity of the base fluid,  $K_f$  is the thermal conductivity of the base fluid,  $K_s$  is the thermal conductivity of the nanoparticle,  $(\rho C_p)_s$  is the heat capacitance of the nanoparticle,  $(\rho C_p)_f$  is the heat capacitance of the base fluid.

#### 1.7.4 Nanoparticles Concentration Equation

This equation is derived based on the Ficks law of mass transfer of nanoparticles and the dispersion rate of nanoparticles in the base fluid coupled with the thermophoresis and Brownian motion effects [63-75] and is stated as,

$$\left( \frac{\partial C}{\partial t} + (\mathbf{V} \cdot \nabla)C \right) = D_B \nabla^2 C + \left( \frac{D_T}{T_w} \right) \nabla^2 T, \quad (1.13)$$

where  $C$  is the nanoparticles concentration,  $D_B$  is the Brownian diffusion coefficient,  $D_T$  is the thermophoresis diffusion coefficient and  $T$  is the prescribed reference temperature.

### 1.7.5 Entropy equation

Entropy is a measure of how energy and other extensive quantities distribute within available constraints in a thermodynamic system. The entropy generation is always a positive quantity or zero (reversible process). Its value depends on the process, thus it is not a property of a system. That is it destroys the available energy in any flow process and thermal system. It has the dimension of energy divided by temperature, which has a unit of Joules per Kelvin ( $J/K$ ) in the international System of units. As entropy-generation takes place the quality of energy decreases, so to preserve the quality of energy entropy generation in fluid flow should be reduced. According to Woods [76] the local volumetric rate of entropy generation is given by [63-75]

$$S^m = \frac{k_f}{T_a^2} \left( \frac{\partial T}{\partial y} \right)^2 + \frac{\mu_f}{T_a} \left( \frac{\partial u}{\partial y} \right)^2 + \frac{D_B}{C_0} \left( \frac{\partial C}{\partial y} \right)^2 + \frac{D_B}{T_a} \frac{\partial T}{\partial y} \frac{\partial C}{\partial y} \quad (1.14)$$

The first term is irreversible and is the irreversibility due to heat transfer, the second term is the entropy generation due to viscous dissipation, while the third and fourth terms are the local entropy generation due to particles mass transfer and complex interaction with base fluid.

### 1.7.6 Prandtl number

The ratio of the momentum diffusivity to the thermal diffusivity is said to be the Prandtl number. It is denoted by  $P_r$  and mathematically, it can be written as

$$P_r = \frac{\nu}{\alpha} \quad (1.15)$$

where  $\nu$ ,  $\alpha$  denote the momentum diffusivity or kinematic diffusivity and the thermal diffusivity respectively. It controls the relative thickness of momentum and temperature.

### 1.7.7 Eckert number

It is a dimensionless number defining the ratio between the kinetic energy of flow and enthalpy. Mathematically,

$$E_c = \frac{u_w^2}{C_p(\Delta T)}, \quad (1.16)$$

where  $u_w^2$  is the characteristic flow velocity,  $C_p$  the specific heat and  $\Delta T$  is the temperature.

### 1.7.8 Skin friction coefficient

Skin friction coefficient occurs between the fluid and the solid surface, which leads to slow down the motion of fluid. The skin friction coefficient can be defined as

$$C_f = \frac{2\tau_w}{\rho U^2}, \quad (1.17)$$

where  $\tau_w$  denotes the wall shear stress,  $\rho$  the density and  $U$  the free-stream velocity, respectively.

### 1.7.9 Sherwood number

It is the ratio of total rate of mass transfer to the rate of diffusive mass transport. Mathematically, it can be expressed as

$$S_h = \frac{kL}{D}, \quad (1.18)$$

where  $k$ ,  $L$  and  $D$  are the mass transfer coefficient, characteristic length and the mass diffusivity, respectively.

### 1.7.10 Nusselt number

It examines the ratio of convective to the conductive heat transfer through the boundary of the surface. It is a dimensionless number which was introduced by the German mathematician Nusselt. It is denoted by  $N_u$  and mathematically, it is expressed by

$$N_u = \frac{h\delta}{k}, \quad (1.19)$$

and where  $h, \delta, k$  denote the coefficient of heat transfer, the characteristic length and the thermal conductivity respectively.

## 1.8 Literature Review

Studies related to heat transfer of variable viscosity nanofluid flow in the space between two parallel plates, one of which is moving relative to the other or both plates stationary have received the attention of several researchers due to numerous industrial and engineering applications. Until today, there have been many studies regarding heat transfer of fluids other than nanofluids. However, the number of articles related to nanofluids has increased exponentially since the discovery of the term nanofluid by Choi [1]. The research on nanofluids has mainly focused on the prediction and measurement techniques in order to evaluate their thermal conductivity.

Some experimental investigations [13, 15, 34, 35] have revealed that the nanofluids have remarkably higher thermal conductivities than those of conventional pure fluids and have shown that the nanofluids have great potential for heat transfer enhancement. It incurs little or no penalty in pressure drop because the nanoparticles are so small that the nanofluid behaves like a pure fluid. Nanofluids are expected to be suitable for the engineering application without severe problems in a pipeline and with little or no pressure drop. Jang *et al.* [36] carried out studies on the role of Brownian motion in the enhancement of thermal conductivity of nanofluids. The role of Brownian motion hydrodynamics on nanofluid thermal conductivity was explained by Evans [37]. Most studies on transport properties of the nanofluids were focused on thermal conductivity.

Convective heat transfer in nanofluids has received much attention in recent years. Chang *et al.* [38], Putra *et al.* [39], Bernaz *et al.* [40], Khanafer *et al.* [41], Wen and Ding [42], Rong *et al.* [43], Chen *et al.* [44], Xuan and Li [45], Pak and Cho [46], Tahery *et al.* [47] and Hakan [48] numerically investigated heat transfer performance of nanofluids. Most of the studies were on free convection; however, Maïga *et al.* [49] carried out studies on forced convection of alumina particles suspended in water and ethylene glycol in a uniformly heated tube. They found that the heat transfer coefficient and the wall shear stress increase with increasing nanoparticle volume fraction and Reynolds number. Peyghambarzadeh *et al.* [50] carried out experiments on forced convective heat transfer in a car radiator using water or a mixture of water and anti-freezing material like ethylene glycol. They noted that the nanofluids significantly increased the heat transfer rates, and the heat transfer rates depended on particle concentration, flow conditions (rate of fluid flow) and weakly depended on temperature. This shows that nanofluids are highly suited for use in effective radiators for cars.

These research findings erase any doubts that adding nanoparticles to a base fluid will increase its thermal conductivity. It can be concluded that improving the thermal conductivity is the key to improving the heat transfer characteristics of convectational fluids. However, it has been observed that the natural convective heat transfer coefficient decrease systematically with increasing nanoparticle concentration and the deterioration is partially attributed to the high viscosity of nanofluids [51]. Lee and Choi [12] applied a nanofluid as a coolant to a microchannel heat exchanger for cooling crystal silicon mirrors used in high-intensity X-ray sources and pointed out that the nanofluid dramatically enhanced the cooling rates compared with the conventional water-cooled and liquid-nitrogen-cooled microchannel heat exchangers. The problem of incompressible, viscous, forced convective laminar boundary layer flow of copper water and alumina water nanofluid over a flat plate was investigated by Anjali and Andrews [52].

Using nanofluids strongly influences the boundary layer thickness by modifying the viscosity of the resulting mixture, which leads to variations in the mass transfer near walls in external boundary layer flows [53]. More recently, heat transfer problems for boundary layer flow with a convective boundary condition for nanofluids were investigated by Aziz [54], Makinde and Aziz [55], and Ishak [56]. A numerical study of MHD generalized Couette flow and heat transfer with variable viscosity and electrical conductivity were investigated by Makinde and

Onyekekwe [57]. Effects of thermal radiation and viscous dissipation on boundary layer flow of nanofluids over a permeable moving plate were investigated by Motsumi and Makinde [59].

Inherent irreversibility in Sakiadis flow nanofluids were reported by Makinde, Khan and Aziz [60]. Entropy generation in a variable viscosity channel flow of nanofluids with convective cooling was investigated by Mkwizu and Makinde [61]. MHD Couette-Poiseuille flow of variable viscosity nanofluids in a rotating permeable channel with Hall effects were investigated by Makinde, Iskander, Mabood, Khan and Tshehla [58]. Analysis of Blasius flow of hybrid nanofluids over a convectively heated surface was investigated by Olatundun and Makinde [62]. To the best of the researcher's knowledge, no one so far has reported the combined effects of thermal radiation, nanoparticles shape and nanoparticles volume fraction on thermal stability and entropy generation rate of variable viscosity Couette-Poiseuille flow of nanofluids. Furthermore, this study is essential for innovative applications in hydrodynamic lubrication and cooling of engineering systems, since these thermal fluids may be hazardous and lose their effectiveness during operation due to their temperature dependent viscosity.

## **1.9 Statement Problem**

The most sensitive property of nanofluid (which is a mixture of base fluids and nanoparticles) to temperature and concentration rise is the viscosity. For instance the viscosity of various base fluids employed to produce nanofluids such as water, mineral oils, ethylene glycol, etc., varies with temperature. This variation in the base fluids' viscosity due to temperature and concentration may affect the flow characteristics as well as the efficient operation of nanofluids used in industrial and engineering processes. Thus, the influence of temperature dependent viscosity on the flow and heat transfer characteristics of nanofluids cannot be overlooked and requires investigation. Hence, it is necessary to ensure that the nanofluids viscosity is at all times maintained at optimum levels.

## **1.10 Research Objectives**

- To formulate nonlinear mathematical models of Couette and Poiseuille flow under various physical situations.
- To apply and compare numerical algorithms for solving the model problems using appropriate software (Maple 18).

- To investigate the differences in flow behaviour of base fluids and nanofluids with variable viscosity.
- To investigate the combined effects of thermophoresis and Brownian motion on the flow and heat transfer characteristics of nanofluids with variable viscosity.
- Determine the thermal stability criteria for channel flow of nanofluids with variable viscosity.

### **1.11 Significance of the Problem**

Theoretical research on Couette, Poiseuille flow and heat transfer of nanofluid is of great importance due to its wide application in engineering and industries. Microscale products such as miniaturized sensors, motors, heat exchangers, pumps, medical devices have great advantage over the conventional systems. Since they are extremely compact and lightweight, their manufacturing costs are lower, their fuel consumption is low and they need less space in buildings and engineering plants. These devices require ultra-high performance cooling, which is a crucial technical challenge facing many industrial and engineering applications. The conventional method for increasing heat transfer is to increase the area available for exchanging heat with a heat transfer fluid. Unfortunately, the convectional heat transfer fluids used have low thermal conductivity; hence, there is an urgent need for new and innovative coolants with improved performance. The recent discovery of nanofluids provides a solution to the cooling technology. This is because nanofluids have fascinating features like high thermal conductivity at very low nanoparticles concentration and a considerable enhancement of forced convective heat transfer. Nanofluids are also used as coolants for computers and nuclear reactors. Their cooling properties are used in many industrial applications. The main driving force for nanofluid research lies in a wide range of applications. In the industry, issues like productivity and competitiveness require engineering solutions that heavily rely on the mathematical model. It is a major goal for the industry to understand the nanofluid flow behaviour and heat transfer accurately in order to predict the flow regime under the influence of temperature dependent nanofluid viscosity.

To have a clear understanding of the nanofluid dynamics in channel flow with two fixed parallel walls or with one wall fixed while the other wall is subjected to a uniform motion, it is very important to incorporate the heat transfer character of the fluid since this plays a very significant role in the handling and processing of the material. The present study provides a platform for a detailed analysis of the impact of nanoparticles on the dynamics of nanofluid and heat transfer under Couette or Poiseuille flow scenario. The results obtained will no doubt enhance the optimal design of such flow process for engineering and industrial applications.

## **1.12 Research Methodology/Computational Approach**

This study employs a numerical approach in solving model equations, which are Boundary Value Problems (BVPs). In numerical methods, the shooting method together with Newton–Raphson shooting method coupled with fourth-order Runge-Kutta-Fehlberg. The Initial Boundary is used to solve the model problem. The shooting method transforms the BVPs into a set of initial value problems (IVP) which contain unknown initial values that need to be determined by guessing in which the Newton-Raphson technique is used to find these unknown initial values iteratively until a fixed number is obtained. Thereafter the fourth-order Runge-Kutta-Fehlberg iteration scheme is employed to integrate the set of IVPs until the given boundary conditions are satisfied. For the case of IBVPs the equations are discretized in space using a semi-discretization finite difference method known as the method of lines to transform BVPs into IVPs which then is solved by using the Runge-Kutta-Fehlberg iteration. This will be implemented on a computer using the Maple software.

### **1.12.1 The Shooting Method**

Many important physical problems always lead to boundary value problems (BVPs). The shooting method is one among the commonly used powerful numerical methods for solving boundary value problems for ordinary differential equations. In our study, we choose the shooting method to solve the boundary value problem, since it has many advantages such as ease of programming in a general form, less storage is required, and its suitability for automatic procedures.

The shooting method is an iterative algorithm that reformulates the original boundary value problem to a related initial value problem (IVPs) with its appropriate initial conditions. The



new problem requires the solution of the IVP with the initial conditions arbitrary chosen to approximate the boundary conditions at the end points. If these boundary conditions are not satisfied to the required accuracy, the procedure is repeated with a new set of initial conditions until the required accuracy is acquired or a limit to the iteration is reached. The resultant IVP is solved numerically using any appropriate method for solving linear ordinary differential equations. In this study the 4<sup>th</sup> order Runge-Kutta method was used, which provides high accuracy results. The solution of the IVP should converge to that of the BVP. The algorithm for the above procedure is achieved by using Maple programming language. The computed results are presented in graphical form. A two-point boundary value problem was considered,

$$y'' = f(x, y, y'), \quad y(a) = \alpha \text{ and } y(b) = \beta \quad (1.20)$$

where  $a < b$  and  $x \in [a, b]$ . The requirement of the shooting method is to convert the BVP to an IVP with appropriate initial condition. Thus we have,

$$y'' = f(x, y, y'), \quad y(a) = \alpha, \quad y'(a) = s \quad (1.21)$$

Introducing the notations  $u(x; s) = y(x; s)$ ,  $v(x; s) = \frac{\partial}{\partial x} y(x; s)$ , equation (1.20) can be rewritten as a system of first order ODEs,

$$\frac{\partial}{\partial x} u(x; s) = v(x; s), \quad u(a; s) = \alpha \quad (1.22)$$

$$\frac{\partial}{\partial x} v(x; s) = f(x, u(x; s), v(x; s)), \quad v(a; s) = \beta \quad (1.23)$$

The solution  $u(x; s)$  of the IVP (1.22), will coincide with the solution  $y(x)$  of the BVP (1.20), as long as a value for  $s$  is found, such that,

$$\phi(s) = u(b; s) - \beta = 0. \quad (1.24)$$

Equation (1.24) is solvable if and only if there exists  $s \in R$ , so that  $\phi(s) = 0$ . The essence of the shooting method for the solution of the BVP (1.20) is to find a root to the equation (1.24). A standard root-finding technique such as Bisection method or Newton-Raphson method is used.

### 1.12.2 The Bisection Method

Suppose the two numbers  $s_1$  and  $s_2$  are known such that  $\phi(s_1) < 0$  and  $\phi(s_2) > 0$ , we also assume that  $s_1 < s_2$ . Since the solution of the IVP depends on the initial conditions there exists at least one value of  $s$  in the interval  $[s_1, s_2]$  such that  $\phi(s) = 0$ . Thus, the interval  $[s_1, s_2]$  contains a root of the equation (1.24). The method of bisection can then be used to approximate the root of (1.23).

We take the midpoint  $s_3$  of the interval  $[s_1, s_2]$ , compute  $u(b, s_3)$  and consider whether  $\phi(s_3) = u(b, s_3) - \beta$  is positive or negative. If  $\phi(s_3) > 0$ , then the root is in the interval  $[s_1, s_3]$  that contain the root of  $\phi$ , whereas if  $\phi(s_3) < 0$  then it is in the interval  $[s_3, s_2]$ . Repeating this procedure generates a sequence of numbers  $\{s_n\}_{n=1}^{\infty}$  converging to  $s$ . The process is terminated after a finite number of steps when the length of the interval containing  $s$  has become sufficiently small.

### 1.12.3 Newton-Raphson Method

This will help compute a sequence  $\{s_n\}_{n=1}^{\infty}$  generated by  $s_{n+1} = s_n - \frac{\phi(s_n)}{\phi'(s_n)}$  (1.25)

Starting with a value  $s_0$  arbitrary chosen.

To calculate  $\phi'(s_n)$  we introduce new independent variables,

$$\xi(x; s) = \frac{\partial u(x; s)}{\partial x}, \quad \eta(x; s) = \frac{\partial v(x; s)}{\partial x} \text{ and differentiate the IVP (3) with respect to } s \text{ to}$$

obtain a 2<sup>nd</sup> IVP,

$$\frac{\partial \xi(x; s)}{\partial x} = \eta(x; s), \quad \xi(a; s) = 0 \quad (1.26)$$

$$\frac{\partial \eta(x; s)}{\partial x} = p(x; s)\xi(x; s) + q(x; s)\eta(x; s) \quad \eta(a; s) = 1$$

$$\text{where } p(x; s) = \frac{\partial f(x, u(x; s), v(x; s))}{\partial u}$$

$$q(x; s) = \frac{\partial f(x, u(x; s), v(x; s))}{\partial v} \quad (1.27)$$

We assign the value  $s_n$  to  $s$ ,  $n \geq 0$ , then the IVP (1.22) and (1.26) can be solved using an numerical method for IVPs such as the 4<sup>th</sup> order Runge-Kutta method in the interval  $[a, b]$ . Thus an approximation of  $u(b; s_n)$  is obtained to calculate  $\phi(s_n) = u(b; s_n) - \beta$  and we also obtain an approximation  $\xi(b; s_n) = \phi'(s_n)$ . The values  $\phi(s_n)$  and  $\phi'(s_n)$  give the next Newton-Raphson iterate  $s_{n+1}$  from (1.24). The process is repeated until the iterate  $s_n$  settle to a fixed number of digits. The problem with the shooting method is that it assumes that the BVP has a unique solution and also there is no guarantee that the IVP has a solution in the interval  $[a, b]$ .

#### 1.12.4 The Runge-Kutta Method

The Runge-Kutta method is a numerical technique used to solve ordinary differential equations. It is based on the first five terms of the Taylors series. The formula used is;

$$y_{i+1} = y_i + \frac{1}{6}(k_1 + 2k_2 + 2k_3 + k_4)h \quad (1.28)$$

where

$$k_1 = f(x_i, y_i) \quad (1.29a)$$

$$k_2 = f\left(x_i + \frac{1}{2}h, y_i + \frac{1}{2}k_1h\right) \quad (1.29b)$$

$$k_3 = f\left(x_i + \frac{1}{2}h, y_i + \frac{1}{2}k_2h\right) \quad (1.29c)$$

$$k_4 = f(x_i + h, y_i + k_3h) \quad (1.29d)$$

#### 1.13 Thesis Outline

The thesis is organised as follows:

## **Chapter One**

This chapter presents the general introduction, definitions, and applications of nanofluids, literature review, research objectives, and significance of study, problem statement and research methodology. The chapter furthermore expresses the basic equations governing nanofluids flow such as continuity equation, momentum equation, energy equation, concentration transport equation, entropy generation equation (both single phase model and two phase model), and provide thermophysical properties of nanoparticles and base fluids.

## **Chapter Two**

This chapter presents an analysis on inherent irreversibility in Cu-H<sub>2</sub>O nanofluid Couette flow with variable viscosity and nonlinear radiative heat transfer. The first, second and third objectives are achieved in this chapter.

## **Chapter Three**

The chapter presents an analysis of the study on entropy analysis of radiating variable viscosity EG/AG nanofluid flow in microchannels with buoyancy force and convective cooling. The first, second and third objectives are achieved in this chapter.

## **Chapter Four**

This chapter presents an analysis of the study on thermophoresis and Brownian motion effects on a reactive variable viscosity Couette flow in a microchannel. All specific objectives are achieved in this chapter.

## **Chapter Five**

The chapter presents an analysis of the study on the modelling nanoparticles distribution pattern in a microchannel flow of nanofluid filled with a porous medium. The first, second and third objectives are achieved in this chapter.

## **Chapter Six**

This chapter presents an analysis of the study on the entropy generation analysis in a microchannel Poiseuille flow of nanofluid with nanoparticles injection and variable properties. All specific objectives are achieved in this chapter

## **Chapter Seven**

This chapter concludes the dissertation with a general discussion, conclusion, recommendations and future research work.

## CHAPTER 2

# INHERENT IRREVERSIBILITY IN CU-H<sub>2</sub>O NANOFLUID COUETTE FLOW WITH VARIABLE VISCOSITY AND NONLINEAR RADIATIVE HEAT TRANSFER<sup>1</sup>

### ABSTRACT

In this paper, combined effects of thermal radiation, variable viscosity, nanoparticles shape and volume fraction on the inherent irreversibility and thermal stability of water base nanofluid Couette flow containing Copper nanoparticles are investigated. The nonlinear governing equations of continuity, momentum and energy balance are obtained and tackled numerically using shooting method with Runge-Kutta-Fehlberg integration scheme. The effects of various emerging thermophysical parameters on the nanofluid velocity, temperature, skin friction, Nusselt number, thermal stability criteria with respect to critical Eckert number, entropy generation rate and Bejan number are presented graphically and discussed. Our results reveal, among others obtained, that thermal radiation enhances the cooling and thermal stability of Cu-H<sub>2</sub>O nanofluid. In addition, both nanoparticles shapes and volume fraction have great influence on the nanofluids thermal stability and entropy generation rate.

### 2.1 Introduction

One of the classical problems in fluid dynamics is the Couette flow where the fluid motion is induced by movement of the bounding surface. It is a shear driven flow between a fixed and a moving parallel flat plates [77]. The investigation of Couette flow with heat and mass transfer has attracted the continual interest of several researchers owing to its widespread application in industries and engineering systems [57, 78-79].

Example of such applications can be found in tribology and lubrication technology, which deals with the design, friction, wear, and lubrication of interacting surfaces in relative motion [80].

---

<sup>1</sup> This chapter is based on the research paper: R.L. Monaledi and O.D. Makinde. Inherent Irreversibility in Cu-H<sub>2</sub>O Nanofluid Couette Flow with variable Viscosity and Nonlinear Radiative Heat Transfer, International Journal of Fluid Mechanics Research, Volume 46(6), 525–543, 2019.

This plays a significant role in transportation and manufacturing industries, with effective lubrication of moving parts being critical to human progress in ensuring the safe, continuous operation of machine components. Other relevant illustration can be found in the shear flow of coolant fluid used in the industrial processes [81]. Meanwhile, the recent introduction of a new class of nanotechnology-based heat transfer fluids known as nanofluid [1] provide a better ultrahigh-performance coolants and lubricants for many industrial technologies.

Nanofluid are obtained by dispersing solid nanometre sized metallic or non-metallic particles (diameter <100 nm) in common fluids such as water, glycol, oils and refrigerants. Nanolubricants enhance thermal dissipation, anti-wear and improve extreme pressure properties of compressors lubricants [82]. Suspension of low concentration of base liquids generates a complex mixture, where the nanometre-size of the particles and their large surface-to-volume ratio produce new physical phenomena. The underlying physics of the nanoparticle-fluid suspension and their mathematical description need to be properly addressed. A number of investigations conducted in the past have revealed that several factors, such as base fluid material, particle material, particle shape, particle size, particle volume fraction, particle clustering, nanoparticle base fluid interfacial layer, nanoparticle Brownian motion and temperature, affect the thermal conductivity of the nanofluids [11, 83].

Kiblinki *et al.* [84] examined the mechanism of heat flow in a fluid containing nano-sized particles. Buongiorno [85] investigated the effects of nanoparticles mass transfer on the nanofluid flow with heat transfer characteristics. Further discussions on transport phenomena and heat transfer of nanofluids can be found in the references [86, 87]. Meanwhile, viscosity of the cooling fluids and lubricants under Couette flow scenario is a crucial parameter, as it affects pressure drop in the interacting surfaces and impedes with its thermal performance [58]. Under film-lubrication conditions, the potential increase of the lubricant's viscosity due to nanoparticle addition is extremely vital to its effective operation.

Similar to most fluids, the viscosity of nanofluids is temperature dependent and decreases with an increase in temperature. For instance, the viscosity of water and lubricating oil are extremely sensitive to the operating temperature. The viscosity of water at 0 degrees Celsius is 7 times more viscous than water at 100 degrees Celsius. Namburu *et al.* [88] reported an exponential decrease in SiO<sub>2</sub>/ethylene glycol mixed with water nanofluids viscosity with an increase in temperature range from 35°C to 50°C. They observed that these nanofluids exhibit non-

Newtonian behaviour at lower temperatures but Newtonian at higher temperatures. Ali and Makinde [89] numerically examined the combined effects of thermophoresis and Brownian motion on unsteady generalized Couette flow of a water base nanofluid with variable viscosity and convective cooling at the moving surface. A number of studies analysing heat transfer in Couette flow of nanofluid with or without variable viscosity include [90, 91] among many others.

The interaction of thermal radiation with nanofluids is of major interest in the design of many advanced energy conversion systems operating at high temperature. The suspended nanoparticles boost the nanofluids surface area for the absorption of incident radiation as well as the fluid heat capacity [92, 93]. This makes nanofluids very useful and effective as solar collector for solar water heater application. Motsumi and Makinde [59] examined the theoretical model describing the influence of thermal radiation absorption on the flow of Cu-water nanofluids past a moving permeable surface. Other relevant investigations on the effects of thermal radiation interaction with nanofluids can be found in the references [94, 95].

Moreover, for efficient operation and design of thermal engineering systems, not only the heat transfer rate has to be enhanced by using nanofluids but the entropy generation rate has to be minimized as well [96]. As entropy generation takes place, the quality of energy in the flow and thermal system diminish and thus reduces its efficiency. The first law of thermodynamics depicts the energy conservation principle while the second law declares that all real process is irreversible. The thermodynamics irreversibility in a system can be easily quantified in terms of entropy generation rate; consequently, the system exergy decreases while the energy increases.

Several factors such as viscous dissipation, heat transfer, mass transfer and chemical reaction between interacting solid surfaces may enhance the entropy production in a thermal system [76]. The incorporation of thermodynamics second law in the analysis of nanofluids flow with heat transfer enables one to determine the appropriate factors contributing to entropy production in order to minimize them for optimum performance. The effect of nanoparticles' shape on entropy generation in Cu-water nanofluid was studied by Ellahi *et al.* [97]. Abolbashari *et al.* [98] theoretically analyzed the effects of entropy generation on boundary layer flow of Casson nanofluid past a stretching surface. Makinde and Eegunjobi [99] studied numerically the effect of nonlinear thermal radiative heat flux on entropy generation in hydromagnetic couple stress nanofluid flow in a channel with permeable walls. Mkwizu *et al.* [100] presented computational



model and thermodynamic analysis of the effects of Navier-slip and wall permeability on entropy generation in generalized Couette flow of nanofluids containing Copper (Cu) and Alumina ( $\text{Al}_2\text{O}_3$ ) as nanoparticles. Other pertinent studies on this topic can be found in references [60-61,101].

To the best of our knowledge, the combined effects of thermal radiation, nanoparticles shape and nanoparticles volume fraction on thermal stability and entropy generation rate of variable viscosity Couette flow of water base nanofluids has not been reported before. Furthermore, this study is very crucial for innovative applications in hydrodynamic lubrication and cooling of engineering systems, since these thermal fluids may be hazardous and loss their effectiveness during operation due to rapid conversion of kinetic energy into internal energy and their temperature dependent viscosity. This may invariably lead to the formation of critical Eckert number above which the flow process is thermally unsafe. The Eckert number describes the ratio of the kinetic energy dissipated in the flow to the thermal energy conducted into or away from the fluid. It is then necessary to determine the critical value of Eckert number for safe and efficient operation of flow and thermal processes. The aim of the present study is to analyse the entropy generation and thermal stability of Cu-water nanofluid Couette flow with temperature dependent viscosity in the presence of thermal radiation absorption. The effects of various thermophysical parameters are presented graphically and discussed quantitatively.

## 2.2 Problem Formulation

We consider a steady flow of an incompressible, temperature dependent variable viscosity and optically dense radiating nanofluid under a single-phase Couette flow scenario as shown in figure 2.1. The water base nanofluid contains Copper nanoparticles. The flow takes place in the  $x$  -direction between two parallel plates of small width  $H$  and very long length  $L$ . The upper plate moves with constant velocity  $U$  while the lower plate is kept stationary. Following [58, 88-91], the temperature dependent nanofluid viscosity  $\mu_{nf}$  can be expressed in Arrhenius type as,

$$\mu_{nf} = \frac{\mu_f e^{\frac{E}{RT}}}{(1 - \phi)^{2.5}}, \quad (2.1)$$

where  $E$  is the activation energy,  $\mu_f$  is the base fluid pre-exponential dynamic viscosity,  $\phi$  is the nanoparticles volume fraction,  $R$  is universal gas constant and  $T$  is the nanofluid temperature.

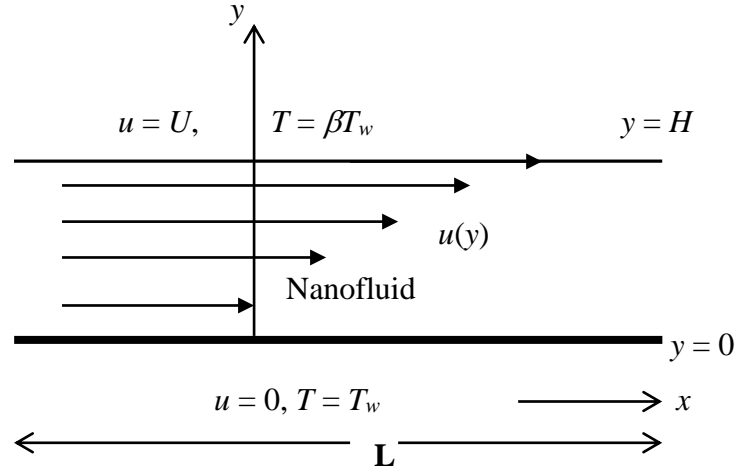


Figure 2.1 Problem geometry

Under these conditions, the continuity, momentum, energy and entropy generation equations governing the problem in two dimensions may be written as [57, 59, 79, 90-95];

$$\frac{\partial u}{\partial x} + \frac{\partial v}{\partial y} = 0, \quad (2.2)$$

$$\left( u \frac{\partial u}{\partial x} + v \frac{\partial u}{\partial y} \right) = -\frac{1}{\rho_{nf}} \frac{\partial p}{\partial x} + \frac{2}{\rho_{nf}} \frac{\partial}{\partial x} \left( \mu_{nf} \frac{\partial u}{\partial x} \right) + \frac{1}{\rho_{nf}} \frac{\partial}{\partial y} \left[ \mu_{nf} \left( \frac{\partial u}{\partial y} + \frac{\partial v}{\partial x} \right) \right], \quad (2.3)$$

$$\left( u \frac{\partial v}{\partial x} + v \frac{\partial v}{\partial y} \right) = -\frac{1}{\rho_{nf}} \frac{\partial p}{\partial y} + \frac{2}{\rho_{nf}} \frac{\partial}{\partial y} \left( \mu_{nf} \frac{\partial v}{\partial y} \right) + \frac{1}{\rho_{nf}} \frac{\partial}{\partial x} \left[ \mu_{nf} \left( \frac{\partial u}{\partial y} + \frac{\partial v}{\partial x} \right) \right], \quad (2.4)$$

$$(\rho C_p)_{nf} \left( u \frac{\partial T}{\partial x} + v \frac{\partial T}{\partial y} \right) = k_{nf} \left( \frac{\partial^2 T}{\partial x^2} + \frac{\partial^2 T}{\partial y^2} \right) + \mu_{nf} \Phi - \frac{\partial q_r}{\partial y}, \quad (2.5)$$

$$E_G = \frac{k_{nf}}{T_w^2} \left( 1 + \frac{16\sigma^* T^3}{3k^* k_{nf}} \right) \left[ \left( \frac{\partial T}{\partial y} \right)^2 + \left( \frac{\partial T}{\partial x} \right)^2 \right] + \frac{\mu_{nf}}{T_w} \Phi, \quad (2.6)$$

and

$$\Phi = \left[ 2 \left( \frac{\partial u}{\partial x} \right)^2 + 2 \left( \frac{\partial v}{\partial y} \right)^2 + \left( \frac{\partial u}{\partial y} + \frac{\partial v}{\partial x} \right)^2 \right]. \quad (2.7)$$

where  $(u, v)$  are the velocity components of the nanofluid in the  $(x, y)$  directions respectively,  $P$  is the nanofluid pressure,  $E_G$  is the entropy generation rate,  $\rho_{nf}$  is the nanofluid density,  $k_{nf}$  is the nanofluid thermal conductivity,  $q_r$  is the radiative heat flux and  $(\rho C_p)_{nf}$  is the nanofluid heat capacitance. By using the Rosseland approximation [59, 92-95] for nonlinear thermal radiation in an optically dense opaque medium, the radiative heat flux  $q_r$  is given as

$$q_r = -\frac{4\sigma^*}{3k^*} \frac{\partial T^4}{\partial y} = -\frac{16\sigma^* T^3}{3k^*} \frac{\partial T}{\partial y} \quad (2.8)$$

where  $\sigma^*$  is the Stefan–Boltzmann constant,  $k^*$  is the mean absorption coefficient. Following [11, 85, 102], the thermophysical expressions of nanofluid with respect to base fluid and nanoparticles are given as

$$\rho_{nf} = (1 - \phi)\rho_f + \phi\rho_s \quad (2.9)$$

$$(\rho C_p)_{nf} = (1 - \phi)(\rho C_p)_f + \phi(\rho C_p)_s \quad (2.10)$$






$$\frac{k_{nf}}{k_f} = \frac{k_s + (m - 1)k_f - (m - 1)\phi(k_f - k_s)}{k_s + (m - 1)k_f + \phi(k_f - k_s)} \quad (2.11)$$

where  $m$  is the nanoparticles shape factor as shown in table 2.2,  $\rho_f$  is the density of the base fluid (mineral oil or water),  $\rho_s$  is the nanoparticles density,  $k_f$  is the thermal conductivity of base fluid,  $k_s$  is the nanoparticles thermal conductivity,  $C_{pf}$  and  $C_{ps}$  are the specific heat at constant pressure for the base fluid and the nanoparticles, respectively (see table 2.1).

Table 2.1 Nanoparticles and base fluid thermophysical properties [11, 83-84]

| Physical Properties | $C_p$ (J/kgK) | $\rho$ (kg/m <sup>3</sup> ) | $k$ (W/mK) |
|---------------------|---------------|-----------------------------|------------|
| Water               | 4183          | 998.2                       | 0.67       |
| Cu                  | 385           | 8933                        | 400        |

Table 2.2 The nanoparticles shape factors (m) [85, 99]

| Nanoparticles Shape | Shape Structure  | Shape Factor (m) |
|---------------------|--|------------------|
| <i>Spherical</i>    |   | 3                |
| <i>Bricks</i>       |   | 3.7              |
| <i>Cylindrical</i>  |   | 4.9              |
| <i>Platelets</i>    |   | 5.7              |
| <i>Blades</i>       |  | 8.6              |

The appropriate boundary conditions are given as follows:

$$u = 0, T = T_w \text{ (for a lower fixed impermeable plate)} \quad \text{at } y = 0 \quad (2.12)$$

$$u=U, T=\beta T_w, \text{ (the upper plate is subjected to a uniform motion) at } y = H \quad (2.13)$$

where  $\beta \geq 1$  is the upper moving plate temperature parameter and  $T_w$  is the lower fixed plate temperature. We introduce the following non-dimensional quantities in equations (2.2)-(2.13):

$$\begin{aligned} \eta &= \frac{y}{\varepsilon L}, X = \frac{x}{L}, W = \frac{u}{U}, V = \frac{v}{\varepsilon U}, \varepsilon = \frac{H}{L}, \theta = \frac{E(T - T_w)}{RT_w^2}, \bar{P} = \frac{H^2 P}{\mu_f L U}, \\ \gamma &= \frac{RT_w}{E}, \text{Re} = \frac{UL}{\nu_f}, \text{Nr} = \frac{16\sigma^* T_w^3}{3k^* k_f}, \nu_f = \frac{\mu_f}{\rho_f}, \text{Ec} = \frac{EU^2}{C_{pf} RT_w^2}, \text{Pr} = \frac{\mu_f C_{pf}}{k_f}, \\ M &= \frac{k_s + (m-1)k_f + \phi(k_f - k_s)}{k_s + (m-1)k_f - (m-1)\phi(k_f - k_s)}, \text{Ns} = \frac{H^2 E_G}{k_f \gamma}, \end{aligned} \quad (2.14)$$

and obtain

$$\begin{aligned} \varepsilon^2 \text{Re} \left( 1 - \phi + \phi \frac{\rho_s}{\rho_f} \right) \left( W \frac{\partial W}{\partial X} + V \frac{\partial W}{\partial \eta} \right) = - \frac{\partial \bar{p}}{\partial X} + \frac{2\varepsilon^2 e^{\frac{1}{\gamma}}}{(1-\phi)^{2.5}} \frac{\partial}{\partial X} \left( e^{-\frac{\theta}{(1+\gamma\theta)}} \frac{\partial W}{\partial X} \right) \\ + \frac{e^{\frac{1}{\gamma}}}{(1-\phi)^{2.5}} \frac{\partial}{\partial \eta} \left[ e^{-\frac{\theta}{(1+\gamma\theta)}} \left( \frac{\partial W}{\partial \eta} + \varepsilon^2 \frac{\partial V}{\partial X} \right) \right], \end{aligned} \quad (2.15)$$

$$\begin{aligned} \varepsilon^4 \text{Re} \left( 1 - \phi + \phi \frac{\rho_s}{\rho_f} \right) \left( W \frac{\partial V}{\partial X} + V \frac{\partial V}{\partial \eta} \right) = - \frac{\partial \bar{p}}{\partial \eta} + \frac{2\varepsilon^2 e^{\frac{1}{\gamma}}}{(1-\phi)^{2.5}} \frac{\partial}{\partial \eta} \left( e^{-\frac{\theta}{(1+\gamma\theta)}} \frac{\partial V}{\partial \eta} \right) \\ + \frac{\varepsilon^2 e^{\frac{1}{\gamma}}}{(1-\phi)^{2.5}} \frac{\partial}{\partial X} \left[ e^{-\frac{\theta}{(1+\gamma\theta)}} \left( \frac{\partial W}{\partial \eta} + \varepsilon^2 \frac{\partial V}{\partial X} \right) \right], \end{aligned} \quad (2.16)$$

$$\begin{aligned} \varepsilon^2 M \text{Pr} \text{Re} \left( 1 - \phi + \phi \frac{(\rho C_p)_s}{(\rho C_p)_f} \right) \left( W \frac{\partial \theta}{\partial X} + V \frac{\partial \theta}{\partial \eta} \right) = \varepsilon^2 \frac{\partial^2 \theta}{\partial X^2} \\ + \left[ 1 + MNr(1 + \gamma\theta)^3 \right] \frac{\partial^2 \theta}{\partial \eta^2} + 3MNr\gamma(1 + \gamma\theta)^2 \left( \frac{\partial \theta}{\partial \eta} \right)^2 \\ + \frac{M \text{Pr} E c e^{\frac{1}{\gamma}} e^{-\frac{\theta}{(1+\gamma\theta)}}}{(1-\phi)^{2.5}} \left[ 2\varepsilon^2 \left( \frac{\partial W}{\partial X} \right)^2 + 2\varepsilon^2 \left( \frac{\partial V}{\partial \eta} \right)^2 + \left( \frac{\partial W}{\partial \eta} + \varepsilon^2 \frac{\partial V}{\partial X} \right)^2 \right], \end{aligned} \quad (2.17)$$

$$\begin{aligned} Ns = \frac{\text{Pr} E c e^{\frac{1}{\gamma}} e^{-\frac{\theta}{(1+\gamma\theta)}}}{\gamma(1-\phi)^{2.5}} \left[ 2\varepsilon^2 \left( \frac{\partial W}{\partial X} \right)^2 + 2\varepsilon^2 \left( \frac{\partial V}{\partial \eta} \right)^2 + \left( \frac{\partial W}{\partial \eta} + \varepsilon^2 \frac{\partial V}{\partial X} \right)^2 \right] \\ + \frac{[1 + MNr(1 + \gamma\theta)^3]}{M} \left[ \left( \frac{\partial \theta}{\partial \eta} \right)^2 + \varepsilon^2 \left( \frac{d\theta}{dX} \right)^2 \right]. \end{aligned} \quad (2.18)$$

where  $\gamma$  is the activation energy parameter,  $Ec$  is the Eckert number,  $\text{Pr}$  is the Prandtl number ( $\text{Pr} \approx 6.2$  for water),  $Re$  is the Reynolds number. Since the channel aspect ratio is very small ( $0 < \varepsilon \ll 1$ ), the lubrication approximation based on asymptotic simplification of the governing equations (2.14)–(2.18) is invoked. For Couette flow in a very long microchannel, the axial pressure gradient is zero (i.e.  $\partial \bar{p} / \partial X = 0$ ) and the flow is solely driven by the uniform motion of the upper wall.

Equations (2.16)–(2.18) then become,

$$(1 + \gamma\theta)^2 \frac{d^2W}{d\eta^2} = \frac{d\theta}{d\eta} \frac{dW}{d\eta}, \quad (2.19)$$

$$\left[1 + MNr(1 + \gamma\theta)^3\right] \frac{d^2\theta}{d\eta^2} + 3MNr\gamma(1 + \gamma\theta)^2 \left(\frac{d\theta}{d\eta}\right)^2 + \frac{M \text{Pr} Ece^{\frac{1}{\gamma}}}{(1 - \phi)^{2.5}} \left(\frac{dW}{d\eta}\right)^2 e^{-\frac{\theta}{(1 + \gamma\theta)}} = 0 \quad (2.20)$$

$$N_s = \frac{\left[1 + MNr(1 + \gamma\theta)^3\right]}{M} \left(\frac{d\theta}{d\eta}\right)^2 + \frac{\text{Pr} Ece^{\frac{1}{\gamma}} e^{-\frac{\theta}{(1 + \gamma\theta)}}}{\gamma(1 - \phi)^{2.5}} \left(\frac{dW}{d\eta}\right)^2, \quad (2.21)$$

with boundary conditions given as

$$W(0) = 0, \theta(0) = 0 \quad (2.22)$$

$$W(1) = 1, \theta(1) = \frac{\beta - 1}{\gamma}. \quad (2.23)$$

Other quantities of interest are the skin friction coefficients ( $C_f$ ), Nusselt number ( $Nu$ ) and the Bejan number ( $Be$ ) which are given as

$$C_f = \frac{H\tau_w}{\mu_f U} = \frac{e^{\frac{1}{\gamma}} e^{-\frac{\theta}{(1 + \gamma\theta)}}}{(1 - \phi)^{2.5}} \frac{dW}{d\eta} \Big|_{\eta=0,1}, \quad (2.24)$$

$$Nu = \frac{HEq_w}{k_f RT_w^2} = -\frac{\left[1 + MNr(1 + \gamma\theta)^3\right]}{M} \frac{d\theta}{d\eta} \Big|_{\eta=0,1}, \quad (2.25)$$

$$Be = \frac{N_i}{N_s} = \frac{1}{1 + B} \quad (2.26)$$

where

$$\tau_w = \mu_{nf} \frac{\partial u}{\partial y}, \quad q_w = -k_{nf} \left( 1 + \frac{M16\sigma^* T^3}{3k_f k^*} \right) \frac{\partial T}{\partial y}, \quad (2.27)$$

$$N_1 = \frac{[1 + MNr(1 + \gamma\theta)^3]}{M} \left( \frac{d\theta}{d\eta} \right)^2, \quad N_2 = \frac{\text{Pr} Ec e^{\frac{1}{\gamma} e^{-\frac{\theta}{(1+\gamma\theta)}}}}{\gamma(1-\phi)^{2.5}} \left( \frac{dW}{d\eta} \right)^2, \quad B = \frac{N_2}{N_1}, \quad (2.28)$$

The symbol  $N_1$  represents thermodynamic irreversibility due to thermal radiation absorption and heat transfer while  $N_2$  corresponds to the entropy generation due to fluid friction. When  $0.5 < Be \leq 1$ , the effects of thermodynamics irreversibility due to thermal radiation absorption and heat transfer dominate the flow system while  $0 \leq Be < 0.5$  corresponds to the dominant effects of fluid friction. When  $Be = 0.5$ ,  $N_1$  and  $N_2$  contribute equally to the entropy generation and  $B$  is the irreversibility ratio.

**Special Case:** It is very important to note that the nonlinear model equations (2.19)-(2.21) do admit an exact solution for a special case when  $Nr = 0$  (i.e. absent of thermal radiation) and  $\gamma \rightarrow \infty$  (i.e. extremely small activation energy or constant nanofluid viscosity), and we obtain the solution for the velocity and temperature field as

$$W(\eta) = \eta, \quad \theta(\eta) = \frac{M \text{Pr} Ec (\eta - \eta^2)}{2(1-\phi)^{2.5}}, \quad Ns(\eta) = M \left( \frac{\text{Pr} Ec (1 - 2\eta)}{2(1-\phi)^{2.5}} \right)^2. \quad (2.29)$$

### 2.3 Numerical Procedure

The dimensionless equations (2.17)-(2.18) coupled with the boundary conditions (2.20)-(2.21) are boundary value problem (BVP). We transformed these equations into a set of nonlinear first order ordinary differential equations with some unknown initial conditions to be calculated by shooting technique [103].

Let,

$$W = y_1, W' = y_2, \theta = y_3, \theta' = y_4. \quad (2.30)$$

The governing equations then become

$$\left. \begin{aligned} y_1' &= y_2, y_2' = \frac{y_2 y_4}{(1 + \gamma_3)^2}, \\ y_3' &= y_4, y_4' = -\frac{1}{(1 + MNr(1 + \gamma_3)^3)} \left[ 3MNr\gamma(1 + \gamma_3)^2 y_4^2 + \frac{M \text{Pr} Ec e^{\frac{1}{\gamma}}}{(1 - \phi)^{2.5}} y_2^2 e^{-\frac{y_3}{(1 + \gamma_3)}} \right] \end{aligned} \right\} \quad (2.31)$$

with the corresponding initial conditions as

$$y_1(0) = 0, y_2(0) = a_1, y_3(0) = 0, y_4(0) = a_2. \quad (2.32)$$

The values for  $a_1$  and  $a_2$  in the equation (2.32) are first guessed and then determined accurately with the shooting method via Newton-Raphson's technique for each set of parameter values in equation (2.29). Thereafter, Runge-Kutta-Fehlberg integration scheme [35] is then employed to tackle the resulting initial value problem numerically with step size  $\Delta\eta=0.01$ . From the numerical solution for velocity and temperature profiles, we compute the values for the skin friction ( $C_f$ ), the Nusselt number ( $Nu$ ) and the entropy generation rate together with Bejan number as given by equations (2.19) and (2.23)-(2.25).

## 2.4 Results and Discussion

In this section, the numerical and graphical results showing the effects of all the emerging thermophysical parameters involved in the flow system are demonstrated. For this purpose, computational results are displayed in tables 2.3-2.4 while figures 2.2–2.22 are sketched to illustrate the nanofluid velocity, temperature, skin friction, Nusselt number, entropy generation rate and Bejan number profiles. Table 2.3 shows a comparison between the analytical and numerical solution for the special case of temperature field with constant viscosity ( $\gamma \rightarrow \infty$ ) and absent of thermal radiation ( $Nr = 0$ ). The results show excellent agreement between the exact solution obtained in equation (2.27) and the numerical solution obtained for equations (2.29)-(2.30).

This validates the accuracy of the results obtained from our numerical procedure. Table 2.4 illustrates the influence of various thermophysical parameters on the critical value of Eckert number ( $Ec^*$ ) for thermal stability of Cu-water nanofluid. The values  $Ec^*$  increases with



increasing values of  $\beta$ ,  $Nr$ ,  $m$  and  $\gamma$ , consequently, thermal stability is enhanced. An increase in the Cu-nanoparticles volume fraction  $\phi$ , decreases the value of  $Ec^*$  and boost early occurrence of thermal instability in the flow field. It is interesting to note that nanofluid with blades shape Cu-nanoparticles ( $m=8.6$ ) is most thermally stable with biggest value of  $Ec^*$  as compare to platelets ( $m=5.7$ ), cylindrical ( $m=4.9$ ) and bricks ( $m=3.7$ ) while nanofluid with spherical ( $m=3$ ) shaped nanoparticles is the least thermally stable with lowest value of  $Ec^*$ . In the meantime, thermal stability is enhanced with a decrease in nanofluid activation energy and an increase in thermal radiation absorption. It is noteworthy that Cu-water nanofluid Couette flow with uniform plates temperature ( $\beta=1$ ) tend to be more thermally unstable in comparison with that of non-uniform plates temperature ( $\beta>1$ ). This can be attributed a rise in thermal energy accumulation within the flow field due to an imposed uniform plates temperature during Couette flow operation.

Table 2.3 Comparison between analytical and numerical results for Cu-Water

| $\eta$ | $\theta(\eta)$<br>Exact Solution | $\theta(\eta)$<br>Numerical Solution | $ \theta_{\text{Exact}}-\theta_{\text{Num.}} $ |
|--------|----------------------------------|--------------------------------------|--|
| 0      | 0                                | 0                                    | 0  |
| 0.1    | 0.27268638                       | 0.27268638                           | $10^{-12}$                                     |
| 0.2    | 0.48477579                       | 0.48477580                           | $10^{-11}$                                     |
| 0.3    | 0.63626823                       | 0.63626822                           | $10^{-10}$                                     |
| 0.4    | 0.72716369                       | 0.72716370                           | $10^{-10}$                                     |
| 0.5    | 0.75746218                       | 0.75746219                           | $10^{-9}$                                      |
| 0.6    | 0.72716369                       | 0.72716370                           | $10^{-10}$                                     |
| 0.7    | 0.63626823                       | 0.63626822                           | $10^{-10}$                                     |
| 0.8    | 0.48477579                       | 0.48477580                           | $10^{-11}$                                     |
| 0.9    | 0.27268638                       | 0.27268638                           | $10^{-12}$                                     |
| 1.0    | 0                                | 0                                    | 0  |

Table 2.4 Computations showing the effect of parameters variation on thermal stability critical Eckert number for Cu-water

| $\phi$ | $\beta$ | $Nr$ | $m$ | $\gamma$ | $Ec^*$   |
|--------|---------|------|-----|----------|----------|
| 0      | 1       | 1    | 3   | 0.3      | 2.178123 |
| 0.05   | 1       | 1    | 3   | 0.3      | 1.942080 |
| 0.1    | 1       | 1    | 3   | 0.3      | 1.733472 |
| 0.1    | 1.2     | 1    | 3   | 0.3      | 1.906881 |
| 0.1    | 1.3     | 1    | 3   | 0.3      | 3.071546 |
| 0.1    | 1       | 3    | 3   | 0.3      | 3.542225 |
| 0.1    | 1       | 5    | 3   | 0.3      | 4.636695 |
| 0.1    | 1       | 1    | 3.7 | 0.3      | 1.752564 |
| 0.1    | 1       | 1    | 4.9 | 0.3      | 1.788244 |
| 0.1    | 1       | 1    | 5.7 | 0.3      | 1.904520 |
| 0.1    | 1       | 1    | 8.6 | 0.3      | 1.914091 |
| 0.1    | 1       | 1    | 3   | 0.2      | 0.264364 |
| 0.1    | 1       | 1    | 3   | 0.15     | 0.175602 |

#### 2.4.1 Effect of Parameter Variation on Velocity Profiles

Figures 2.2-2.5 show the effects of parameters variation on Cu-water nanofluid velocity profiles. An increase in the upper moving plate temperature parameter ( $\beta$ ) decreases the velocity profiles within the channel as shown in figure 2. Figures 2.3-2.4 indicate that Cu-water nanofluid velocity increases near the lower fixed plate and decreases near the upper moving plate due to an increase in the values of both activation energy parameter ( $\gamma$ ) and thermal radiation parameter ( $Nr$ ). Consequently, an inflexion point occurs in the nanofluid velocity. This presence of inflexion point may lead to the onset of hydrodynamics instability in the flow field. Figure 2.5 shows that a rise in the value of Eckert number boosts the Cu-water velocity profiles. This is expected since viscous heating due to velocity gradient is enhanced with an increase in  $Ec$ , consequently, the fluid becomes lighter and flow faster.

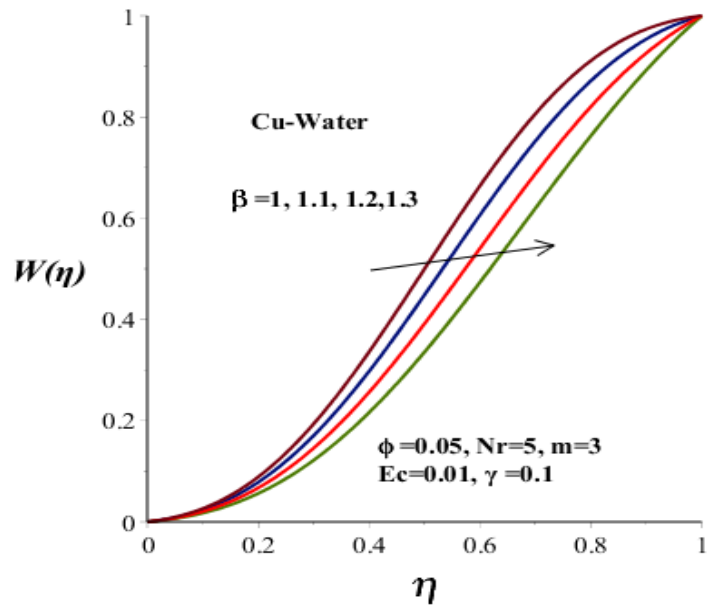


Figure 2.2 Velocity profiles with  $\beta$

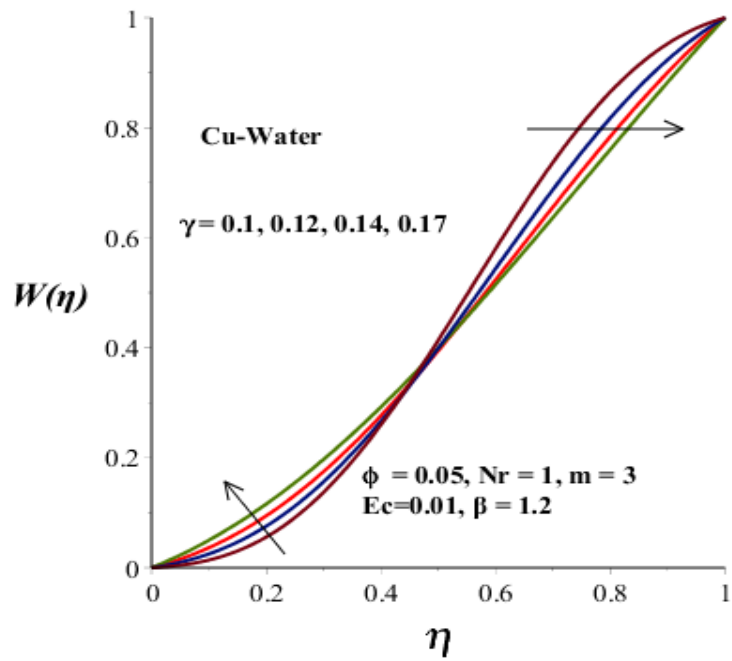


Figure 2.3: Velocity profiles with  $\gamma$

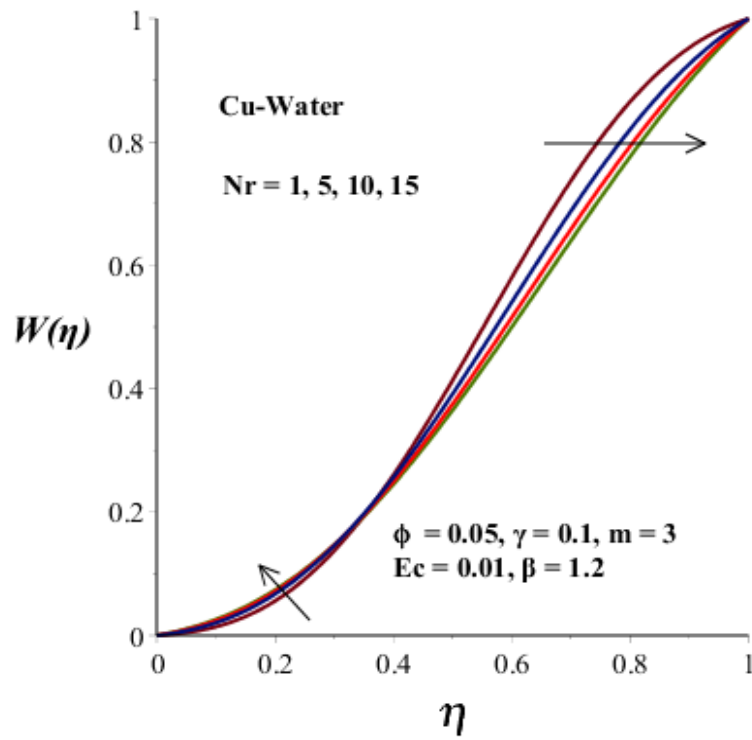


Figure 2.4 Velocity profiles Nr

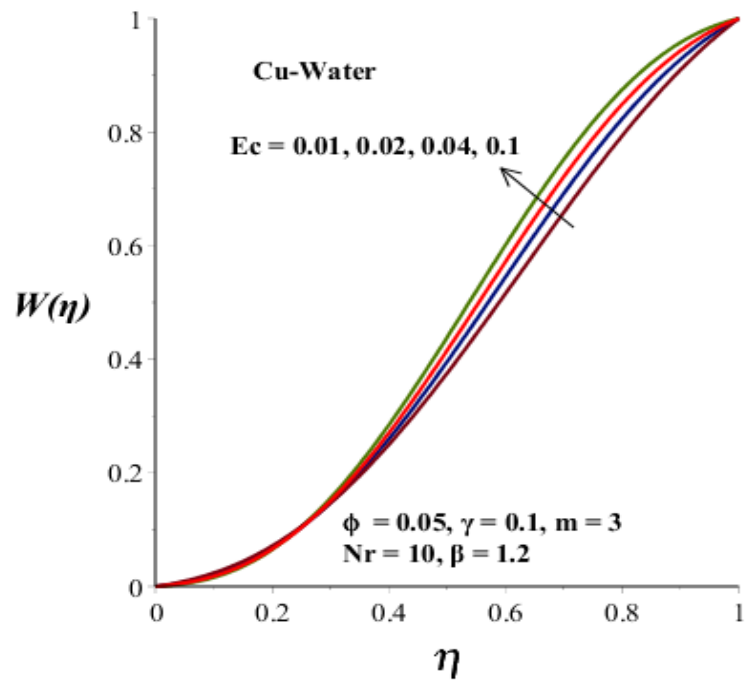


Figure 2.5 Velocity profiles Ec

## 2.4.2 Effect of Parameter Variation on Temperature Profiles

Figures 2.6-2.9 illustrate the Cu-water nanofluid temperature profiles under different parametric conditions. In figure 2.6, we observed that the nanofluid temperature diminishes near the lower fixed plate but rises near the upper moving plate region with an increase value of  $\beta > 1$ . This is expected since when  $\beta=1$  both plates are subjected to the same uniform temperature, as  $\beta > 1$  increases, the upper moving plate temperature increases while lower fixed plate temperature does not change, consequently, the Cu-water temperature augments in the upper moving plate region due to convective heat transfer from the plate to the fluid. Figures 2.7-2.8 depict the effects of nanoparticles volume fraction, Eckert number, radiation parameter and activation energy parameter on the nanofluid temperature. As  $\phi$  and  $Ec$  raise in values, the Cu-water temperature amplifies while the trend is opposite when the values of  $Nr$  and  $\gamma$  ascend. Increase in  $\phi$  will raise the thermal conductivity which invariably boosts the Cu-water temperature. Similarly, as  $Ec$  rises in value, the effect of viscous dissipation intensifies and consequently, Cu-water temperature increases. Meanwhile, an increase in the value of  $\gamma$  decreases the Cu-water activation energy, leading to a fall in Cu-water temperature. In figure 2.9, we observed that the Cu-water temperature lessens with a rise in the value of nanoparticles shape parameter ( $m$ ). Consequently, the temperature of Cu-water nanofluid with spherical shape nanoparticles is maximum, followed by bricks shape, cylindrical shape, platelet shape nanoparticles, respectively, while blade shape nanoparticles produce the lowest Cu-water nanofluid temperature.

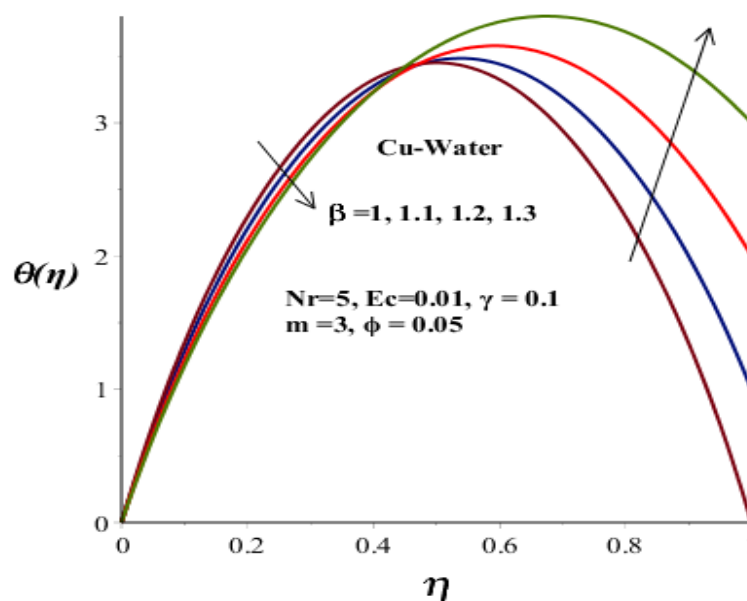


Figure 2.6 Temperature profiles with  $\beta$

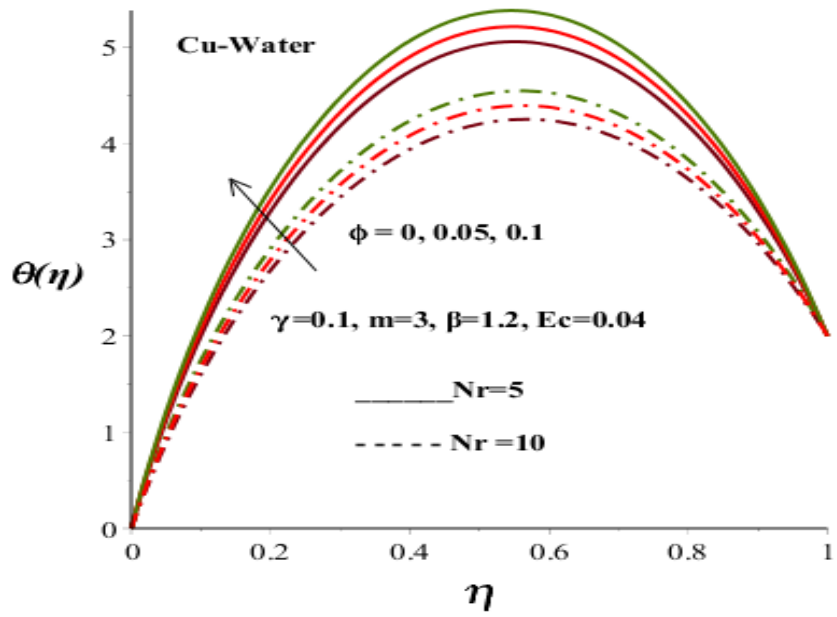


Figure 2.7 Temperature profiles with  $Nr$  and  $\phi$

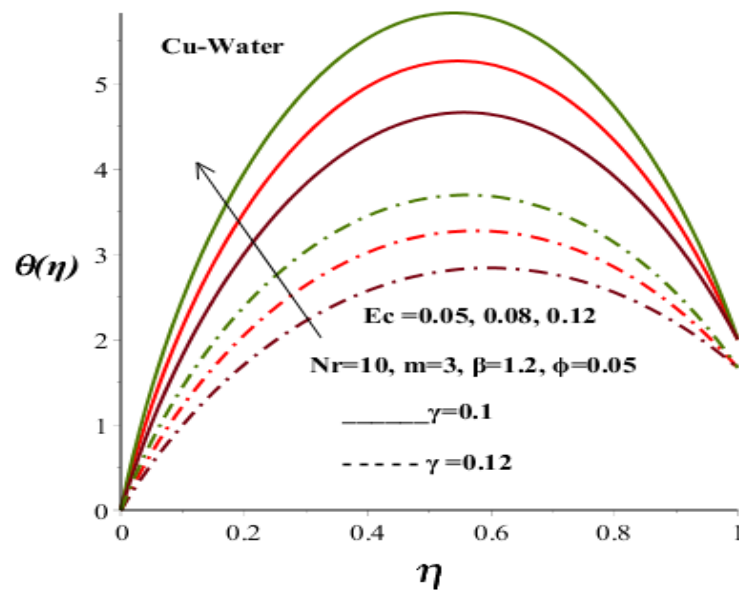


Figure 2.8 Temperature profiles with  $Ec$  and  $\gamma$

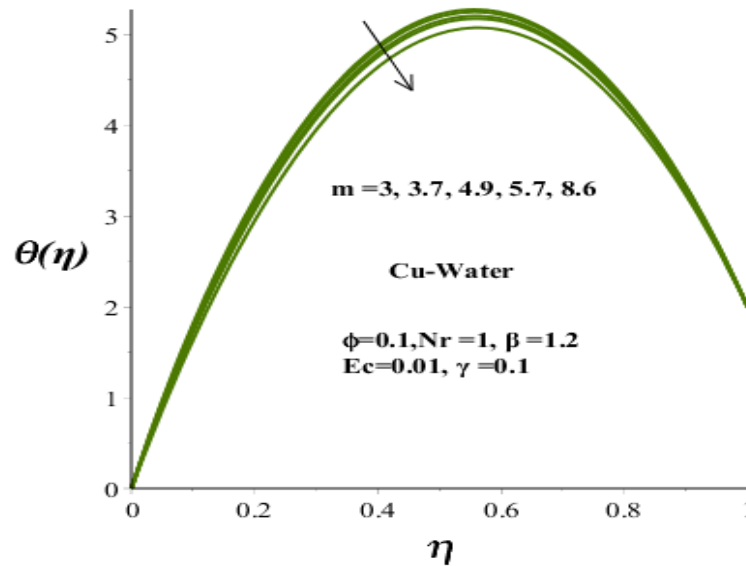


Figure 2.9: Temperature profiles with  $m$

### 2.4.3 Skin Friction, Nusselt Number and Thermal Stability Conditions

Figures 2.10-2.11 depict the effects of parameter variations on the skin friction. A rise in the skin friction coefficient at the channel inner surface is observed with increasing nanoparticles volume fraction ( $\phi$ ), nanoparticles shape parameter ( $m$ ) and thermal radiation absorption ( $Nr$ ). The increase in the skin friction may be attributed to a rise in the velocity gradient at the channel inner surface as the value of these parameters increases. The trend is opposite with a decrease in skin friction as the value of Eckert number ( $Ec$ ), upper plate temperature parameter ( $\beta$ ) and the activation energy parameter ( $\gamma$ ) increase. In figures 2.12-2.13, it is observed that the heat transfer rate at the channel surface rises with escalating values of  $\phi$ ,  $Nr$ ,  $Ec$ ,  $m$  and  $\beta$ , but diminishes with an increase in  $\gamma$  value. The increase in Nusselt number may be attributed to a rise in the temperature gradient at the channel surface as these parameter increases. Figures 2.14-2.15 show the effects on various parameters on the critical value of  $Ec^*$  for the onset of thermal instability in the Cu-water flow field. In particular, for  $0 < Ec < Ec^*$  the Cu-water Couette flow system is thermally stable. It is noteworthy that thermal stability interval for the Eckert number diminishes with an increase in Cu-nanoparticles volume fraction but increases with a rise in thermal radiation absorption. This is in agreement with the results displayed in table 2.4.

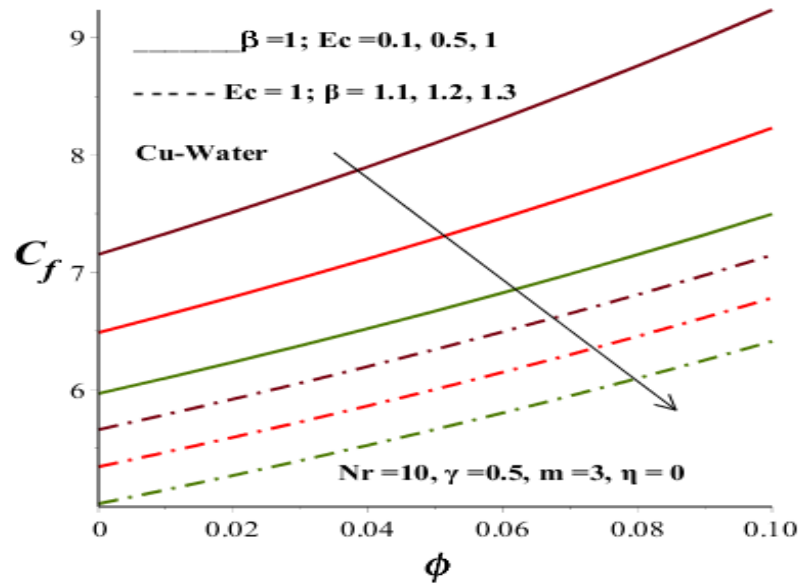


Figure 2.10: Skin friction with  $\phi, Ec$  and  $\beta$

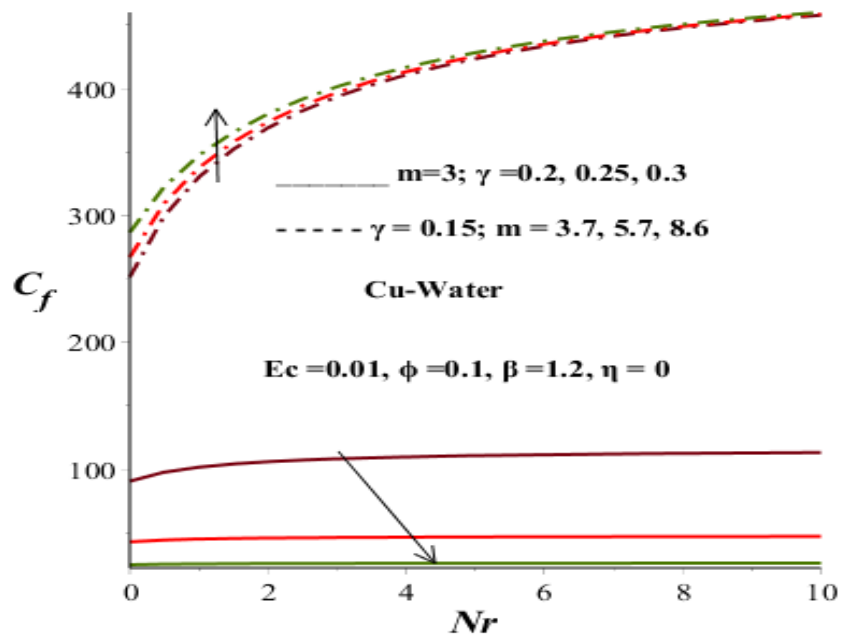


Figure 2.11 Skin friction with  $Nr, m$  and  $\gamma$



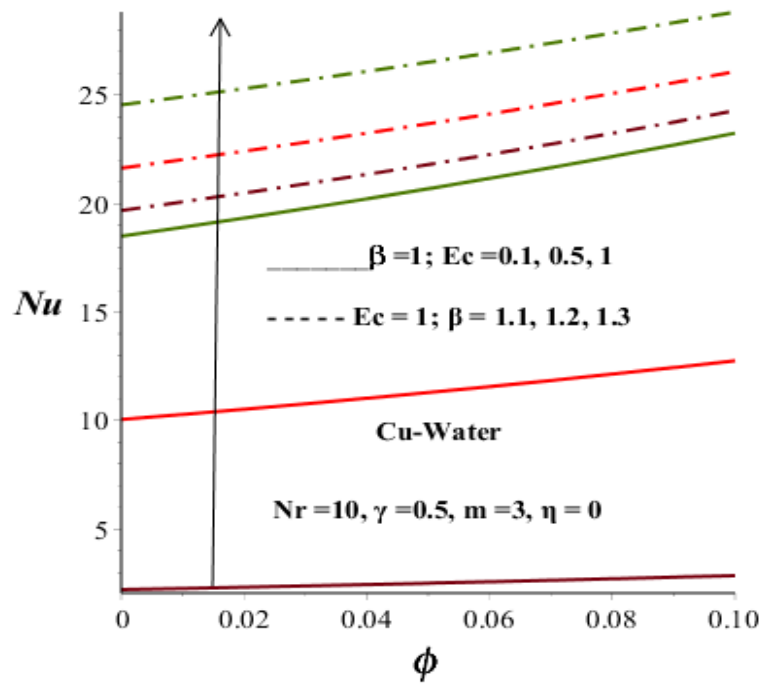


Figure 2.12 Nusselt number with  $\phi$ ,  $Ec$  and  $\beta$

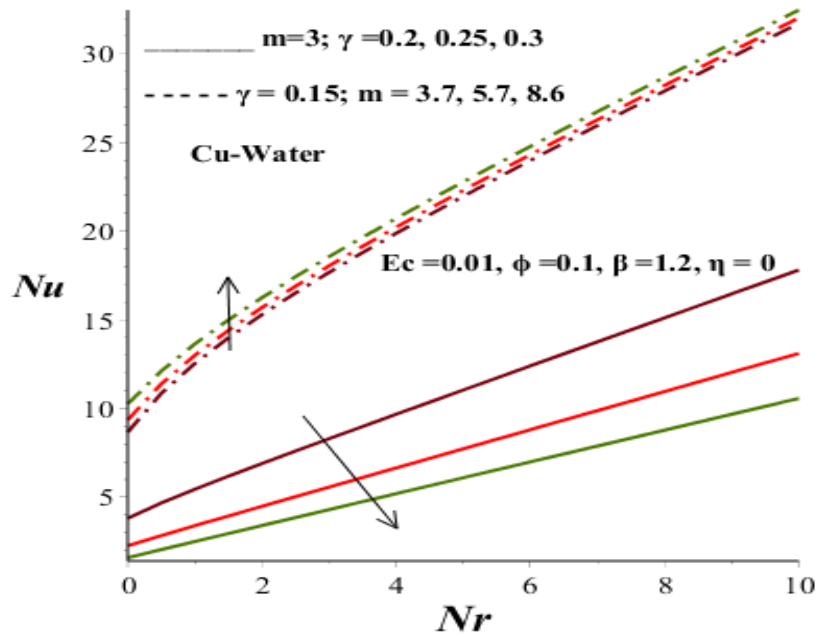


Figure 2.13 Nusselt number with  $Nr$ ,  $m$  and  $\gamma$

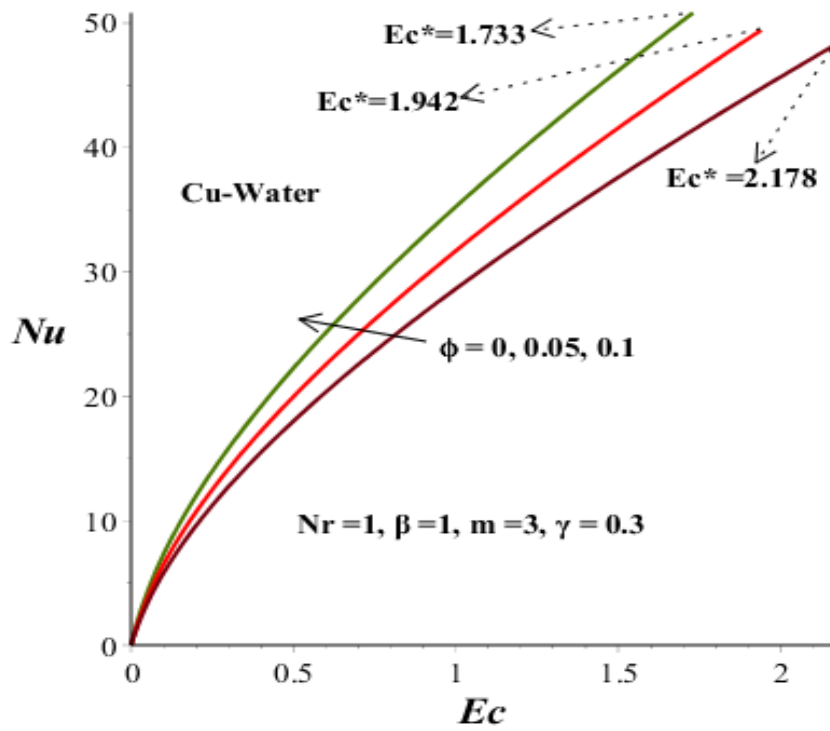


Figure 2.14 Thermal stability criticality with  $\phi$

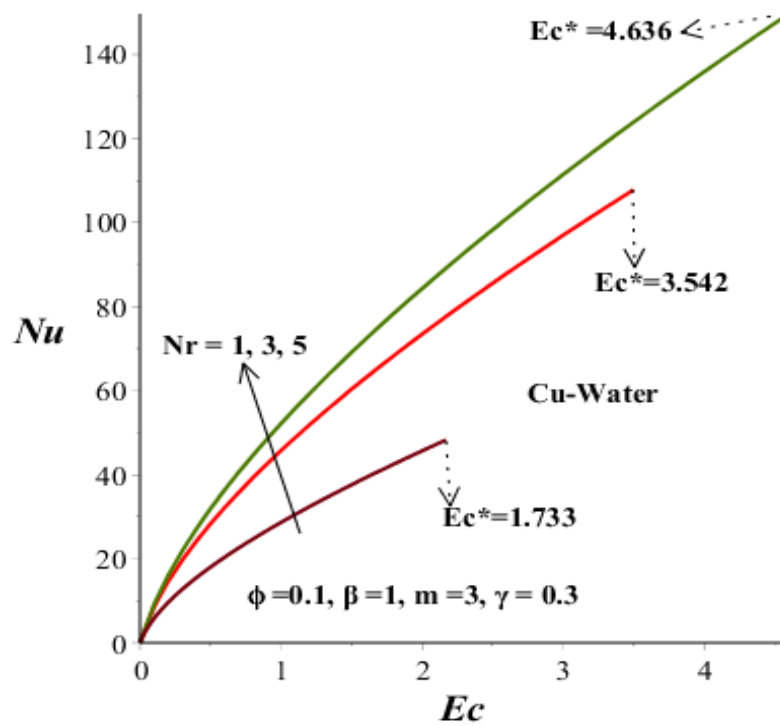


Figure 2.15 Thermal stability criticality with  $Nr$

#### 2.4.4 Effect of Parameter Variation on Entropy Generation Rate

The influence of various thermophysical parameters on the entropy production rate is displayed in figures 2.16-2.19. Generally, the entropy production is higher at the lower fixed plate as compare to that of the moving upper plate. A rise in the upper plate temperature (see figure 2.16) lessens the entropy generation rate within the channel. In figures 2.17-2.18, it can be seen that the entropy production within the channel amplifies with rising values of thermal radiation absorption, nanoparticles volume fraction and shape parameter. This implies that Cu-water nanofluid with blade shape Cu-nanoparticle generates maximum entropy while the nanofluid with spherical shape Cu-nanoparticle generates minimum entropy under Couette flow scenario. Figure 2.19 reveal entropy production enhancement with increasing values of  $Ec$  and  $\gamma$ . This is expected, as increasing the values of Eckert number result in more viscous dissipation, which augments the entropy generation effects.

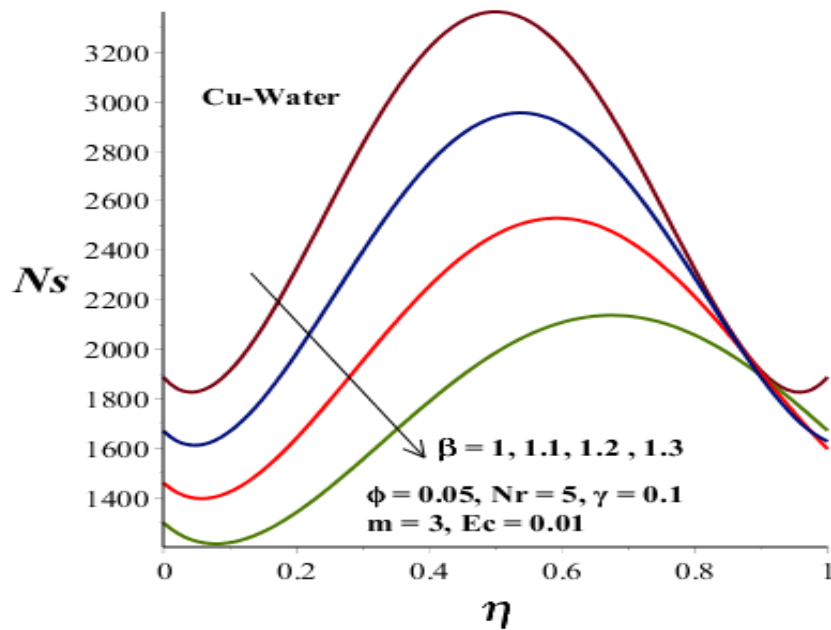


Figure 2.16 Entropy generation rate with  $\beta$

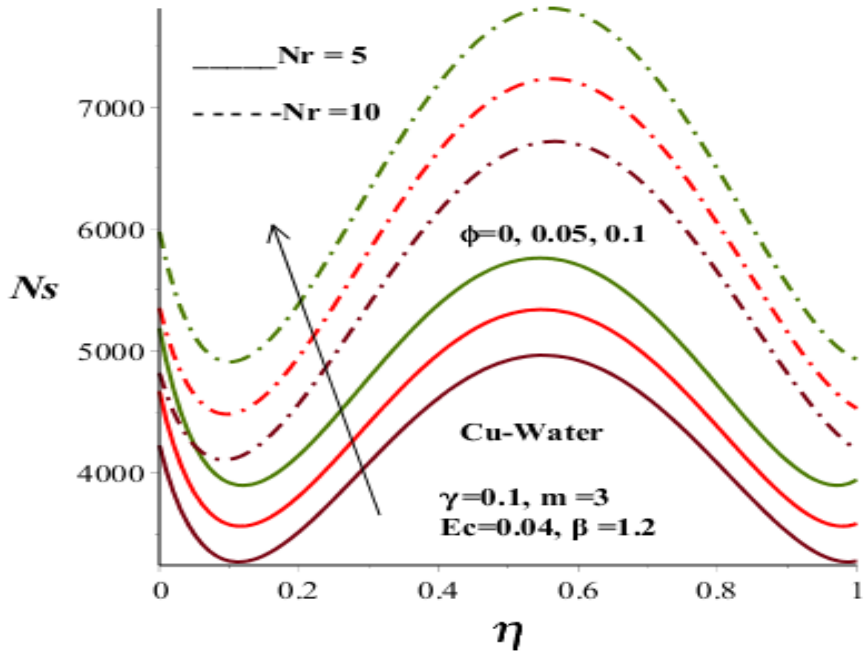


Figure 2.17 Entropy generation rate with  $Nr$  and  $\phi$

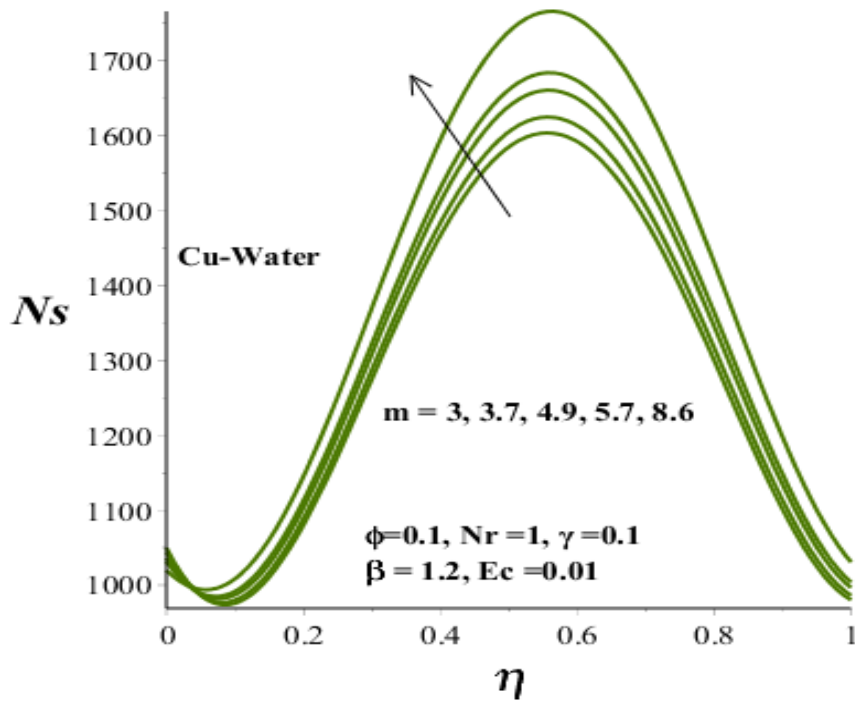


Figure 2.18 Entropy generation rate with  $m$

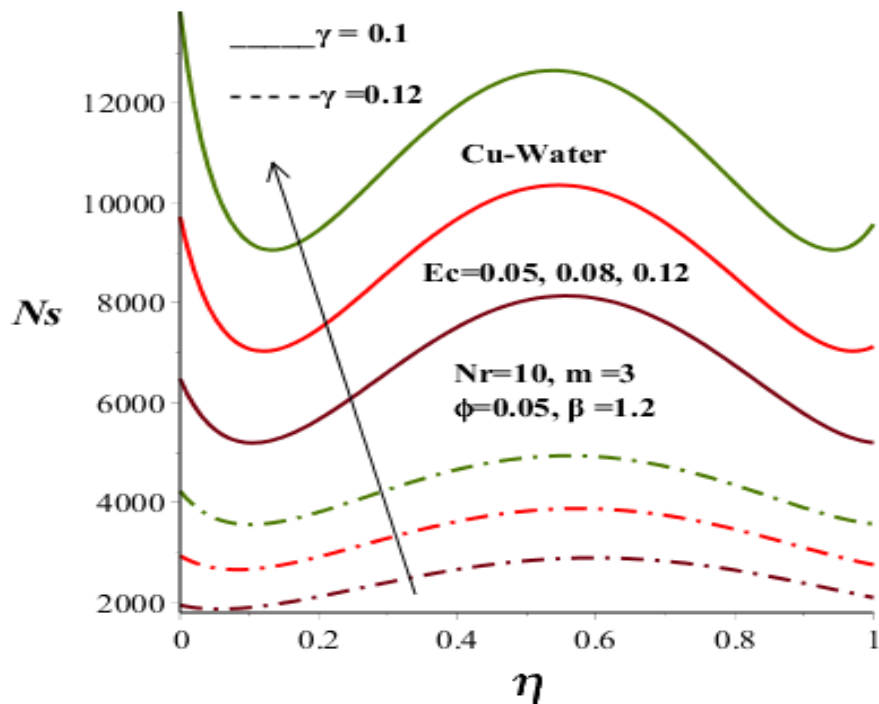


Figure 2.19 Entropy generation rate with  $Ec$  and  $\gamma$

#### 2.4.5 Effect of Parameter Variation on Bejan Number

The parametric effects on the Bejan number are displayed in figures 2.20-2.22. From these figures the dominance effects of heat transfer irreversibility at both fixed and moving plates is observed, while the fluid friction irreversibility effects tend to dominate the channel core region. A rise in the value of moving upper plate temperature ( $\beta > 1$ ) boosts the intensity of both heat transfer irreversibility at the lower fixed plate region and the fluid friction irreversibility at the upper moving plate region as shown in figure 2.20. In figures 2.21-2.22, the value of Bejan number amplifies near the two plates with increasing values on Cu-nanoparticles volume fraction ( $\phi$ ) and Eckert number ( $Ec$ ) but diminishes with a rise in thermal radiation absorption ( $Nr$ ) and activation energy ( $\gamma$ ) parameters. Consequently, the effect of heat transfer irreversibility is absolute with rising values of ( $\phi$ ) and ( $Ec$ ), whereas, the effect of heat transfer irreversibility lessened with escalating values of ( $Nr$ ) and ( $\gamma$ ). Meanwhile, the dominance effect of fluid friction irreversibility is manifest within the channel core region.

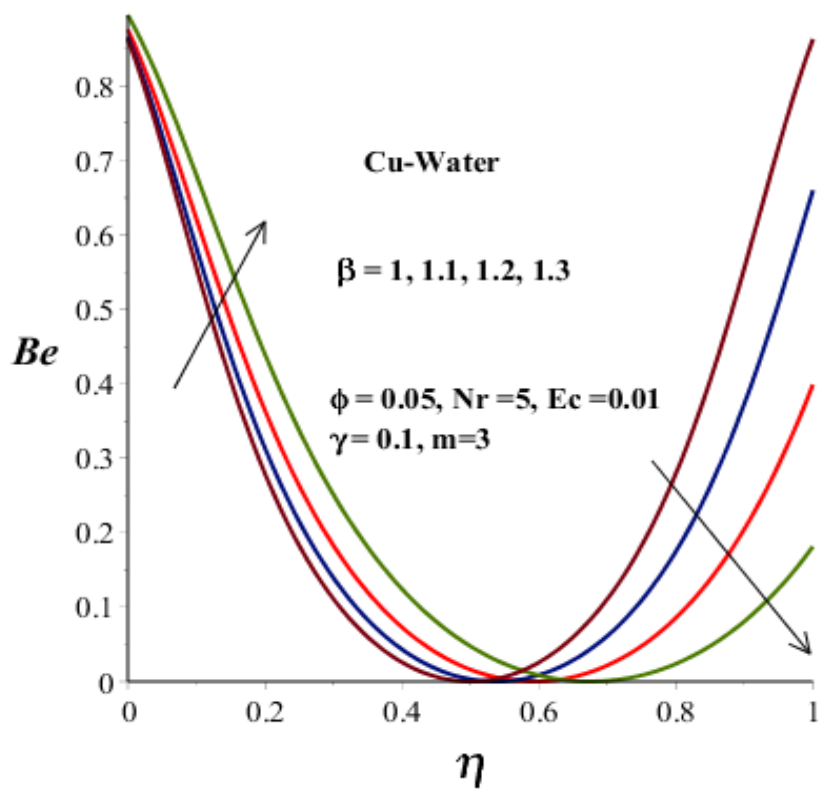


Figure 2.20 Bejan number with  $\beta$

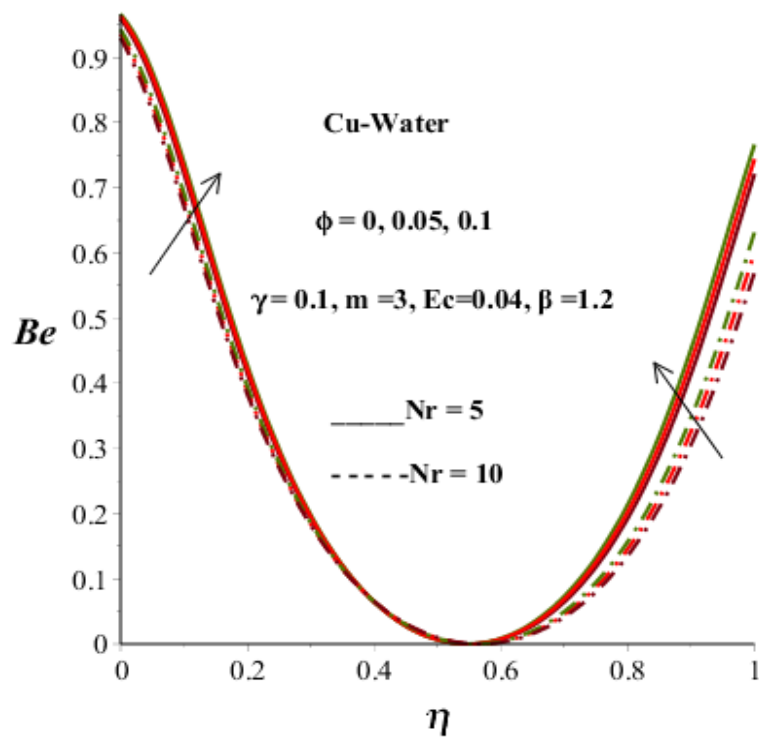


Figure 2.21 Bejan number with  $Nr$  and  $\phi$ .

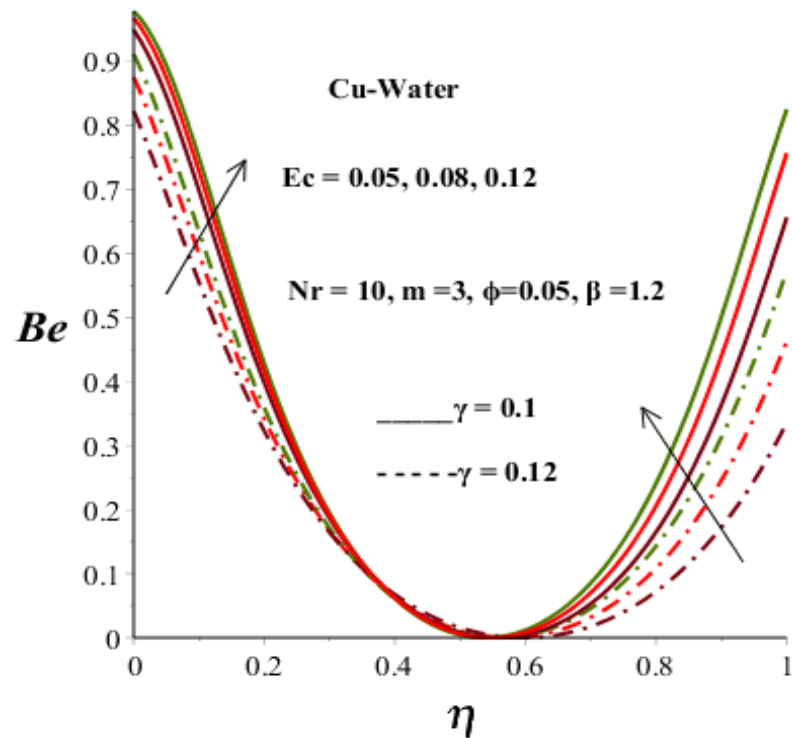


Figure 2.22 Bejan number with  $Ec$  and  $\gamma$

## 2.5 Conclusion

Theoretical model based on the first-law and second-law of thermodynamics is developed for the combined effects of nonlinear thermal radiation and variable viscosity on Couette flow of water base nanofluid containing Cu-nanoparticles. The nonlinear problem is numerically tackled using shooting method with Runge-Kutta-Fehlberg integration scheme. Some of the pertinent results can be summarized as follows:

- The Cu-water Couette flow velocity profiles shows an inflexion point when the values of  $Nr$  and  $\gamma$  increase.
- As  $\phi$  and  $Ec$  ascend, the Cu-water temperature amplifies while the trend is opposite when  $Nr$  and  $\gamma$  increase.
- Cu-water temperature lessens with a rise in the value of nanoparticle shape parameter  $m$ .
- Thermal stability is enhanced with escalating values of  $\beta$ ,  $Nr$ ,  $m$  and  $\gamma$ , while an increase in  $\phi$  may facilitate the onset of thermal instability in Cu-water Couette flow.
- Entropy production is enhanced with increasing values of  $Nr$ ,  $m$  and  $Ec$ , but diminished with increasing values of  $\gamma$  and  $\beta$ .

- The dominance effects of heat transfer irreversibility is manifest near the two plates region and enhanced with escalating values of  $\phi$  and  $Ec$  while dominance effect of fluid friction irreversibility is evident within the channel core region.

- 

Finally, using Cu-nanoparticles as additives to lubricants or coolant can greatly improve their tribological properties by reducing friction, wear and heat transfer enhancement. The rise in entropy production and thermal instability during Couette flow situation may be detrimental to both cooling and lubrication processes. However, with appropriate regulation of the emerging thermophysical parameters, this challenge can be easily overcome for optimum performance.



## CHAPTER 3

# ENTROPY ANALYSIS OF A RADIATING VARIABLE VISCOSITY EG/AG NANOFLUID FLOW IN MICROCHANNELS WITH BUOYANCY FORCE AND CONVECTIVE COOLING<sup>2</sup>

### ABSTRACT

The inherent irreversibility of a variable viscosity ethylene glycol/silver (EG/Ag) nanofluid single-phase Poiseuille flow in a vertical microchannel with convective cooling under the combined influence of buoyancy force, nonlinear thermal radiation, nanoparticles shape and volume fraction is investigated. The nonlinear model equations are obtained and numerically solved via shooting method with Runge-Kutta-Fehlberg integration scheme. Pertinent results with respect to the effects of emerging thermophysical parameters on the nanofluid velocity, temperature, skin friction, Nusselt number, thermal stability criteria, entropy generation rate and Bejan number are presented graphically and discussed. It is observed that thermal radiation, Biot number and buoyancy force boost the release of heat energy thereby cooling the flow system. Meanwhile, an increase in nanoparticles volume fraction lessens the entropy generation rate, which augment the exergetic effectiveness and thermal stability of the flow system.

### 3.1 Introduction

Convection in microchannels or channels of small aspect ratio do occur in various thermal engineering equipment, for example, collector of solar energy, heat flux removal in miniaturized electronic devices, heat exchangers, transformer cooling, etc. Due to its wide applications, numerous investigations have been done towards the understanding of fully developed mixed convection flow in a microchannel [81, 104-106].

---

<sup>2</sup> This chapter is based on the research paper: R.L. Monaledi and O.D. Makinde. Entropy Analysis of a Radiating Variable Viscosity EG/Ag Nanofluid Flow in Microchannels with Buoyancy Force and Convective Cooling. *Defect and Diffusion Forum*, 387, 273–285, 2018.

The convective flow induced by density variation within the fluid due to temperature gradient known as buoyancy or free convection is highly desired in many thermal engineering processes for heat-removal mechanism as it requires small power consumption and produces negligible operating noise [107-109]. Meanwhile, the inherent low thermal conductivity of the conventional working fluid coupled with poor energy efficiency of the free convection in comparison to forced convection has become a challenging issue. The recent advancement in science and engineering with advent of nanotechnology as reported by Choi [1], provides an innovative method of improving the heat transfer performance of the conventional fluid containing nanosized metallic or non-metallic particles known as nanofluid. Thereafter, the great potential of nanofluid have been investigated by several authors with respect to its hydrodynamic and thermal characteristics [11, 62, 86, 110–111]. Peyghambarzadeh *et al.* [112] numerically analysed the heat transfer performance of nanofluid with Copper Oxide and Aluminium Oxide nanoparticles in a rectangular microchannels. Makinde *et al.* [58] studied the combined effects of magnetic field and variable viscosity on rotating channel flow of nanofluid. The problem of peristaltic transport of non-Newtonian nanofluid in an asymmetric channel was investigated by Reddy and Makinde [113].

Several engineering flow processes do take place at high temperatures where the effect of thermal radiation plays a very important role in the overall surface heat transfer [93]. Thermal radiation refers to the emission of electromagnetic waves from all matter that has a temperature greater than absolute zero. Studies related to thermal radiation interaction with nanofluid is very significant because of the manner in which radiant emission depends on temperature and nanoparticles volume fraction. The suspended nanoparticles boost the surface area of the base fluid for radiation harvesting and make nanofluid very useful as solar collector [114]. Khan *et al.* [115] studied the effects of temperature dependent viscosity and radiative heat flux on hydromagnetic stagnation point flow of nanofluid over a stretching sheet. Motsumi and Makinde [59] examined the effect of thermal radiation on boundary layer flow of nanofluid over a permeable heated surface.

The magneto-nanofluid bioconvection with thermal radiation past the paraboloid of revolution surface was theoretically analysed by Makinde and Animasaun [94]. Irreversibility lessens the efficiency of various heat transfer and fluids engineering devices and can be measured in terms of entropy generation rate [96]. The main goal in the design of any thermodynamic flow process is to achieve optimal energy utilization through entropy generation minimization.

This can be theoretically analysed using the first and second laws of thermodynamics with the principles of fluid mechanics [76]. In general, the irreversibility phenomena in nanofluid flow are mainly due to heat transfer and viscous dissipation. The viscous dissipation effect is particularly significant in a microchannel due to its large length-to-diameter ratio, and is further enhanced in nanofluids with temperature dependent viscosity.

The experimental observation of Nguyen *et al.* [116] revealed that the nanofluid viscosity drops sharply with temperature especially for high concentration of nanoparticles. Some noteworthy studies related to the inherent irreversibility in nanofluid can be found in Refs. [60, 101, 117–119]. To the best of our knowledge, no one so far has discussed the combined effects of nonlinear thermal radiation, buoyancy force, convective cooling and viscous dissipation on inherent irreversibility and thermal stability of temperature dependent variable viscosity EG/Ag nanofluid flow in microchannels. The major use of ethylene glycol (EG) is for convective heat transfer medium in automobiles and liquid-cooled computers. Ethylene glycol is also used in chilled-water air-conditioning. Silver (Ag) nanoparticles is one of the most thermally conductive metallic particles and its use in cooling applications would be interesting. The underlying physical significance of the EG/Ag viscous dissipation effect is articulated through Eckert number ( $Ec$ ) and Prandtl number ( $Pr$ ). For large ( $EcPr$ ) the energy dissipated is an important parameter in the heat transfer process and the kinetic energy can play a very significant role in determining the fluid temperature, thermal stability criteria, entropy generation rate and the overall heat transfer process in the microchannel.

Our analysis would serve as a useful tool for obtaining the necessary conditions for thermal stability and exergetic effectiveness enhancement needed for design of such an integrated system. In the following sections, the problem is formulated, analysed are solved. Pertinent results and displayed graphically and discussed.

### 3.2 Model Problem

We consider a steady Poiseuille flow of an incompressible, temperature dependent variable viscosity and optically dense radiating ethylene glycol base nanofluid containing silver nanoparticles as shown in figure 3.1. The flow takes place in the  $x$ -direction in a microchannel of width  $2H$  and length  $L$ . It is assumed that heat exchange between the nanofluid and the ambient environment does occur through the walls with heat transfer coefficient  $h$ . Following [58, 111, 115], the temperature dependent nanofluid viscosity ( $\mu_{nf}$ ) can be expressed as,

$$\mu_{nf} = \frac{\mu_f e^{-b(T-T_w)}}{(1-\phi)^{2.5}} \quad (3.1)$$

where  $\mu_f$  is the ethylene glycol dynamic viscosity at the ambient temperature  $T_w$ ,  $\phi$  is the nanoparticles volume fraction,  $b$  is the viscosity variation parameter and  $T$  is the nanofluid temperature.

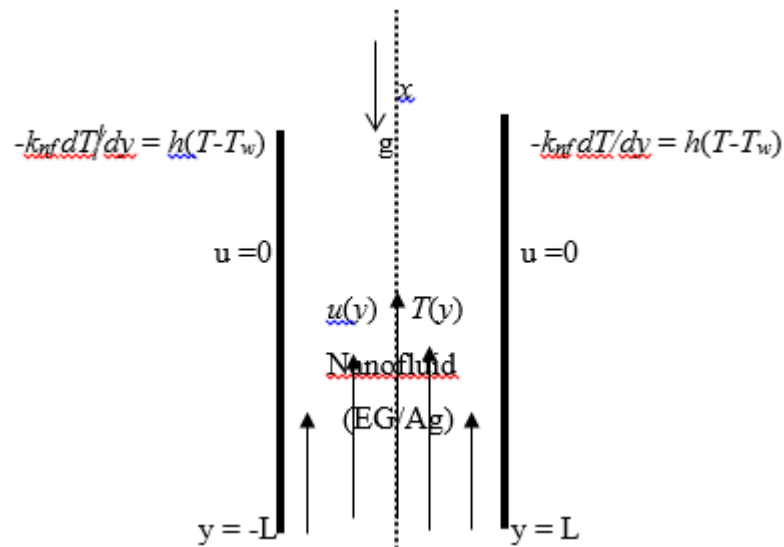


Figure 3.1: Problem geometry

Under these conditions, the continuity, momentum, energy and entropy generation equations governing the problem may be written as [104-106, 110, 111, 117 ];

$$\frac{\partial u}{\partial x} = 0 \quad (3.2)$$

$$-\frac{1}{\rho_{nf}} \frac{\partial p}{\partial x} + \frac{1}{\rho_{nf}} \frac{\partial}{\partial y} \left[ \mu_{nf} \left( \frac{\partial u}{\partial y} \right) \right] + \beta_{nf} g (T - T_w) = 0 \quad (3.3)$$

$$k_{nf} \frac{\partial^2 T}{\partial y^2} + \mu_{nf} \left( \frac{\partial u}{\partial y} \right)^2 - \frac{\partial q_r}{\partial y} = 0, \quad (3.4)$$

$$E_G = \frac{k_{nf}}{T_w^2} \left( 1 + \frac{16\sigma^* T^3}{3k^* k_{nf}} \right) \left( \frac{\partial T}{\partial y} \right)^2 + \frac{\mu_{nf}}{T_w} \left( \frac{\partial u}{\partial y} \right)^2, \quad (3.5)$$

where  $u$  is the nanofluid velocity in the  $x$ -direction,  $P$  is the nanofluid pressure,  $\beta_{nf}$  is the nanofluid thermal expansion coefficient,  $g$  is the gravitational acceleration,  $E_G$  is the entropy generation rate,  $\rho_{nf}$  is the nanofluid density,  $k_{nf}$  is the nanofluid thermal conductivity,  $q_r$  is the radiative heat flux and  $(\rho C_p)_{nf}$  is the nanofluid heat capacitance. By using the Rosseland approximation [93] for nonlinear thermal radiation in an optically dense opaque medium, the radiative heat flux  $q_r$  is given as,

$$q_r = -\frac{4\sigma^* \partial T^4}{3k^* \partial y} = -\frac{16\sigma^* T^3 \partial T}{3k^* \partial y} \quad (3.6)$$

where  $\sigma^*$  is the Stefan–Boltzmann constant,  $k^*$  is the mean absorption coefficient. Following [11, 62, 86], the thermophysical expressions of nanofluid with respect to base fluid and nanoparticles are given as,

$$\rho_{nf} = (1 - \phi) \rho_f + \phi \rho_s \quad (3.7)$$

$$(\rho C_p)_{nf} = (1 - \phi) (\rho C_p)_f + \phi (\rho C_p)_s \quad (3.8)$$

$$\frac{k_{nf}}{k_f} = \frac{k_s + (m-1)k_f - (m-1)\phi(k_f - k_s)}{k_s + (m-1)k_f + \phi(k_f - k_s)} \quad (3.9)$$






$$(\rho\beta)_{nf} = (1-\phi)(\rho\beta)_f + \phi(\rho\beta)_s \quad (3.10)$$

where  $m$  is the nanoparticles shape factor as shown in table 3.2,  $\rho_f$  is the density of the base fluid (EG),  $\rho_s$  is the nanoparticles density,  $\beta_f$  is the base fluid (EG) thermal expansion coefficient,  $\beta_s$  is the nanoparticles thermal expansion coefficient,  $k_f$  is the thermal conductivity of base fluid,  $k_s$  is the nanoparticles thermal conductivity,  $C_{pf}$  and  $C_{ps}$  are the specific heat at constant pressure for the base fluid and the nanoparticles, respectively (see table 3.1).

Table 3.1 Nanoparticles and base fluid thermophysical properties [11, 58, 62, 86, 110-112]

| Physical Properties  | $C_p$ (J/kgK) | $\rho$ (kg/m <sup>3</sup> ) | $k$ (W/mK) | $\beta$ (K <sup>-1</sup> ) |
|----------------------|---------------|-----------------------------|------------|----------------------------|
| Ethylene Glycol (EG) | 2415          | 4111                        | 0.252      | $57 \times 10^{-5}$        |
| Silver(Ag)           | 235           | 10500                       | 429        | $1.89 \times 10^{-5}$      |

Table 3.2 The nanoparticles shape factors ( $m$ ) [11, 62]

| Nanoparticles<br>Shape | Shape<br>Structure  | Shape Factor<br>( $m$ ) |
|------------------------|---|-------------------------|
| <i>Spherical</i>       |  | 3                       |
| <i>Bricks</i>          |  | 3.7                     |
| <i>Cylindrical</i>     |  | 4.9                     |
| <i>Platelets</i>       |  | 5.7                     |
| <i>Blades</i>          |  | 8.6                     |

The appropriate boundary conditions are given as follows:

$$\frac{\partial u}{\partial y} = \frac{\partial T}{\partial y} = 0 \text{ at } y = 0, \text{ (axial symmetric condition)} \quad (3.11)$$

$$u = 0, -k_{nf} \frac{\partial T}{\partial y} = h(T - T_w) \text{ at } y = \mp L \quad (3.12)$$

Equations (3.2)-(3.9) are rendered dimensionless by incorporating the following variables and parameters;

$$\begin{aligned} \eta = \frac{y}{L}, X = \frac{x}{L}, W = \frac{uL}{\nu_f}, \theta = \frac{T - T_w}{T_w}, \bar{P} = \frac{L^2 P}{\rho_f \nu_f^2}, Gr = \frac{g\beta_f T_w L^3}{\nu_f^2}, \\ Nr = \frac{16\sigma^* T_w^3}{3k^* k_f}, \nu_f = \frac{\mu_f}{\rho_f}, Ec = \frac{\nu_f^2}{C_{pf} T_w L^2}, Pr = \frac{\mu_f C_{pf}}{k_f}, \lambda = bT_w, Bi = \frac{hL}{k_f}, \\ M = \frac{k_s + (m-1)k_f + \phi(k_f - k_s)}{k_s + (m-1)k_f - (m-1)\phi(k_f - k_s)}, Ns = \frac{L^2 E_G}{k_f}, -\frac{\partial \bar{P}}{\partial X} = A, \end{aligned} \quad (3.13)$$

and obtain

$$\frac{d^2 W}{d\eta^2} - \lambda \frac{d\theta}{d\eta} \frac{dW}{d\eta} = -A(1-\phi)^{2.5} e^{\lambda\theta} - (1-\phi)^{2.5} \left[ (1-\phi) + \phi \frac{(\rho\beta)_s}{(\rho\beta)_f} \right] Gr \theta e^{\lambda\theta}, \quad (3.14)$$

$$\left[ 1 + MNr(1+\theta)^3 \right] \frac{d^2 \theta}{d\eta^2} + 3MNr(1+\theta)^2 \left( \frac{d\theta}{d\eta} \right)^2 + \frac{M Pr Ec e^{-\lambda\theta}}{(1-\phi)^{2.5}} \left( \frac{dW}{d\eta} \right)^2 = 0, \quad (3.15)$$

$$Ns = \frac{\left[ 1 + MNr(1+\theta)^3 \right] \left( \frac{d\theta}{d\eta} \right)^2 + \frac{Pr Ec e^{-\lambda\theta}}{(1-\phi)^{2.5}} \left( \frac{dW}{d\eta} \right)^2}{M}, \quad (3.16)$$

with boundary conditions given as,

$$\frac{dW}{d\eta}(0) = \frac{d\theta}{d\eta}(0) = 0, W(1)=0, \frac{d\theta}{d\eta}(1) = -MBi\theta(1) \quad (3.17)$$

where  $\lambda$  is the variable viscosity parameter, Bi is the Biot number, Ec is the Eckert number, Gr is the Grashof number and Pr is the Prandtl number (Pr  $\approx$  137.48 for ethylene glycol). Other quantities of interest are the skin friction coefficients ( $C_f$ ), Nusselt number (Nu) and the Bejan number (Be) which are given as

$$C_f = \frac{L^2 \tau_w}{\mu_f \nu_f} = - \frac{e^{-\lambda \theta}}{(1-\phi)^{2.5}} \frac{dW}{d\eta} \Big|_{\eta=1}, \quad (3.18)$$

$$Nu = \frac{Lq_w}{k_f T_w} = - \frac{[1 + MNr(1+\theta)^3]}{M} \frac{d\theta}{d\eta} \Big|_{\eta=1}, \quad (3.19)$$

$$Be = \frac{N_1}{N_s} = \frac{1}{1+B} \quad (3.20)$$

where

$$\tau_w = \mu_{nf} \frac{\partial u}{\partial y}, \quad q_w = -k_{nf} \left( 1 + \frac{M16\sigma^* T^3}{3k_f k^*} \right) \frac{\partial T}{\partial y}, \quad (3.21)$$

$$N_1 = \frac{[1 + MNr(1+\theta)^3]}{M} \left( \frac{d\theta}{d\eta} \right)^2, \quad N_2 = \frac{\text{Pr} Ece^{-\lambda \theta}}{(1-\phi)^{2.5}} \left( \frac{dW}{d\eta} \right)^2, \quad B = \frac{N_2}{N_1}. \quad (3.22)$$

The symbol  $N_1$  represents thermodynamic irreversibility due to thermal radiation absorption and heat transfer while  $N_2$  corresponds to the entropy generation due to fluid friction. When  $0.5 < Be \leq 1$ , the effects of thermodynamics irreversibility due to thermal radiation absorption and heat transfer dominate the flow system while  $0 \leq Be < 0.5$  corresponds to the dominant effects of fluid friction. When  $Be = 0.5$ ,  $N_1$  and  $N_2$  contribute equally to the entropy generation and  $B$  is the irreversibility ratio.

### 3.3 Numerical Procedure

The dimensionless equations (3.11)-(3.12) coupled with the boundary conditions in equation (3.14) are boundary value problem (BVP). We transformed these equations into a set of nonlinear first order ordinary differential equations with some unknown initial conditions to be calculated by shooting technique [103] Let,

$$W = y_1, W' = y_2, \theta = y_3, \theta' = y_4. \quad (3.23)$$



The governing equations then become

$$\left. \begin{aligned} y_1' = y_2, y_2' &= \lambda y_4 y_2 - A(1-\phi)^{2.5} - (1-\phi)^{2.5} \left[ (1-\phi) + \phi \frac{(\rho\beta)_s}{(\rho\beta)_f} \right] Gry_3 e^{\lambda y_3}, \\ y_3' = y_4, y_4' &= -\frac{1}{(1+MNr(1+y_3)^3)} \left[ 3MNr(1+y_3)^2 y_4^2 + \frac{M \text{Pr} Ec e^{-\lambda y_3}}{(1-\phi)^{2.5}} y_2^2 \right] \end{aligned} \right\} \quad (3.24)$$

with the corresponding initial conditions as

$$y_1(0) = a_1, y_2(0) = 0, y_3(0) = a_2, y_4(0) = 0. \quad (3.25)$$

The values for  $a_1$  and  $a_2$  in the equation (3.26) are first guessed and then determined accurately with shooting method via Newton-Raphson's technique for each set of parameter values in equation (3.21). Thereafter, Runge-Kutta-Fehlberg integration scheme [103] is then employed to tackle the resulting initial value problem numerically with step size  $\Delta\eta=0.01$ . From the numerical solution for velocity and temperature profiles, we compute the values for the entropy generation rate, skin friction ( $C_f$ ), the Nusselt number ( $Nu$ ) and the Bejan number as given by equations (3.13) and (3.15)-(3.17).

### 3.4 Results and Discussion

Numerical results showing the influence of various thermophysical parameters on the nanofluid velocity, temperature, skin friction, thermal stability conditions, Nusselt number, entropy generation rate and Bejan number are displayed graphically in figures 3.2-3.21 and tables 3.3-3.4. In all our computations, the value of dimensionless axial pressure gradient is taken as  $A=1$  and that of the EG Prantdl number as  $\text{Pr} \approx 137.48$ . The numerical values of critical Eckert number ( $Ec^*$ ) for thermal stability of EG/Ag nanofluid in microchannel are shown in table 3.3. In essence, the flow is thermally stable within the range of Eckert number  $0 \leq Ec \leq Ec^*$ . Interestingly, EG/Ag nanofluid becomes thermally unstable for  $Ec > Ec^*$  and no real solution exist for the nonlinear model equations (3.11)-(3.14).

The critical Eckert number  $Ec^*$  occurs whenever the internal heat generated within the nanofluid due to viscous dissipation increases more rapidly than can be removed, consequently,

thermal runaway or even destruction of the entire flow process may happen. It is noteworthy that the magnitude of critical Eckert number ( $Ec^*$ ) increases with rising values of  $\phi$ ,  $Bi$  and  $Nr$ , consequently, the range of thermal stability for Eckert number is enhanced (see also figures 3.11 and 3.12). Opposite trend of reduction in the thermal stability interval for Eckert number is observed with amplified values of  $\lambda$ ,  $m$  and  $Gr$ . Table 3.4 illustrates effects of thermophysical parameters on the skin friction and Nusselt number. It is seen that with the increase in the nanoparticles volume fraction, Biot number and thermal radiation parameter both the skin-friction and Nusselt number diminish. On the contrary, as the values of  $\lambda$ ,  $m$ ,  $Ec$  and  $Gr$  amplified, skin-friction and rate of heat transfer at the microchannel wall increase.

Table 3.3: Computations showing the effect of parameters variation on thermal stability critical Eckert number ( $Ec^*$ ) for Silver-Ethylene Glycol nanofluid ( $A=1$ ,  $Pr = 137.48$ )

| $\phi$ | $\lambda$ | $Nr$ | $m$ | $Gr$ | $Bi$ | $Ec^*$  |
|--------|-----------|------|-----|------|------|---------|
| 0      | 0.1       | 1    | 3   | 0.1  | 1    | 1.86227 |
| 0.05   | 0.1       | 1    | 3   | 0.1  | 1    | 2.05431 |
| 0.1    | 0.1       | 1    | 3   | 0.1  | 1    | 2.29196 |
| 0.1    | 0.2       | 1    | 3   | 0.1  | 1    | 0.75058 |
| 0.1    | 0.3       | 1    | 3   | 0.1  | 1    | 0.49453 |
| 0.1    | 0.1       | 2    | 3   | 0.1  | 1    | 3.47717 |
| 0.1    | 0.1       | 3    | 3   | 0.1  | 1    | 4.65769 |
| 0.1    | 0.1       | 1    | 3.7 | 0.1  | 1    | 2.24558 |
| 0.1    | 0.1       | 1    | 4.9 | 0.1  | 1    | 2.17560 |
| 0.1    | 0.1       | 1    | 5.7 | 0.1  | 1    | 2.13455 |
| 0.1    | 0.1       | 1    | 8.6 | 0.1  | 1    | 2.01398 |
| 0.1    | 0.1       | 1    | 3   | 0.3  | 1    | 0.53548 |
| 0.1    | 0.1       | 1    | 3   | 0.5  | 1    | 0.23724 |
| 0.1    | 0.1       | 1    | 3   | 0.1  | 0.8  | 1.89298 |
| 0.1    | 0.1       | 1    | 3   | 0.1  | 0.4  | 1.01202 |

Table 3.4 Computations showing the effect of parameters variation on skin friction and Nusselt number ( $A=1$ ,  $Pr = 137.48$ )

| $\phi$ | $\lambda$ | $Nr$ | $m$ | $Gr$ | $Bi$ | $Ec$ | $C_f$     | $Nu$       |
|--------|-----------|------|-----|------|------|------|-----------|------------|
| 0      | 0.1       | 1    | 3   | 0.1  | 1    | 0.1  | 1.0993283 | 6.11448946 |
| 0.05   | 0.1       | 1    | 3   | 0.1  | 1    | 0.1  | 1.0922054 | 5.29433535 |
| 0.1    | 0.1       | 1    | 3   | 0.1  | 1    | 0.1  | 1.0849777 | 4.54961155 |

|     |     |   |     |     |     |     |           |            |
|-----|-----|---|-----|-----|-----|-----|-----------|------------|
| 0.1 | 0.3 | 1 | 3   | 0.1 | 1   | 0.1 | 1.0944910 | 5.72052846 |
| 0.1 | 0.6 | 1 | 3   | 0.1 | 1   | 0.1 | 1.1165947 | 9.28057921 |
| 0.1 | 0.1 | 2 | 3   | 0.1 | 1   | 0.1 | 1.0618279 | 4.24862264 |
| 0.1 | 0.1 | 3 | 3   | 0.1 | 1   | 0.1 | 1.0505711 | 4.10810299 |
| 0.1 | 0.1 | 1 | 3.7 | 0.1 | 1   | 0.1 | 1.0864934 | 4.56999412 |
| 0.1 | 0.1 | 1 | 4.9 | 0.1 | 1   | 0.1 | 1.0889828 | 4.60362614 |
| 0.1 | 0.1 | 1 | 5.7 | 0.1 | 1   | 0.1 | 1.0905730 | 4.62521222 |
| 0.1 | 0.1 | 1 | 8.6 | 0.1 | 1   | 0.1 | 1.0959409 | 4.69867197 |
| 0.1 | 0.1 | 1 | 3   | 0.3 | 1   | 0.1 | 1.3044940 | 6.72801674 |
| 0.1 | 0.1 | 1 | 3   | 0.5 | 1   | 0.1 | 1.6144566 | 10.5929096 |
| 0.1 | 0.1 | 1 | 3   | 0.1 | 0.8 | 0.1 | 1.0930438 | 4.65881257 |
| 0.1 | 0.1 | 1 | 3   | 0.1 | 0.4 | 0.1 | 1.1231392 | 5.08499154 |
| 0.1 | 0.1 | 1 | 3   | 0.1 | 1   | 0.5 | 1.1821729 | 30.0282130 |
| 0.1 | 0.1 | 1 | 3   | 0.1 | 1   | 1.0 | 1.2443439 | 71.1988029 |

### 3.4.1 Effect of Parameters Variation on Velocity Profiles

The effects of various thermophysical parameters on the EG/Eg nanofluid velocity profiles are depicted in figures 3.2-3.5. The parabolic profile with maximum velocity along the microchannel centreline and zero velocity at the wall is observed. It is seen in figures 3.2-3.4 that the nanofluid velocity lessens with a rise in the nanoparticles volume fraction, Biot number and thermal radiation parameter but increases with an elevation in the Eckert number, Grashof number and variable viscosity parameter. This may be attributed to the fact that as  $\phi$ ,  $Bi$  and  $Nr$  increases, nanofluid viscosity augments with more radiative and convective heat loss, consequently, the velocity profiles diminish.

On the contrary, as the values of  $Ec$ ,  $Gr$  and  $\lambda$  increase, the nanofluid becomes lighter and flow faster due to a rise in the internal heat generation within the flow system. Figure 3.5 shows that the nanofluid velocity is enhanced with increasing value of nanoparticles shape parameter ( $m$ ). This simply implies that EG/Ag nanofluid with blade shape nanoparticles produced maximum velocity while the lowest velocity is observed for nanofluid with spherical shape nanoparticles.

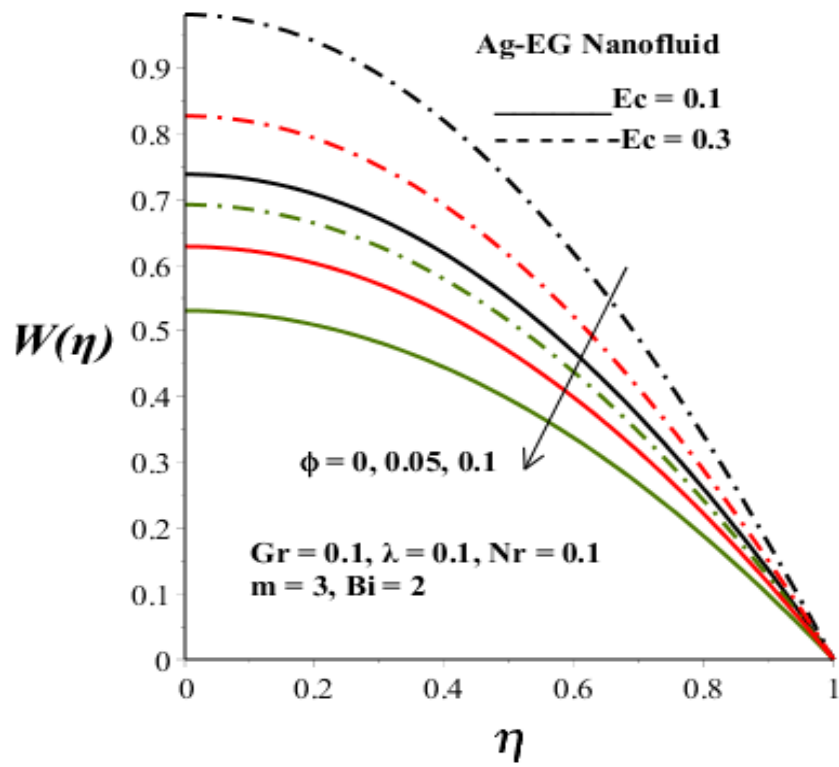


Figure 3.2: Velocity profile with  $Ec$  and  $\phi$

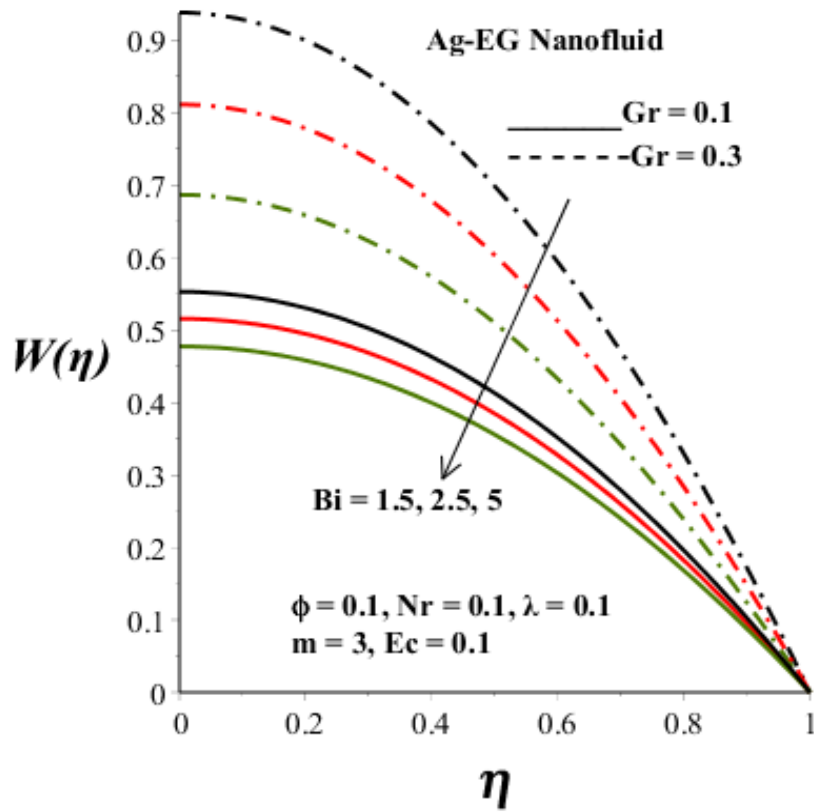


Figure 3.3 Velocity profile with  $Bi$  and  $Gr$

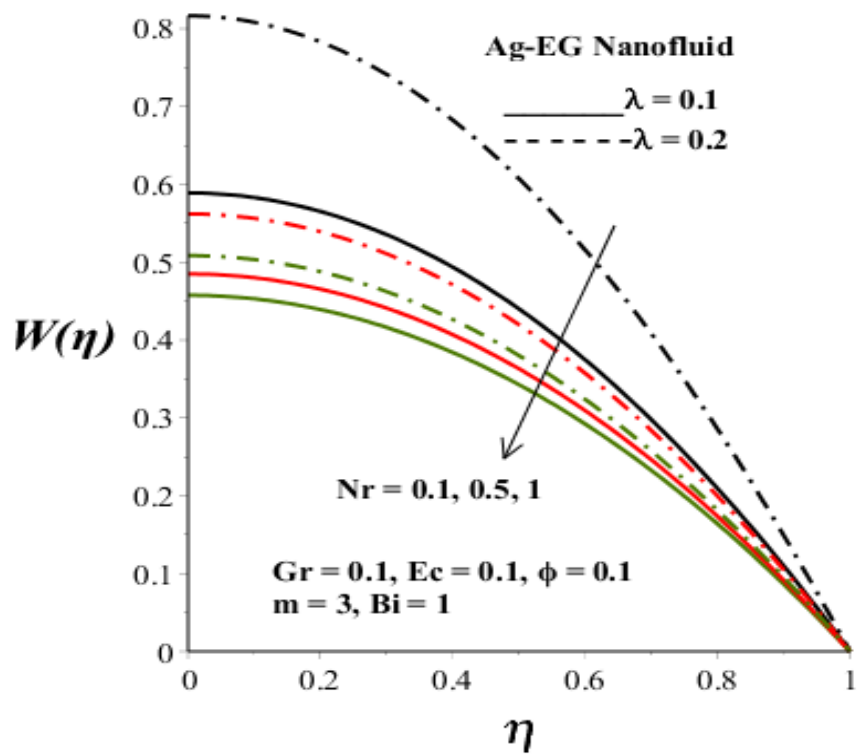


Figure 3.4 Velocity profile with  $Nr$  and  $\lambda$

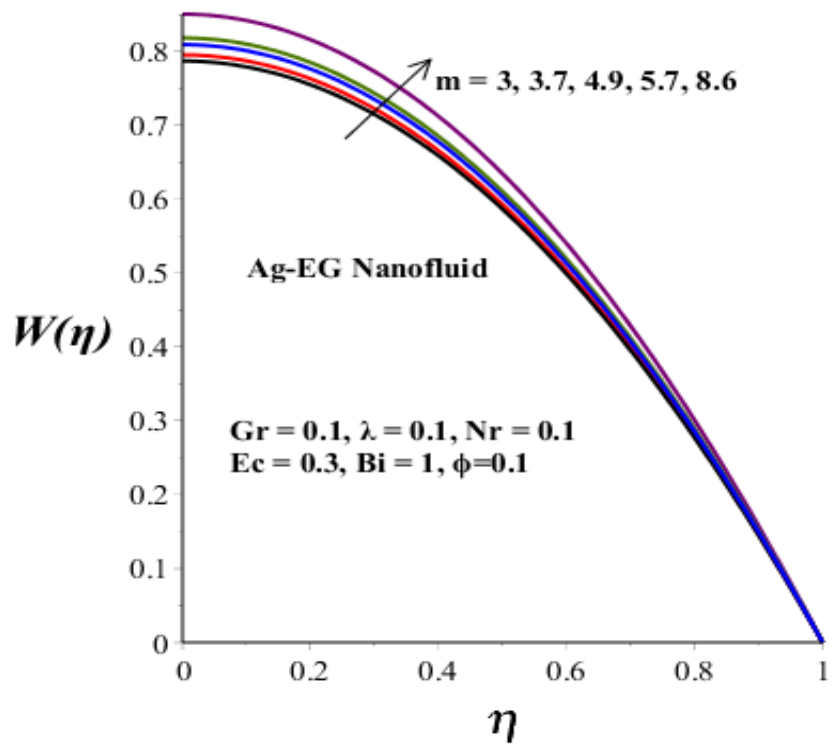


Figure 3.5: Velocity profile with  $m$

### 3.4.2 Effect of Parameters Variation on Temperature Profiles

Figures 3.6-3.9 portray the temperature profiles of AG/Eg nanofluid under different parametric conditions. Maximum temperature is observed along the microchannel centreline and minimum at the wall due to convective heat loss to the ambient environment. As  $\phi$ , Bi and Nr increase, the nanofluid temperature lessens as shown in figures 3.6-3.8. The trend is opposite with escalating nanofluid temperature as the values of Ec, Gr and  $\lambda$  amplify. The lowering of EG/Ag temperature can be ascribed to the cooling effects of radiative and convective heat loss while the elevation of temperature can be attributed to a boost in the internal heat generation within the flow system. In figure 3.9, it is seen that EG/Ag nanofluid with blade shape nanoparticles produced maximum temperature while the lowest temperature is observed for nanofluid with spherical shape nanoparticles.

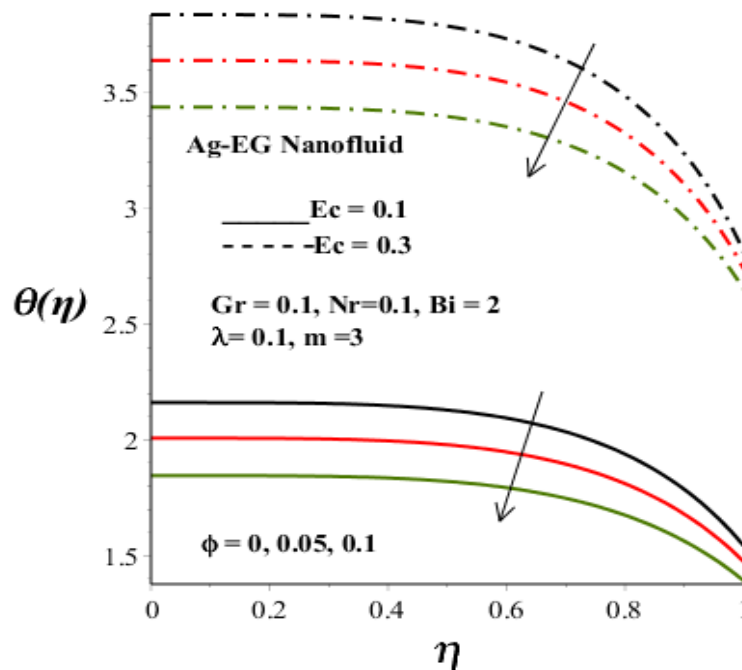


Figure 3.6 Temperature profiles with Ec and  $\phi$

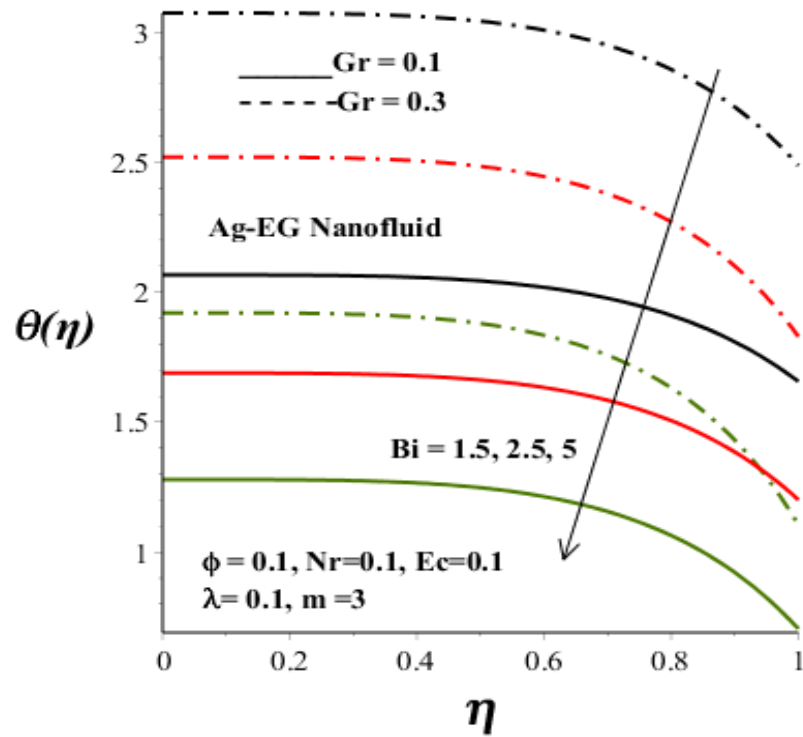


Figure 3.7 Temperature profiles with  $Bi$  and  $Gr$

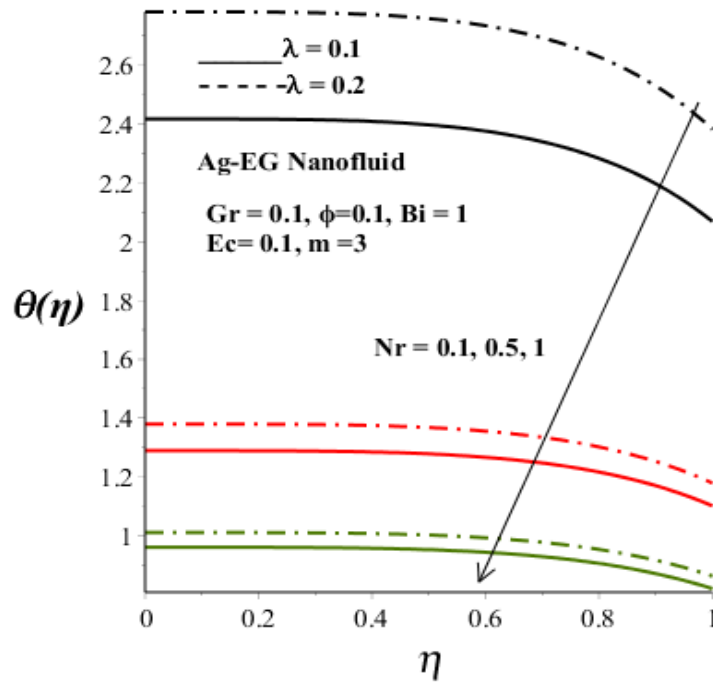


Figure 3.8 Temperature profiles with  $Nr$  and  $\lambda$

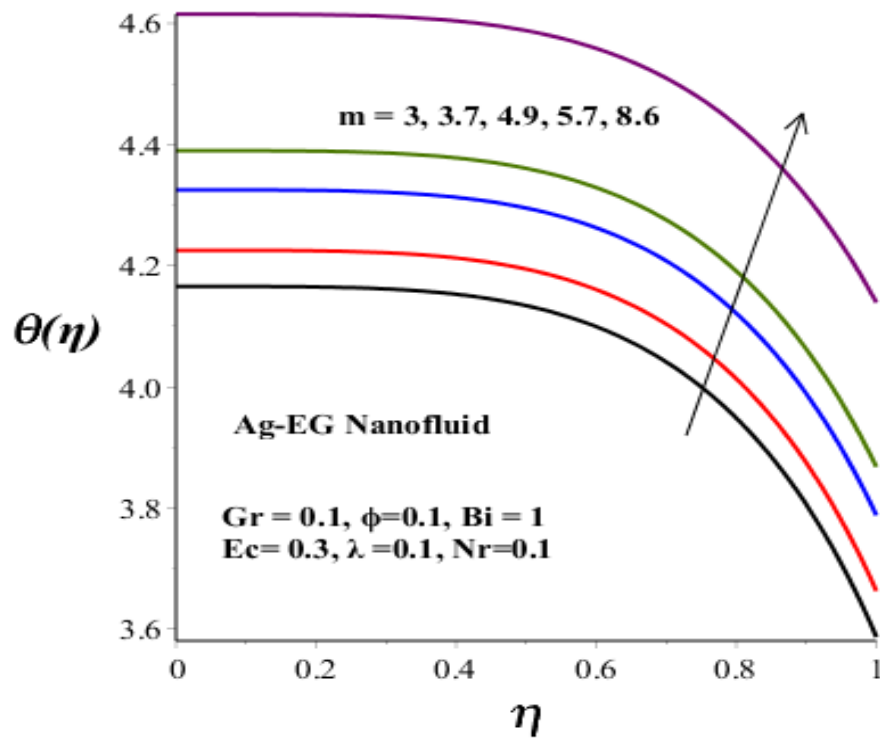


Figure 3.9 Temperature profiles with  $m$

### 3.4.3 Skin Friction, Nusselt Number and Thermal Stability Conditions

The effects of parameter variation on the skin friction, Nusselt number and thermal stability conditions are illustrated graphically in figures 3.10-3.13. As the convective and radiative heat loss amplify, the both skin friction and Nusselt number diminish as illustrated in figures 3.10 and 3.13. Meanwhile, the skin friction and Nusselt number escalate with an increase in Eckert number due to a combined effect of velocity and temperature gradients at the wall. Figure 3.11 shows a dwindling skin friction as the nanoparticles volume fraction augments. Similar trend of a lessen Nusselt number is observed in figure 3.12 with increasing value of  $\phi$ . This is in agreement with the results displayed in table 3.4. Moreover, the critical Eckert number  $Ec^*$  depicting the stability condition is obtained such that for  $Ec > Ec^*$ , the flow is thermally unstable and no real solution exist for the problem as described in table 3.3.



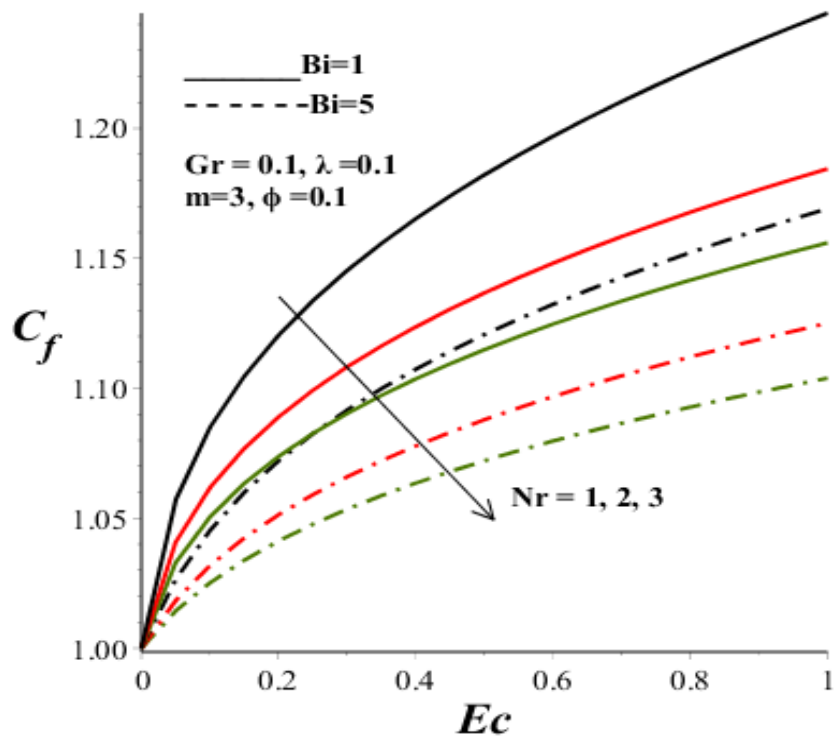


Figure 3.10 Skin friction with Bi, Nr and Ec \*

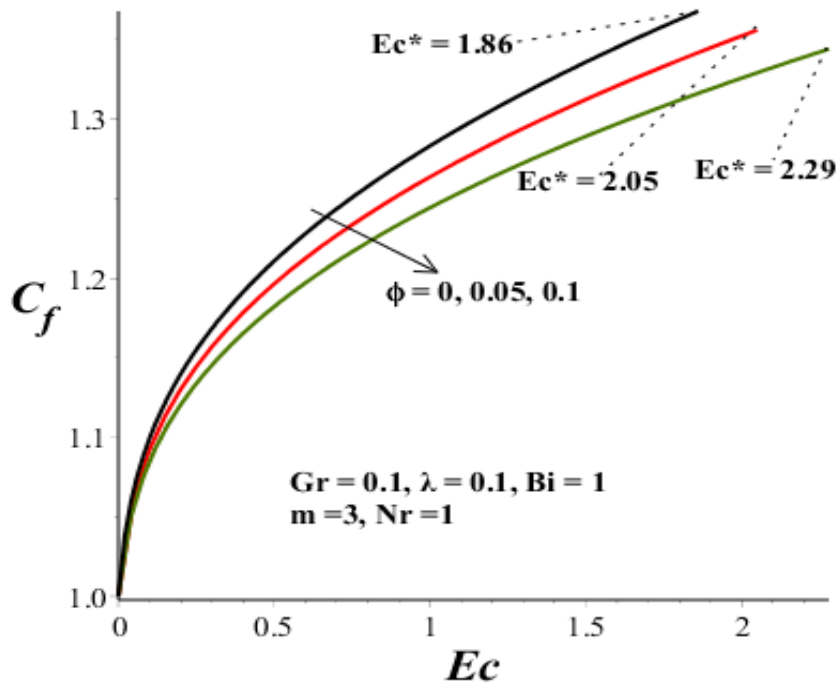


Figure 3.11 Skin friction with  $\phi$  and Ec

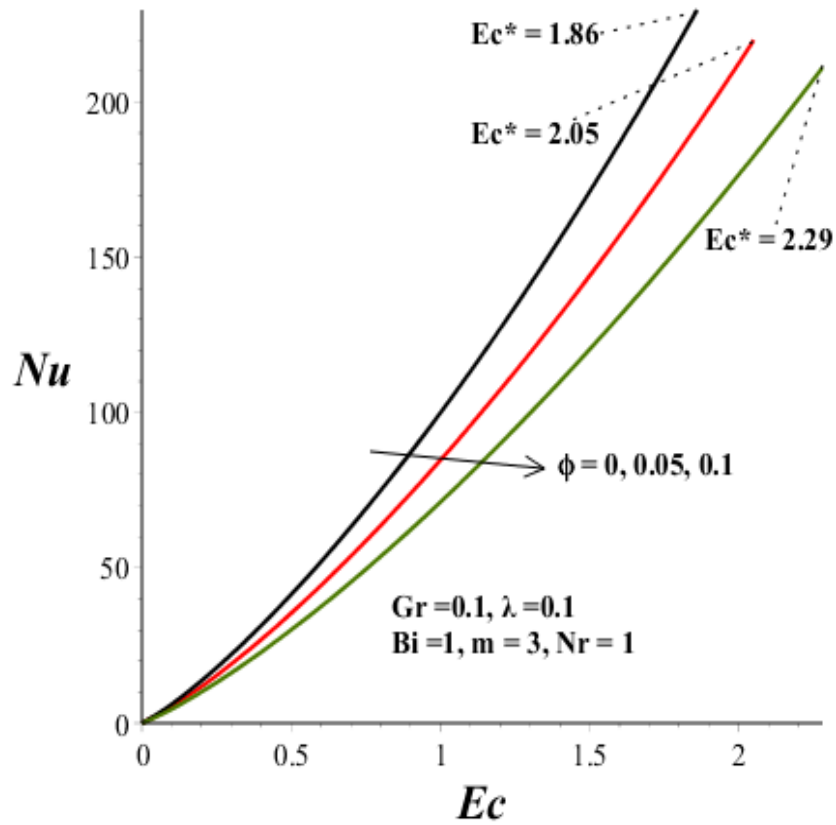


Figure 3.12 Nusselt number with  $\phi$  and  $Ec^*$

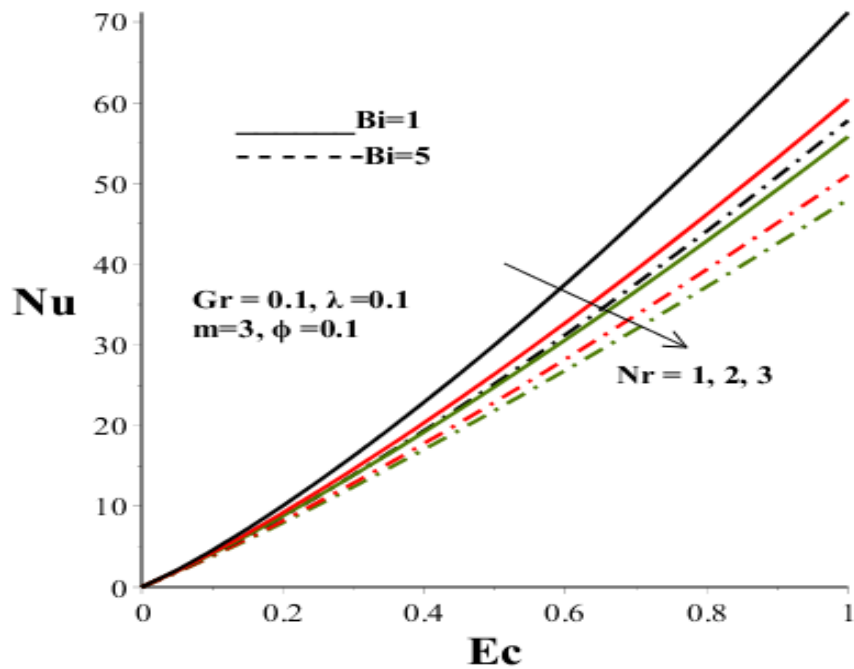


Figure 3.13 Nusselt with  $Bi$ ,  $Nr$  and  $Ec$

### 3.4.4 Effect of Parameters Variation on Entropy Generation Rate

The effects of parametric condition on entropy generation rate that determines the second-law performance of EG/Ag nanofluid flow in a microchannel are displayed in figures 3.14-3.17. It is noteworthy that no entropy is produced along the microchannel centreline. Moreover, the production of entropy increases gradually with maximum value at the wall.

The suspension of Ag nanoparticles in the EG fluid lowers the entropy generation in the flow significantly, hence, the thermodynamic efficiency is enhanced as shown in figure 3.14. In figures 3.15-3.16, similar trend of dwindling entropy production is observed with increasing convective cooling and radiative heat loss. Therefore, increase in the Biot number  $Bi$  and radiation parameter  $Nr$  enhances exergetic effectiveness of the system. On the contrary, the entropy generation rate escalates with an increase in Grashof number ( $Gr$ ), Eckert number ( $Ec$ ) and variable viscosity parameter ( $\lambda$ ), inducing a penalty in exergetic effectiveness.

This may be attributed to a drop in fluid viscosity due to a rise in the internal heat generation, leading to elevation in velocity and temperature gradients. In figure 3.17, it is seen that the entropy production ascend slightly as the value of nanoparticles shape parameter ( $m$ ) increases. This implies that the thermodynamic performance of AG/Ag nanofluid with spherical shape nanoparticles in microchannel is slightly higher than that of nanofluid with blade shape nanoparticles.

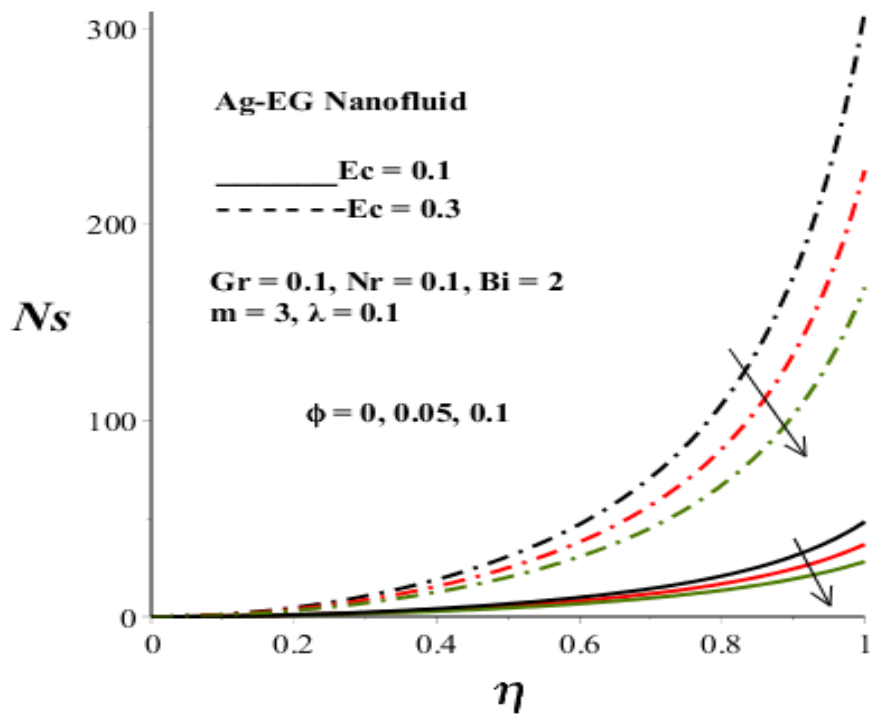


Figure 3.14 Entropy generation rate with  $Ec$  and  $\phi$ .

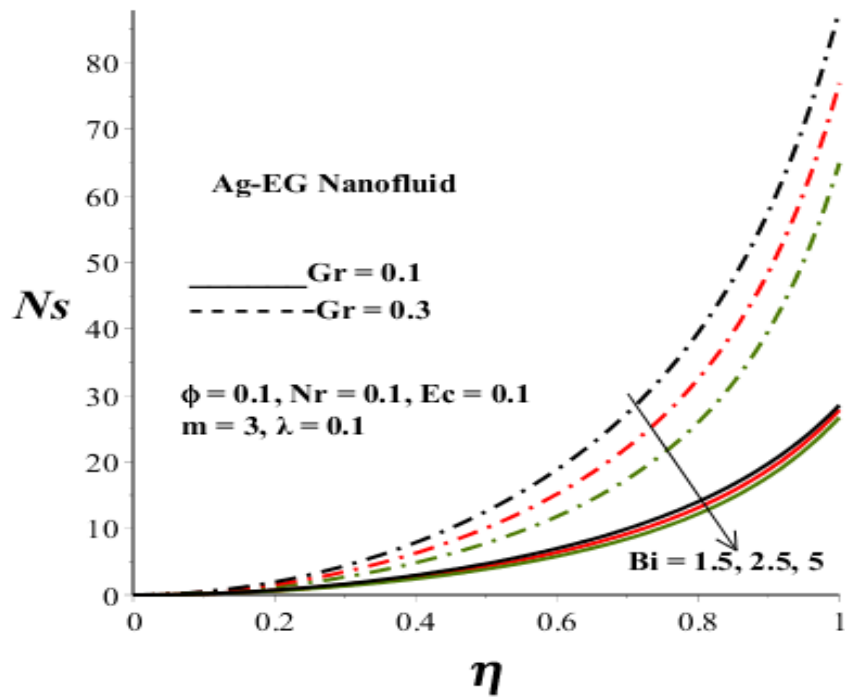


Figure 3.15 Entropy generation rate with  $Bi$  and  $Gr$

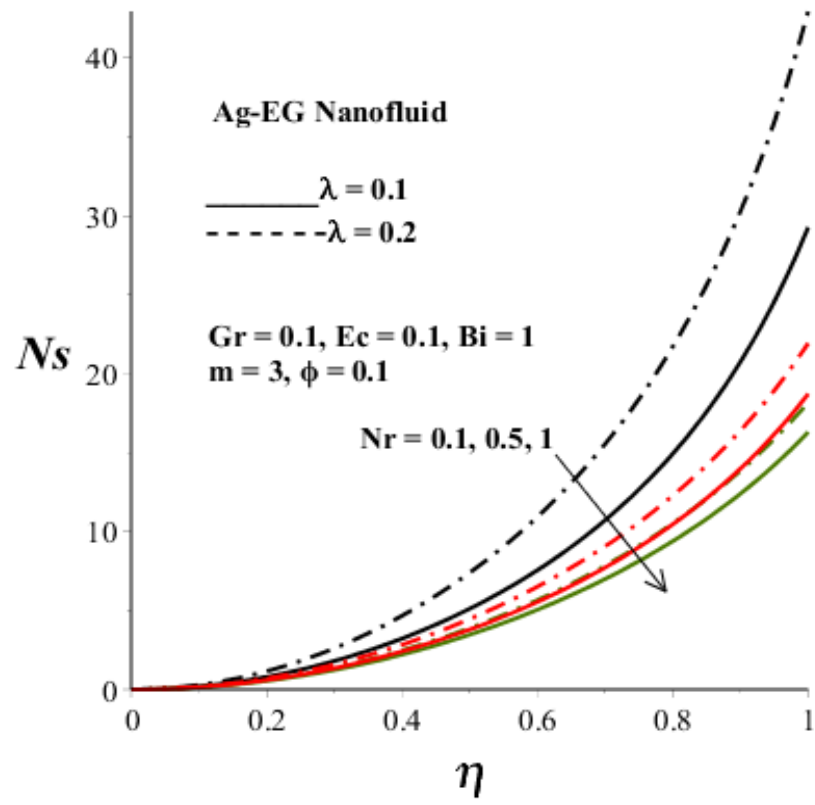


Figure 3.16 Effects of  $Nr$  and  $\lambda$  on  $Ns$ .

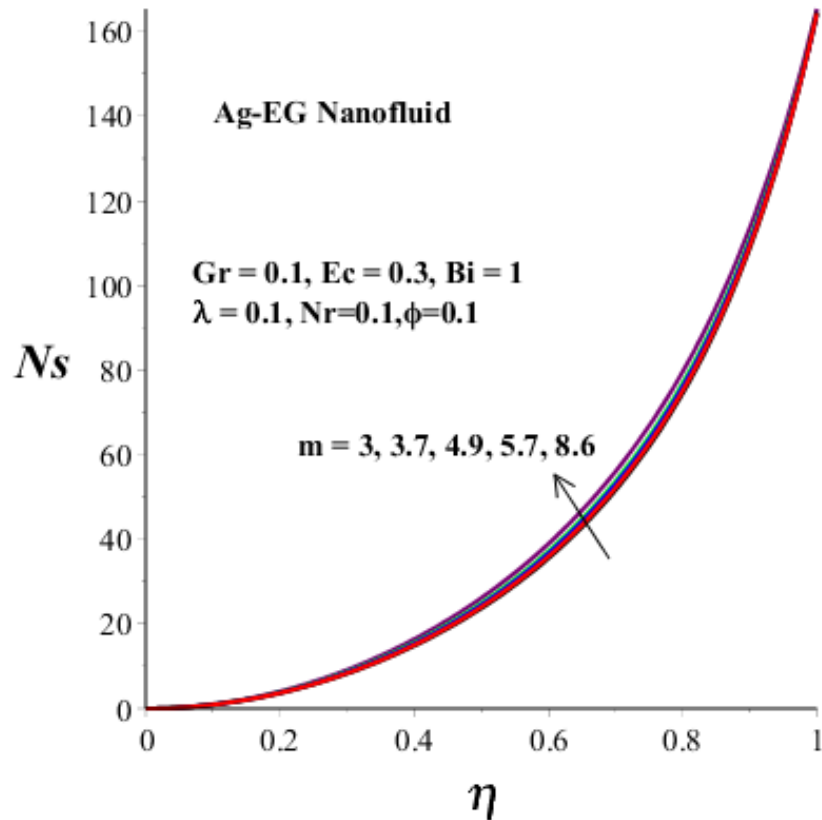


Figure 3.17 Effects of  $m$  on  $N_s$ .

### 3.4.5 Effect of Parameters Variation on Bejan Number

Figures 3.18-3.21 illustrate the parametric effects on the Bejan number. Interestingly, the Bejan number is zero along the microchannel centreline indicating the strong dominant effects of fluid friction irreversibility. The value of Bejan number amplifies towards the wall with increasing effects of heat transfer irreversibility. Moreover, it is noteworthy that the Bejan number decreases with increasing values of nanofluid volume fraction  $\phi$  and thermal radiation parameter  $N_r$ , consequently, the dominant effects of fluid friction irreversibility intensifies. On the contrary, Bejan number escalates as the parameter values of  $Ec$ ,  $Bi$ ,  $Br$  and  $\lambda$  amplify, leading to a rise in the dominant effects of heat transfer irreversibility.

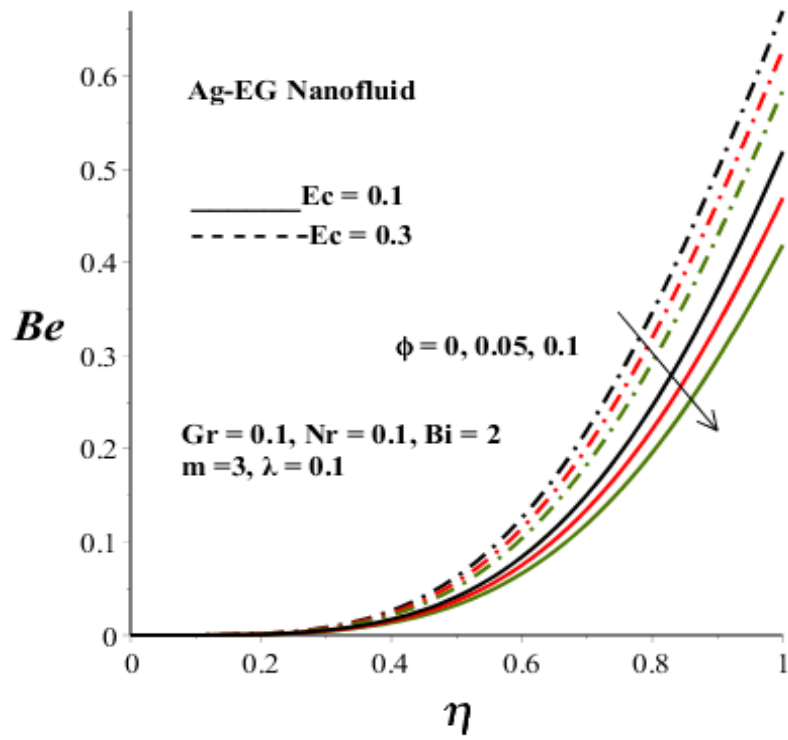


Figure 3.18 Bejan number with  $Ec$  and  $\phi$

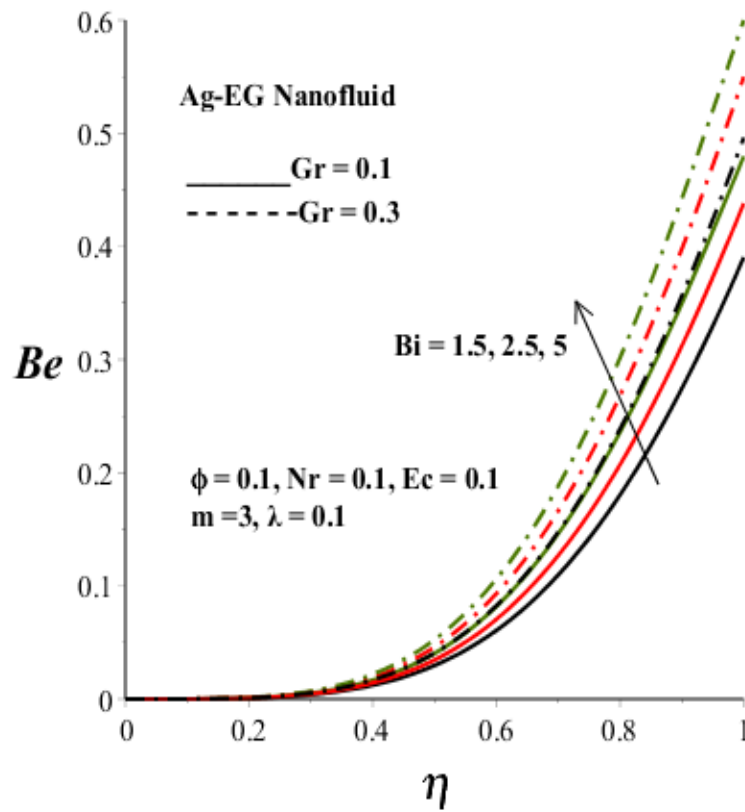


Figure 3.19 Bejan number with  $Bi$  and  $Gr$

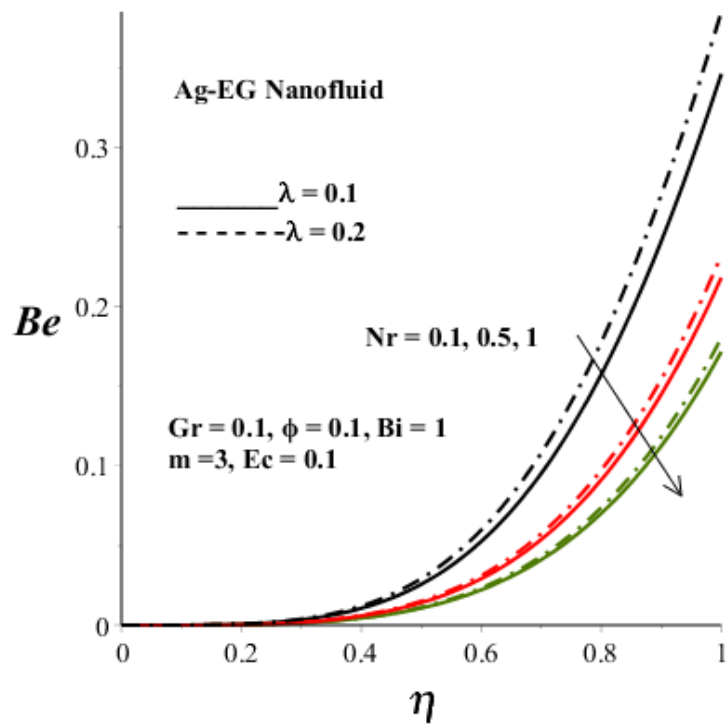


Figure 3.20 Bejan number with  $Nr$  and  $\lambda$ .

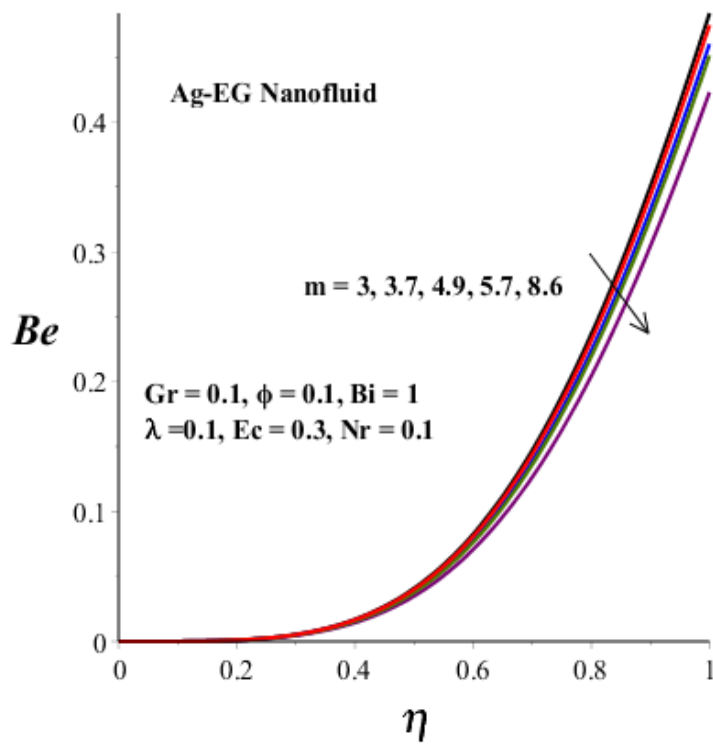


Figure 3.21 Bejan number with  $m$ .



### 3.5 Conclusion

A nonlinear model based on the first-law and second-law of thermodynamics is developed for a variable viscosity EG/Ag nanofluids flow in a vertical microchannel with convective cooling under the combined action of thermal radiation and buoyancy force.

Numerical results for the axial velocity, temperature, skin friction, Nusselt number, thermal stability condition, entropy generation rate and Bejan number are obtained using shooting method with Runge-Kutta-Fehlberg integration scheme. Pertinent results obtained from this study can be summarized as follow:

- Velocity profiles diminished with rising values of  $\phi$ ,  $Bi$  and  $Nr$  but enhanced with increasing values of  $Gr$ ,  $Ec$ ,  $\lambda$ ,  $m$ .
- Temperature profiles rise with amplifying values of  $Gr$ ,  $Ec$ ,  $\lambda$ ,  $m$  but diminished with rising values of  $\phi$ ,  $Bi$  and  $Nr$ .
- Increase in  $\lambda$ ,  $m$ ,  $Ec$  and  $Gr$  escalate the skin-friction and Nusselt number while increases in  $\phi$ ,  $Bi$ ,  $Nr$  lessen the skin-friction and Nusselt number.
- Critical Eckert number  $Ec^*$  exist such that for  $0 \leq Ec \leq Ec^*$  the flow is thermally stable and for  $Ec > Ec^*$  the flow is thermally unstable.
- The magnitude of  $Ec^*$  is enhanced with rising values of  $\phi$ ,  $Bi$  and  $Nr$ , but diminished with an increase in  $\lambda$ ,  $m$ ,  $Ec$  and  $Gr$ .
- Increase in  $\phi$ ,  $Bi$  and  $Nr$  enhance the thermodynamic efficiency while an increase in  $\lambda$ ,  $m$ ,  $Ec$  and  $Gr$  lessen the flow exergetic effectiveness.
- Increase in  $\phi$ ,  $Nr$  and  $m$  enhance the dominance effects of fluid friction irreversibility, while an increase in  $\lambda$ ,  $Bi$ ,  $Ec$  and  $Gr$  boost dominance effects of heat transfer irreversibility.

Finally, it is very obvious from our above results that the thermodynamic performance and thermal stability of EG/Ag nanofluid flow in a microchannel can be enhanced with appropriate regulation of the emerging thermophysical parameter values. Our analysis would undoubtedly serve as a useful tool for obtaining the conditions needed for design of such an integrated system in order to achieve optimal performance.

## CHAPTER 4

# THERMOPHORESIS AND BROWNIAN MOTION EFFECTS ON A REACTIVE VARIABLE VISCOSITY COUETTE FLOW IN A MICROCHANNEL<sup>3</sup>

### ABSTRACT

This paper examines the combined effects of thermophoresis, Brownian motion and viscous dissipation on the thermal performance of a reactive variable viscosity nanofluid in a microchannel under a Couette flow scenario. The nonlinear governing equations are obtained and tackled numerically using shooting method with Runge-Kutta-Fehlberg integration scheme. The effects of the pertinent parameters on the nanofluid velocity, temperature, skin friction, Nusselt number, entropy generation rate and Bejan number are presented in graphical form and discussed in detail. It is observed that a boost in thermophoresis is thermally destabilizing and enhances entropy production while an augment in Brownian motion lessens entropy generation rate and promotes thermal stability.

### 4.1 Introduction

Fluid motion induced by movement of the bounding surfaces do occur in various engineering and industrial processes. This shear driven fluid motion known as Couette flow is one of the classical problems in fluid mechanics with relevant applications in engineering tribology with respect to lubricant hydrodynamics involving loaded journal bearings and in viscometry as well as in coolant heat transfer operation [77]. A few core studies on Couette flow can be found in [57, 80, 120-121]. Meanwhile, some of the lubricants utilized in engineering and industrial processes under Couette flow scenario are very reactive e.g. hydrocarbon oils, polyglycols, synthetic esters, and polyphenylethers and their efficiency depends largely on variation in the temperature and concentration. For instance, lubricants with antioxidant will fail much faster when operating in a high-oxygen environment due to chemical reaction [122-125].

---

<sup>3</sup> This chapter is based on the research paper: R. L. Monaledi and O. D. Makinde. Thermophoresis and Brownian Motion Effects on a Reactive Variable Viscosity Couette Flow in a Microchannel. Accepted in Defect and Diffusion Forum, 2020.

The development of nanotechnology-based heat transfer fluids known as nanofluid provides a better ultrahigh-performance nanolubricants for many industrial technologies [1, 85]. Ali *et al.*[90] numerically examined effects of magnetic field on the Couette flow of nanofluid in a rotating system. Das *et al.* [126] studied the buoyancy effects on Couette flow of a reactive nanofluid between two concentric tubes. The numerical solution for combined effects of magnetic field and variable viscosity on Couette flow of nanofluid in a rotating system was reported by Makinde *et al.*[58]. Khalil *et al.* [82] investigated the effects of nanolubricant on tool wear during turning process of AISI 1050 steel material.

Meanwhile, Couette flow process of nanofluid is closely associated with thermodynamic irreversibilities due to combined effects of heat transfer, viscous dissipation and nanoparticles mass transfer. This may invariably lead to increasing entropy generation in the flow system. Consequently, the quality of energy in the system diminishes and thus reduces its efficient operation. Therefore, implementation of entropy generation minimization is extremely necessary in order to enhance the efficiency of the flow process [60, 76, 96]. Theoretically, this involves modelling and optimization of the devices by accounting for heat transfer, fluid friction and nanoparticles irreversibilities. Das *et al.* [101] presented a numerical solution for the inherent irreversibilities in hybrid nanofluid flow through a porous channel. Monaledi and Makinde [127] investigated the combined effects of thermal radiation, variable viscosity and buoyancy force on the entropy generation rate in EG/Ag nanofluid flow through a microchannel. The entropy analysis of Couette slip flow of nanofluid with convective cooling has been reported by Mkwizu *et al.* [61, 100]. Makinde and Eegunjobi [99] studied the effects of magnetic field and thermal radiation on the entropy generation rate in a non-Newtonian nanofluid flow through a permeable channel.

From the literature survey, it is observed that the combined effects of thermophoresis and Brownian motion on entropy generation rate in a microchannel Couette flow of a reactive variable viscosity nanofluid has not been reported. Our objective in this present study is to fill this gap in the literature. Moreover, the entropy analysis in microchannel with one plate moving is a different fundamental problem worth pursuing. This study is necessary specifically in the design of effective nanolubricants and coolants for microchannel with interacting surfaces in relative motion and heat exchangers. In the following sections, the model problem is formulated, analysed and solved. Pertinent results for the velocity, temperature and nanoparticles concentration profiles as well as the skin friction, Nusselt number, Sherwood

number and the flow thermal stability condition are obtained. Effects of various thermophysical parameters are presented graphically and discussed quantitatively.

## 4.2 Model Problem

The Buongiorno model for a Couette flow of an incompressible, variable viscosity nanofluid in a microchannel is considered as shown in figure 4.1. The flow takes place in the  $x$ -direction between two parallel plates of small width  $h$  and very long length  $L$ . The upper plate moves with constant velocity  $U$  while the lower plate is kept stationary. The temperature and concentration dependent nanofluid viscosity ( $\mu$ ) can be expressed as,

$$\mu = \mu_0 e^{-\beta_1(T-T_w)+\beta_2(C-C_w)} \quad (4.1)$$

where  $\mu_0$  is the nanofluid viscosity at the channel walls,  $T_w$  is the wall temperature,  $C_w$  is the wall concentration,  $T$  is the nanofluid temperature,  $C$  is the nanofluid concentration,  $\beta_1$ ,  $\beta_2$  are the variable viscosity parameters due to temperature and concentration variation, respectively.

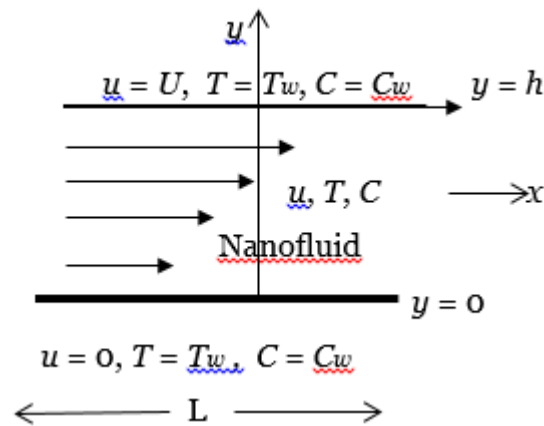


Figure 4.1 Problem geometry

Under these conditions, the continuity, momentum, energy, concentration and entropy generation equations governing the problem may be written as [61, 127];

$$\frac{\partial u}{\partial x} = 0 \quad (4.2)$$

$$\frac{\partial}{\partial y} \left( \mu \frac{\partial u}{\partial y} \right) = 0, \quad (4.3)$$

$$\alpha \frac{\partial^2 T}{\partial y^2} + \frac{\mu}{(\rho c_p)_f} \left( \frac{\partial u}{\partial y} \right)^2 + \tau \left[ D_B \frac{\partial C}{\partial y} \frac{\partial T}{\partial y} + \frac{D_T}{T_w} \left( \frac{\partial T}{\partial y} \right)^2 \right] = 0 \quad (4.4)$$

$$D_B \frac{\partial^2 C}{\partial y^2} + \frac{D_T}{T_w} \frac{\partial^2 T}{\partial y^2} - \gamma (C - C_w) = 0 \quad (4.5)$$

$$E_g = \frac{k}{T_w^2} \left( \frac{\partial T}{\partial y} \right)^2 + \frac{\mu}{T_w} \left( \frac{\partial u}{\partial y} \right)^2 + \frac{RD_B}{C_w} \left( \frac{\partial C}{\partial y} \right)^2 + \frac{RD_T}{T_w} \frac{\partial C}{\partial y} \frac{\partial T}{\partial y}, \quad (4.6)$$

with the boundary conditions given as

$$\left. \begin{aligned} u=0, \quad T=T_w, \quad C=C_w, \quad \text{at } y=0 \\ u=U, \quad T=T_w, \quad C=C_w, \quad \text{at } y=h \end{aligned} \right\} \quad (4.7)$$

where  $R$  is the universal gas constant,  $U$  is the uniform velocity of the upper wall,  $E_g$  is the entropy generation rate,  $k$  is the fluid thermal conductivity,  $D_B$  is the Brownian motion mass diffusivity,  $D_T$  is thermophoresis mass diffusivity,  $\rho_f$  is the base fluid density,  $\tau$  is the specific heat capacity ratio,  $c_{pf}$  is the fluid specific heat capacity at constant pressure,  $\gamma$  is the reaction rate parameter and  $\alpha$  is the fluid thermal diffusivity coefficient. We introduce the following non-dimensional quantities in equations (4.2)-(4.7):

$$\begin{aligned} \eta = \frac{y}{h}, \quad W = \frac{u}{U}, \quad \theta = \frac{T - T_w}{T_w}, \quad \phi = \frac{C}{C_w}, \quad \text{Pr} = \frac{\nu}{\alpha}, \quad \nu = \frac{\mu_0}{\rho_f}, \quad \lambda_1 = \beta_1 T_w, \\ \lambda_2 = \beta_2 C_w, \quad Ec = \frac{U^2}{c_{pf} T_w}, \quad Nb = \frac{\tau D_B C_w}{\nu}, \quad Nt = \frac{\tau D_T}{\nu}, \quad m = \frac{\gamma h^2}{\nu}, \\ \alpha = \frac{k}{(\rho c_p)_f}, \quad n = \frac{RD_B}{k}, \quad Ns = \frac{E_g h^2}{k}, \quad Sc = \frac{\nu}{D_B}, \quad \text{Re} = \frac{Uh}{\nu}, \end{aligned} \quad (4.8)$$

and obtain

$$\frac{dW}{d\eta} = Ae^{\lambda_1\theta - \lambda_2(\phi-1)} \quad (4.9)$$

$$\frac{d^2\theta}{d\eta^2} + \text{Pr} Ec A^2 e^{\lambda_1\theta - \lambda_2(\phi-1)} + \text{Pr} Nb \frac{d\phi}{d\eta} \frac{d\theta}{d\eta} + \text{Pr} Nt \left( \frac{d\theta}{d\eta} \right)^2 = 0 \quad (4.10)$$

$$\frac{d^2\phi}{d\eta^2} + \frac{Nt}{Nb} \frac{d^2\theta}{d\eta^2} - Scm(\phi-1) = 0 \quad (4.11)$$

$$Ns = \left( \frac{d\theta}{d\eta} \right)^2 + \text{Pr} Ec A^2 e^{\lambda_1\theta - \lambda_2(\phi-1)} + n \left[ \left( \frac{d\phi}{d\eta} \right)^2 + \frac{d\phi}{d\eta} \frac{d\theta}{d\eta} \right] \quad (4.12)$$

with boundary conditions given as,

$$\left. \begin{aligned} W(0) = 0, \quad \theta(0) = 0, \quad \phi(0) = 1, \\ W(1) = 1, \quad \theta(1) = 0, \quad \phi(1) = 1. \end{aligned} \right\} \quad (4.13)$$

where  $A$  corresponds to the skin friction value at the walls,  $\text{Pr}$  is Prandtl number,  $Sc$  is the Schmidt number,  $Ec$  is the Eckert number,  $Nt$  is the thermophoresis parameter,  $Nb$  is Brownian motion parameter,  $n$  is the irreversibility parameter due to nanoparticles concentration.  $Ns$  is the entropy generation rate and  $\lambda_1, \lambda_2$  are variable viscosity parameters due to temperature and nanoparticles concentration, respectively.

Other quantities of interest are the skin friction coefficients ( $C_f$ ), Nusselt number ( $Nu$ ), Sherwood number and the Bejan number ( $Be$ ) which are given as

$$\text{Re} C_f = \frac{h\tau_w}{\mu_0 U} = \frac{dW}{d\eta} \Big|_{\eta=0,1} = A \quad (4.14)$$

$$Nu = \frac{hq_w}{kT_w} = - \frac{d\theta}{d\eta} \Big|_{\eta=0,1}, \quad (4.15)$$

$$Sh = \frac{hq_m}{D_B C_w} = -\left. \frac{d\phi}{d\eta} \right|_{\eta=0,1}, \quad (4.16)$$

$$Be = \frac{N_1}{N_s} = \frac{1}{1+F} \quad (4.17)$$

where

$$\tau_w = \mu_0 \frac{\partial u}{\partial y}, \quad q_w = -k \frac{\partial T}{\partial y}, \quad q_m = -D_B \frac{\partial C}{\partial y}, \quad N_1 = \left( \frac{d\theta}{d\eta} \right)^2, \quad (4.18)$$

$$N_2 = \text{Pr} Ec A^2 e^{\lambda_1 \theta - \lambda_2 (\phi-1)}, \quad N_3 = n \left[ \left( \frac{d\phi}{d\eta} \right)^2 + \frac{d\phi}{d\eta} \frac{d\theta}{d\eta} \right], \quad F = \frac{N_2 + N_3}{N_1}. \quad (4.19)$$

The variable  $F$  represents the irreversibility ratio. The symbol  $N_1$  represents thermodynamic irreversibility due to heat transfer;  $N_2$  corresponds to the entropy generation due to fluid friction while  $N_3$  represents irreversibility due to nanoparticles concentration. Whenever  $0 \leq Be < 0.5$ , entropy generation due to fluid friction and nanoparticles concentration dominates the flow system while heat transfer irreversibility dominates when  $0.5 < Be \leq 1$ .

### 4.3 Numerical Procedure

Equations (4.9)-(4.11) with the boundary conditions in equation (4.13) are solved numerically using shooting method with Runge-Kutta-Fehlberg integration scheme. The procedure involves transforming the model boundary value problem into a set of nonlinear first order ordinary differential equations with some unknown initial conditions to be calculated by shooting technique [58, 61, 90, 99-100, 126-127], Let

$$\theta = y_1, \theta' = y_2, \phi = y_3, \phi' = y_4. \quad (4.20)$$

The governing equations then become

$$\left. \begin{aligned} W' &= Ae^{\lambda_1 y_1 - \lambda_2 (y_3 - 1)}, \\ y_1' &= y_2, \\ y_2' &= -\text{Pr} EcA^2 e^{\lambda_1 y_1 - \lambda_2 (y_3 - 1)} - \text{Pr} Nby_2 y_4 - \text{Pr} Nty_2^2, \\ y_3' &= y_4, \\ y_4' &= \frac{Nt}{Nb} \left( \text{Pr} EcA^2 e^{\lambda_1 y_1 - \lambda_2 (y_3 - 1)} + \text{Pr} Nby_2 y_4 + \text{Pr} Nty_2^2 \right) + Scm(y_3 - 1), \end{aligned} \right\} \quad (4.21)$$

with the corresponding initial conditions as

$$W(0) = 0, W'(0) = A, y_1(0) = 0, y_2(0) = a_1, y_3(0) = 1, y_4(0) = a_2. \quad (4.22)$$

Initially, we guess the values of  $a_1$  and  $a_2$  in the equation (4.22) and thereafter determine the accurate values of the unknown initial conditions via shooting method with Newton-Raphson's iteration technique for each set of parameter values in equation (4.19). With step size of  $\Delta\eta=0.01$ , the initial value problem is solved numerically using Runge-Kutta-Fehlberg integration scheme. Solutions obtained for the velocity, temperature and nanoparticles concentration profiles are utilized to compute the values for the skin friction, Nusselt number, Sherwood number, entropy generation rate and Bejan number as given in equations (4.12) and (4.14)-(4.15).

#### 4.4 Results and Discussion

In order to gain an insight into the overall flow structure with heat and mass transfer characteristics, numerical solution for the velocity, temperature and nanoparticles concentration profiles are presented graphically in figures 4.2-4.20. We also compute the results for the skin friction ( $C_f$ ), the Nusselt number ( $Nu$ ), Sherwood number, entropy generation rate and Bejan number as depicted in table 4.1 and figures 4.21-4.39. The effects of thermophysical parameters on the critical value of Eckert number ( $Ec^*$ ) for thermal stability is displayed in table 4.1 and also demonstrated in figures 4.24-4.25. Eckert number refers to the relationship between the dissipated flow kinetic energy and the thermal energy conducted into the fluid. Determination of critical value of Eckert number will enhance safe and efficient operation of flow and thermal processes.



Interestingly, the values of  $Ec^*$  increase with a rise in the values of  $Nb$ ,  $m$  and  $Sc$ , consequently, the flow thermal stability is enhanced. However, the trend is opposite with an escalation in the parameter values of  $Nt$ ,  $\lambda_1$  and  $\lambda_2$ , leading to a reduction in the  $Ec^*$  and early occurrence of thermal instability in the flow field. This implies that a boost in thermophoresis coupled with a decrease in fluid viscosity is thermally destabilizing while an augment in Brownian motion promotes thermal stability.

Table 4.1 Computations showing the effect of parameters variation on thermal stability critical Eckert number  $Pr = 6.2$

| $Nb$ | $Nt$ | $\lambda_1$ | $\lambda_2$ | $m$ | $Sc$ | $Ec^*$    |
|------|------|-------------|-------------|-----|------|-----------|
| 0.1  | 0.5  | 0.5         | 0.5         | 0.1 | 0.6  | 1.151786  |
| 0.2  | 0.5  | 0.5         | 0.5         | 0.1 | 0.6  | 2.356651  |
| 0.3  | 0.5  | 0.5         | 0.5         | 0.1 | 0.6  | 3.533653  |
| 0.1  | 0.3  | 0.5         | 0.5         | 0.1 | 0.6  | 1.964840  |
| 0.1  | 0.2  | 0.5         | 0.5         | 0.1 | 0.6  | 2.944305  |
| 0.1  | 0.5  | 0.4         | 0.5         | 0.1 | 0.6  | 1.152486  |
| 0.1  | 0.5  | 0.1         | 0.5         | 0.1 | 0.6  | 1.155291  |
| 0.1  | 0.5  | 0.5         | 0.3         | 0.1 | 0.6  | 1.090410  |
| 0.1  | 0.5  | 0.5         | 0.1         | 0.1 | 0.6  | 1.119099  |
| 0.1  | 0.5  | 0.5         | 0.5         | 0.3 | 0.6  | 1.152239  |
| 0.1  | 0.5  | 0.5         | 0.5         | 0.5 | 0.6  | 1.152691  |
| 0.1  | 0.5  | 0.5         | 0.5         | 0.1 | 6.0  | 1.153820  |
| 0.1  | 0.5  | 0.5         | 0.5         | 0.1 | 10   | 1.1553178 |

#### 4.4.1 Velocity Profiles

Figures 4.2-4.6 illustrate the effects of parameters variation on nanofluid velocity profiles. Generally, the velocity is zero at the lower fixed plate due to no slip condition and gradually increases to its maximum values at the upper moving plate. A rise in the parameter values  $\lambda_1$ ,  $\lambda_2$ ,  $Nt$  and  $Ec$  drops the velocity near the lower fixed plate region and boosts the velocity near the upper moving plate as shown in figure 4.2-4.5.

The trend is reversed in figure 4.6 with increasing Brownian motion ( $Nb$ ), consequently, the nanofluid velocity rises near the lower fixed wall but diminishes near the upper moving wall.

It is noteworthy that at the channel centreline ( $\eta=0.5$ ) the velocity is not affected by parameter variation. Therefore, the Couette flow velocity is general enhanced with nanof fluid viscosity variation and thermophoresis activities.

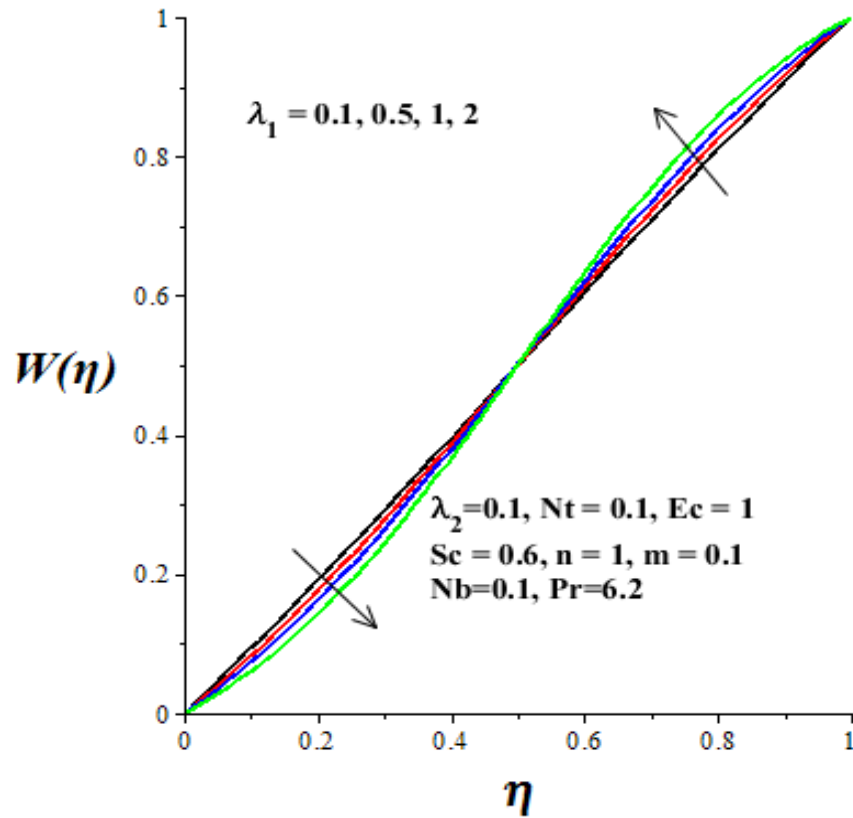


Figure 4.2: Velocity profiles with increasing  $\lambda_1$

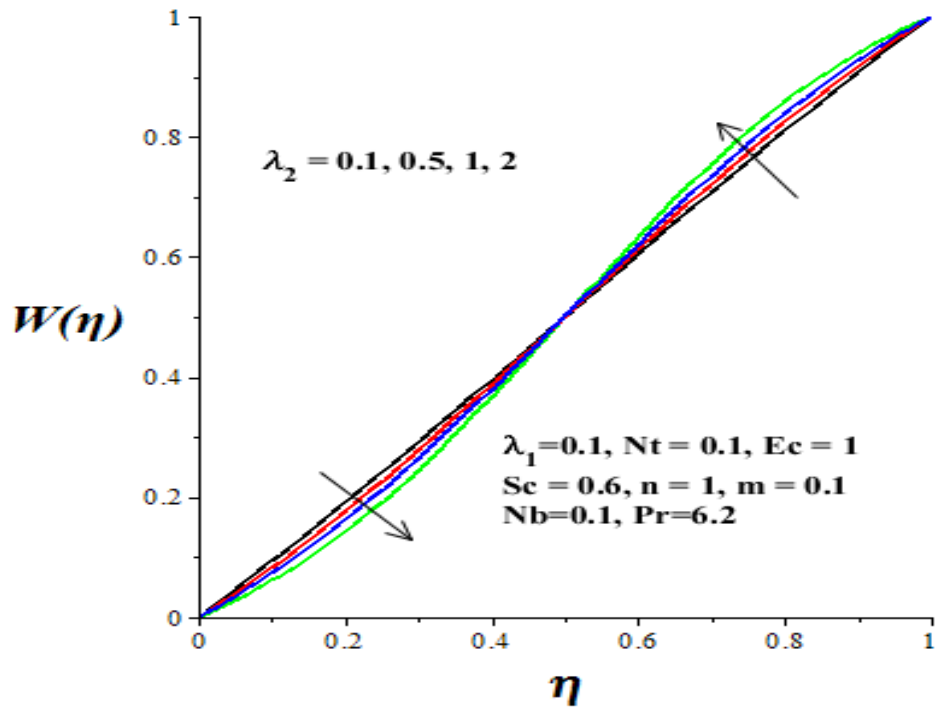


Figure 4.3: Velocity profiles with increasing  $\lambda_2$

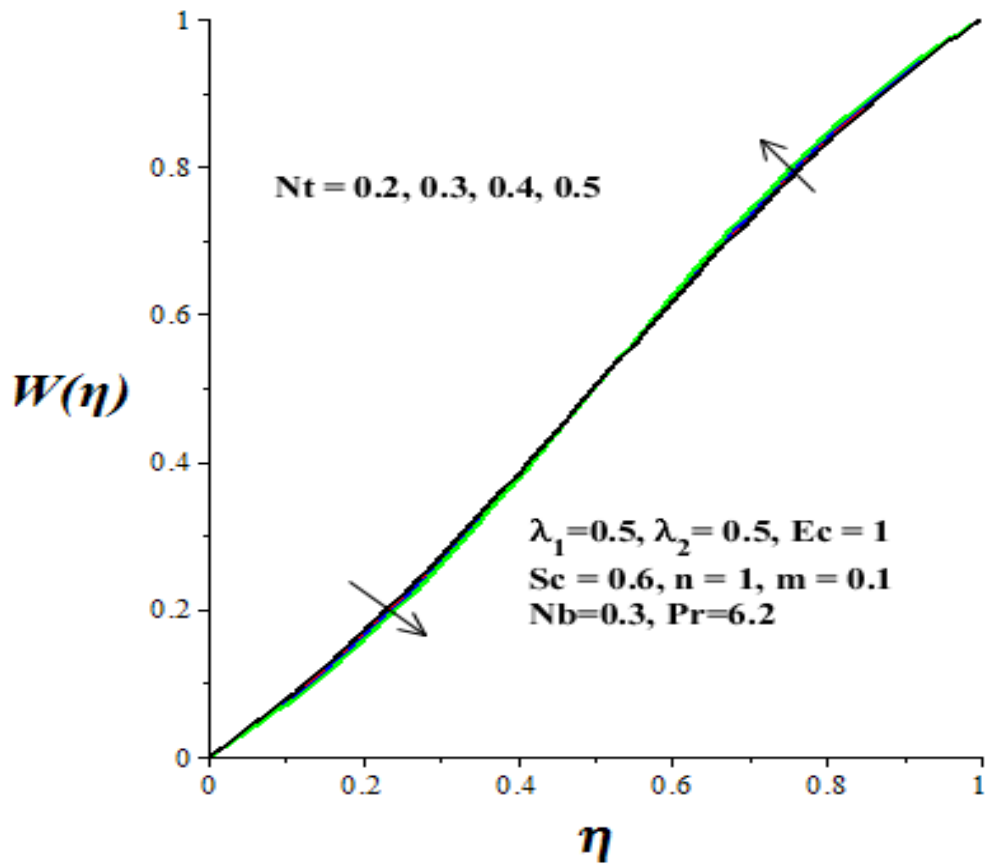


Figure 4.4: Velocity profiles with increasing  $Nt$

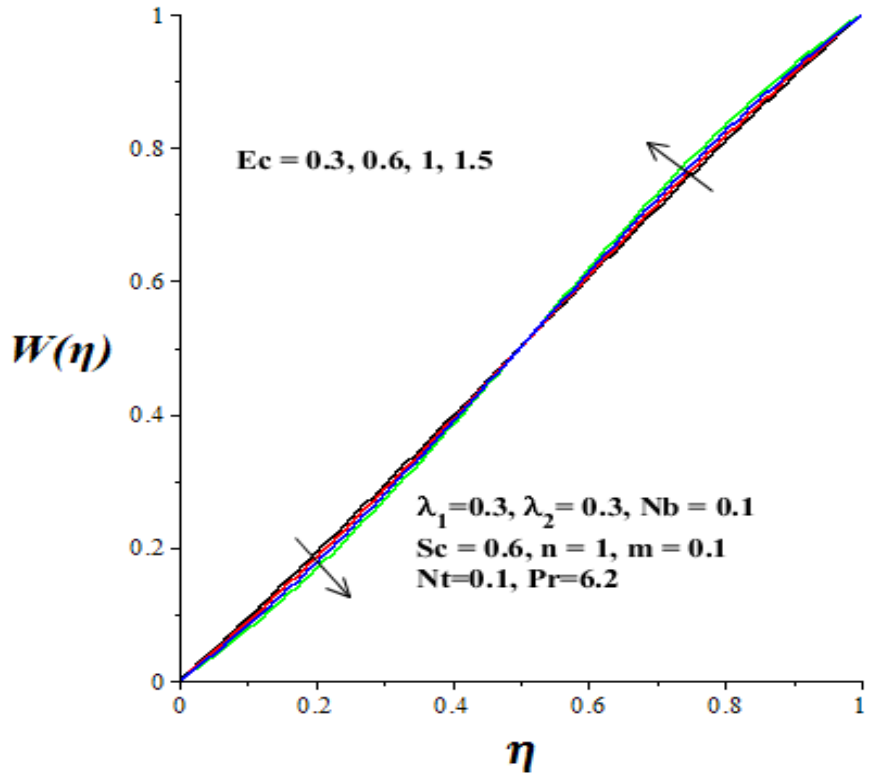


Figure 4.5: Velocity profiles with increasing  $Ec$

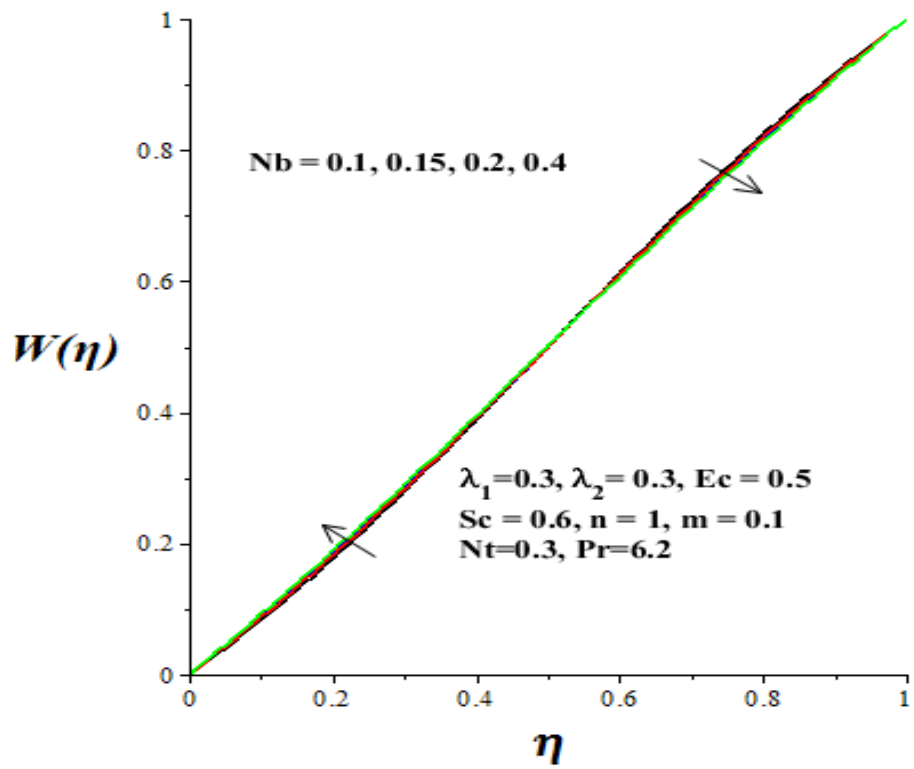


Figure 4.6: Velocity profiles with increasing  $Nb$

#### 4.4.2 Temperature Profiles

Figures 4.7-4.13 illustrate the temperature profiles of nanofluid under different parametric conditions. Generally, the nanofluid temperature is lowest at both fixed and moving walls but attained its maximum value along the plate's centreline. Meanwhile, a decrease in nanofluid temperature is observed with increasing parameter values of  $\lambda_1$ ,  $\lambda_2$  and  $Nt$  as shown in figures 4.7-4.9. The trend is opposite in figures 4.10-4.13 with a rise in nanofluid temperature as the parameters  $Nb$ ,  $Ec$ ,  $m$  and  $Sc$  increased. This may be attributed to the increasing interaction between the nanoparticles and the base fluid under the Couette flow process.

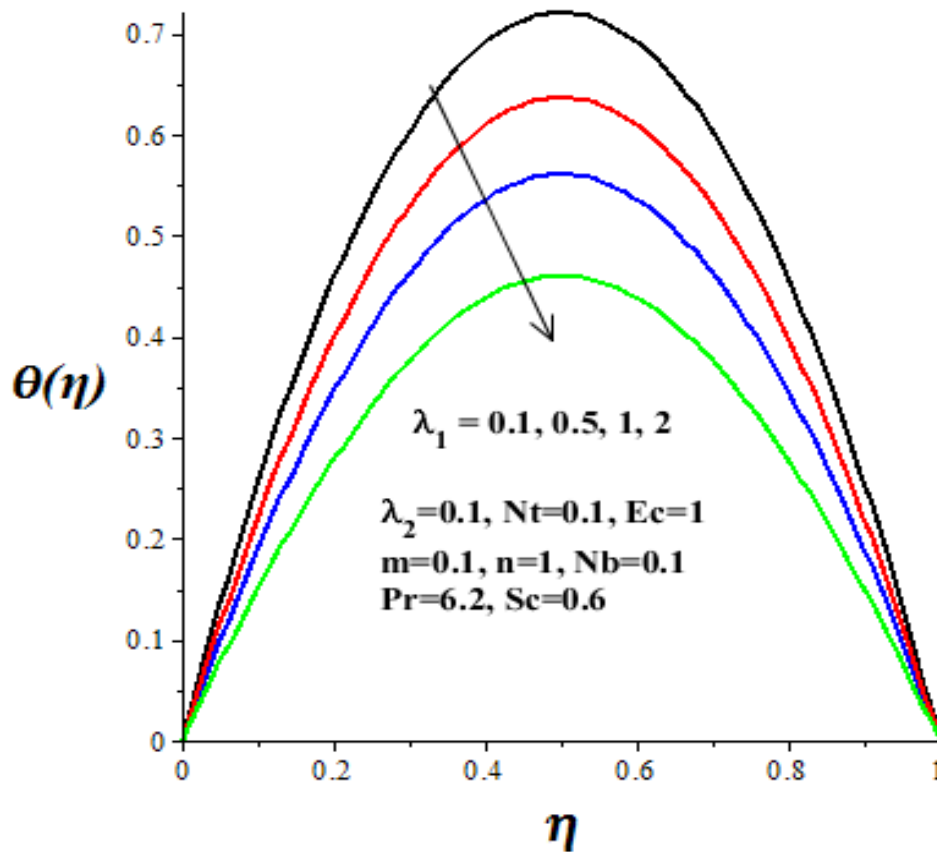


Figure 4.7: Effects of  $\lambda_1$  on temperature profiles.

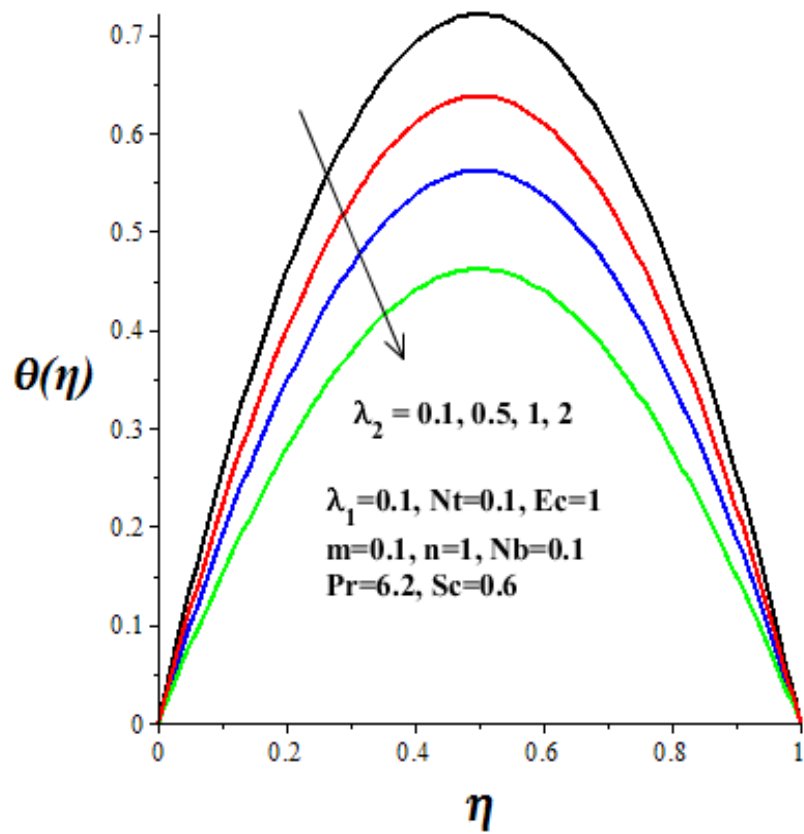


Figure 4.8: Effects of  $\lambda_2$  on temperature profiles

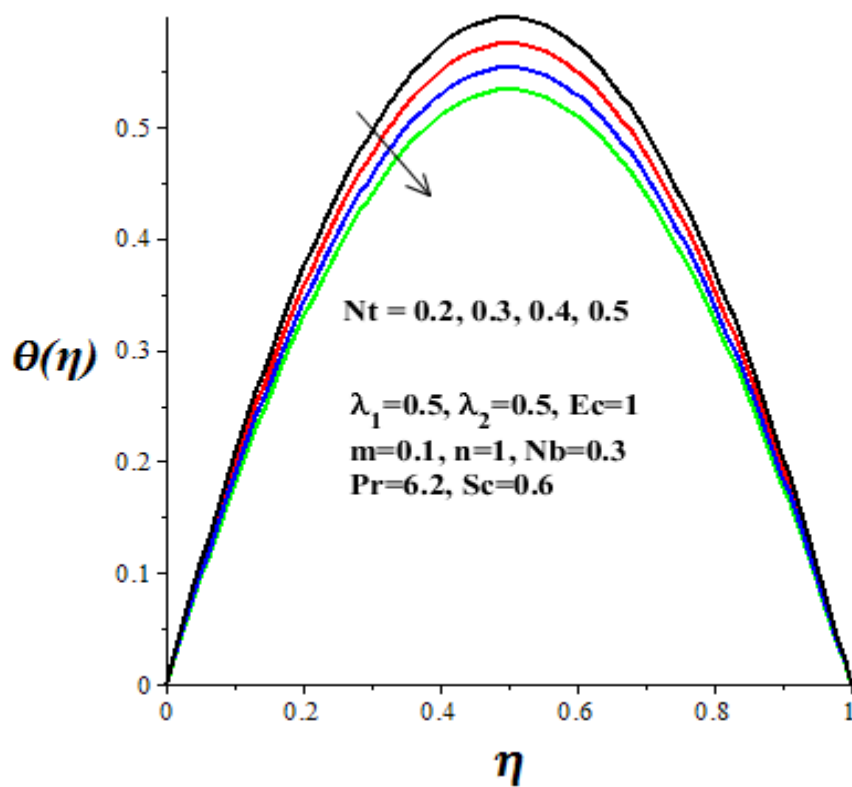


Figure 4.9: Temperature profiles with increasing  $Nt$

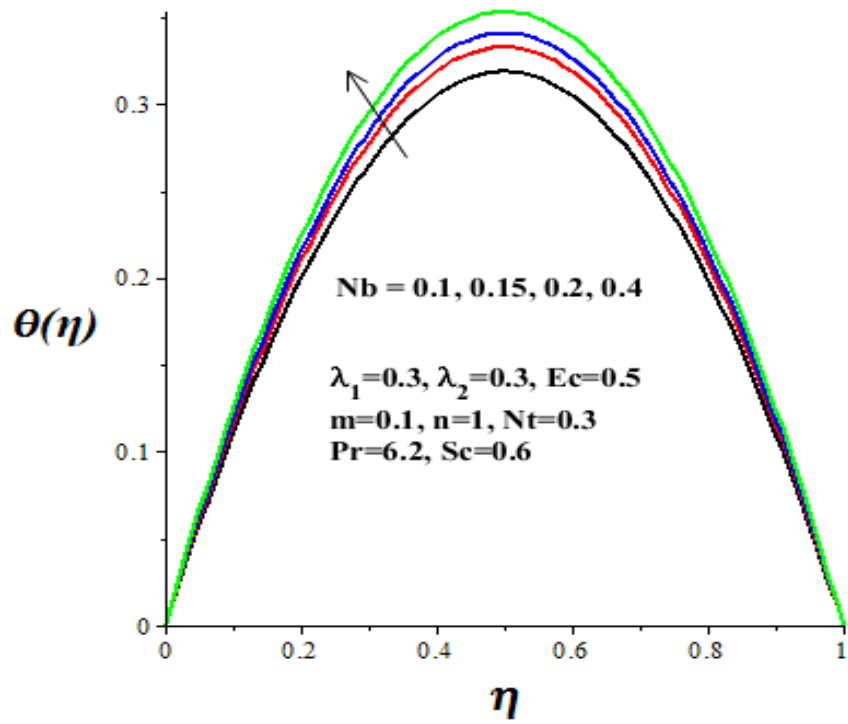


Figure 4.10: Temperature profiles with increasing Nb

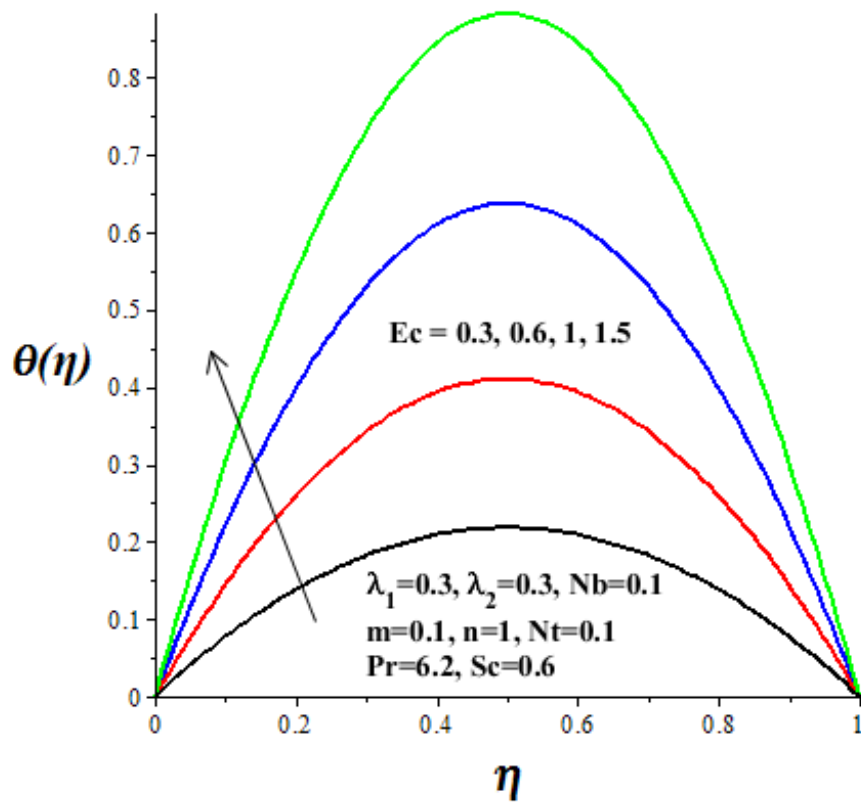


Figure 4.11: Temperature profiles with increasing Ec

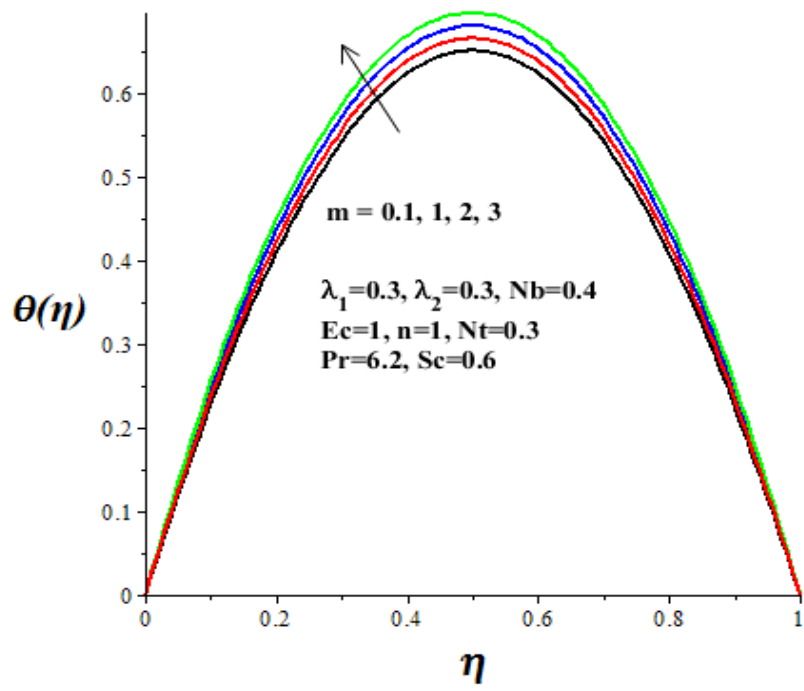


Figure 4.12: Temperature profiles with increasing  $m$

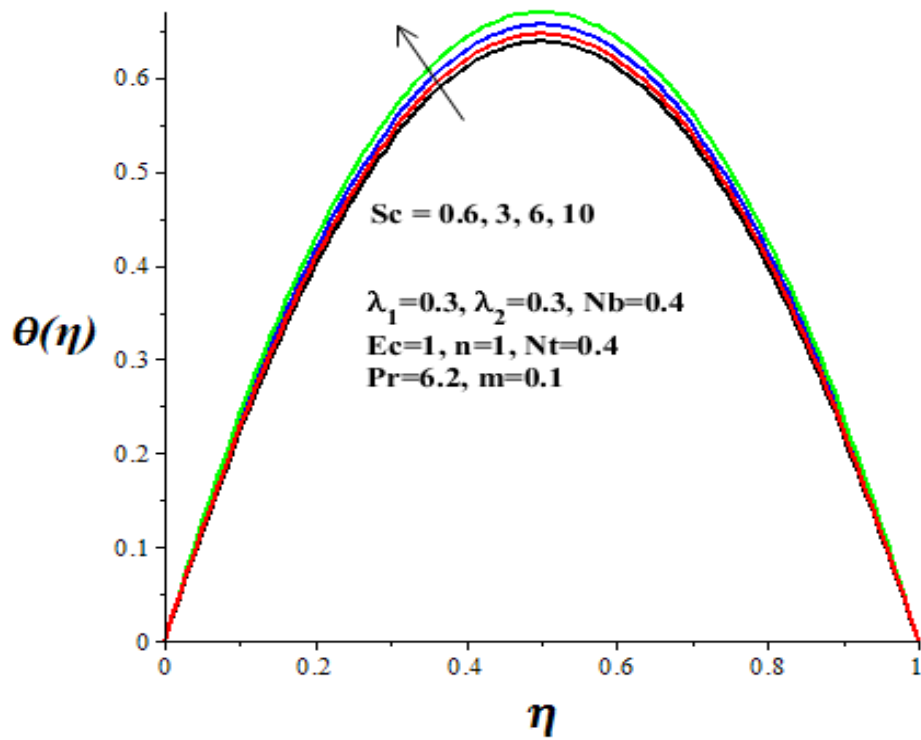


Figure 4.13: Temperature profiles with increasing  $Sc$



### 4.4.3 Nanoparticles Concentration Profiles

Figures 4.14-4.20 demonstrate the effects of various parameters on the nanoparticles concentration profiles. Generally, a minimum concentration is noticed in all figures around the microchannel centreline and the profiles increase gradually towards the fixed and moving walls. It is interesting to note that the nanoparticles concentration is enhanced with an escalation in the parameter values of  $\lambda_1$ ,  $\lambda_2$ ,  $Nb$ ,  $m$  and  $Sc$  as shown in figure 4.14-4.18, while a reduction in the concentration is observed in figures 4.19-4.20 with a rise in parameter values of  $Ec$  and  $Nt$ . As the nanofluid viscosity varies, the nanoparticles concentration increases towards the microchannel centreline due to a rise in Brownian motion activities and chemical reaction.

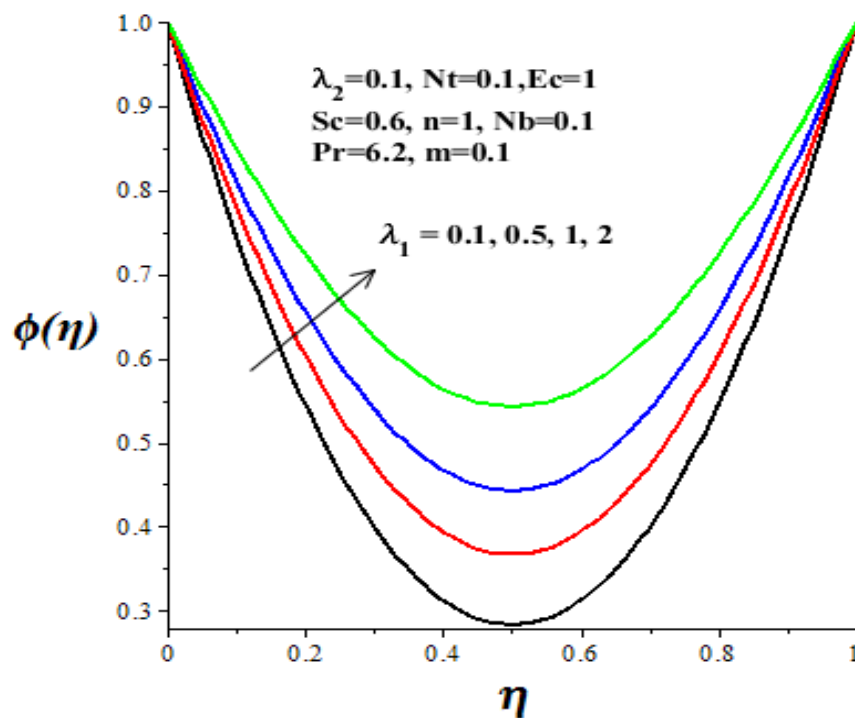


Figure 4.14: Concentration profiles with  $\lambda_1$ .

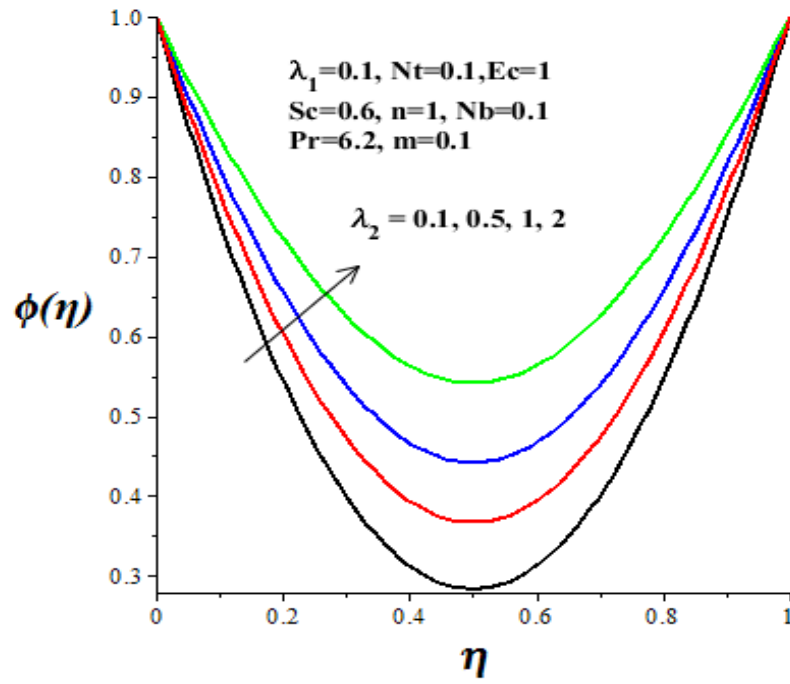


Figure 4.15: Concentration profiles with  $\lambda_2$

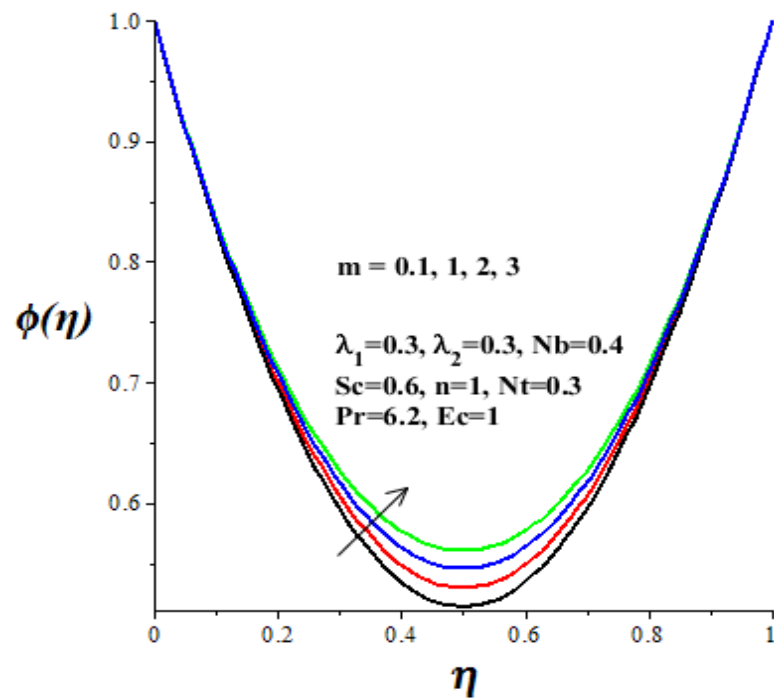


Figure 4.16: Concentration profiles with  $m$ .

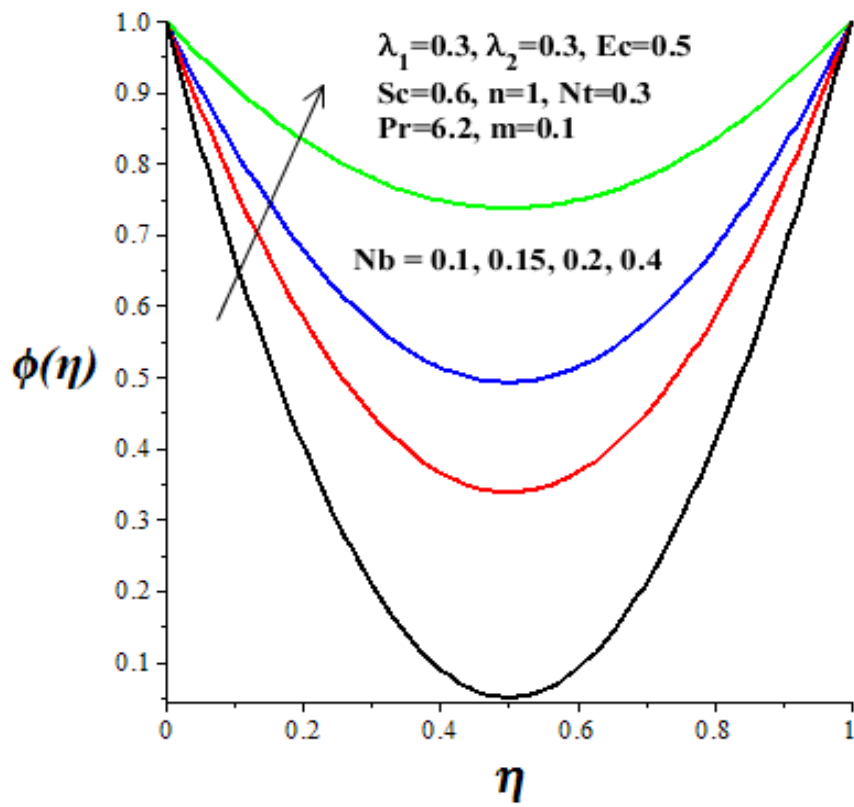


Figure 4.17: Concentration profiles with Nb.

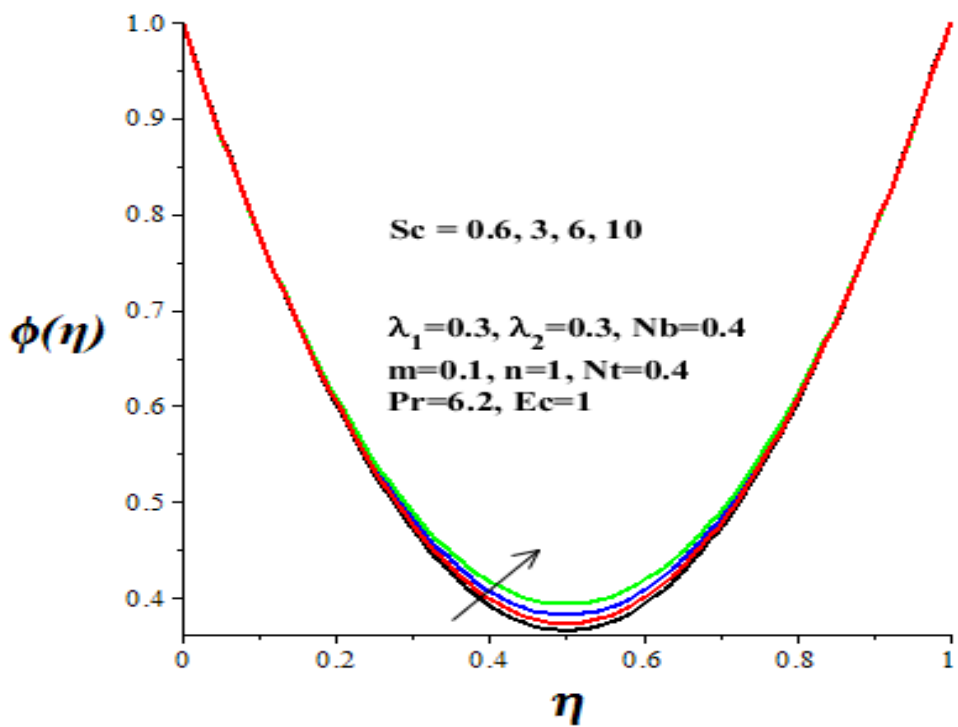


Figure 4.18: Concentration profiles with Sc.

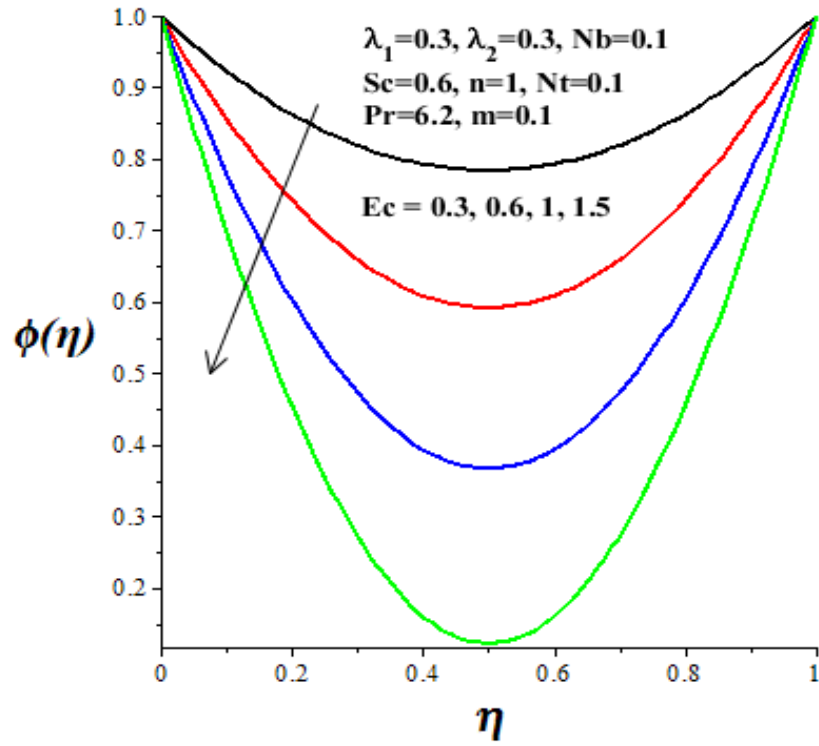


Figure 4.19: Concentration profiles with  $Ec$ .

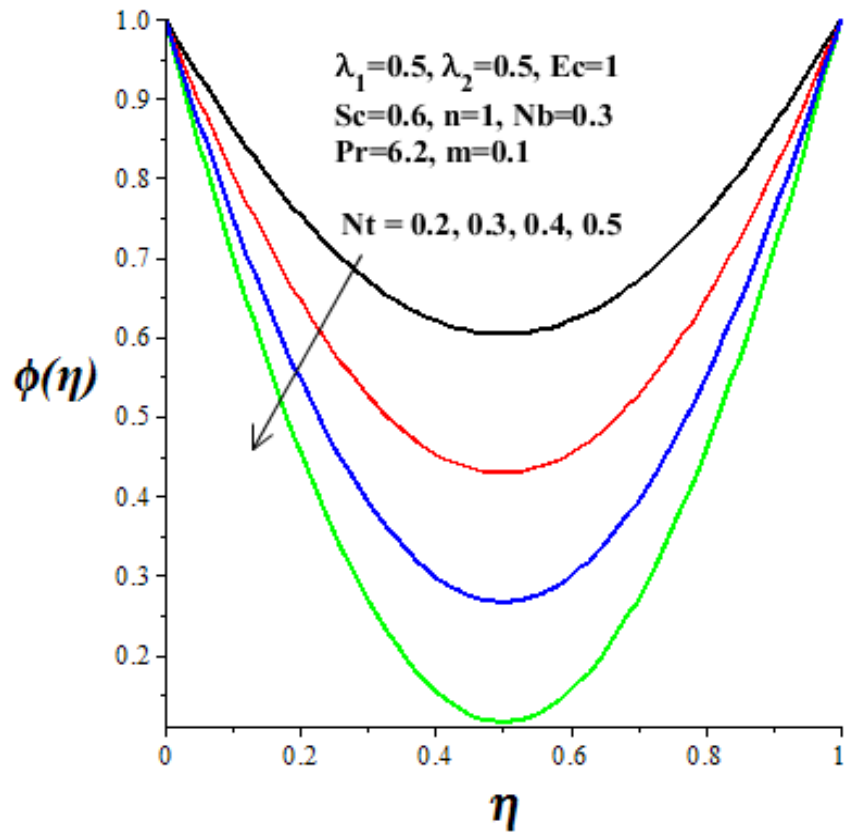


Figure 4.20: Concentration profiles with  $Nt$ .

#### 4.4.4 Skin Friction, Nusselt Number, Sherwood Number and Thermal Stability Criteria

Figure 4.21 shows that the shear stress (skin friction) at the microchannel wall lessens with a rise in parameter values of  $\lambda_1$ ,  $\lambda_2$  and  $Ec$ . This may be attributed to a decrease in the nanofluid velocity gradient at the wall as the parameters increase. Consequently, the nanofluid viscosity decreases and dissipation rate increases. Figure 4.22 reveals that the heat flux at the microchannel wall represented by Nusselt number rises with amplification of Eckert number due to viscous dissipation but diminishes with a reduction in nanofluid viscosity (i.e.  $\lambda_1$ ,  $\lambda_2$  increase). Similar trend is observed in figure 4.23 for Sherwood number.

The nanoparticle mass transfer rate increases with  $Ec$  but decreases with  $\lambda_1$  and  $\lambda_2$ . Figures 4.24-4.25 show that the Brownian motion boosts the Nusselt number and enhances flow thermal stability while thermophoresis lessens it.

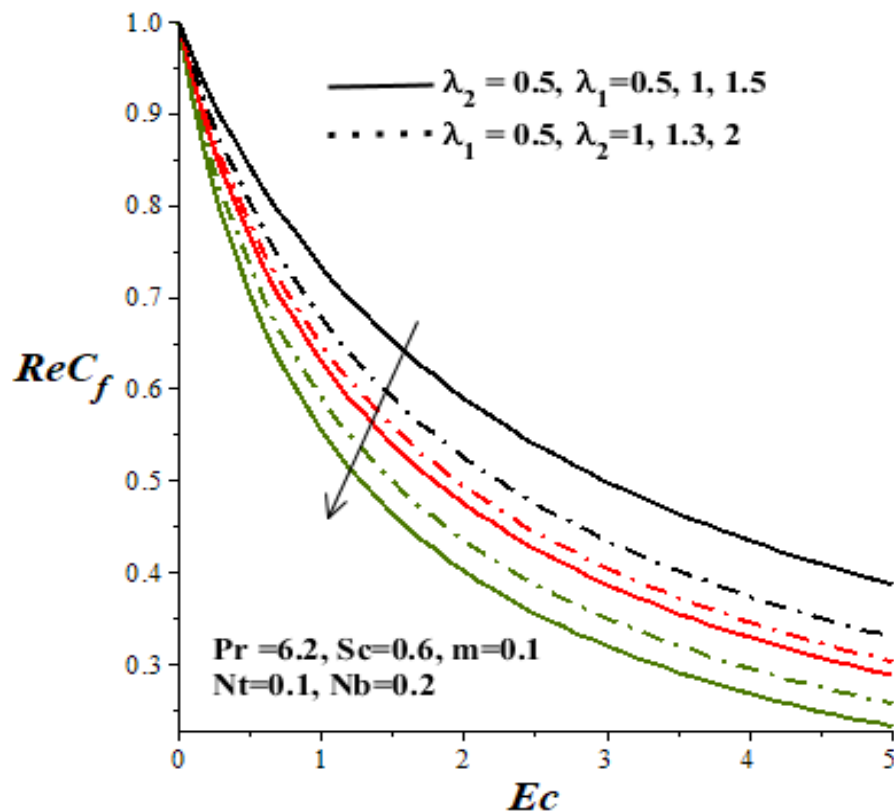


Figure 4. 21: Skin friction with  $Ec$ ,  $\lambda_1$  and  $\lambda_2$

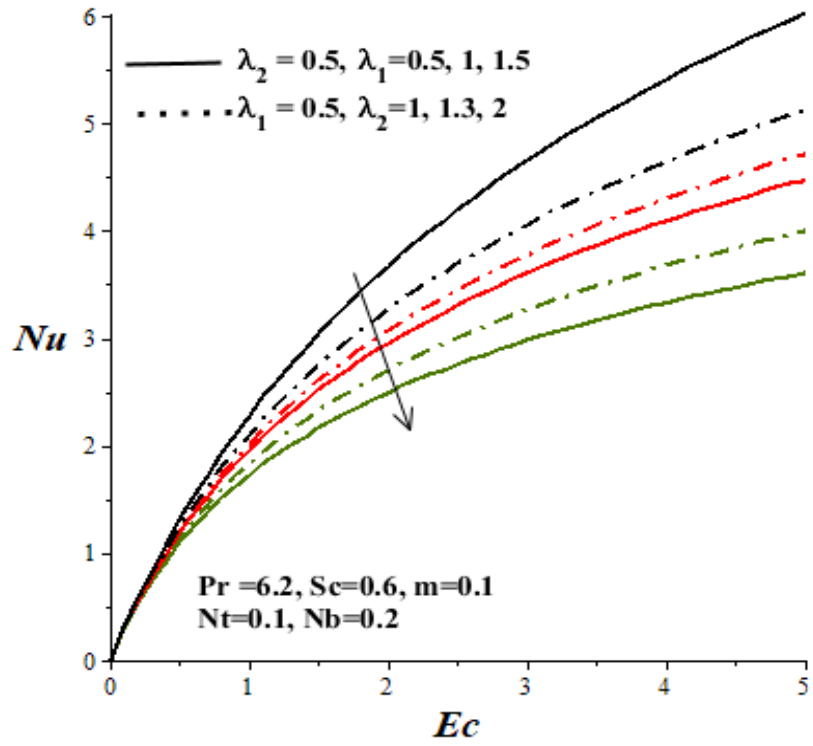


Figure 4.22: Nusselt number with  $Ec, \lambda_1$  and  $\lambda_2$

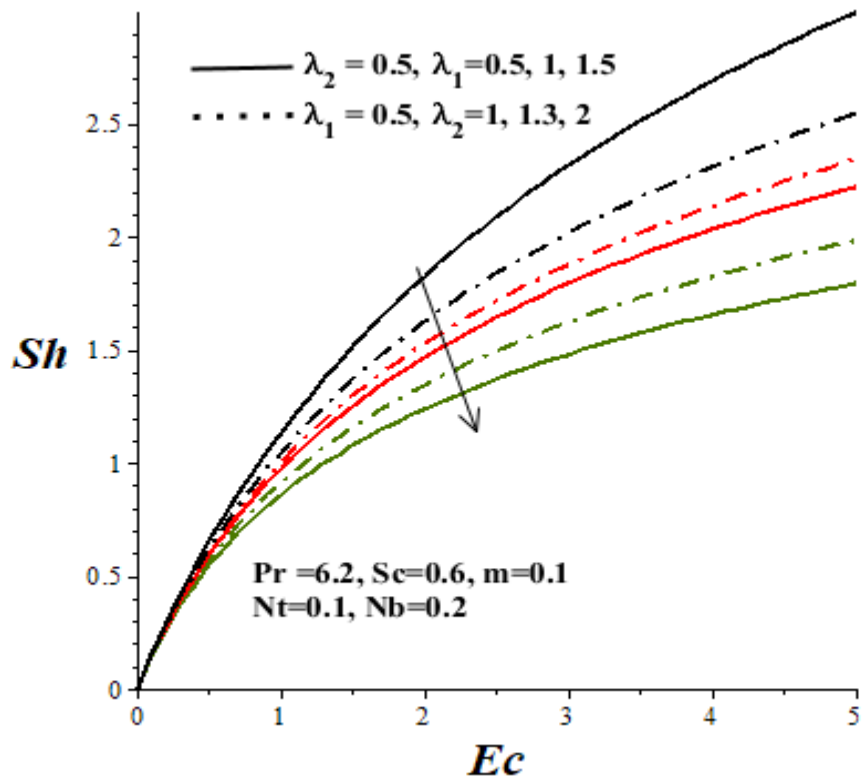


Figure 4.23: Sherwood number with  $Ec, \lambda_1$  and  $\lambda_2$

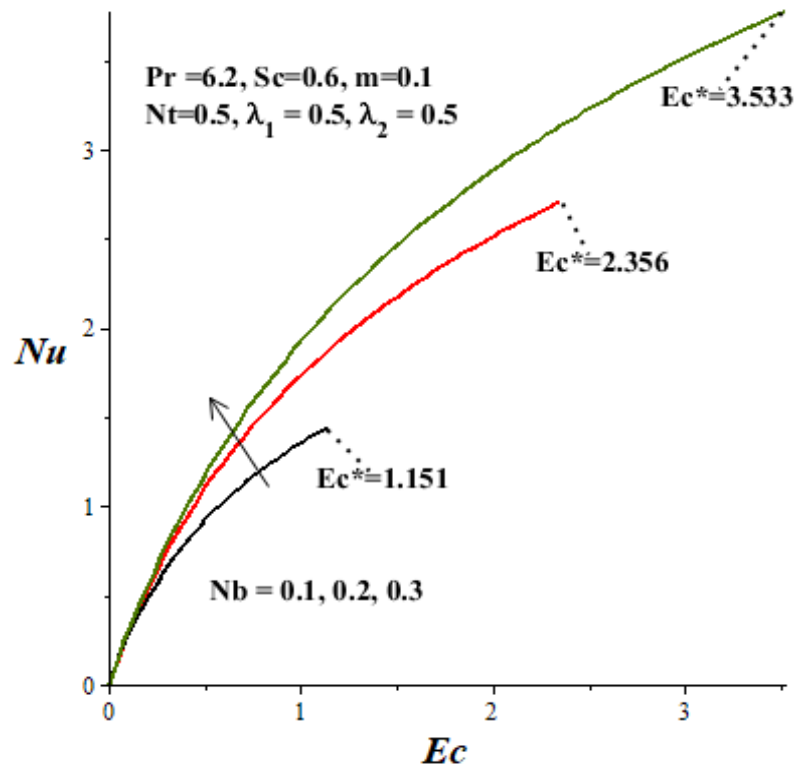


Figure 4.24: Critical Eckert number  $Ec^*$  with  $Nb$

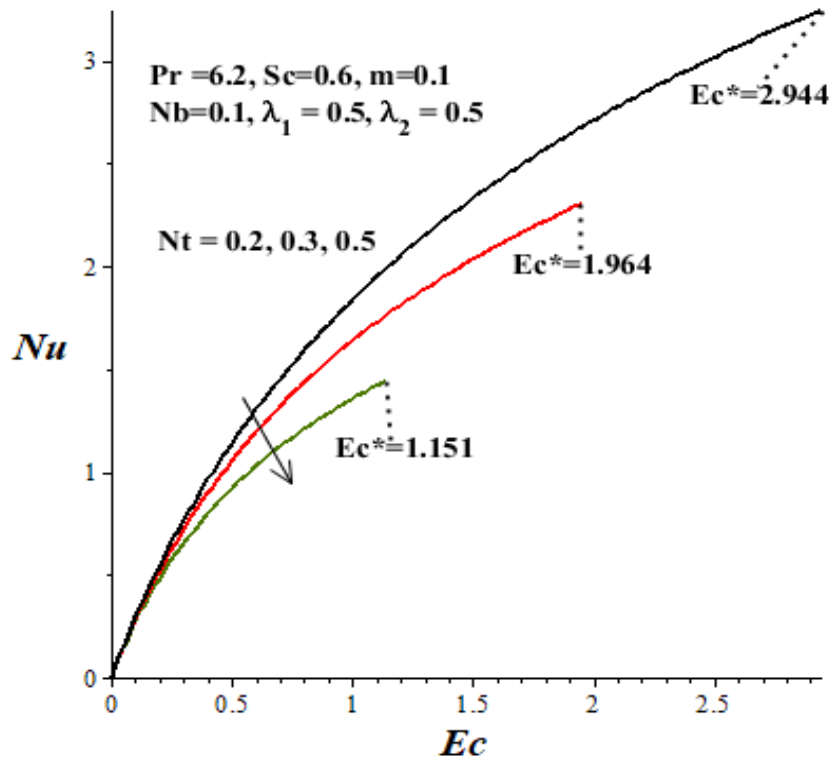


Figure 4.25: Critical Eckert number  $Ec^*$  with  $Nt$

#### 4.4.5 Entropy Generation Rate

The effects of thermophysical parameters on the entropy generation rate are displayed in figures 4.26-4.32. Generally, the entropy production is higher at both the lower fixed plate and the upper moving plate as compared to that of the centreline region. An increase in viscosity variation parameters and Brownian motion activities (see figures 4.26-4.28) lessens the entropy generation rate within the microchannel. Meanwhile, a rise in thermophoresis, viscous dissipation represented by Eckert number, reaction rate and Schmidt number enhances the rate of entropy production in the nanofluid Couette flow process as shown in figures 4.29-4.32.

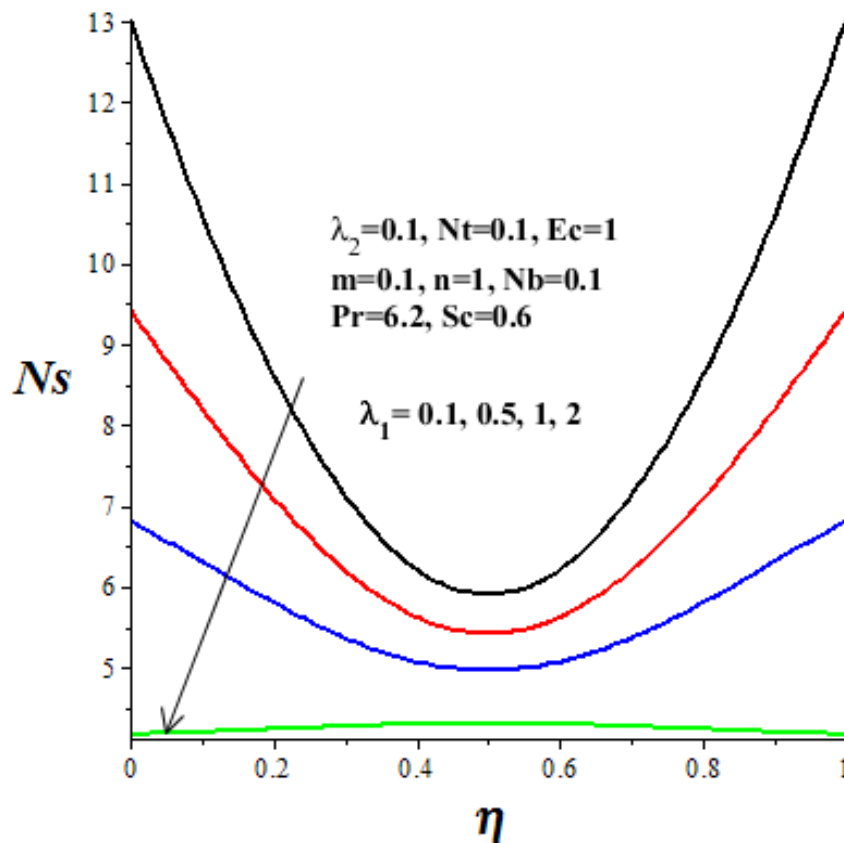


Figure 4.26: Entropy generation rate with  $\lambda_1$



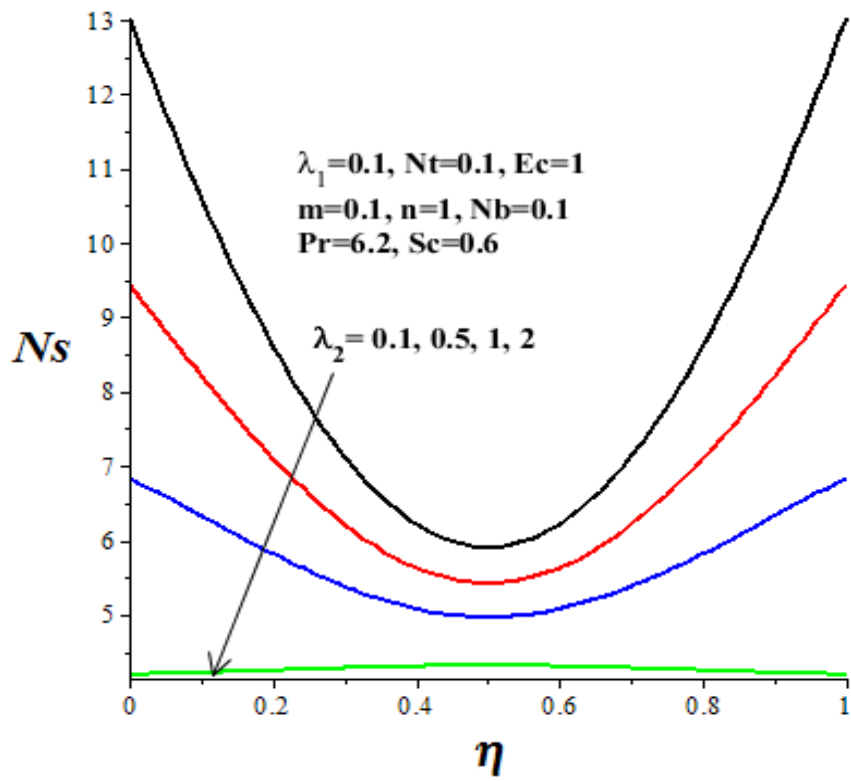


Figure 4.27: Entropy generation rate with  $\lambda_2$

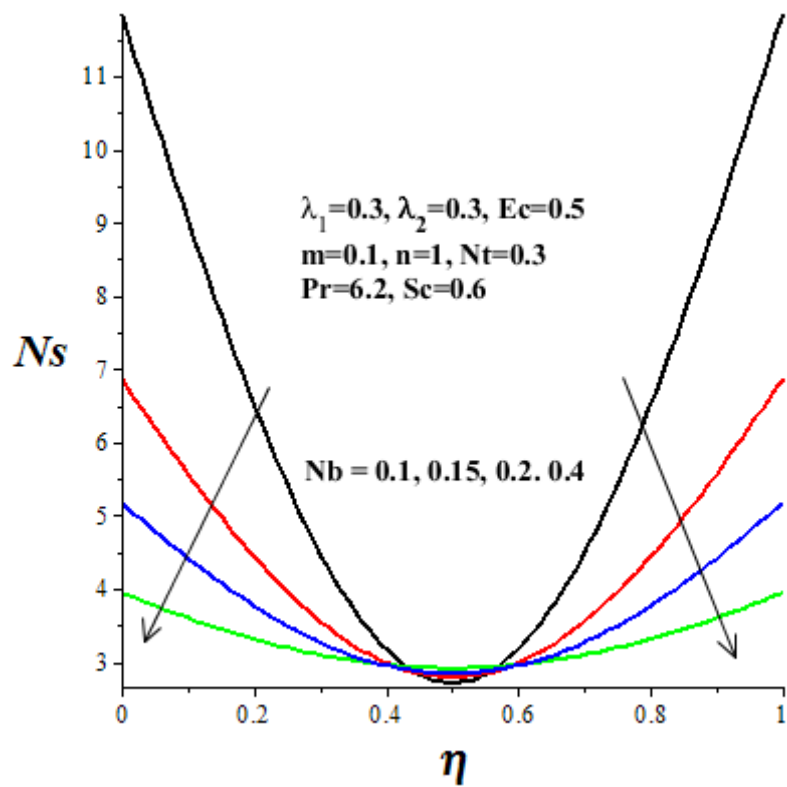


Figure 4.28: Entropy generation rate with  $Nb$

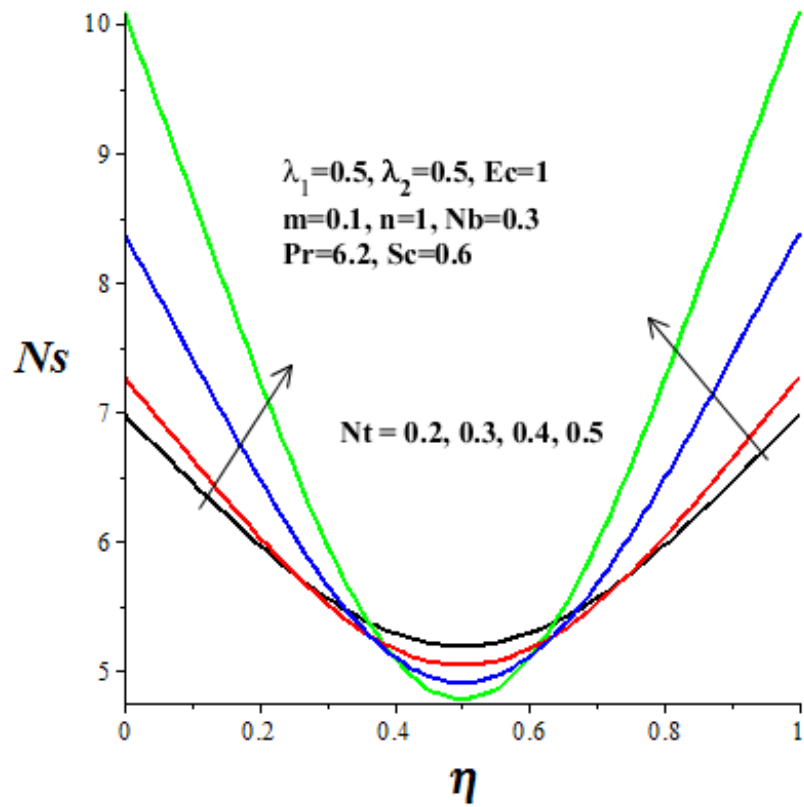


Figure 4.29: Entropy generation rate with  $Nt$

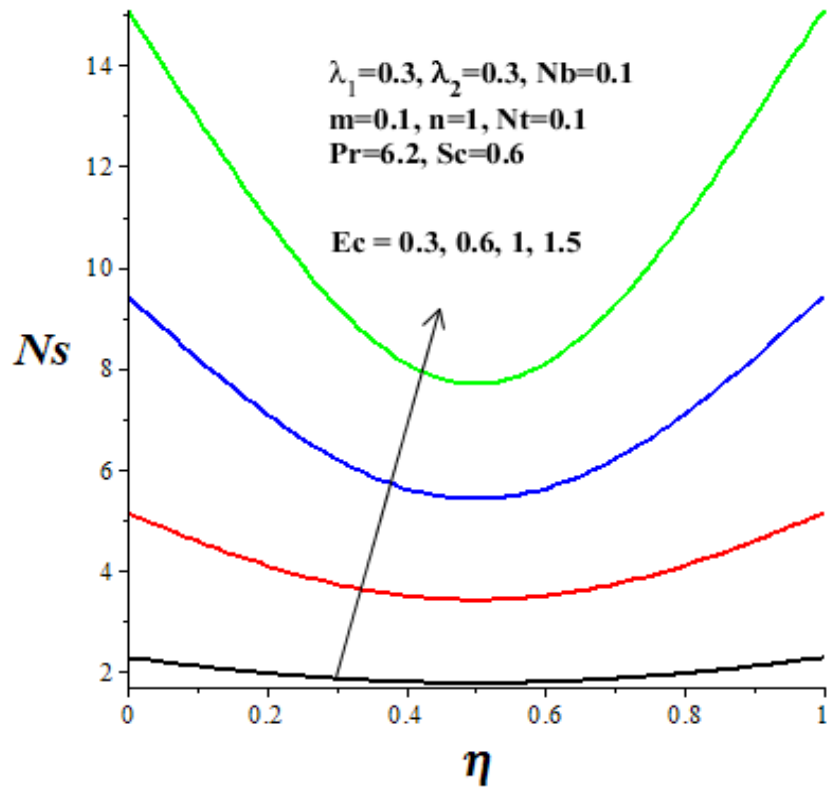


Figure 4.30: Entropy generation rate with  $Ec$

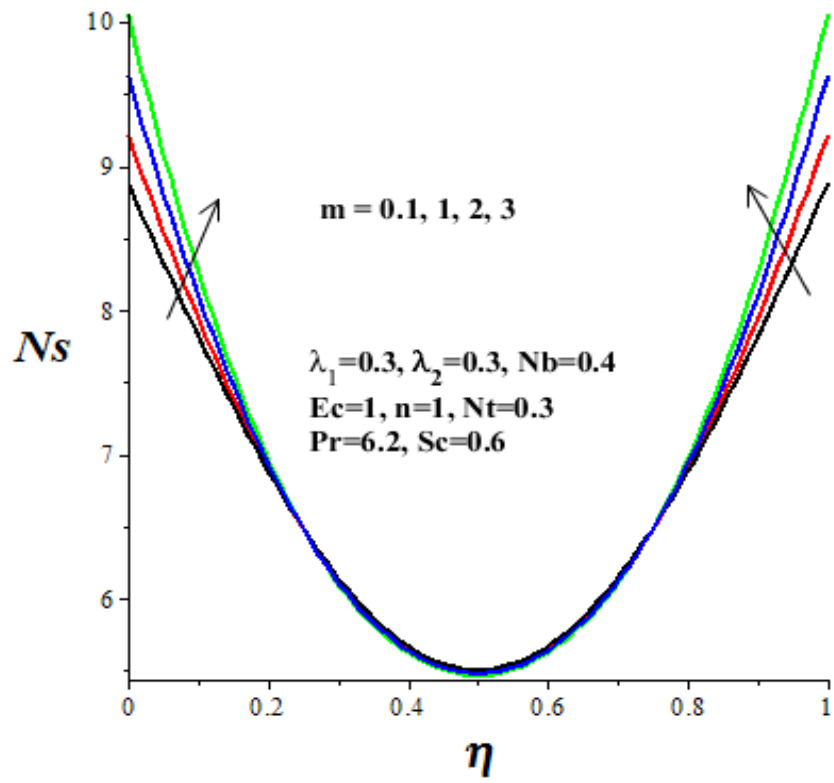


Figure 4.31: Entropy generation rate with  $m$

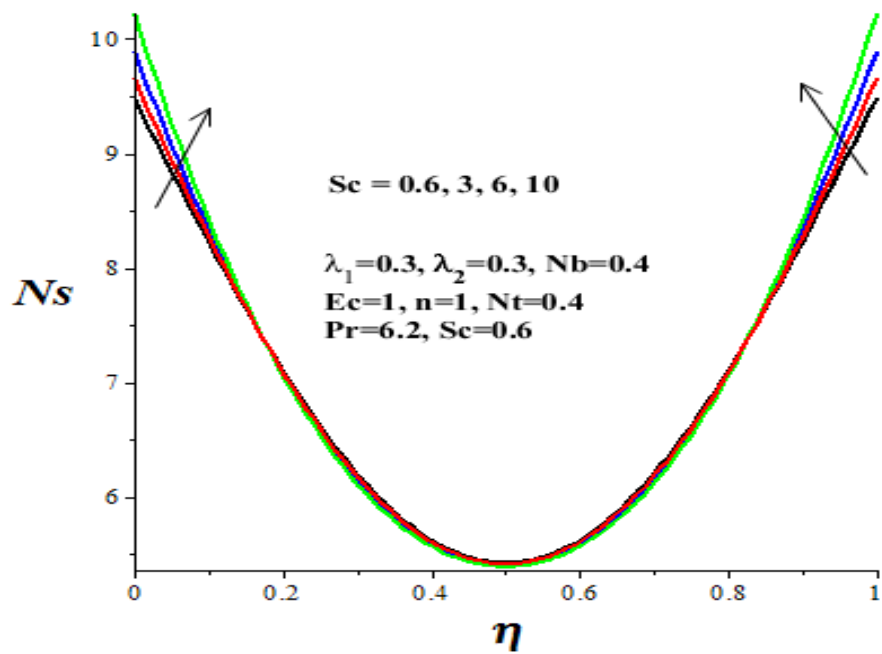


Figure 4.32: Entropy generation rate with  $Sc$

#### 4.4.6 Bejan Number

Figures 4.33-4.39 reveal the effects of various parameters on the Bejan number. From these figures, it is interesting to note the dominant effects of heat transfer irreversibility at both fixed and moving plates while the fluid friction irreversibility completely dominates the channel core region. A rise in the value of viscosity variation parameters  $\lambda_1$ ,  $\lambda_2$  and the thermophoresis parameter  $Nt$  lessens the strength of heat transfer irreversibility at both fixed and moving plate region as shown figures 4.33-4.35. In figures 4.36-4.39, the value of Bejan number escalates near the two plates with increasing values on Brownian motion ( $Nb$ ), Eckert number ( $Ec$ ), reaction parameter ( $m$ ) and Schmidt number ( $Sc$ ). Consequently, the effect of heat transfer irreversibility is absolute near both the fixed and moving plates. However, fluid friction irreversibility still dominates entropy production within the microchannel core region.

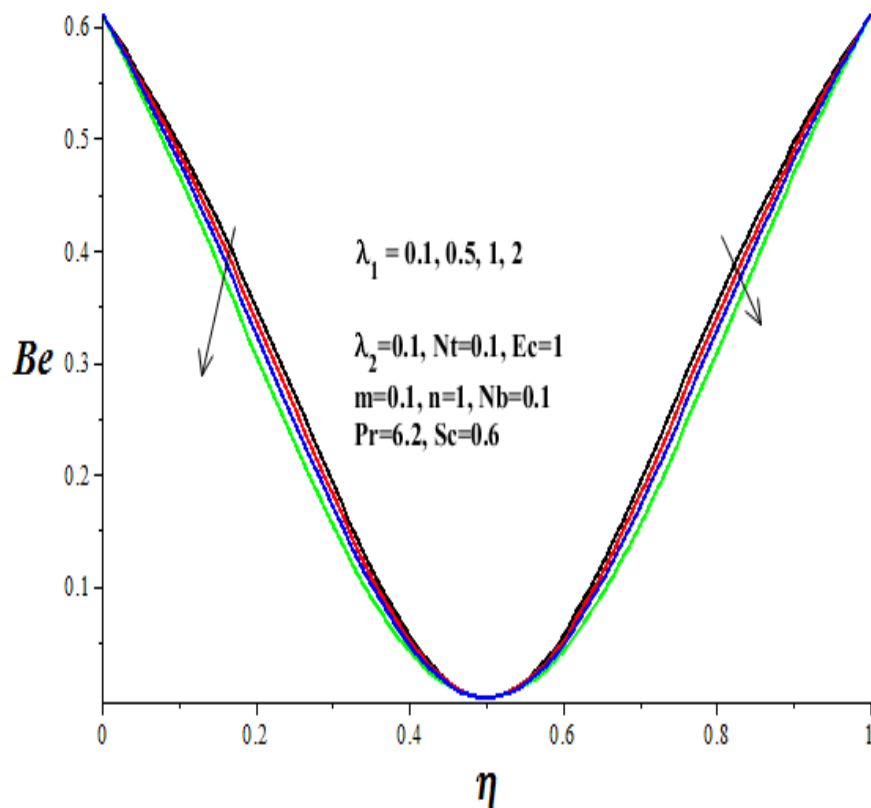


Figure 4.33: Bejan number with increasing  $\lambda_1$

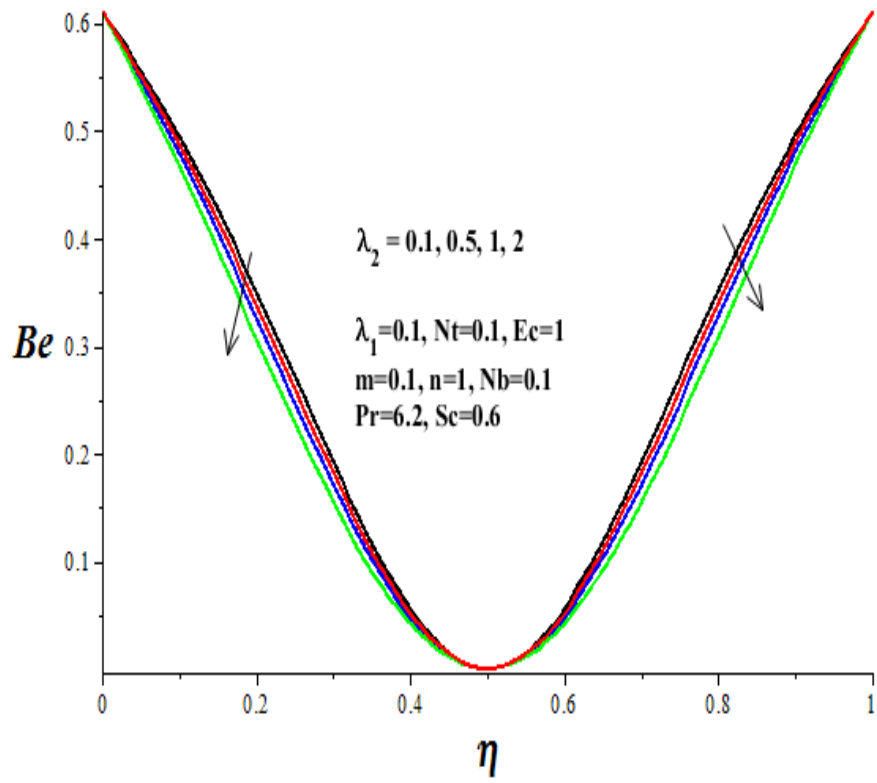


Figure 4.34: Bejan number with increasing  $\lambda_2$

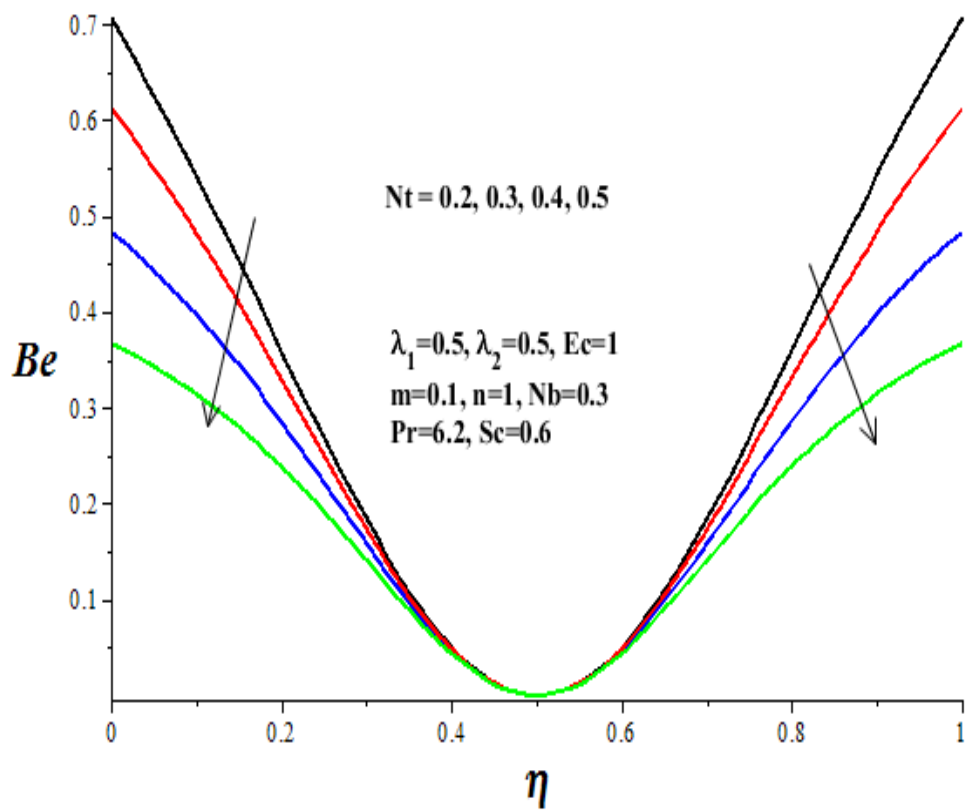


Figure 4.35: Bejan number with increasing  $Nt$

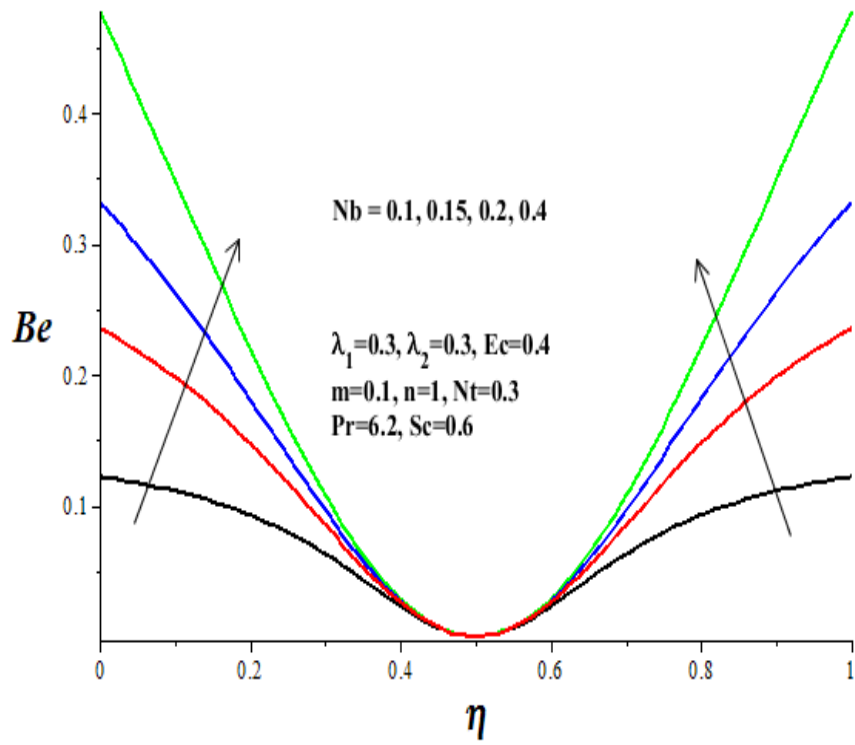


Figure 4.36: Bejan number with increasing Nb

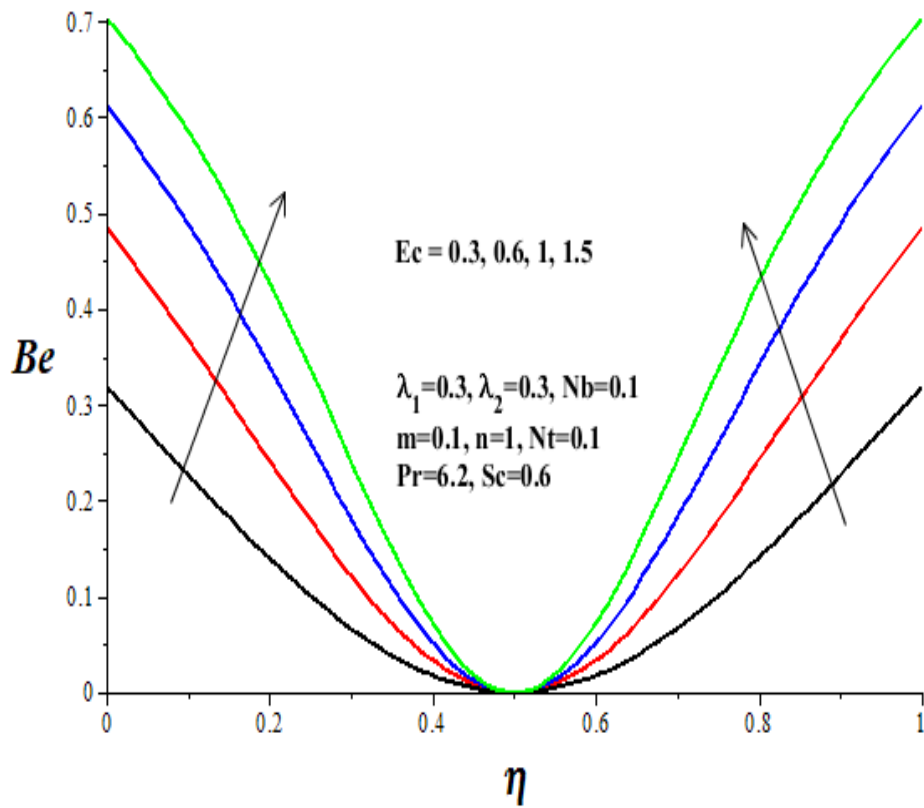


Figure 4.37: Bejan number with increasing Ec

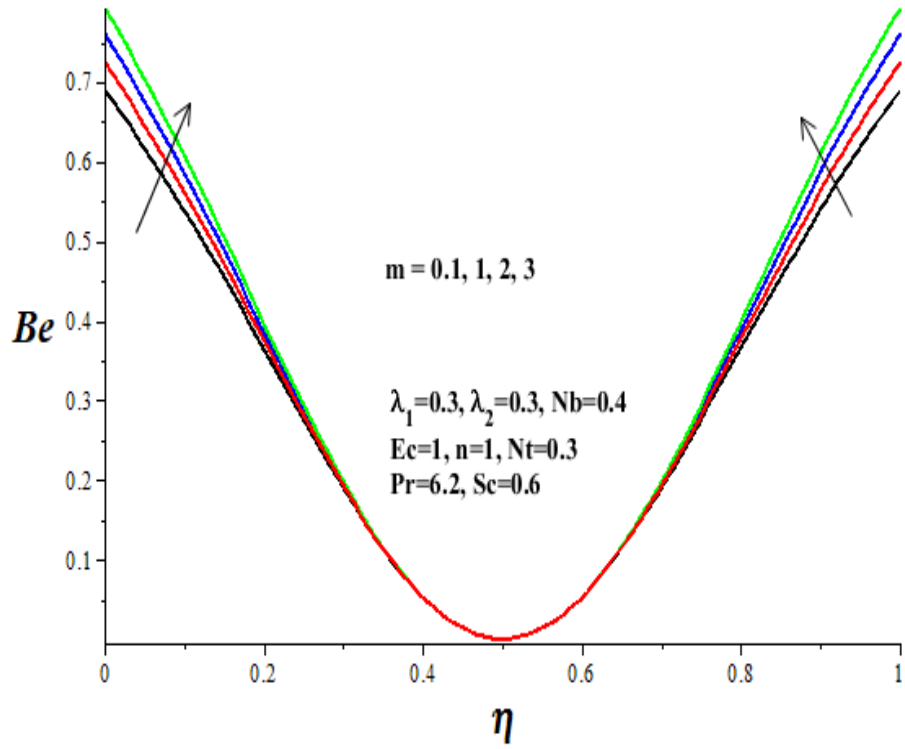


Figure 4.38: Bejan number with increasing  $m$

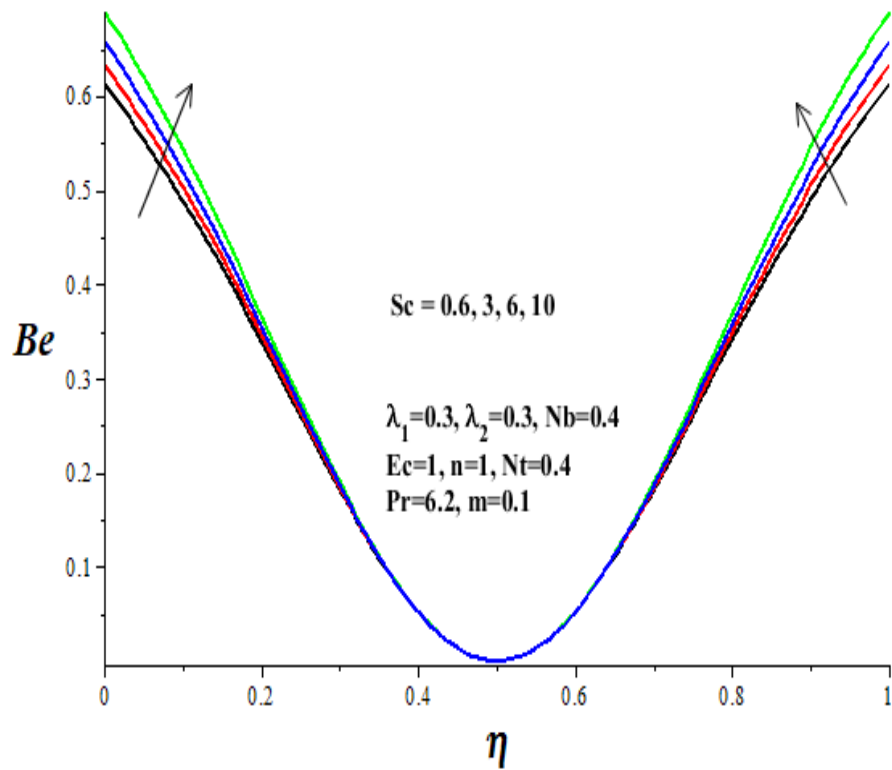


Figure 4.39: Bejan number with increasing  $Sc$

## 4.5 Conclusions

In this study, the inherent irreversibility for Buongiorno model of a reactive variable viscosity nanofluid Couette flow in a microchannel has been investigated numerically using shooting method coupled with Runge-Kutta-Fehlberg integration scheme. Pertinent results can be summarized as follows:

- An increase in  $Ec$ ,  $Nt$ ,  $\lambda_1$ ,  $\lambda_2$  enhances the velocity near the moving upper plate but decreases the velocity near the lower fixed plate.

Meanwhile as  $Nb$  increases, the velocity declines near the moving plate but increases near the fixed plate. It is interesting to note that a turning point occurs in the velocity profiles at the microchannel centreline.

- Generally, the nanofluid temperature is highest along the microchannel centreline and minimum at the walls. The temperature drops with increasing values of  $Nt$ ,  $\lambda_1$ ,  $\lambda_2$  but rises with increasing values of  $Nb$ ,  $m$ ,  $Ec$  and  $Sc$ .
- The nanoparticles concentration is lowest along the microchannel centreline and highest at the walls. Moreover, an increase in  $Sc$ ,  $m$ ,  $Nb$ ,  $\lambda_1$ ,  $\lambda_2$  enhances the nanoparticles concentration across the microchannel, while an increase in  $Ec$  and  $Nt$  lessens the concentration.
- The skin friction, Nusselt number and Sherwood number diminish with an increasing values of  $Ec$ ,  $\lambda_1$  and  $\lambda_2$ . In addition, an increase in  $Nb$  and  $Ec$  boosts the Nusselt number while an increase in  $Nt$  lowers the Nusselt number. Interestingly, a critical Eckert number  $Ec^*$  exist such that for  $0 \leq Ec \leq Ec^*$  the flow is thermally stable and for  $Ec > Ec^*$ , the flow is thermally unstable.
- It is noteworthy that the flow thermal stability is enhanced with increasing values of  $Nb$  and  $m$  while an increase in  $Nt$ ,  $\lambda_1$ ,  $\lambda_2$  and  $Sc$  expedite thermal instability in the flow field.



- Entropy production is more pronounced at the walls and less along the microchannel core region. However, an increase in  $Ec$ ,  $Nt$ ,  $m$ ,  $Sc$ , expedites entropy generation rate while an increase in  $Nb$ ,  $\lambda_1$ ,  $\lambda_2$  lessens the entropy production.
- Generally, Bejan number is highest at the walls with dominant effect of heat transfer irreversibility and lowest along the microchannel core region with dominant effects of fluid friction and nanoparticles concentration irreversibility. An increase in  $Ec$ ,  $Nb$ ,  $m$ ,  $Sc$ , expedites domination of heat transfer irreversibility near the walls by increasing Bejan number, while an increase in  $Nt$ ,  $\lambda_1$ ,  $\lambda_2$  lessens the Bejan number and heightens fluid friction and nanoparticles concentration irreversibility effects.

Finally, the rise in entropy production and thermal instability due to thermophoresis activities during Couette flow of nanofluid may be detrimental to efficient operation. However, with appropriate regulation of the emerging thermophysical processes such as Brownian motion, this challenge can be easily overcome for optimum performance.

## CHAPTER 5

# MODELLING NANOPARTICLES DISTRIBUTION PATTERN IN A MICROCHANNEL FLOW OF NANOFLUID FILLED WITH A POROUS MEDIUM<sup>4</sup>

### ABSTRACT

In this paper, a modified Buongiorno model is proposed and utilized to examine the nanoparticles distribution pattern in a nanofluid flow through a microchannel filled with a porous medium. The governing nonlinear differential equations are obtained and tackled numerically by using shooting method coupled with Runge-Kutta-Fehlberg integration scheme. Graphical results showing the effects of the pertinent parameters on the nanofluid velocity, nanoparticles concentration, skin friction and Sherwood number are presented and discussed quantitatively. It is found that nanoparticles tend to aggregate with high concentration along the microchannel centreline region, thus, lessens the skin friction and boosts the Sherwood number.

### 5.1 Introduction

Microfluidics has become an emerging science and technology of systems that process nano-sized fluid materials using channels with dimensions of tens to hundreds of micrometres [128-130]. Adequate knowledge of fluid flows in microchannels is crucial for the effective control of dynamic effects associated with transport phenomena such as momentum, heat and mass transfer for different applications in micro-system technology. Moreover, the enormously small aspect ratio characteristics of microchannels offer a veritable platform for enhanced flow rate with heat and mass transfer processes such as the transportation of fluids for chemical or biological processing, micro-mixing of different fluids or separating different species and micro-scaled cooling systems of electronic devices [131, 132]. Meanwhile, it is reported that the surface contact area to-volume ratio of the flow is enhanced by incorporating porous media into the microchannels [104, 105].

---

<sup>4</sup> This chapter is based on the research paper: O.D. Makinde and R. L. Monaledi. Modelling Nanoparticles Distribution Pattern in a Microchannel Flow of Nanofluid Filled with a Porous Medium. Num. Com. Meth. Sci. Eng., 1 No. 3, 111- 116 (2019)

Consequently, the embedment of porous media in microchannels will further improve the local velocity mixing of working fluid and provide a high-mass-flux removal method in miniaturized devices. Recently, the advancement in the field of nanotechnology has led to the advent of a new generation of coolants known as nanofluids [1, 85]. It is engineered by colloidal suspensions of functionalized nano-sized particles composite materials into the base fluid. Some typical nanofluids are ethylene glycol based copper or silver nanofluids and water based copper oxide or iron oxide nanofluids [101, 127]. In spite of the existence of numerous experimental and theoretical investigations [99, 133-135] on micro-porous channel hydrodynamics of nanofluids, a number of principal problems are not well studied especially with respect to the impact of nanoparticles distribution pattern on flow rate and mass flux. In the present studies, the objective is to fill this gap by theoretically examining the combined effects of porous medium permeability and nanoparticles distribution pattern on both flow rate and mass transfer rate in a micro-porous channel. In the following sections, the model problem is formulated, analysed and numerically tackled. Pertinent results for the velocity and nanoparticles concentration profiles as well as the skin friction and Sherwood number are obtained. Effects of various physical parameters are displayed graphically and discussed.

## 5.2 Model Problem

The modified Buongiorno [85] model for a Poiseuille flow of an incompressible nanofluid with variable viscosity in a microchannel filled with a porous medium is considered as shown in figure 5.1. The flow takes place in the  $x$  - direction between two parallel plates of small width  $h$  and very long length  $L$ .

Following [102], the nanoparticle concentration dependent nanofluid dynamic viscosity ( $\mu_{nf}$ ) can be expressed as

$$\mu_{nf} = \frac{\mu_f (C_s - C_w)^{2.5}}{(C_s - C)^{2.5}} \quad (5.1)$$

where  $C_s$  is the total concentration of nanoparticles such that  $C_w < C \ll C_s$ ,  $\mu_f$  is the base fluid dynamic viscosity,  $C_w$  is the nanoparticles concentration at the microchannel walls and  $C$  is the nanofluid concentration.

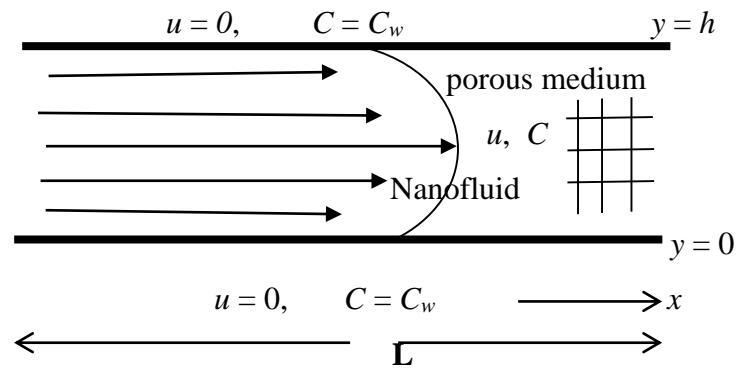


Figure 5.1: Schematic diagram of the problem

Under these conditions, the continuity, momentum and nanoparticles concentration equations governing the problem may be written as [99, 127, 134-135];

$$\frac{\partial u}{\partial x} = 0 \quad (5.2)$$

$$\frac{\partial}{\partial y} \left( \mu_{nf} \frac{\partial u}{\partial y} \right) - \frac{\mu_{nf} u}{K} - \frac{\partial P}{\partial x} = 0, \quad (5.3)$$

$$D_B \frac{\partial^2 C}{\partial y^2} + \gamma(C_s - C) = 0 \quad (5.4)$$

with the boundary conditions given as

$$\left. \begin{array}{l} u = 0, \quad C = C_w, \quad \text{at } y = 0 \\ u = 0, \quad C = C_w, \quad \text{at } y = \square \end{array} \right\} \quad (5.5)$$

where  $D_B$  is the nanoparticles mass diffusivity,  $\rho_f$  is the base fluid density,  $P$  is the nanofluent pressure,  $\gamma$  relates to the source rate of nanoparticles into the nanofluent.

We introduce the following non-dimensional quantities in equations (5.2) - (5.5):

$$\eta = \frac{y}{h}, W = \frac{uh}{\nu_f}, \phi = \frac{C - C_w}{C_s - C_w}, \nu_f = \frac{\mu_f}{\rho_f}, \lambda = \frac{\gamma h^2}{\nu_f}, \quad (5.6)$$

$$A = -\frac{\partial \bar{P}}{\partial X}, \bar{P} = \frac{\rho_f h^2 P}{\mu_f^2}, X = \frac{x}{h}, Sc = \frac{\nu_f}{D_B}, Da = \frac{K}{h^2},$$

and obtain

$$\frac{d^2 W}{d\eta^2} + \frac{5}{2(1-\phi)} \frac{dW}{d\eta} \frac{d\phi}{d\eta} - \frac{W}{Da} + A(1-\phi)^{\frac{5}{2}} = 0 \quad (5.7)$$

$$\frac{d^2 \phi}{d\eta^2} + Sc\lambda(1-\phi) = 0 \quad (5.8)$$

with boundary conditions given as

$$\left. \begin{aligned} W(0) = \phi(0) = 0, \\ W(1) = \phi(1) = 0, \end{aligned} \right\} \quad (5.9)$$

where A corresponds to the constant axial pressure gradient, Sc is the Schmidt number, Da is the Darcy number and  $\lambda$  is the parameter that relates to the rate of injection of nanoparticles into the base fluid. Other quantities of interest are the skin friction coefficients ( $C_f$ ) and the Sherwood number ( $Sh$ ) which are given as

$$C_f = \frac{h^2 \tau_w}{\rho_f \nu_f^2} = \frac{dW}{d\eta} \Big|_{\eta=0,1}, \quad (5.10)$$

$$Sh = \frac{hq_m}{D_B(C_1 - C_w)} = -\frac{d\phi}{d\eta} \Big|_{\eta=0,1}, \quad (5.11)$$

Where

$$\tau_w = \mu_{nf} \frac{\partial u}{\partial y}, \quad q_m = -D_B \frac{\partial C}{\partial y}. \quad (5.12)$$

### 5.3 Numerical Procedure

The nonlinear model boundary value problem in equations (5.7)-(5.9) are transformed into a set of first order ordinary differential equations with some unknown initial conditions and tackled numerically using shooting method with Runge-Kutta-Fehlberg integration scheme [103]. Let

$$W = y_1, W' = y_2, \phi = y_3, \phi' = y_4. \quad (5.13)$$

The governing equations then become

$$\left. \begin{aligned} y_1' &= y_2 \\ y_2' &= -\frac{5y_2y_4}{2(1-y_3)} + \frac{y_1}{Da} - A(1-y_3)^{\frac{5}{2}} \\ y_3' &= y_4 \\ y_4' &= Sc\lambda(y_3-1) \end{aligned} \right\} \quad (5.14)$$

with the corresponding initial conditions as

$$y_1(0) = 0, y_2(0) = a_1, y_3(0) = 0, y_4(0) = a_2 \quad (5.15)$$

The values of  $a_1$  and  $a_2$  in the equation (5.14) are initially guessed and thereafter accurately determined via shooting method with Newton-Raphson's iteration technique for each set of parameter values in equation (5.13) with step size of  $\Delta\eta=0.01$ . Solutions obtained for the velocity and nanoparticles concentration profiles are utilized to compute the values for the skin friction and Sherwood number as given in equation (5.10) and equation (5.11).

### 5.4 Results and Discussion

In order to gain an insight into the overall flow structure with mass transfer characteristics, numerical solution for the velocity and nanoparticles concentration profiles are presented graphically in figures 5.2-5.6. We also compute the results for the skin friction ( $C_f$ ) and Sherwood number (Sh) as depicted in figures 5.7-5.9. Generally, the velocity profiles as illustrated in figures 5.2-5.4 are parabolic with maximum value along the microchannel centreline region and zero at the walls due to no slip condition. It is noteworthy that an increase

in the Darcy number ( $Da$ ) enhances the nanofluid velocity due to an enlarged permeability of the porous media (see figure 5.2). Meanwhile, the velocity profiles lessens with a rise in the parameter values of  $Sc$  and  $\lambda$ . This can be attributed to the thickening of the nanofluid due to increasing concentration of nanoparticles, consequently, the nanofluid viscosity rises and the flow rate diminishes as depicted in figures 5.3-5.4.

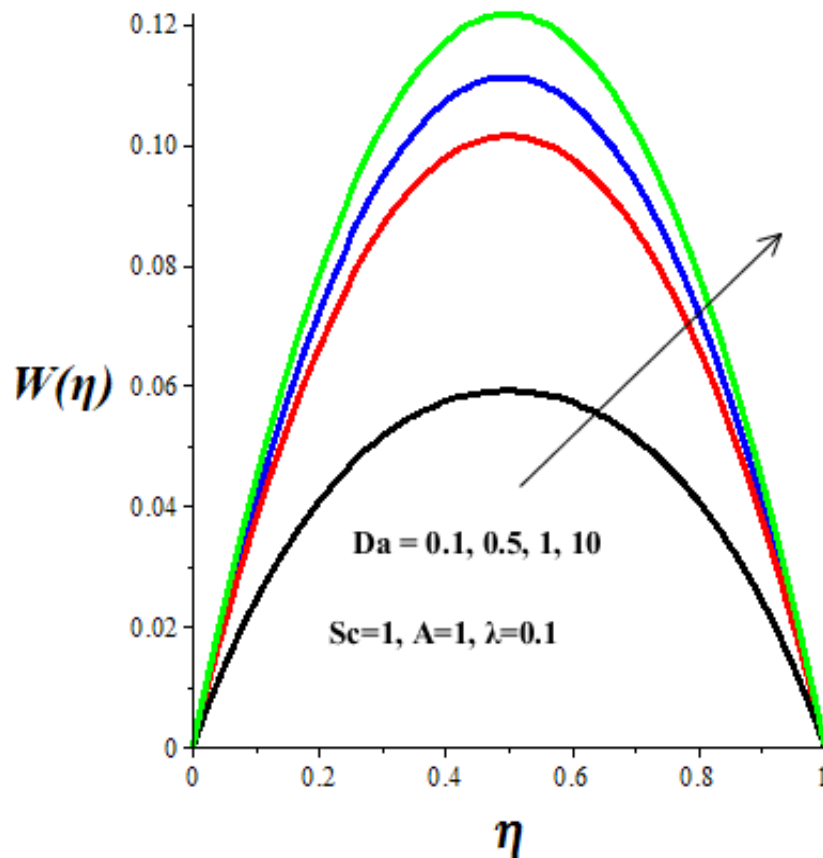


Figure 5.2: Effect of  $Da$  on velocity profiles

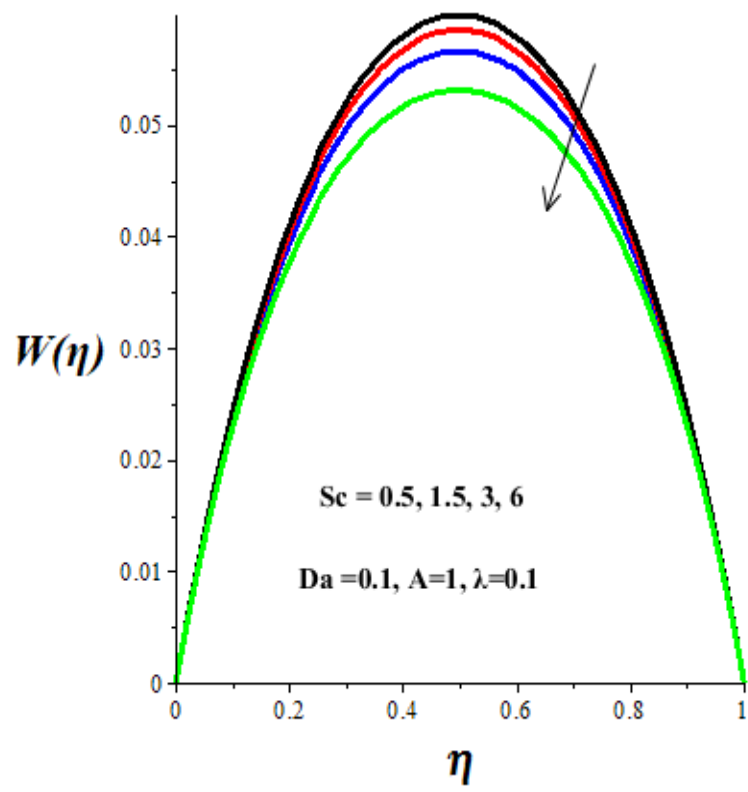


Figure 5.3: Effect of  $Sc$  on velocity profiles

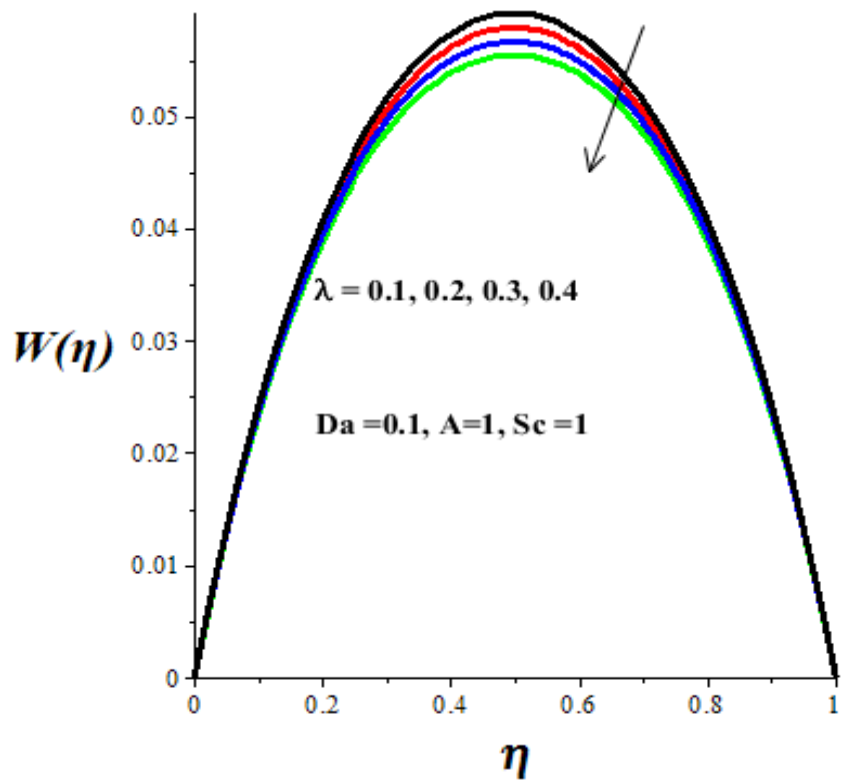


Figure 5.4: Effect of  $\lambda$  on velocity profiles



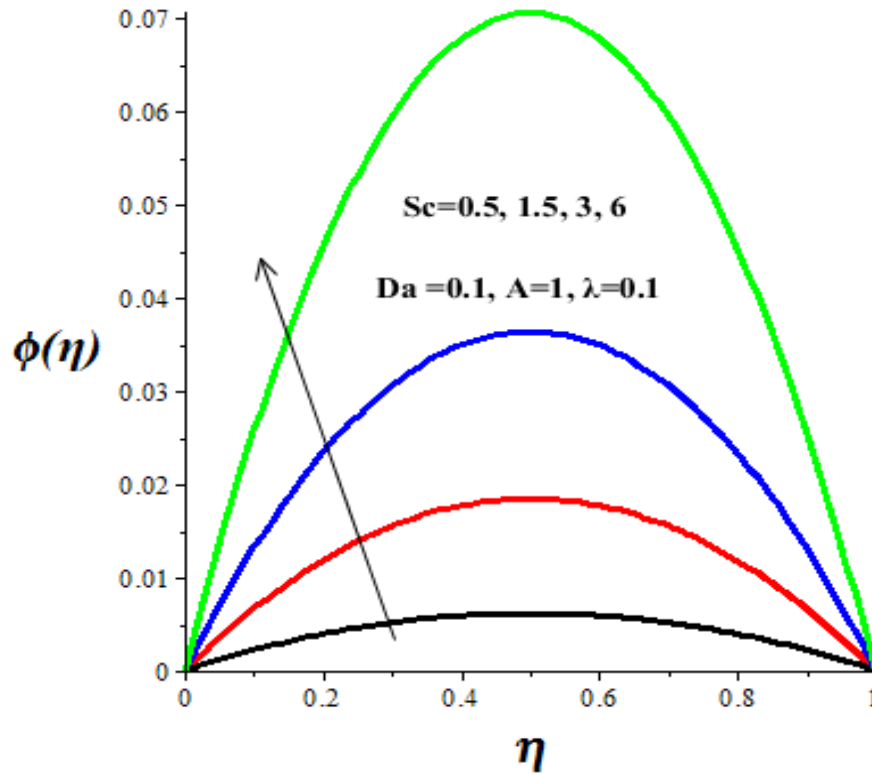


Figure 5.5: Nanoparticles concentration profiles with Sc

In figures 5.5-5.6, we observed that nanoparticles tend to aggregate more towards the microchannel centreline region with high concentration as compared to the wall region. Moreover, this distribution pattern of nanoparticles is enhanced with an amplification in the parameter values of Sc and  $\lambda$ . This is expected, since an increase in the values Sc and  $\lambda$  implies more injection of nanoparticles into the base fluid, leading to a rise in the concentration of nanoparticles towards the microchannel centreline region.

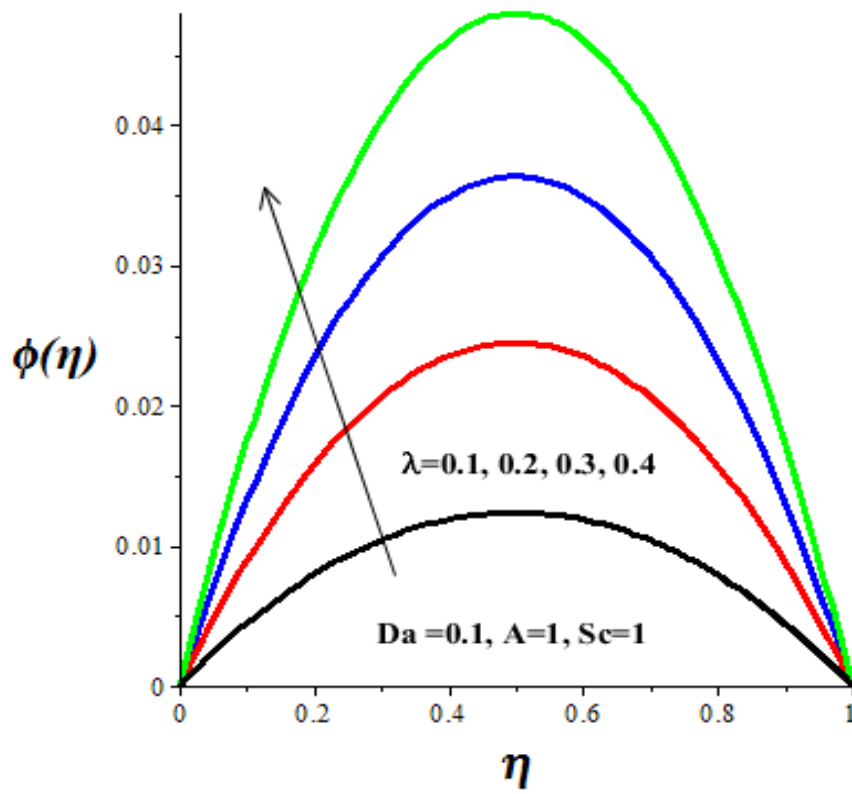


Figure 5.6: Nanoparticles concentration profiles with  $\lambda$

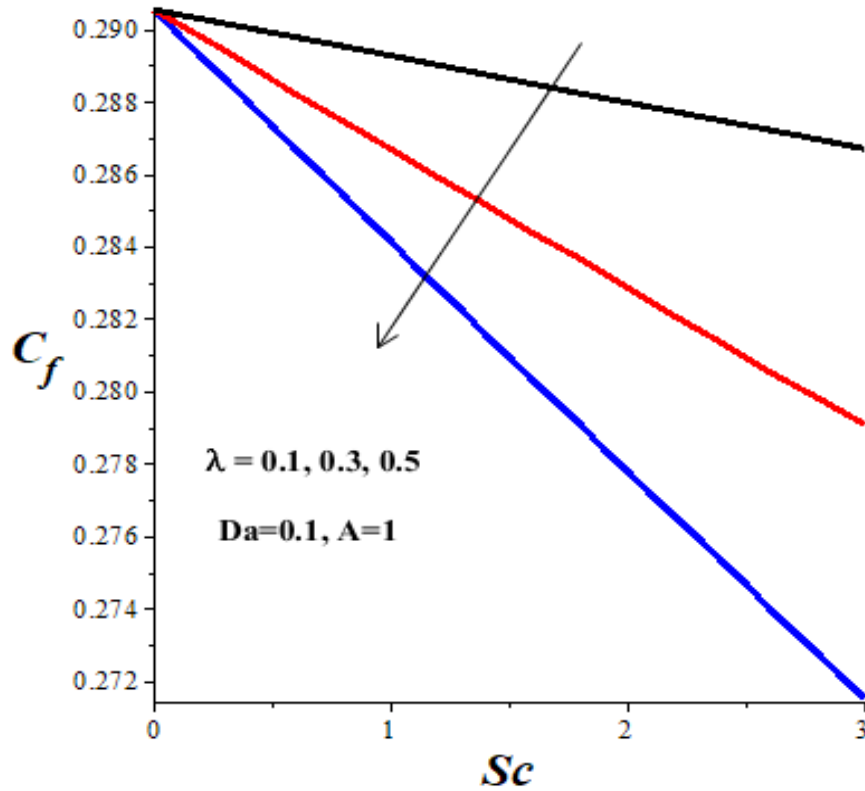


Figure 5.7: Skin friction with  $Sc$  and  $\lambda$

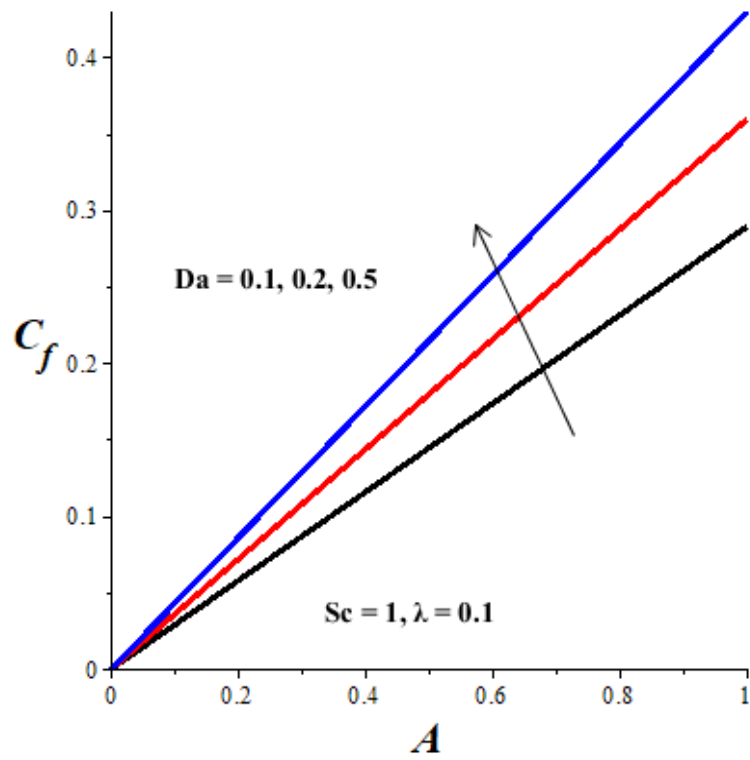


Figure 5.8: Skin friction with  $A$  and  $Da$

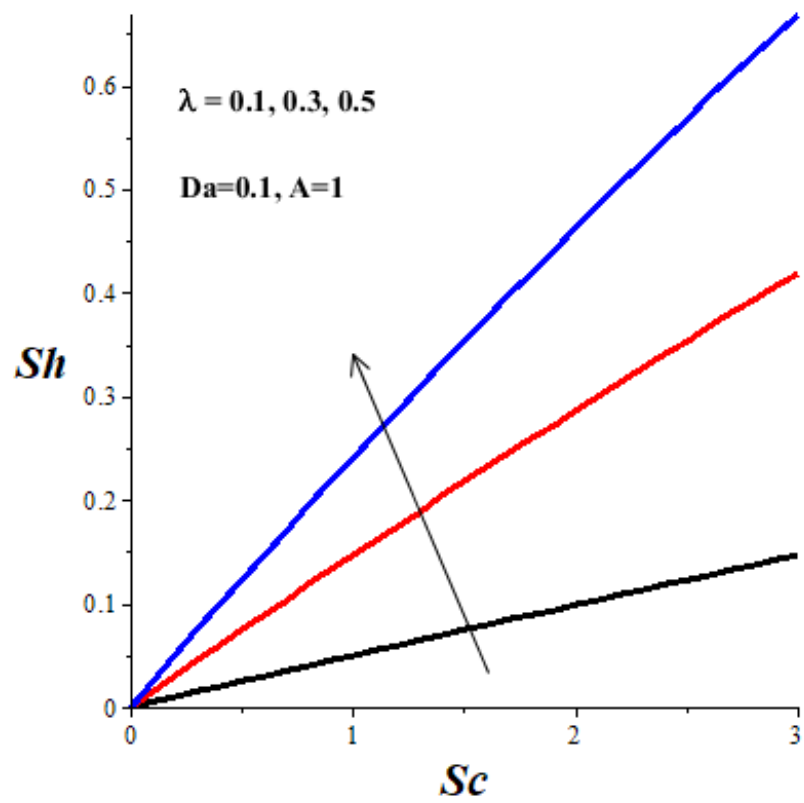


Figure 5.9: Sherwood number with  $Sc$  and  $\lambda$

Figures 5.7-5.8 show that the shear stress (skin friction) at the microchannel wall lessens with a rise in parameter values of  $Sc$  and  $\lambda$ , but escalates with an increase in parameter values of  $A$  and  $Da$ . Since the nanofluid viscosity is augmented with increasing values of  $Sc$  and  $\lambda$ , consequently, velocity gradient at the wall is diminished, leading to a fall in skin friction. Meanwhile, as  $A$  and  $Da$  values increase, the velocity gradient at the wall is enhanced, leading to skin friction amplification. In figure 5.9, it is seen that nanoparticles mass transfer rate at the wall increases with both  $Sc$  and  $\lambda$ . This is expected since the injection of nanoparticles into the base fluid rises with increased values of  $Sc$  and  $\lambda$ , leading to a boost in the nanoparticles concentration gradient at the wall and enhanced Sherwood number.

## 5.5 Conclusions

In this study, variable viscosity nanofluid Poiseuille flow in a microchannel filled with a porous medium has been investigated numerically using shooting method coupled with Runge-Kutta-Fehlberg integration scheme. Pertinent results can be summarized as follows:

- Increase in  $Sc$  and  $\lambda$  lessen the velocity profiles but enhance the nanoparticles concentration profiles.
- Increase in  $Da$  boosts the velocity profiles.
- Nanoparticles tend to aggregate more towards the microchannel centreline region as compare to the wall region
- Skin friction diminishes with a rise in  $Sc$  and  $\lambda$ , but amplifies with an increase in  $A$  and  $Da$ .
- Increase in  $Sc$  and  $\lambda$  boost the Sherwood number.

Finally, it is worth mentioning that the observed distribution pattern of nanoparticles with high concentration along the microchannel centreline region augments the efficient flow process through the reduction of the skin friction and enhancement of the Sherwood number.

## CHAPTER 6

# ENTROPY GENERATION ANALYSIS IN A MICROCHANNEL POISEUILLE FLOWS OF NANOFLUID WITH NANOPARTICLES INJECTION AND VARIABLE PROPERTIES<sup>5</sup>

### ABSTRACT

In this study, a more realistic modified Buongiorno's nanofluid model is proposed and utilized to examine the impact of nanoparticles injection and distribution on inherent irreversibility in a microchannel Poiseuille flow of nanofluid with variable properties. The governing nonlinear differential equations are obtained and tackled numerically using shooting method coupled with Runge-Kutta-Fehlberg integration scheme. Graphical results showing the effects of the pertinent parameters on the nanofluid velocity, temperature, nanoparticles concentration, skin friction, Nusselt number, Sherwood number, entropy generation rate and Bejan number are presented and discussed quantitatively. It is found that the aggregation of nanoparticles toward the microchannel centreline region lessens the skin friction and boosts the heat and mass transfer rate. While thermophoresis of mobile nanoparticles escalates entropy production rate, nanoparticles injection with the Brownian motion lessens it.

### 6.1 Introduction

Heat transfer seems to pervade all aspects of engineering systems and efficient management of heat transfer process may enhance new product development, create a saving in energy, reduce process time, raise thermal rating and lengthen the working life of the equipment. The advent of nanotechnology in recent time has greatly improved the ability to augment heat transfer processes through an innovative mixture of conventional fluid with nano-sized solid metallic or non-metallic particles (1–100nm diameters) known as nanoparticles. This new type of heat transfer enhancement fluid known as nanofluid was pioneered by Choi [1].

---

<sup>5</sup> This chapter is based on the research paper: R. L. Monaledi and O. D. Makinde: Entropy Generation Analysis in a Microchannel Poiseuille Flows of Nanofluid with Nanoparticles Injection and Variable Properties. Submitted to Journal of Thermal Analysis and Calorimetry, 2020.

The process invariably boosts the thermal conductivity of the convective fluid and its heat transfer capability. Several experimental and theoretical investigations were conducted in order to establish the efficacy of nanofluids in dealing with various heat transfer challenges arising from engineering and industrial processes. An extensive review of combined heat and mass transfer characteristics in nanofluids has been provided by Pang *et al.* [136]. Numerical study of both single and two-phase models of turbulent forced convection of Cu–water nanofluid in a heated tube was performed by Ganesan *et al.* [137]. The effects of thermal buoyancy on nanofluid convection in partially heated rectangular enclosures were numerically studied by Oztop and Abu-Nada [11]. Buongiorno [85] pioneered a two-phase model of convective transport of nanofluids with emphases on the thermophoresis and Brownian motion effects. Makinde and Aziz [138] employed the two phase model to examine the combined effects of thermophoresis and Brownian motion on thermal boundary layer flow of nanofluid problem. Elias *et al.* [83] investigated the impact of nanoparticles shape on the heat transfer enhancement capability of nanofluids. Several other relevant studies have been done on this topic such as [58, 80–81, 90].

The thermodynamic irreversibility in thermal engineering systems is closely associated with the entropy generation rate. An increase in entropy production lessens the system efficiency. Bejan [96] underscored the importance of entropy reduction in convective heat transfer and argued that entropy must be minimized in order to optimize system efficiency. Das *et al.* [101] studied the effects of entropy generation on hybrid nanofluid flow through a porous channel. Monaledi and Makinde [127] examined the impact of thermal radiation, variable viscosity and buoyancy force on thermodynamic irreversibility in EG/Ag nanofluid flow through a microchannel. Mayeli *et al.* [139] numerically investigated the MHD forced convection and entropy generation in a straight duct with walls containing water–Al<sub>2</sub>O<sub>3</sub> nanofluid.

The effects of magnetic field and thermal radiation on the entropy production in a non-Newtonian nanofluid flow through a permeable channel were reported by Makinde and Eegunjobi [99]. Abbaszadeh *et al.* [140] investigated the effects of magnetic field on entropy generation rate in CuO–water nanofluid flow in a slippery microchannel with temperature jump. Recently, Monaledi and Makinde [141] numerically studied the combined effects of thermal radiation and variable viscosity on entropy production rate in Cu–H<sub>2</sub>O nanofluid under Couette flow scenario.

From the literature survey, it is observed that the impact of nanoparticles injection and distribution on entropy generation rate in a microchannel Poiseuille flow of variable properties nanofluid with Brownian motion and microscopic thermophoresis effects are not studied yet. Hence, the present work aims to fill this gap in literature by considering a more realistic modified Buongiorno's nanofluid two-phase model with variable viscosity and thermal conductivity due to temperature and nanoparticles injection rate. In the following sections, the model problem is formulated, analysed and solved. Pertinent results for the velocity, temperature and nanoparticles concentration profiles as well as the skin friction, Nusselt number, Sherwood number and the flow thermal stability condition are obtained. The effects of various thermophysical parameters are presented graphically and discussed quantitatively.

## 6.2 Model Problem

The modified Buongiorno model for a Poiseuille flow of an incompressible water base nanofluid with variable viscosity and thermal conductivity in a microchannel is considered as shown in figure 6.1. The flow takes place in the  $x$ -direction between two parallel plates of small width  $h$  and very long length  $L$ . Following [102, 127, 141], the temperature and concentration dependent nanofluid viscosity ( $\mu_{nf}$ ) and thermal conductivity ( $k_{nf}$ ) can be expressed as

$$\mu_{nf} = \frac{\mu_f (C_s - C_w)^{2.5} e^{-\beta(T-T_w)}}{(C_s - C)^{2.5}} \quad (6.1)$$

$$\frac{k_{nf}}{k_f} = \frac{(C_s - C_w)(k_s + 2k_f) - 2(C - C_w)(k_f - k_s)}{(C_s - C_w)(k_s + 2k_f) + (C - C_w)(k_f - k_s)} \quad (6.2)$$

where  $C_s$  is the total concentration of nanoparticles such that  $C_w < C \ll C_s$ ,  $\mu_f$  is the base fluid (water) viscosity at the channel walls,  $T_w$  is the wall temperature,  $C_w$  is the nanoparticles concentration at the microchannel walls,  $T$  is the nanofluid temperature,  $C$  is the nanofluid concentration,  $\beta$  is the variable viscosity parameters due to temperature,  $k_f$  is the thermal conductivity of based fluid and  $k_s$  is the nanoparticles thermal conductivity.

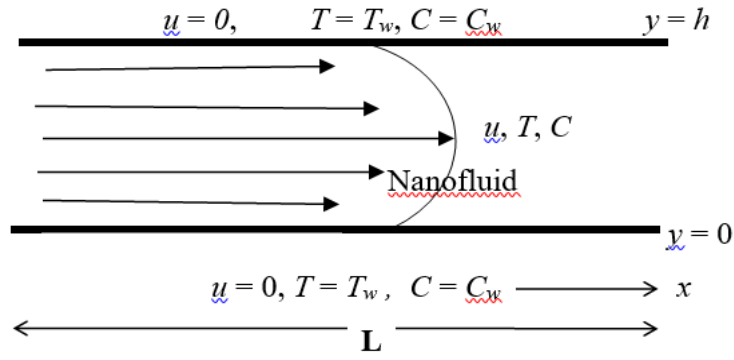


Figure 6.1: Problem geometry

Under these conditions, the continuity, momentum, energy, concentration and entropy generation equations governing the problem may be written as [58, 90, 96, 101, 127, 141];

$$\frac{\partial u}{\partial x} = 0 \quad (6.3)$$

$$\frac{\partial}{\partial y} \left( \mu_{nf} \frac{\partial u}{\partial y} \right) - \frac{\partial P}{\partial x} = 0, \quad (6.4)$$

$$\frac{\partial}{\partial y} \left( k_{nf} \frac{\partial T}{\partial y} \right) + \mu_{nf} \left( \frac{\partial u}{\partial y} \right)^2 + (\rho c_p)_f \tau \left[ D_B \frac{\partial C}{\partial y} \frac{\partial T}{\partial y} + \frac{D_T}{T_w} \left( \frac{\partial T}{\partial y} \right)^2 \right] = 0 \quad (6.5)$$

$$D_B \frac{\partial^2 C}{\partial y^2} + \frac{D_T}{T_w} \frac{\partial^2 T}{\partial y^2} + \delta(C_s - C) = 0 \quad (6.6)$$

$$E_G = \frac{k_{nf}}{T_w^2} \left( \frac{\partial T}{\partial y} \right)^2 + \frac{\mu_{nf}}{T_w} \left( \frac{\partial u}{\partial y} \right)^2 + \frac{RD_B}{(C_s - C_w)} \left( \frac{\partial C}{\partial y} \right)^2 + \frac{RD_B}{T_w} \frac{\partial C}{\partial y} \frac{\partial T}{\partial y}, \quad (6.7)$$

with the boundary conditions given as

$$\left. \begin{aligned} u=0, \quad T=T_w, \quad C=C_w, \quad \text{at } y=0 \\ u=0, \quad T=T_w, \quad C=C_w, \quad \text{at } y=h \end{aligned} \right\} \quad (6.8)$$



where  $R$  is the universal gas constant,  $E_g$  is the entropy generation rate,  $D_B$  is the Brownian motion mass diffusivity,  $D_T$  is thermophoresis mass diffusivity,  $\rho_f$  is the base fluid density,  $\tau$  is the specific heat capacity ratio,  $c_{pf}$  is the base fluid specific heat capacity at constant pressure,  $\delta$  is the nanoparticles injection rate and  $P$  is the nanofluid pressure. The thermophysical properties of the base fluid and nanoparticles are shown in table 6.1 below:

Table 6.1 Nanoparticles and base fluid thermophysical properties [101,137,140-141].

| Physical Properties | $C_p$ (J/kgK) | $\rho$ (kg/m <sup>3</sup> ) | $k$ (W/mK) |
|---------------------|---------------|-----------------------------|------------|
| Water               | 4183          | 998.2                       | 0.67       |
| Cu                  | 385           | 8933                        | 401        |

We introduce the following non-dimensional quantities in equations (6.2) - (6.7):

$$\begin{aligned}
 \eta &= \frac{y}{h}, W = \frac{uh}{\nu_f}, \theta = \frac{T - T_w}{T_w}, \phi = \frac{C - C_w}{C_s - C_w}, \text{Pr} = \frac{\nu_f}{\alpha_f}, \nu_f = \frac{\mu_f}{\rho_f}, \lambda = \beta T_w, \\
 Ec &= \frac{\nu_f^2}{c_{pf} T_w h^2}, Nb = \frac{\tau D_B (C_s - C_w)}{\nu_f}, Nt = \frac{\tau D_T}{\nu_f}, \gamma = \frac{\delta h^2}{\nu_f}, A = -\frac{\partial \bar{P}}{\partial X}, \bar{P} = \frac{\rho_f h^2 P}{\mu_f^2} \quad (6.9) \\
 X &= \frac{x}{h}, \alpha_f = \frac{k_f}{(\rho c_p)_f}, n = \frac{R D_B (C_s - C_w)}{k_f}, Ns = \frac{E_g h^2}{k_f}, Le = \frac{\alpha_f}{D_B}, \\
 M_1 &= \frac{k_s + 2k_f + \phi(\eta)(k_s - k_f)}{k_s + 2k_f - 2\phi(\eta)(k_s - k_f)}, M_2 = \frac{(1 + 2M_1)(k_s - k_f)}{k_s + 2k_f + \phi(\eta)(k_s - k_f)}
 \end{aligned}$$

and obtain

$$\frac{d^2 W}{d\eta^2} - \lambda \frac{dW}{d\eta} \frac{d\theta}{d\eta} + \frac{5}{2(1-\phi)} \frac{dW}{d\eta} \frac{d\phi}{d\eta} + A e^{\lambda\theta} (1-\phi)^{\frac{5}{2}} = 0 \quad (6.10)$$

$$\frac{d^2 \theta}{d\eta^2} - M_2 \frac{d\phi}{d\eta} \frac{d\theta}{d\eta} + \frac{\text{Pr} Ec M_1}{(1-\phi)^{\frac{5}{2}}} \left( \frac{dW}{d\eta} \right)^2 e^{-\lambda\theta} + \text{Pr} M_1 \left( Nb \frac{d\phi}{d\eta} \frac{d\theta}{d\eta} + Nt \left( \frac{d\theta}{d\eta} \right)^2 \right) = 0 \quad (6.11)$$

$$\frac{d^2\phi}{d\eta^2} + \frac{Nt}{Nb} \frac{d^2\theta}{d\eta^2} + \text{Pr} \text{Le} \gamma (1 - \phi) = 0 \quad (6.12)$$

$$Ns = \frac{1}{M_1} \left( \frac{d\theta}{d\eta} \right)^2 + \frac{\text{Pr} \text{Ec}}{(1 - \phi)^{\frac{5}{2}}} \left( \frac{dW}{d\eta} \right)^2 e^{-\lambda\theta} + n \left[ \left( \frac{d\phi}{d\eta} \right)^2 + \frac{d\phi}{d\eta} \frac{d\theta}{d\eta} \right] \quad (6.13)$$

with boundary conditions given as

$$\left. \begin{aligned} W(0) = \theta(0) = \phi(0) = 0, \\ W(1) = \theta(1) = \phi(1) = 0, \end{aligned} \right\} \quad (6.14)$$

where  $A$  corresponds to the constant axial pressure gradient,  $\text{Pr}$  ( $\approx 6.2$ ) is Prandtl number, of the based fluid (water),  $\text{Le}$  is the Lewis number,  $\text{Ec}$  is the Eckert number,  $Nt$  is the thermophoresis parameter,  $\gamma$  nanoparticles injection rate parameter,  $Nb$  is Brownian motion parameter,  $n$  is the irreversibility parameter due to nanoparticles concentration.  $Ns$  is the entropy generation rate and  $\lambda$  is the variable viscosity parameters due to temperature. Other quantities of interest are the skin friction coefficients ( $C_f$ ), Nusselt number ( $Nu$ ), Sherwood number ( $Sh$ ) and the Bejan number ( $Be$ ) which are given as

$$C_f = \frac{h^2 \tau_w}{\rho_f \nu_f^2} = \frac{dW}{d\eta} \Big|_{\eta=0,1}, \quad (6.15)$$

$$Nu = \frac{hq_w}{k_f T_w} = -\frac{d\theta}{d\eta} \Big|_{\eta=0,1}, \quad (6.16)$$

$$Sh = \frac{hq_m}{D_B (C_s - C_w)} = -\frac{d\phi}{d\eta} \Big|_{\eta=0,1}, \quad (6.17)$$

and

$$Be = \frac{N_1}{Ns} = \frac{1}{1 + F} \quad (6.18)$$

where

$$\tau_w = \mu_{nf} \frac{\partial u}{\partial y}, \quad q_w = -k_{nf} \frac{\partial T}{\partial y}, \quad q_m = -D_B \frac{\partial C}{\partial y}, \quad N_1 = \frac{1}{M_1} \left( \frac{d\theta}{d\eta} \right)^2, \quad (6.19)$$

$$N_2 = \frac{\text{Pr} Ec}{(1-\phi)^{\frac{5}{2}}} \left( \frac{dW}{d\eta} \right)^2 e^{-\lambda\theta}, \quad N_3 = n \left[ \left( \frac{d\phi}{d\eta} \right)^2 + \frac{d\phi}{d\eta} \frac{d\theta}{d\eta} \right], \quad F = \frac{N_2 + N_3}{N_1}. \quad (6.20)$$

The variable  $F$  represents the irreversibility ratio. The symbol  $N_1$  represents thermodynamic irreversibility due to heat transfer;  $N_2$  corresponds to the entropy generation due to fluid friction while  $N_3$  represents irreversibility due to nanoparticles concentration. Whenever  $0 \leq \text{Be} < 0.5$ , entropy generation due to fluid friction and nanoparticles concentration dominates the flow system while heat transfer irreversibility dominates when  $0.5 < \text{Be} \leq 1$ .

Special Case: (H<sub>2</sub>O-Base Fluid Only)

In the absent of nanoparticles, the model equations (6.10)–(6.13) will reduce to the followings:

$$\frac{d^2W}{d\eta^2} - \lambda \frac{dW}{d\eta} \frac{d\theta}{d\eta} + Ae^{\lambda\theta} = 0 \quad (6.21)$$

$$\frac{d^2\theta}{d\eta^2} + \text{Pr} Ec \left( \frac{dW}{d\eta} \right)^2 e^{-\lambda\theta} = 0 \quad (6.22)$$

$$Ns = \left( \frac{d\theta}{d\eta} \right)^2 + \text{Pr} Ec \left( \frac{dW}{d\eta} \right)^2 e^{-\lambda\theta} \quad (6.23)$$

with boundary conditions given as

$$\left. \begin{aligned} W(0) = \theta(0) = 0, \\ W(1) = \theta(1) = 0. \end{aligned} \right\} \quad (6.24)$$

### 6.3 Numerical Procedure

The Runge-Kutta-Fehlberg integration scheme coupled with the shooting numerical method [20] is employed in order to tackle the nonlinear boundary value problem described by model equations (6.10)-(6.13). Let

$$W = y_1, W' = y_2, \theta = y_3, \theta' = y_4, \phi = y_5, \phi' = y_6. \quad (6.25)$$

The governing equations are then transformed into a set on nonlinear initial value problem as

$$\left. \begin{aligned} y_1' &= y_2 \\ y_2' &= \lambda y_2 y_4 - \frac{5y_2 y_6}{2(1-y_5)} - Ae^{\lambda y_3} (1-y_5)^{5/2} \\ y_3' &= y_4 \\ y_4' &= M_2 y_4 y_6 - \frac{\text{Pr} Ec M_1 y_2^2}{(1-y_5)^{5/2}} e^{-\lambda y_2} - \text{Pr} M_1 (Nby_4 y_6 + Nty_4^2) \\ y_5' &= y_6 \\ y_6' &= -\frac{Nt}{Nb} \left[ M_2 y_4 y_6 - \frac{\text{Pr} Ec M_1 y_2^2}{(1-y_5)^{5/2}} e^{-\lambda y_2} - \text{Pr} M_1 (Nby_4 y_6 + Nty_4^2) \right] - \text{Pr} Le \gamma (1-y_5) \end{aligned} \right\} \quad (6.26)$$

with the corresponding initial conditions given as

$$y_1(0) = 0, y_2(0) = a_1, y_3(0) = 0, y_4(0) = a_2, y_5(0) = 0, y_6(0) = a_3 \quad (6.27)$$

where

$$M_1 = \frac{k_s + 2k_f + y_5(k_s - k_f)}{k_s + 2k_f - 2y_5(k_s - k_f)}, M_2 = \frac{(1 + 2M_1)(k_s - k_f)}{k_s + 2k_f + y_5(k_s - k_f)} \quad (6.28)$$

The unknown initial values of  $a_1$ ,  $a_2$  and  $a_3$  in the equation (6.27) are first guessed and thereafter determined accurately via shooting method with Newton-Raphson's iteration technique with step size of  $\Delta\eta=0.01$ . Numerical solutions obtained for the velocity, temperature and nanoparticles concentration profiles are utilized to compute the values for the skin friction, Nusselt number, Sherwood number, entropy generation rate and Bejan number as stipulated in equations (6.12) and (6.14)-(6.15).

## 6.4 Results and Discussion

In order to gain an insight into the overall flow structure with heat and mass transfer characteristics, numerical solution for the velocity, temperature and nanoparticles concentration profiles are presented graphically in figures 6.2-6.21. We also compute the results for the skin friction ( $C_f$ ), the Nusselt number ( $Nu$ ), Sherwood number (Sh), entropy generation rate (Ns) and Bejan number (Be) as depicted in figures 6.22-6.41.

### 6.4.1 Velocity Profiles

Figures 6.2-6.8 depict the nanofluid velocity profiles within the microchannel. It is noteworthy that the profiles are parabolic in shape with zero velocity at the walls due to no slip condition and maximum velocity along the microchannel core region. Figure 6.2, shows that the nanofluid (Cu-water) flow rate is lower than that of based fluid (water). This may be accredited to viscosity elevation in nanofluid due to the presence of nanoparticles. Thus, nanofluid becomes slightly heavier as compared with ordinary base fluid and the flow rate is affected. The effects of various parameters on the velocity profiles are displayed in figures 6.3-6.8. Interestingly, the velocity diminished with an increase in the parameter values of  $Le$ ,  $\gamma$  and  $Nb$  but enhanced with a boost in the parameter values of  $Nt$ ,  $\lambda$  and  $Ec$ . This is expected, since a rise in Eckert number ( $Ec$ ), thermophoresis ( $Nt$ ) and variable viscosity parameter ( $\lambda > 0$ ) escalates the internal heat generation within the flow system, consequently, the nanofluid becomes lighter and flow faster. The flow trend is opposite with an increase in Lewis number ( $Le$ ), nanoparticles injection rate ( $\gamma$ ) and Brownian motion ( $Nb$ ), thus, the velocity decreases due to an augmentation in concentration of nanoparticles in the nanofluid.

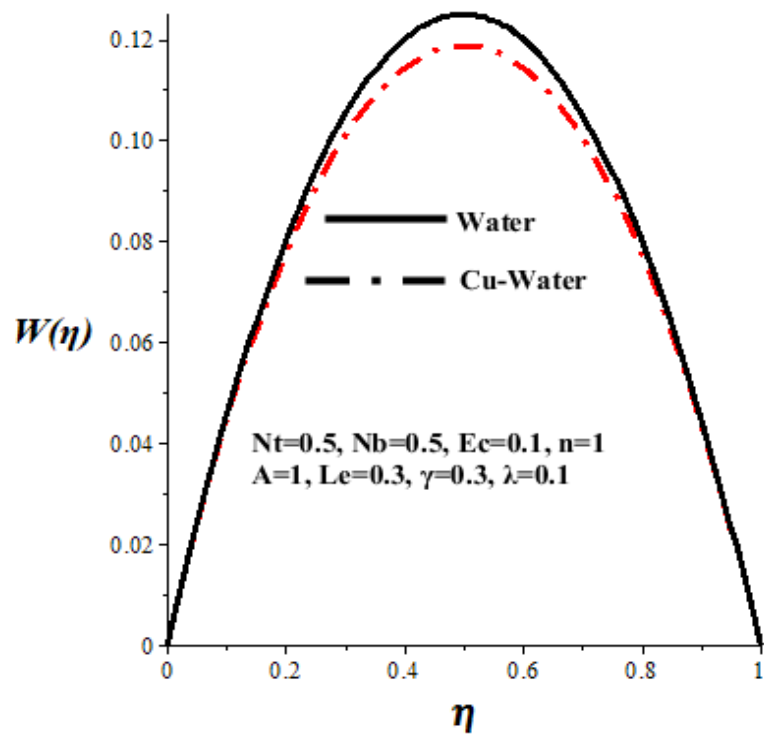


Figure 6.2 Velocity profiles with Cu-nanoparticles

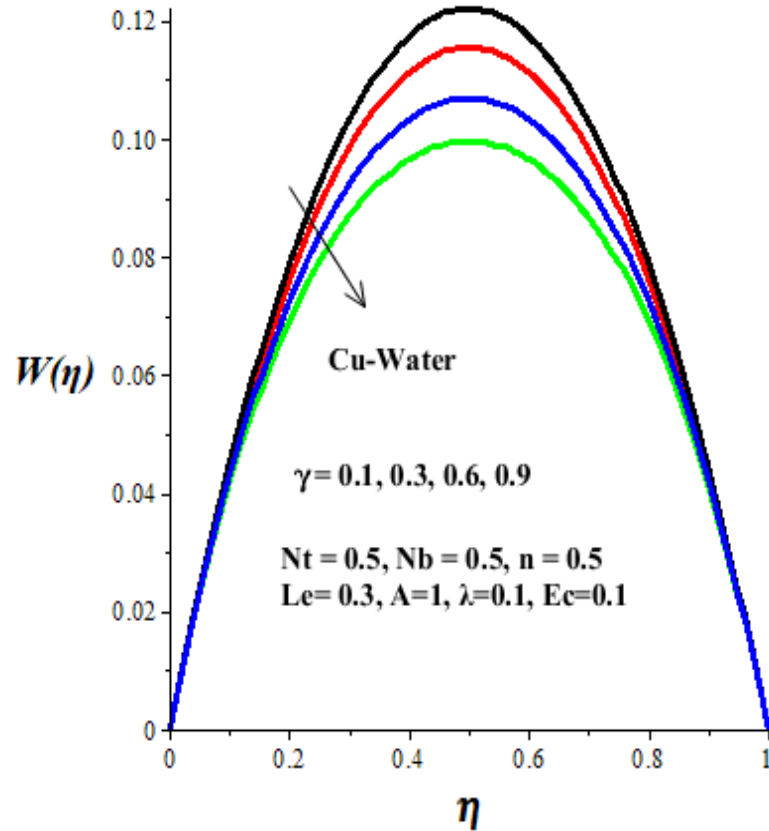


Figure 6.3 Velocity profiles with  $\gamma$

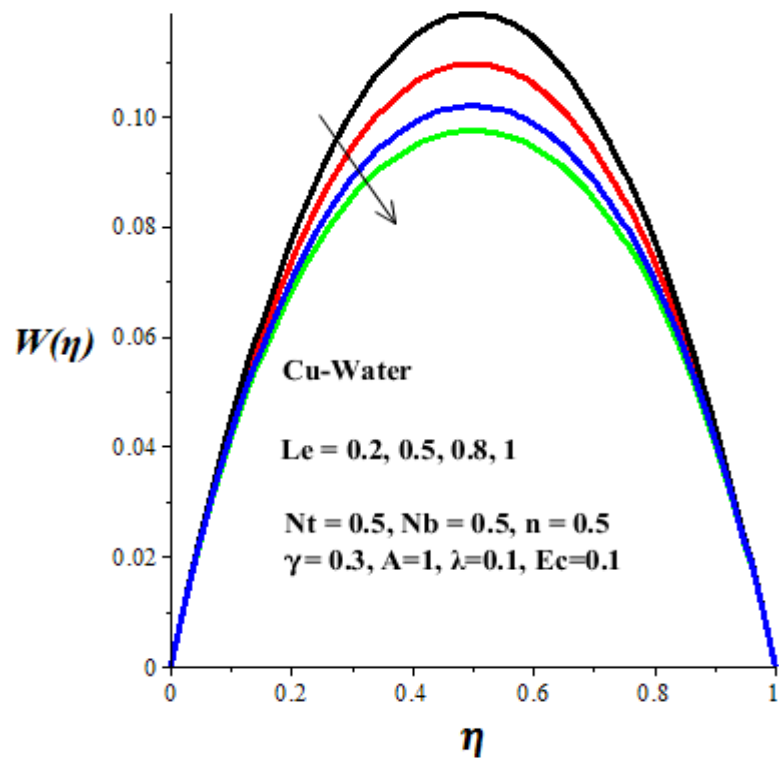


Figure 6.4 Velocity profiles with Le

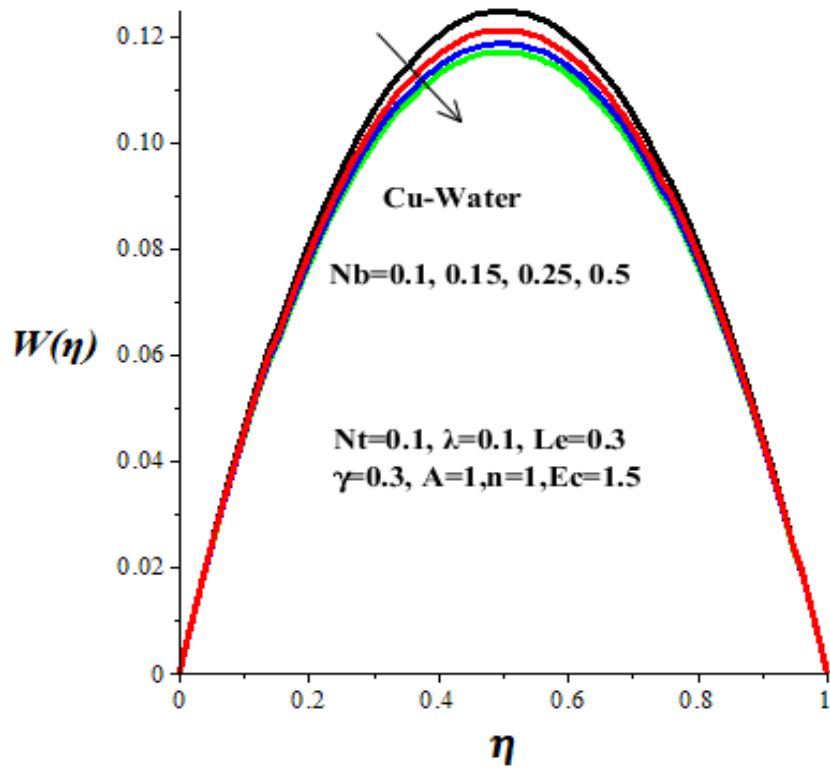


Figure 6.5 Velocity profiles with Nb

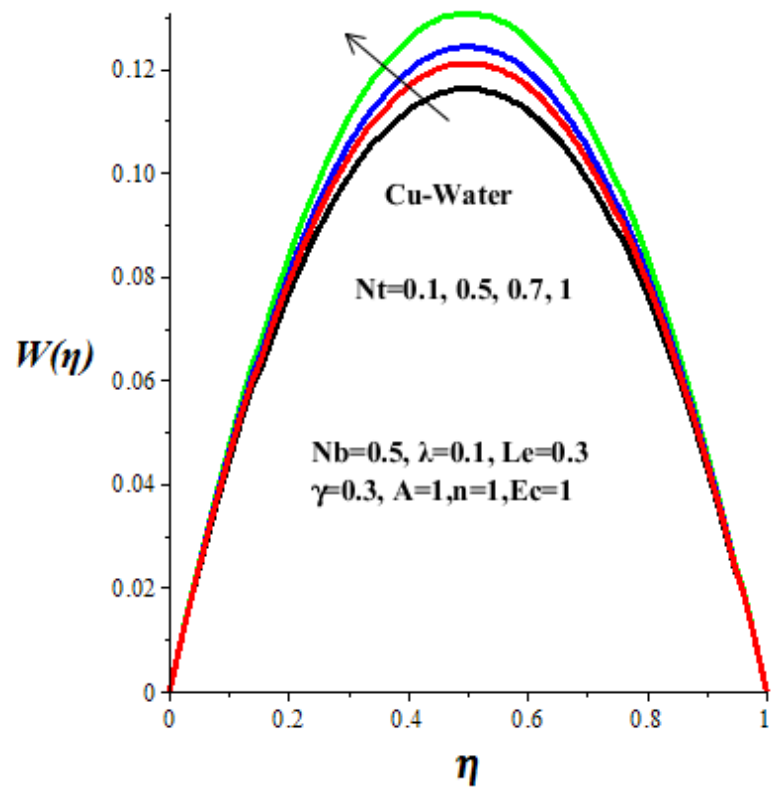


Figure 6.6 Velocity profiles with  $Nt$

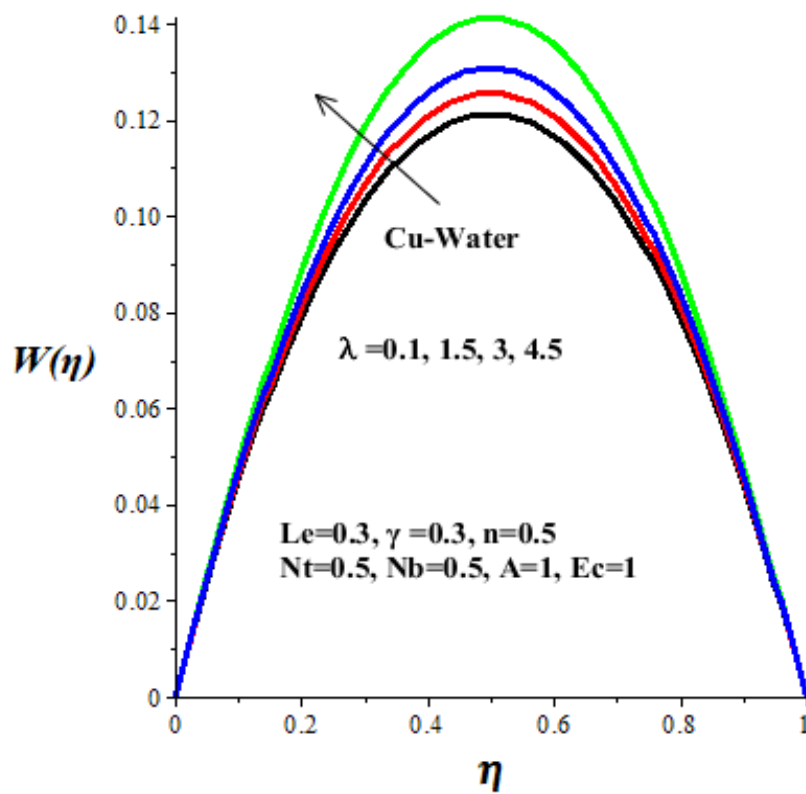
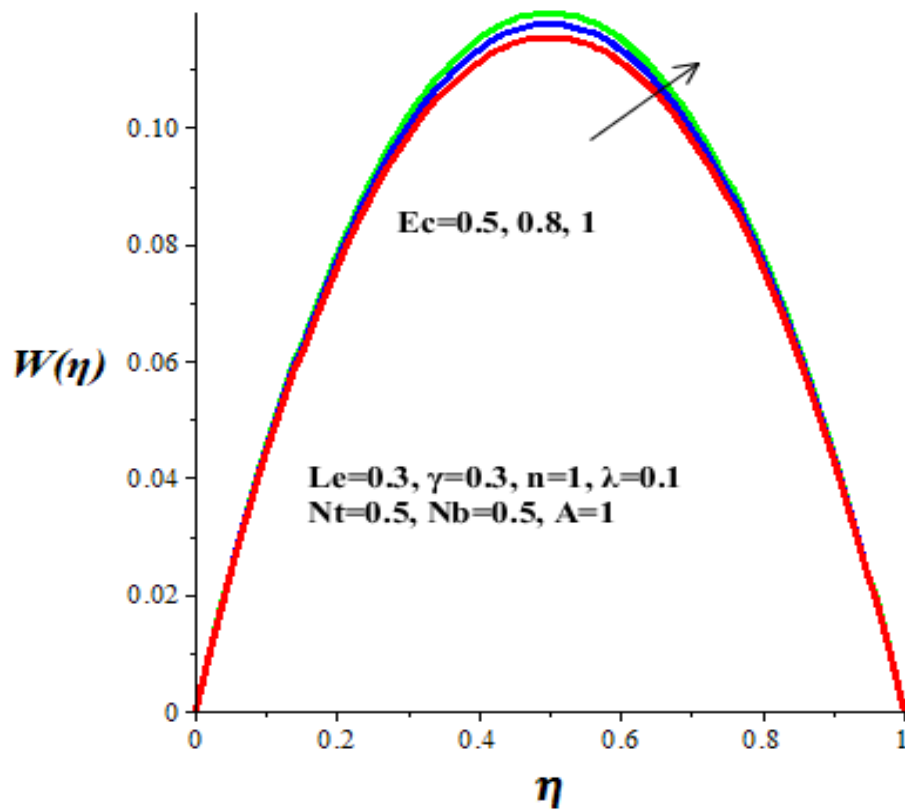


Figure 6.7 Velocity profiles with  $\lambda$



Figure 6.8 Velocity profiles with  $Ec$ 

#### 6.4.2 Temperature Profiles

Figures 6.9-6.15 illustrate the temperature profiles of nanofluid under different parametric conditions. In all the figures, the temperature is lowest at walls but attained its maximum value at the microchannel core region. Figure 6.9 reveals that nanofluid temperature is lower than that of base fluid (water). This may be attributed to nanofluid heat transfer enhancement property as compare to base fluid (water). Therefore, the base fluid tends to conserve more heat leading to its temperature elevation. It can also be perceived from figures 6.10-6.15 that nanofluid temperature drops with increasing values of  $Nb$ ,  $Le$  and  $\gamma$  but rises with increasing values of  $Nt$ ,  $Ec$  and  $\lambda$ . These effects can be ascribed to the fact that the internal heat generation within the flow system is heightened with amplification of Eckert number ( $Ec$ ) due to viscous dissipation, thermophoresis ( $Nt$ ) due to nanoparticles interaction and variable viscosity parameter ( $\lambda > 0$ ). Moreover, the nanofluid temperature declines with an upsurge in Lewis number ( $Le$ ), nanoparticles injection parameter ( $\gamma$ ) and Brownian motion ( $Nb$ ).

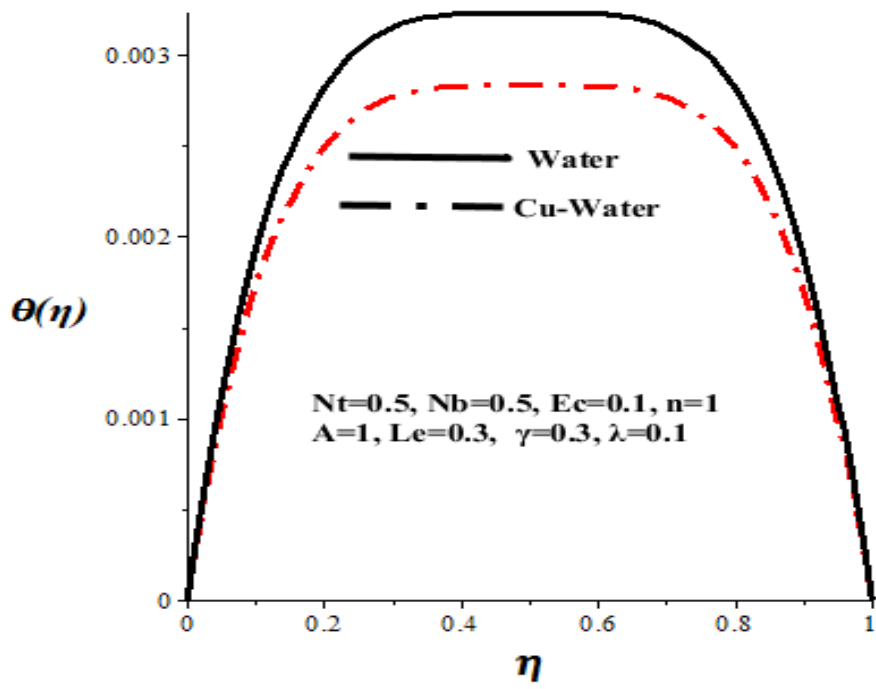


Figure 6.9 Temperature profiles with Cu-nanoparticles

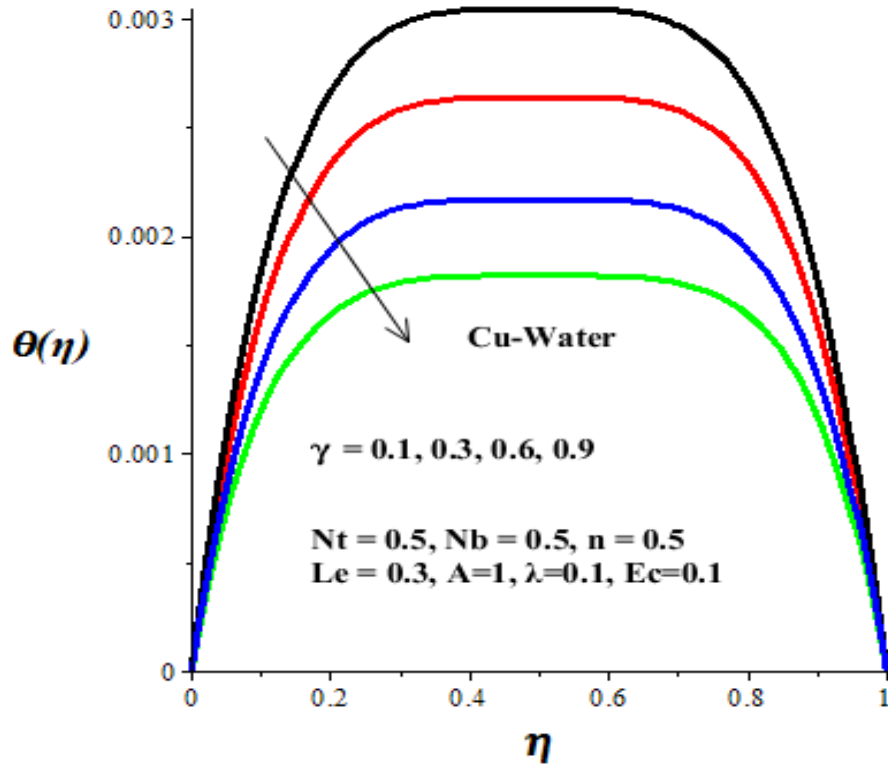


Figure 6.10 Temperature profiles with  $\gamma$

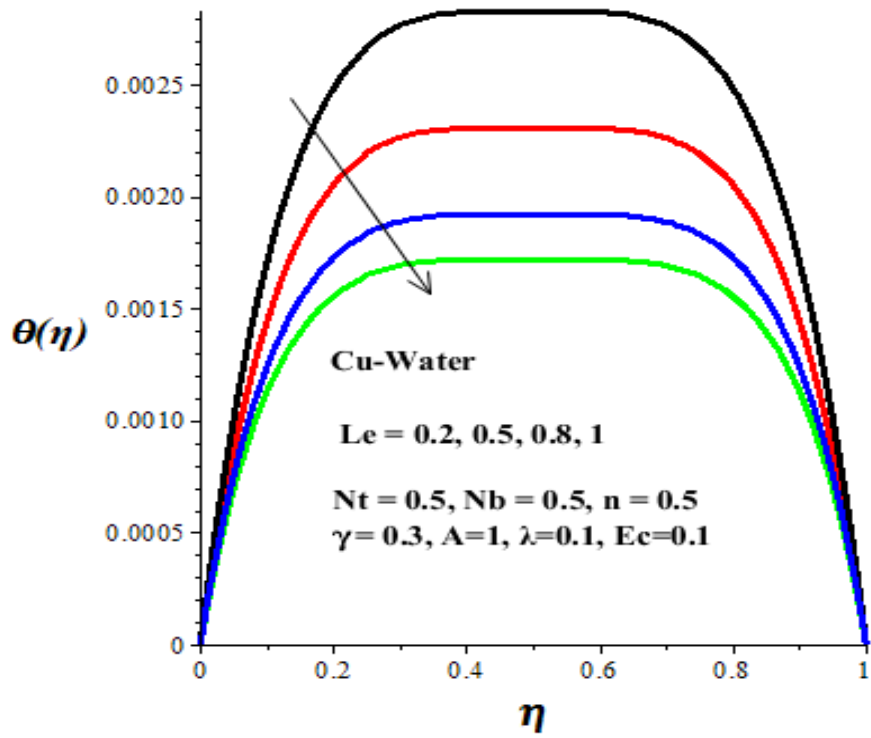


Figure 6.11 Temperature profiles with Le

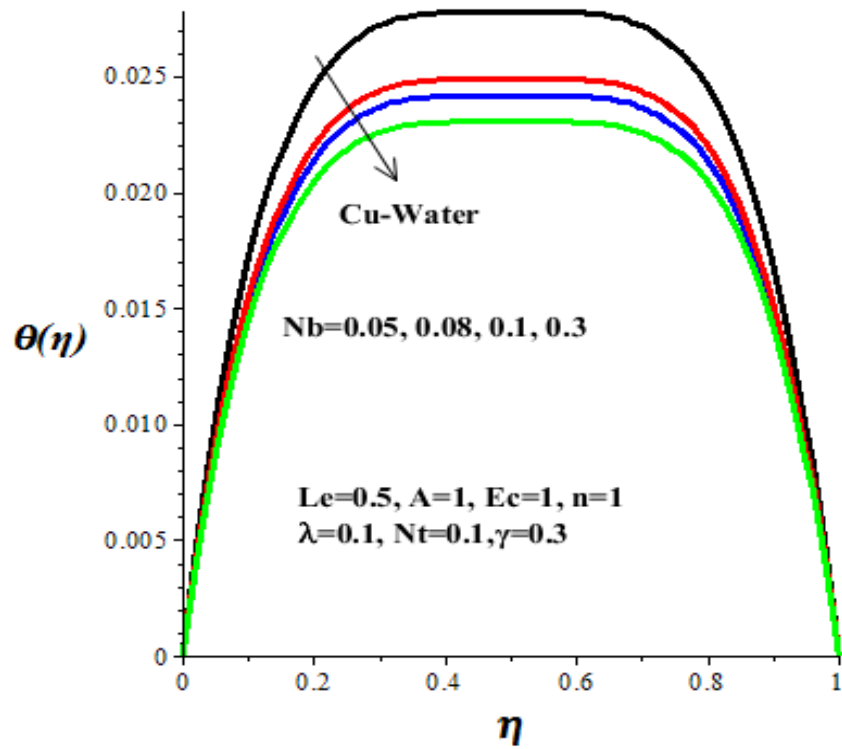


Figure 6.12 Temperature profiles with Nb

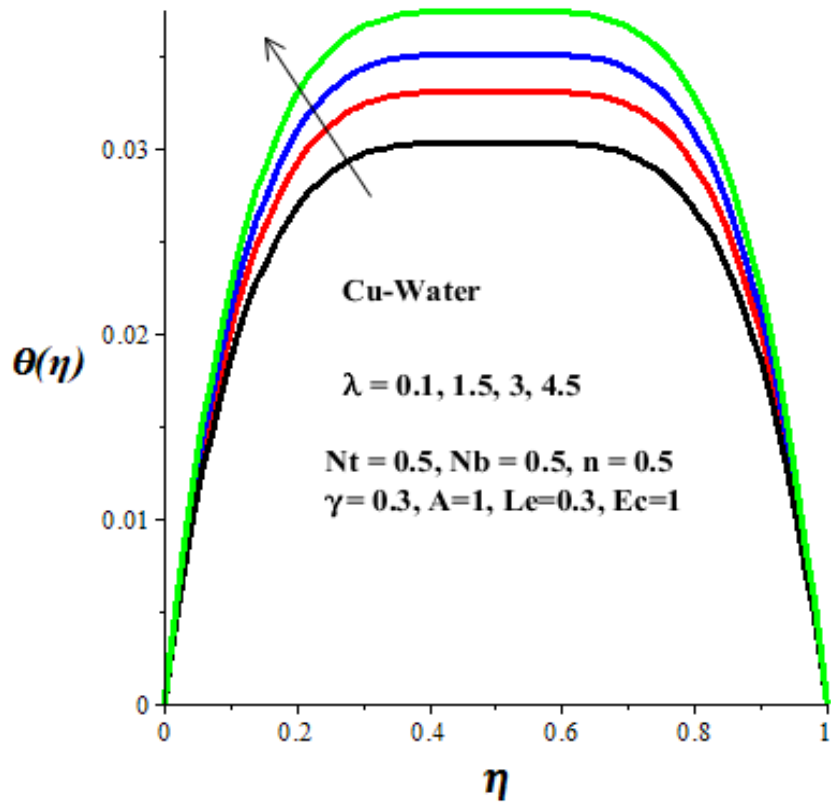


Figure 6.13 Temperature profiles with  $\lambda$

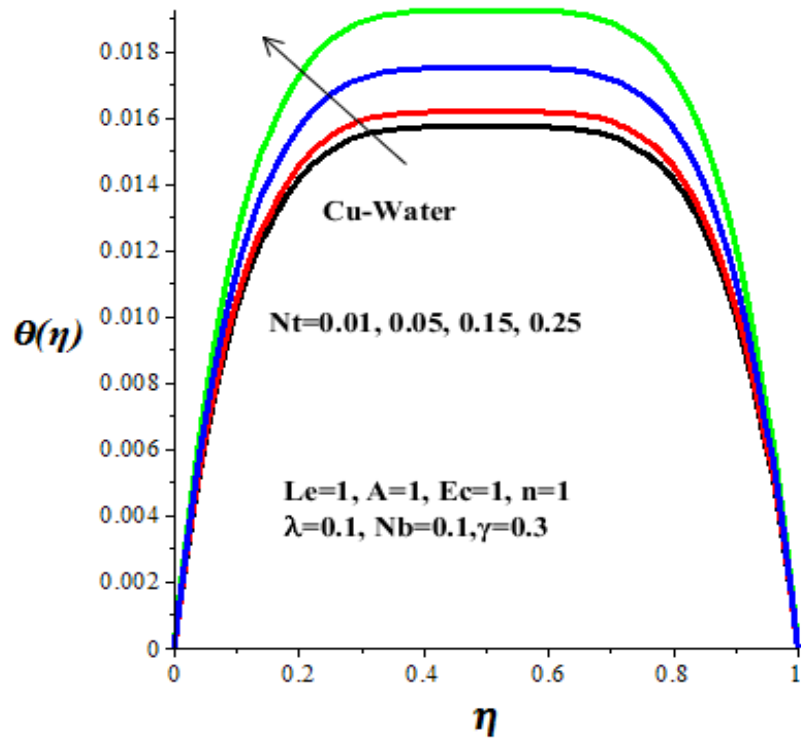


Figure 6.14 Temperature profiles with  $Nt$

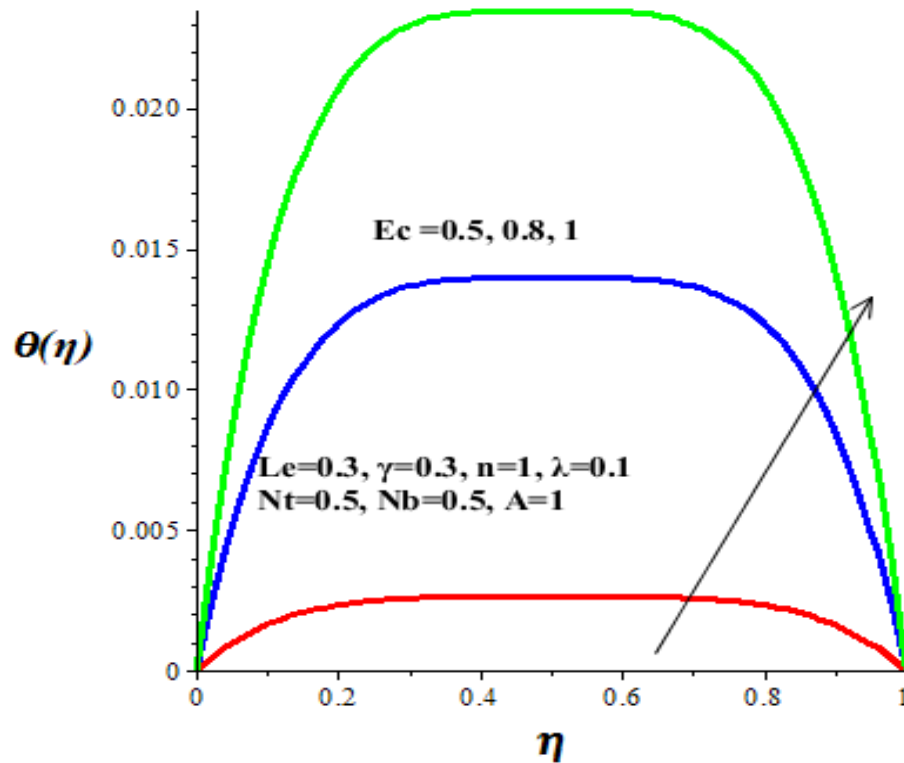


Figure 6.15 Temperature profiles with  $Ec$

### 6.4.3 Nanoparticles Concentration Profiles

Figures 6.16-6.21 depict the parametric effects on the nanoparticles concentration distribution profiles. In general, a parabolic shape distribution pattern is observed with minimum concentration at the walls while majority of the nanoparticles aggregate along the microchannel core region. It is interesting to note that the nanoparticles concentration is enhanced with an escalation in the parameter values of  $\gamma$ ,  $Le$  and  $Nb$  as shown in figures 6.16-6.18, while a decline in the concentration profiles is observed in figures 6.19-6.21 with an upsurge in parameter values of  $\lambda$ ,  $Nt$  and  $Ec$ . As Lewis number ( $Le$ ), nanoparticles injection rate ( $\gamma$ ) and Brownian motion ( $Nb$ ) intensify, nanoparticles injection and distribution within the base fluid increases. Opposite trend of a declining nanoparticles concentration is observed with a rise in Eckert number ( $Ec$ ) due to viscous dissipation, thermophoresis ( $Nt$ ) due to nanoparticles interaction and variable viscosity parameter ( $\lambda > 0$ ). This is expected, since nanofluid becomes lighter with an increase in the parameter values.

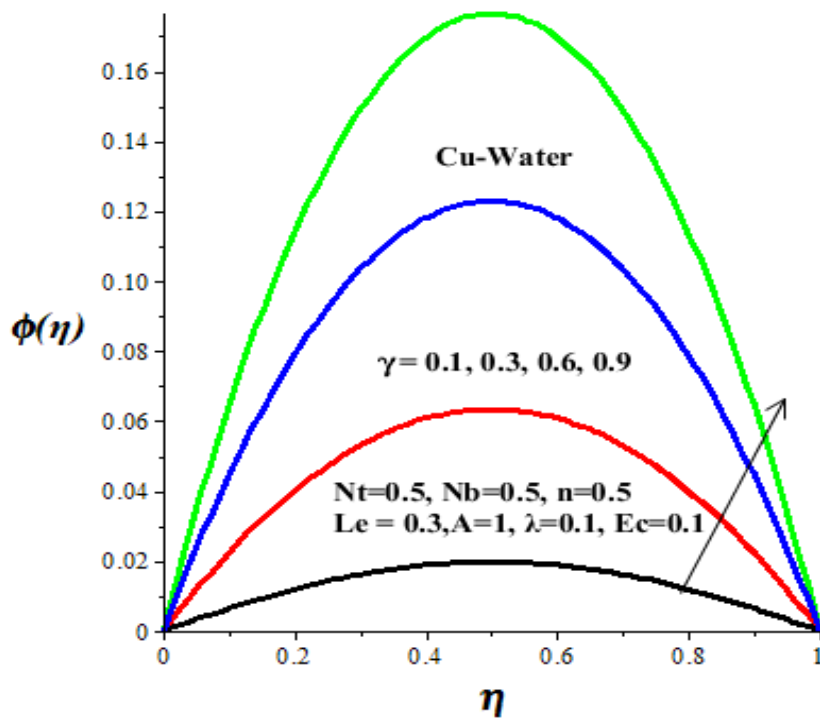


Figure 6.16 Concentration profiles with  $\gamma$

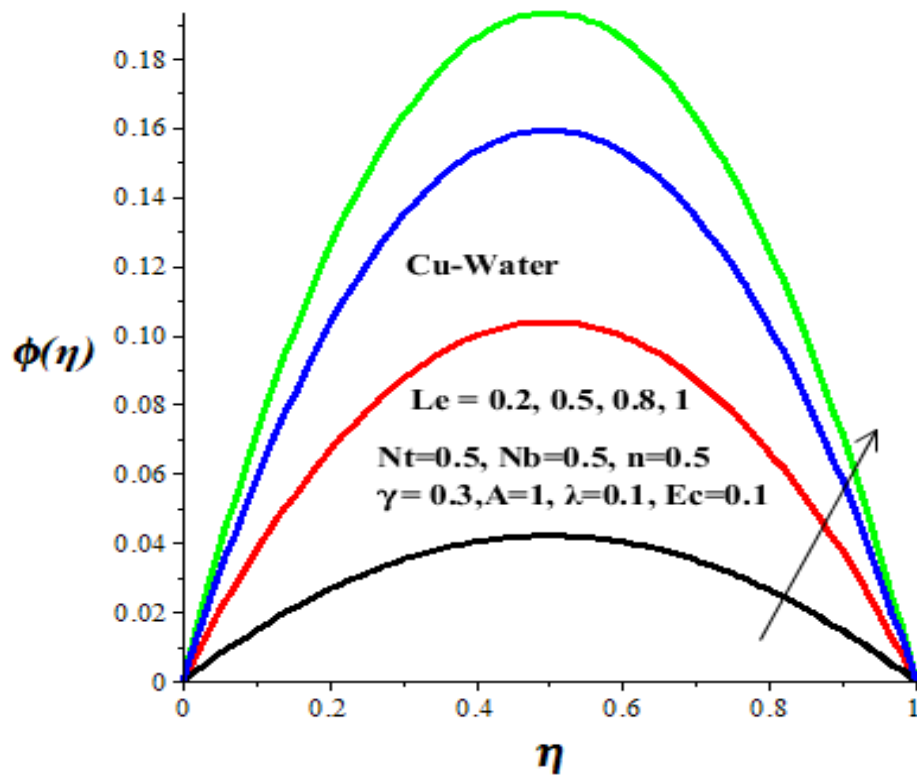


Figure 6.17 Concentration profiles with  $Le$

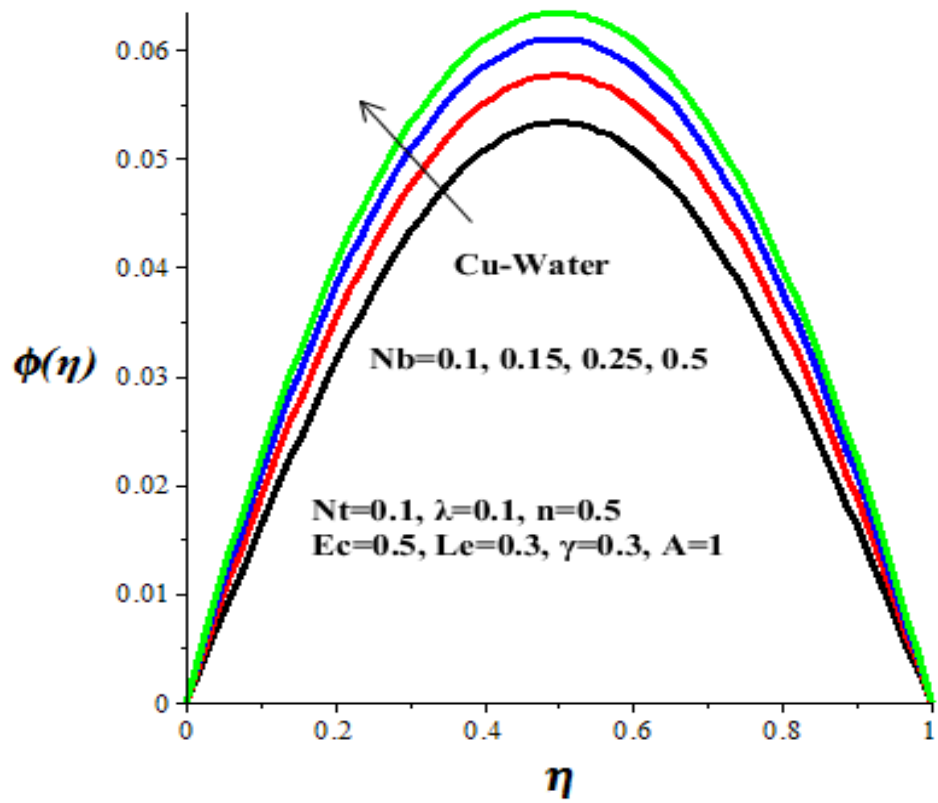


Figure 6.18 Concentration profiles with  $Nb$

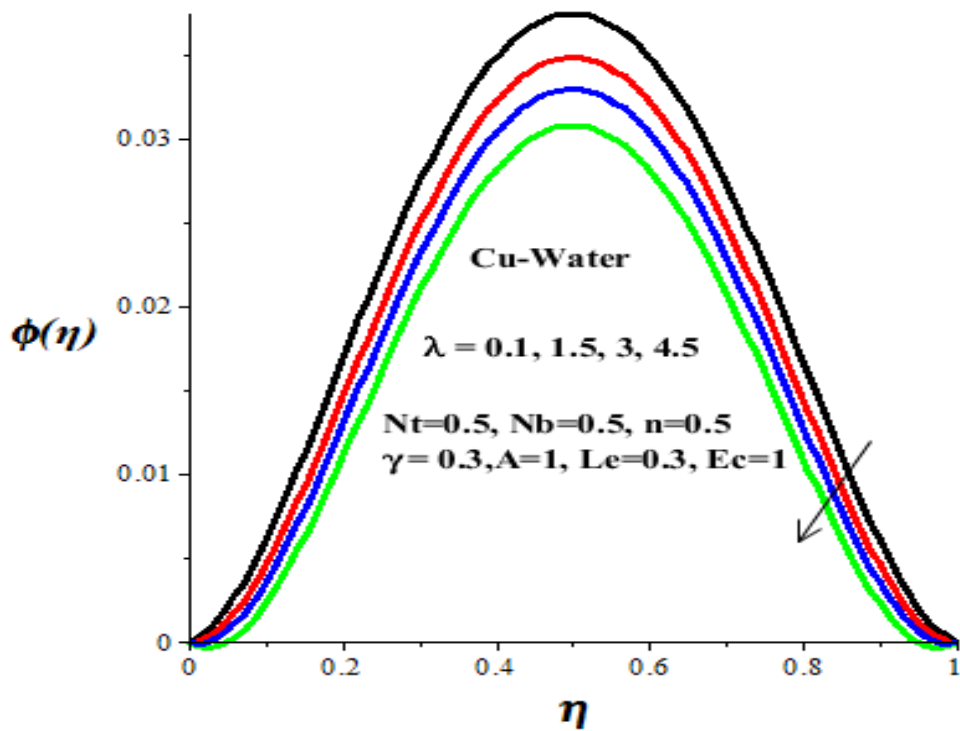


Figure 6.19 Concentration profiles with  $\lambda$

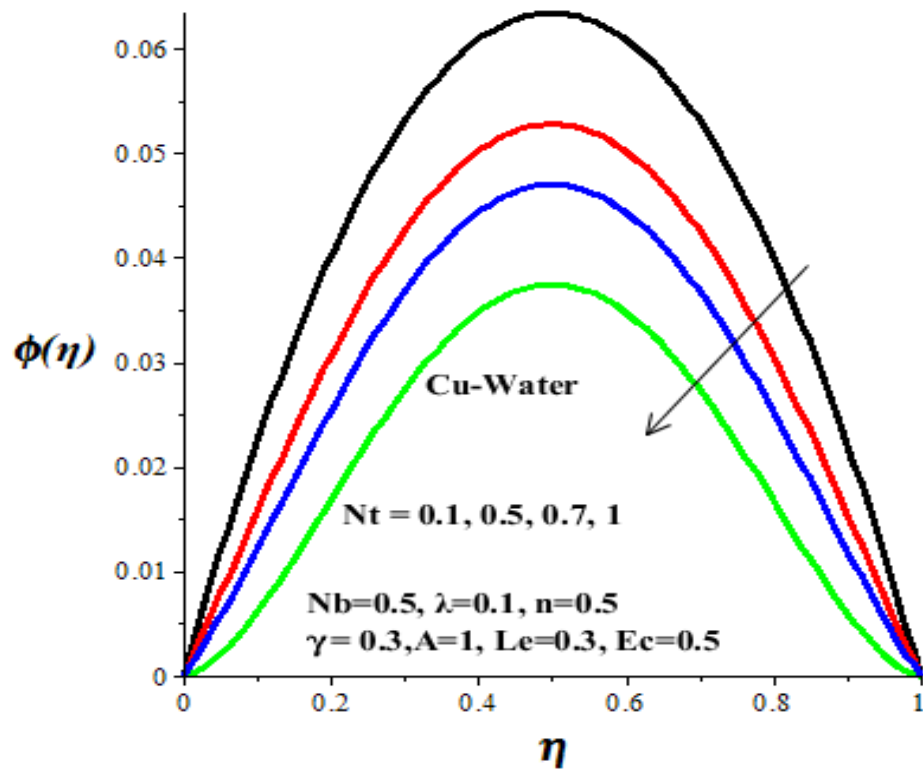


Figure 6.20 Concentration profiles with Nt

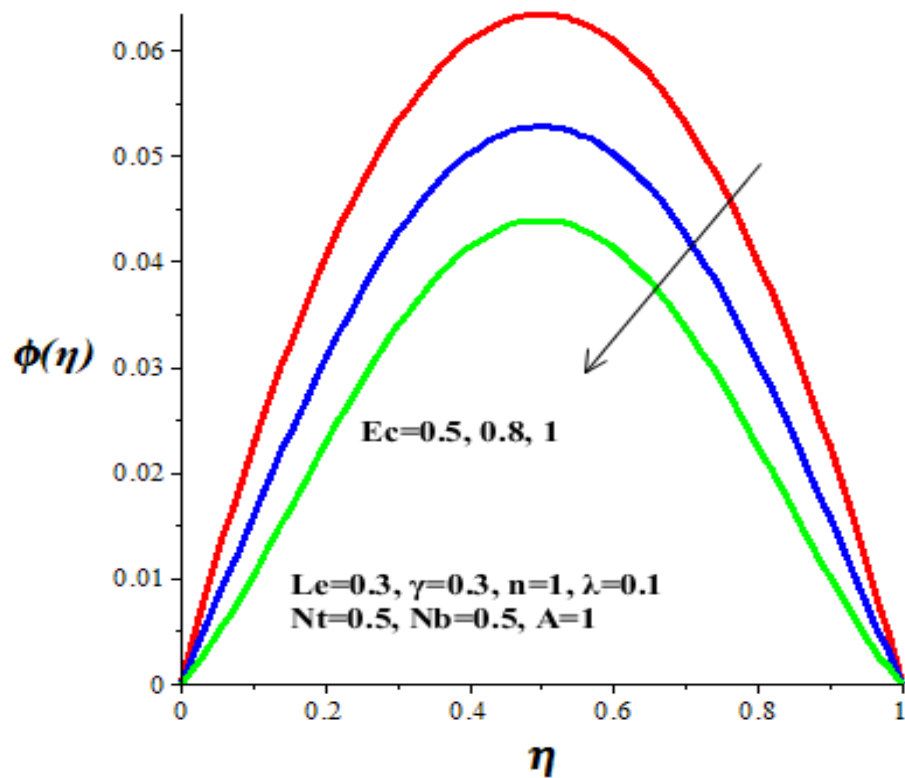


Figure 6.21 Concentration profiles with Ec



#### 6.4.4 Skin Friction

Figure 6.22 depicts the skin friction profile. From model equation (6.1), it can be seen that at the microchannel walls, both the variable viscosity and the variable thermal conductivity depend on base fluid (water) only, given as  $\mu_f$  and  $k_f$ . Therefore, the solution to the model momentum equation (6.9) near the walls is  $dW/d\eta \approx A(1-2\eta)/2$ . Subsequently, the skin friction at microchannel walls is given as  $C_f \approx A/2$ , where A is the axial pressure gradient parameter. This simply implies that an increase in axial pressure gradient will boost the frictional force on the microchannel inner surface.

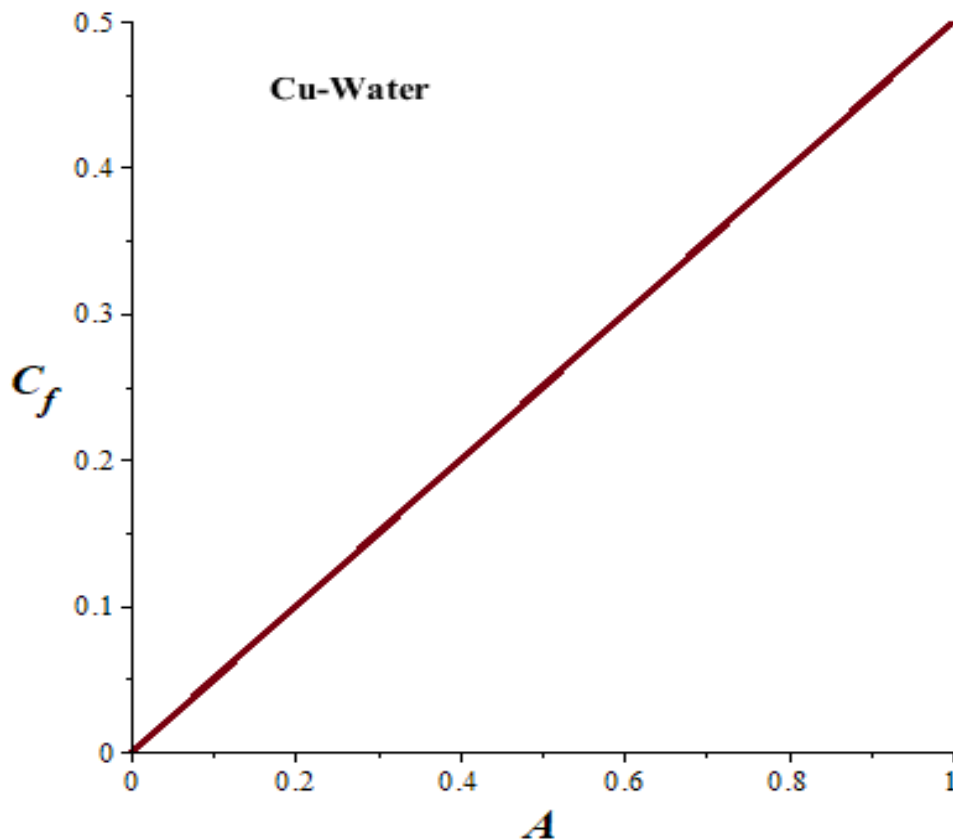


Figure 6.22 Skin friction with increasing A

### 6.4.5 Nusselt Number and Sherwood Number

Figures 6.23-6.27 demonstrate the effects of various thermophysical parameters on the heat and mass transfer rate at the microchannel walls. As expected, figure 6.23 shows that Nusselt number for nanofluid (Cu-water) is higher than that of base fluid (Water). This superior heat transfer enhancement property of nanofluid is the major reason why it is widely utilized in managing engineering and industrial heat transfer processes. In figure 6.24-6.25, it is observed that the heat transfer rate at the walls diminished with increasing parameter values of  $\gamma$  and  $Le$ , but amplified with increasing parameter values of  $Ec$ ,  $\lambda$ ,  $Nt$  and  $Nb$ . The rise in wall heat flux can be ascribed to an escalation in temperature gradient due to combined effects of nanoparticles thermophoresis and Brownian motion coupled with an upsurge in viscous dissipation. Meanwhile, figures 6.26-6.27 revealed an upsurge in mass transfer rate at the microchannel walls as the parameter values of  $Le$ ,  $Nb$  and  $\gamma$  increase. This may be due to a rise in nanoparticles concentration and concentration gradient at the walls. The Sherwood number lessened as viscous dissipation represented by Eckert number ( $Ec$ ) and thermophoresis ( $Nt$ ) activities intensified.

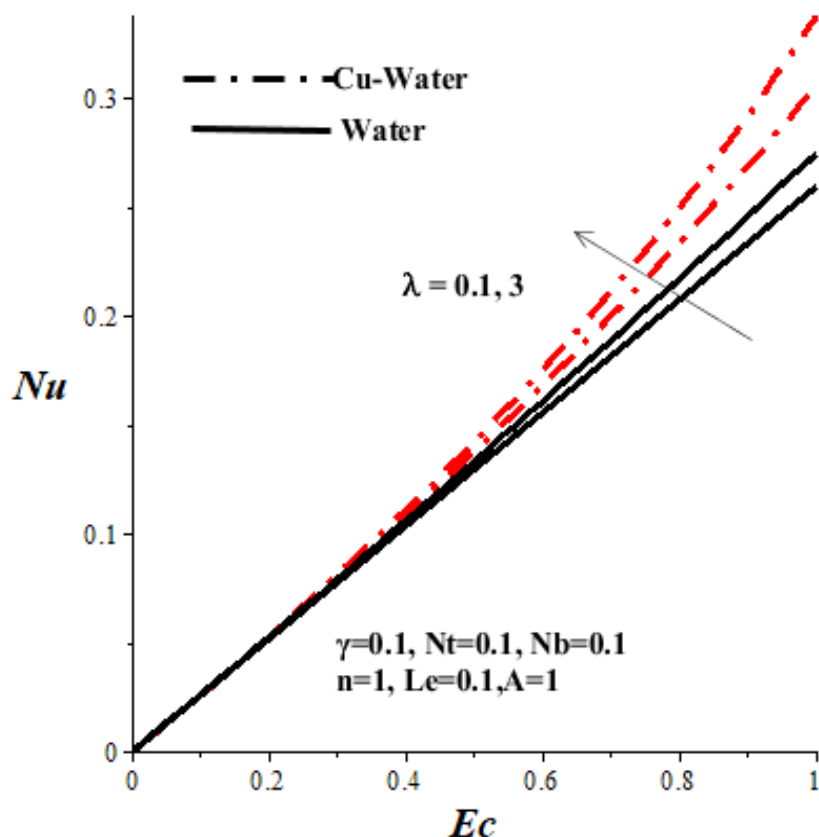


Figure 6.23 Nusselt number with  $Ec$  and  $\lambda$

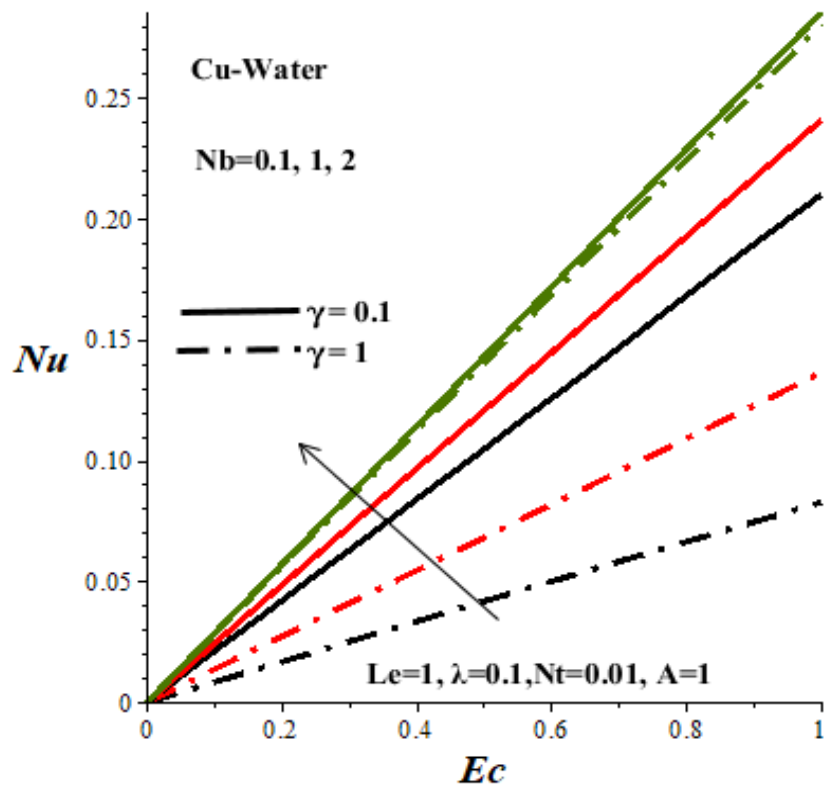


Figure 6.24 Nusselt number with  $Ec, Nb$  and  $\gamma$

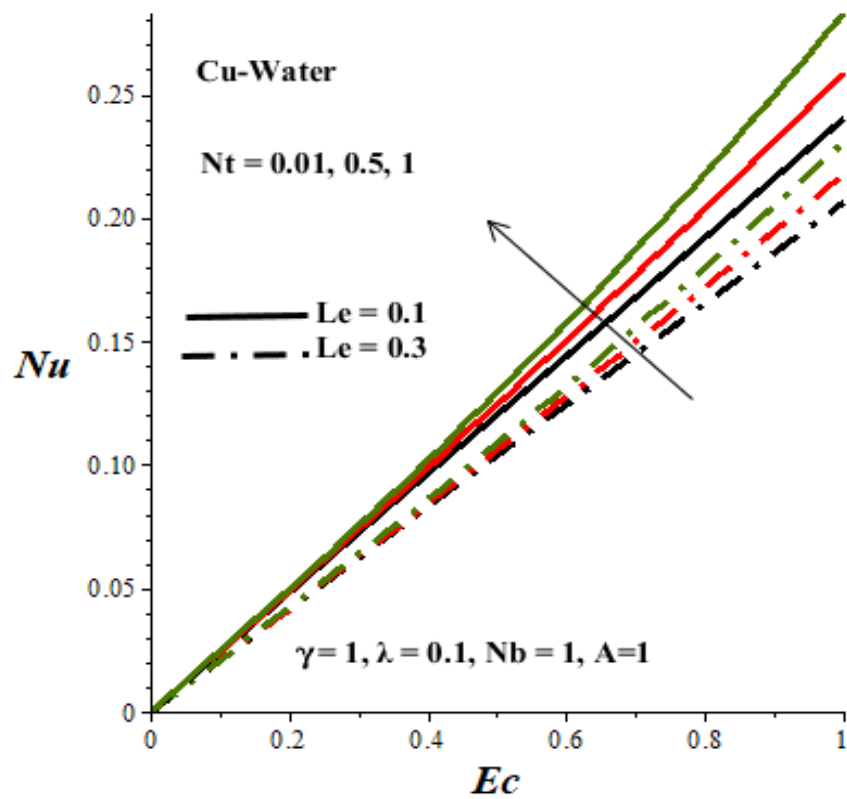


Figure 6.25 Nusselt number with  $Ec, Nt$  and  $Le$

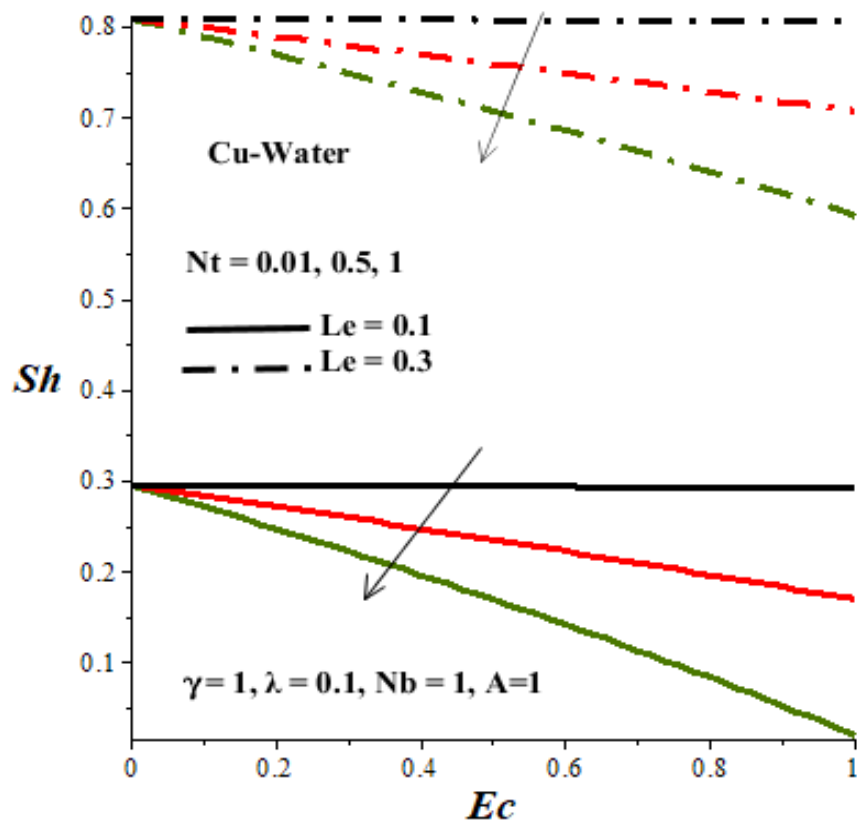


Figure 6.26 Sherwood number with  $Ec$ ,  $Nt$  and  $Le$

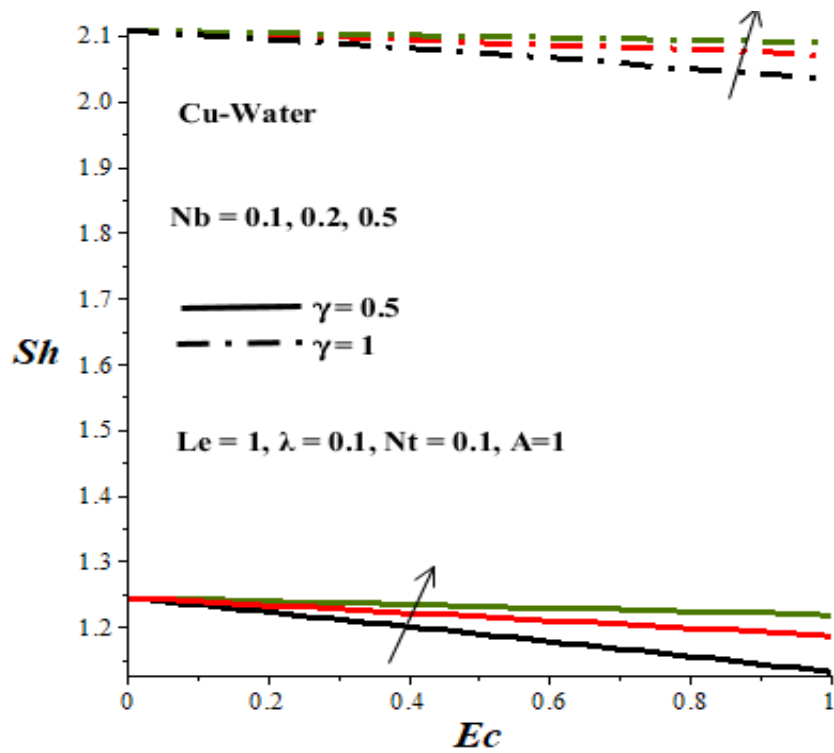


Figure 6.27 Sherwood number with  $Ec$ ,  $Nb$  and  $\gamma$

### 6.4.6 Entropy Generation Rate

The effects of thermophysical parameters on the entropy generation rate are displayed in figures 6.28-6.34. Generally, the entropy production rate is highest at the walls but decreases to its zero value along the microchannel centreline region. The zero entropy along the centreline of microchannel may be attributed to the imposed symmetric conditions in model equation (6.7) which invariably lead to zero velocity gradient, zero temperature gradient, and zero concentration gradient along the microchannel centreline. Moreover, it is noteworthy that the entropy generated by nanofluid is higher than that of base fluid only as illustrated in figure 6.28. The rate of entropy production in the flow system increases with a rise in Brownian motion ( $N_b$ ), Eckert number ( $Ec$ ), Lewis number ( $Le$ ), nanoparticles injection rate ( $\gamma$ ) and variable viscosity parameter ( $\lambda$ ) but lessens with an upsurge in thermophoresis ( $N_t$ ) activities (see figures 6.29-6.34). The augmentation in entropy can be attributed to the enhanced heat and mass transfer properties of nanofluid coupled with an escalation in nanoparticles concentration.

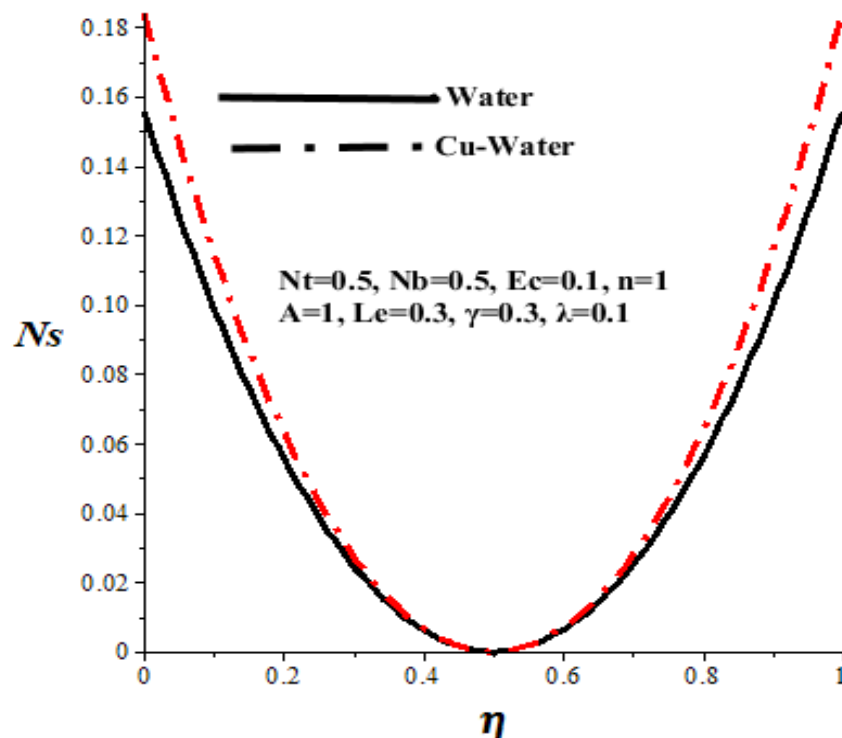


Figure 6.28 Effects of Cu-nanoparticles on  $N_s$

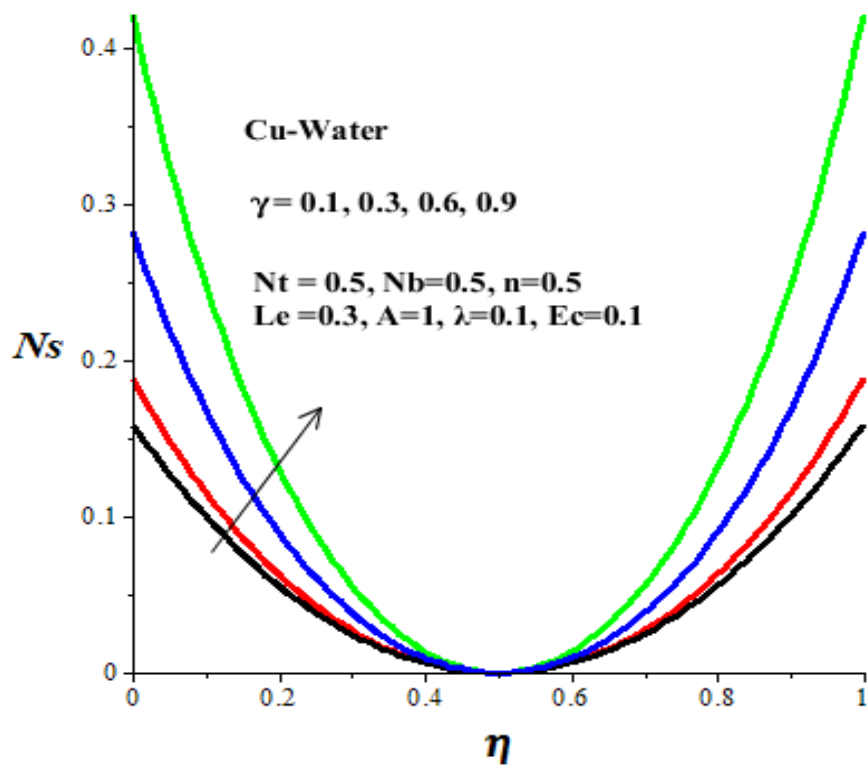


Figure 6.29 Entropy generation rate with  $\gamma$ .

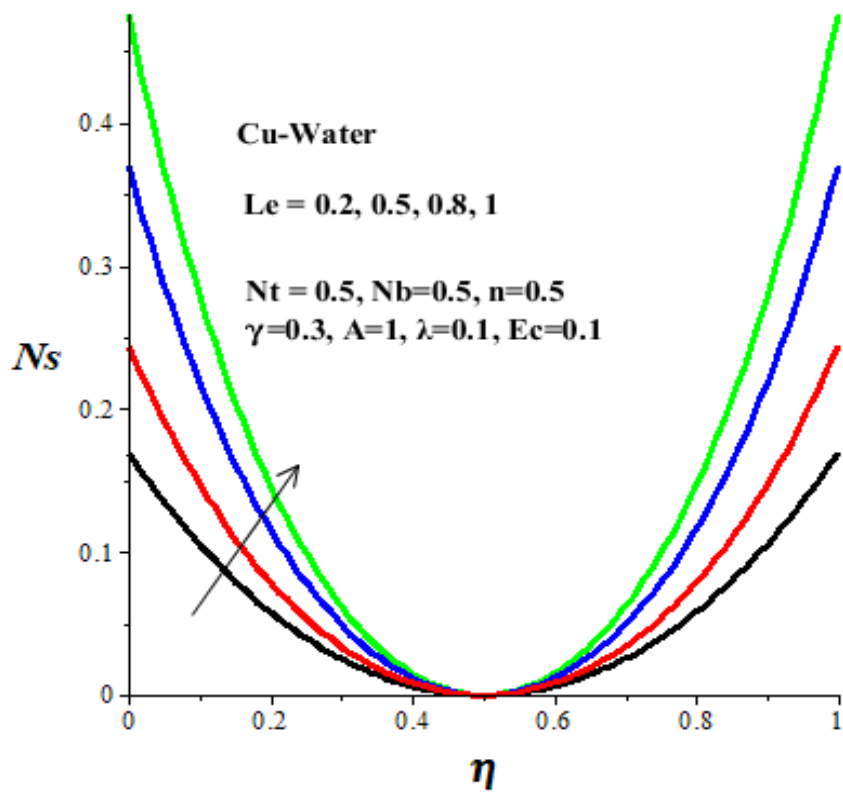


Figure 6.30 Entropy generation rate with  $Le$

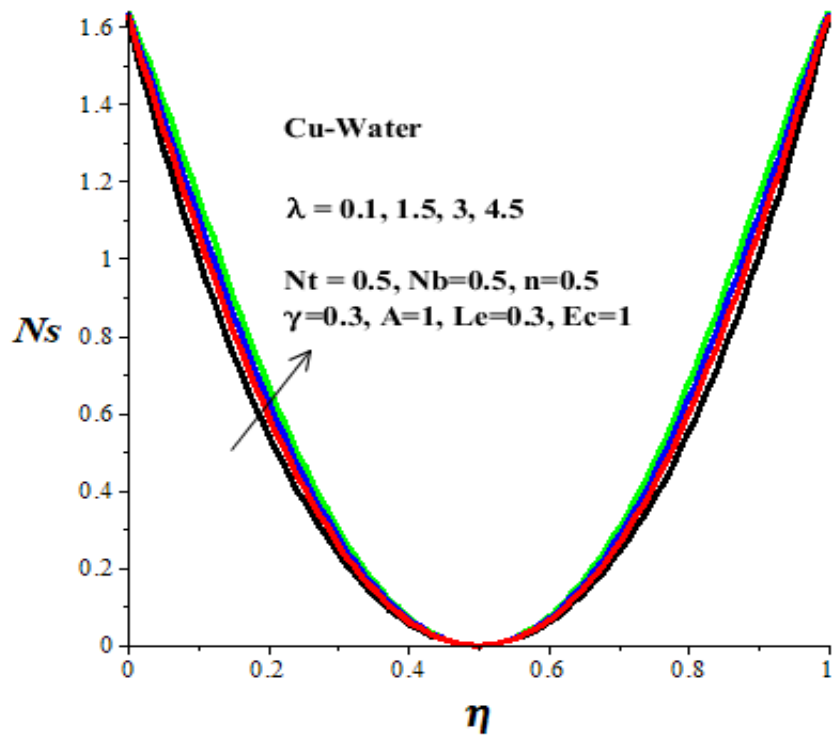


Figure 6.31 Entropy generation rate with  $\lambda$ .

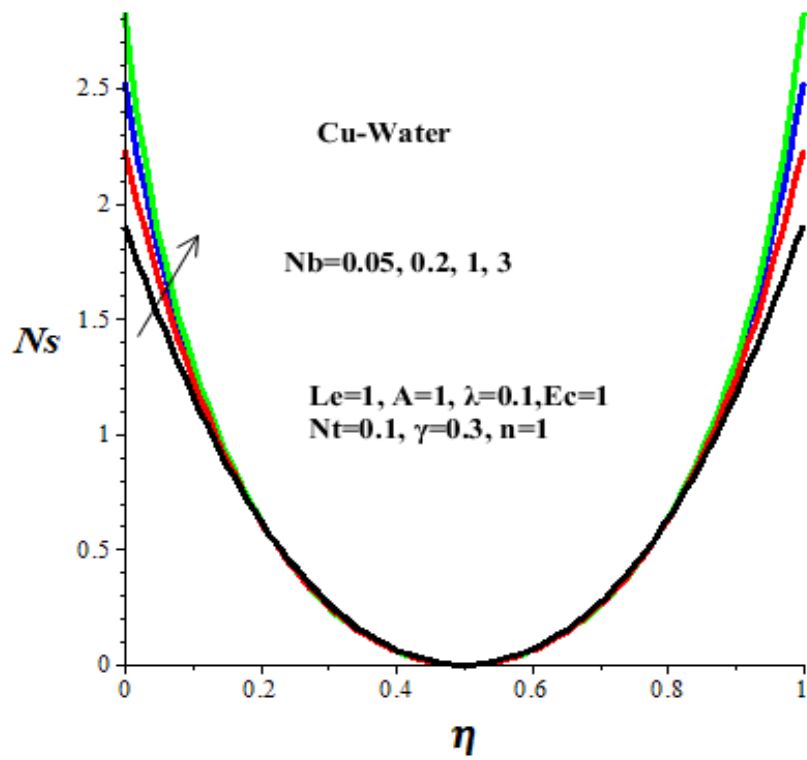


Figure 6.32 Entropy generation rate with  $Nb$

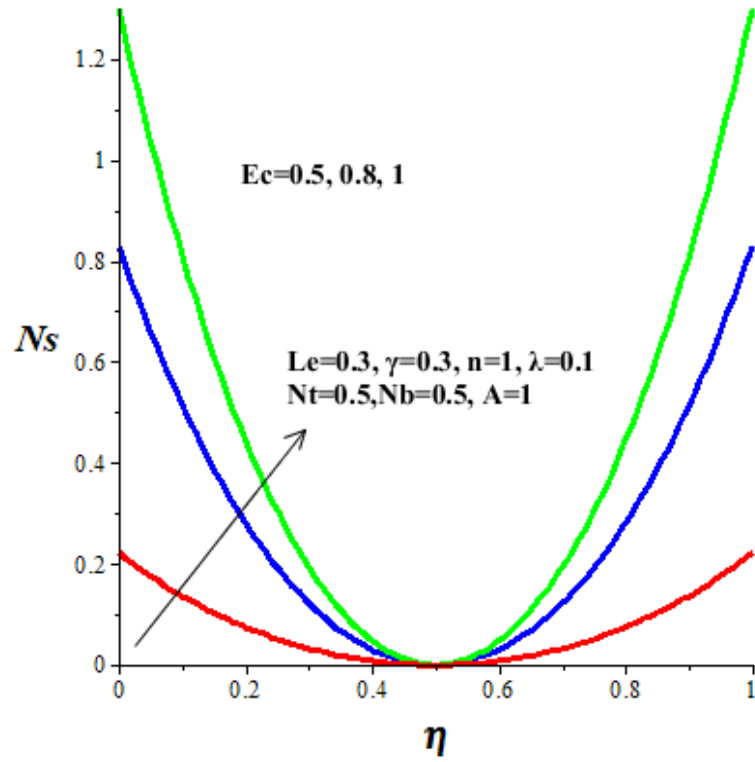


Figure 6.33 Entropy generation rate with Ec

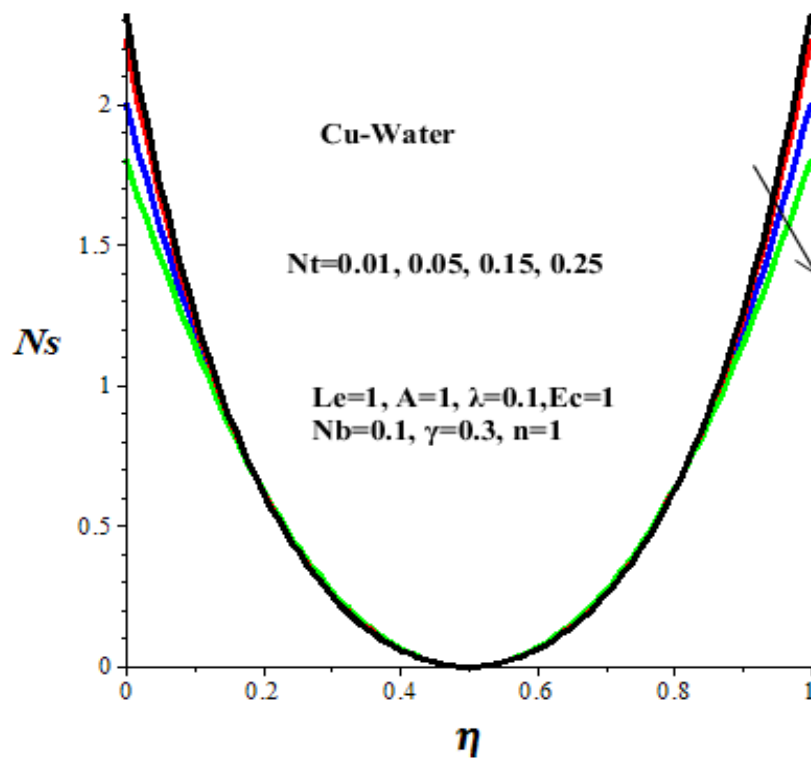


Figure 6.34 Entropy generation rate with Nt



### 6.4.7 Bejan Number

Figures 6.35-6.41 illustrate the effects of various parameters on the Bejan number. From these figures, the increasing dominant effects of heat and mass transfer irreversibility at the walls is noticed, while the fluid friction irreversibility completely dominates the microchannel core region. Meanwhile, the Bejan number produced by nanofluid is lower than that of base fluid only as shown in figure 6.35. This reveals that the contribution of heat transfer irreversibility in base fluid (water) coupled with fluid friction irreversibility to entropy production is more than the combined effects of heat and mass transfer irreversibility together with the fluid friction irreversibility in nanofluid. The Bejan number declines with an upsurge in the parameter values of nanoparticles injection rate  $\gamma$ , Lewis number  $Le$  and Brownian motion  $Nb$ , thus, lessens the strength of heat and mass transfer irreversibility at the walls as demonstrated in figures 6.36-6.38. As parameter values of  $\lambda$ ,  $Nt$  and  $Ec$  amplify, the Bejan number escalates, leading to increasing impact of heat and mass transfer irreversibility at the walls (see figure 6.39-6.41). Moreover, the impact of fluid friction irreversibility is absolute within the microchannel core region.

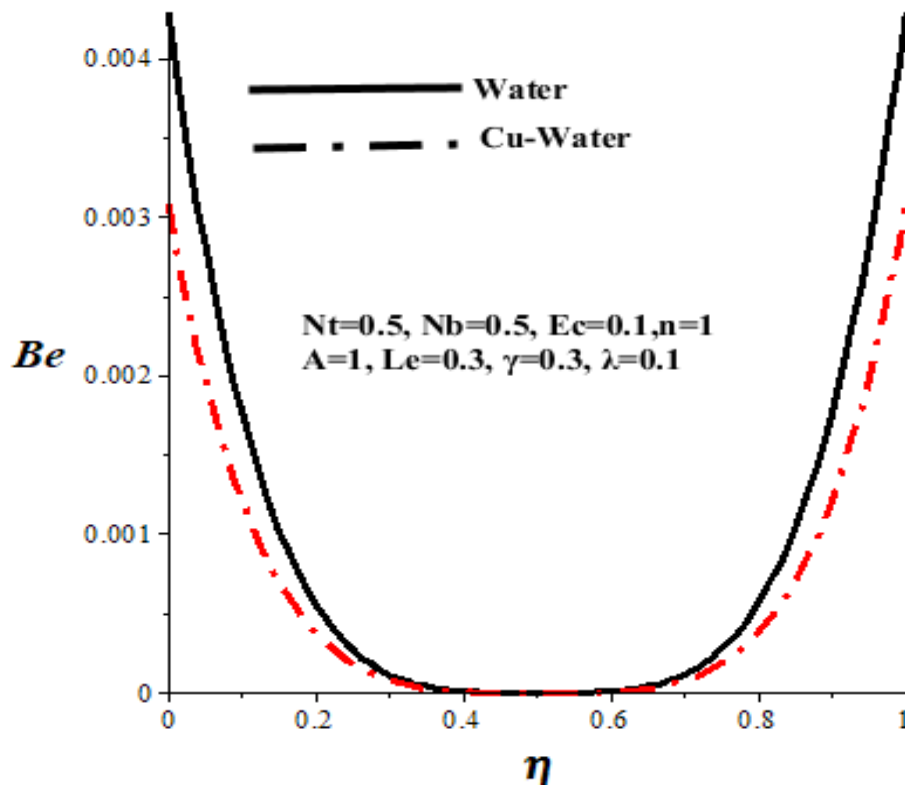


Figure 6.35 Bejan number with Cu-nanoparticles

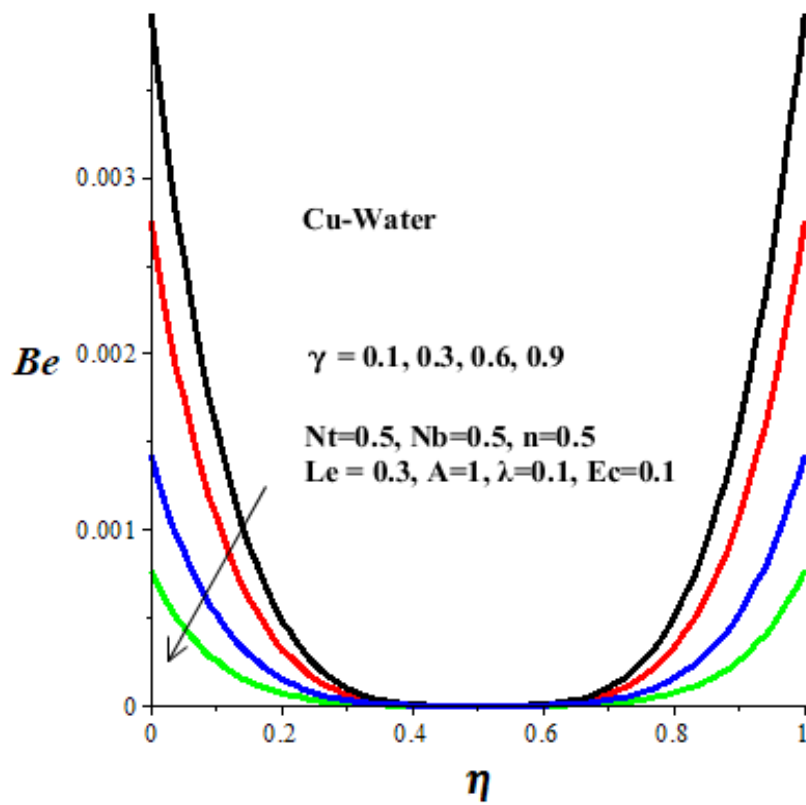


Figure 6.36 Bejan number with  $\gamma$

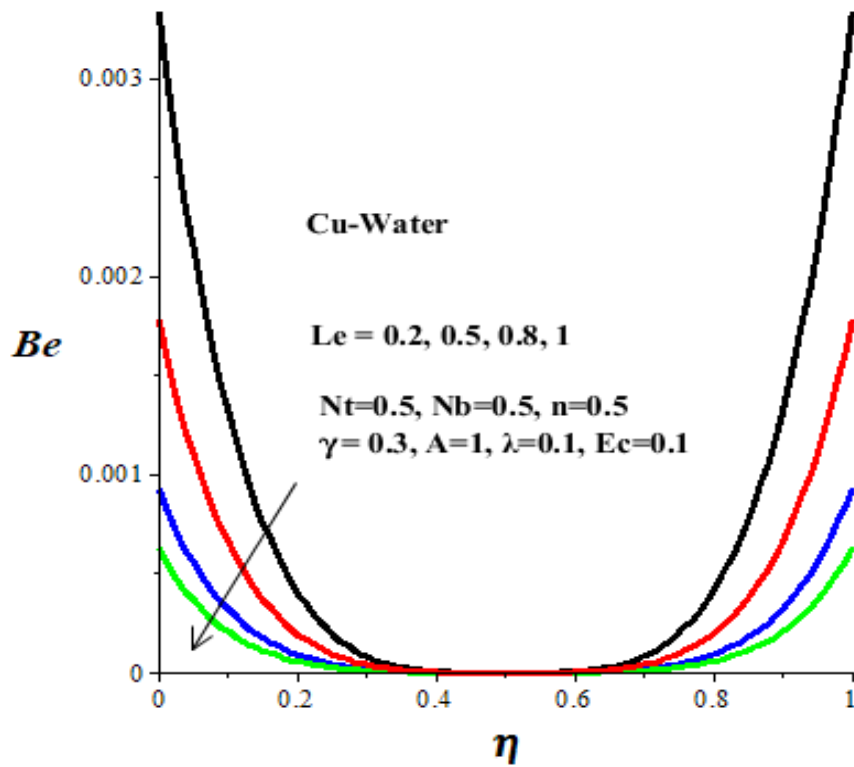


Figure 6.37 Bejan number with  $Le$

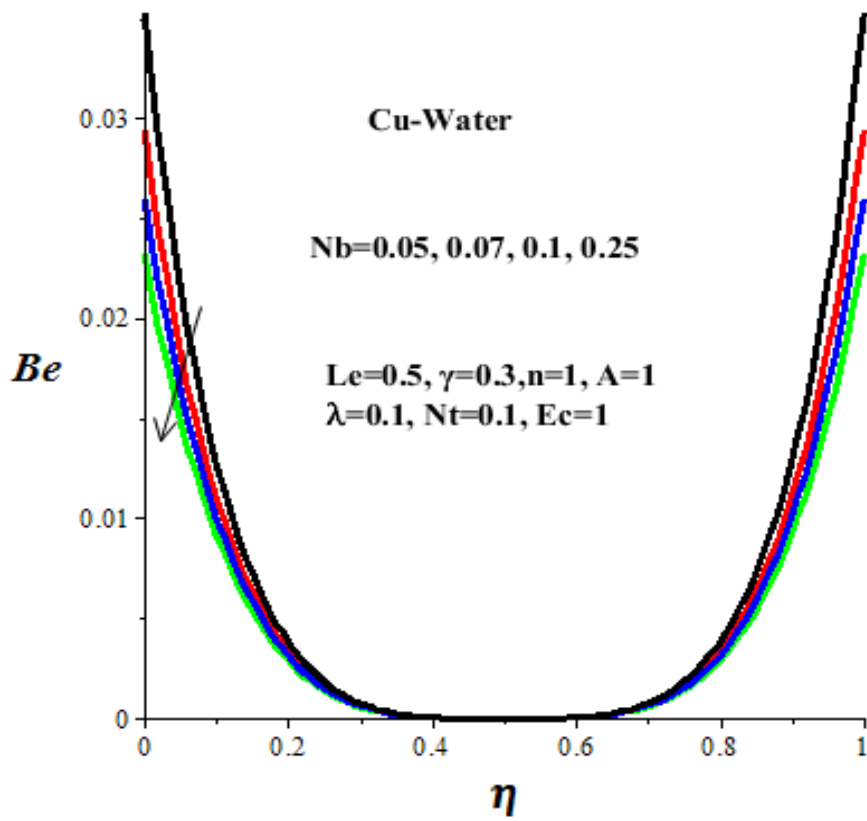


Figure 6.38 Bejan number with Nb

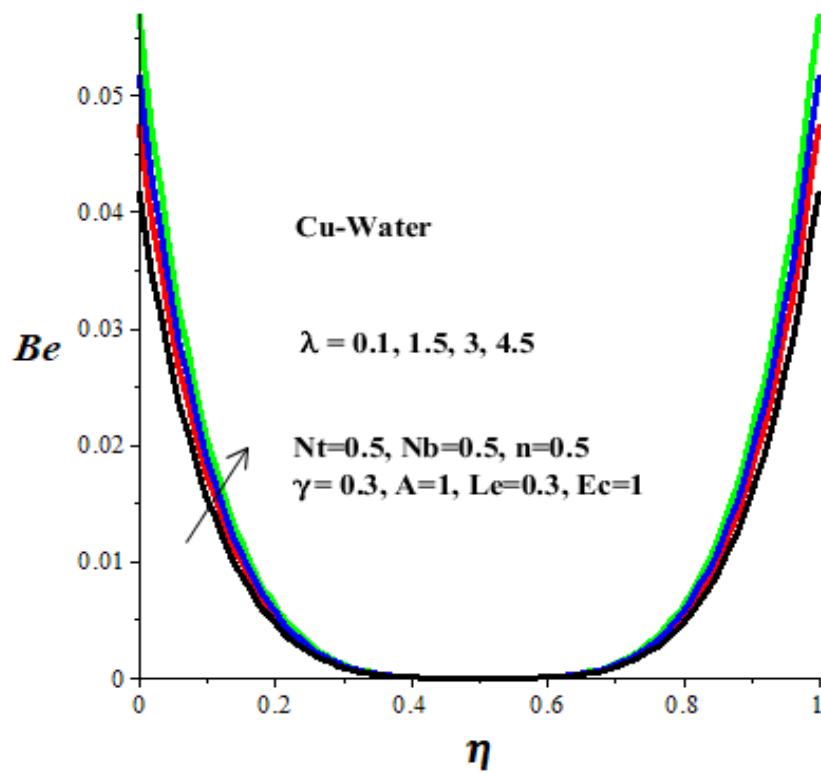


Figure 6.39 Bejan number with  $\lambda$

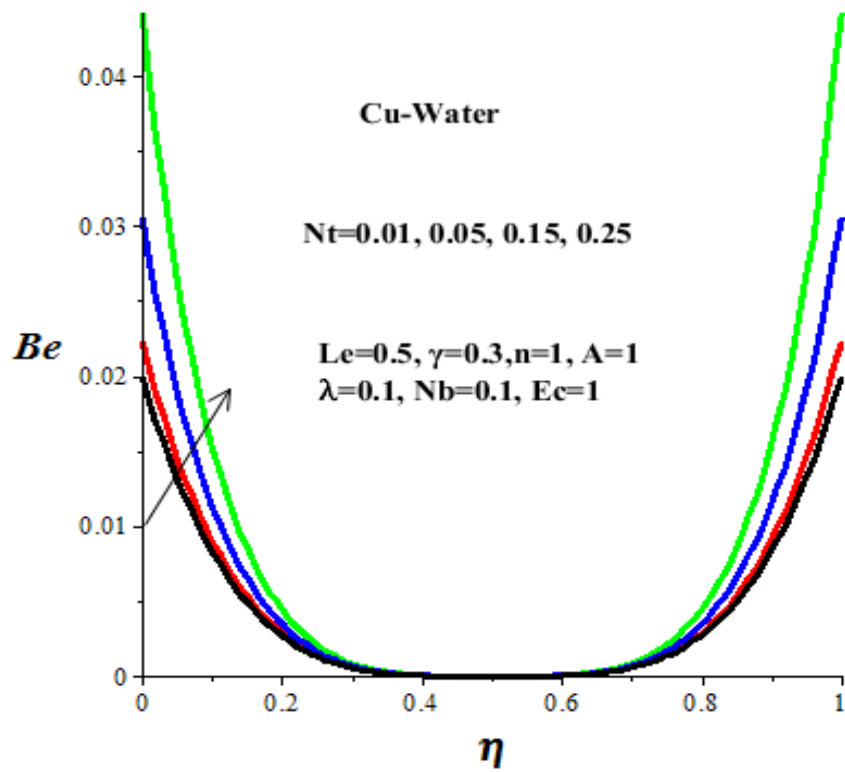


Figure 6.40 Bejan number with  $Nt$

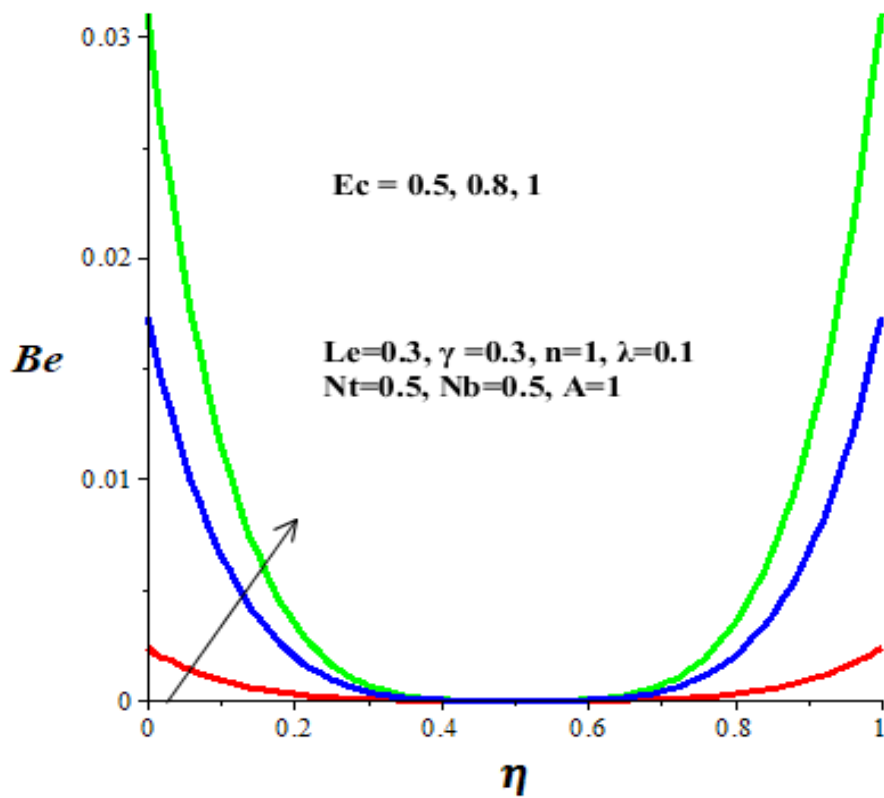


Figure 6.41 Bejan number with  $Ec$

## 6.5. Conclusions

The impact of nanoparticles injection and distribution on entropy generation rate in addition to heat and mass transfer characteristics of microchannel Poiseuille flow of Cu-water nanofluid with variable properties is theoretically examined. Modified Buongiorno's two-phase nanofluid model is employed and numerically tackled using shooting method coupled with Runge-Kutta-Fehlberg integration scheme. Our results can be summarised as follows:

- The flow rate of nanofluid (Cu-water) is lower than that of base fluid (water) in the microchannel. Velocity profiles is enhanced with a rise in  $Ec$ ,  $Nt$  and  $\lambda$  but lessened with an increase in  $Le$ ,  $Nb$  and  $\gamma$ .
- The nanofluid (Cu-Water) temperature is lower than that of base fluid (water) in the microchannel. The temperature drops with increasing values of  $Nb$ ,  $Le$  and  $\gamma$  but rises with increasing values of  $Nt$ ,  $Ec$  and  $\lambda$ .
- The nanoparticles concentration is highest along the microchannel centreline region but lowest at the walls. An increase in  $\gamma$ ,  $Le$  and  $Nb$  enhances the nanoparticles concentration across the microchannel, while an increase in  $\lambda$  and  $Nt$  lessens the concentration.
- The skin friction only depends on axial pressure gradient and is constant throughout the flow.
- Nusselt number for nanofluid (Cu-water) is higher than that of base fluid (Water). The Nusselt number reduces with an increase in  $\gamma$  and  $Le$ , but increases with an increase in  $Ec$ ,  $\lambda$ ,  $Nb$  and  $Nt$ .
- Nanofluid generates more entropy as compare to base fluid. Entropy production is more pronounced at the walls and less along the microchannel core region. An increase in  $\gamma$ ,  $Le$ ,  $\lambda$ ,  $Nb$  and  $Ec$  expedites entropy generation rate while an increase in  $Nt$  lessens the entropy production.
- Nanofluid Bejan number is lower than that of base fluid. Fluid friction irreversibility is absolute along the microchannel core region while the dominant effect of heat and mass transfer irreversibility rises along the walls. Bejan number lessens with  $\gamma$ ,  $Nb$  and  $Le$  but increases with  $\lambda$ ,  $Nt$  and  $Ec$ .

Finally, nanofluid provides technologically advanced heat transfer fluid. The aggregation of nanoparticles toward the microchannel centreline region boosts the heat and mass transfer rate while ensuring the maintenance and control of skin friction. With the appropriate regulation of the emerging thermophysical parameters such as Brownian motion, thermophoresis, nanoparticles injection rate, Eckert number, Lewis number and viscosity variations parameter, heat and mass transfer rate can be further enhanced and entropy generation rate minimized for optimum performance.

## CHAPTER 7

### GENERAL DISCUSSION, CONCLUSION AND RECOMMENDATIONS

#### 7.1. General Discussion

In this thesis, some problems in different geometries were studied. The problems have been solved either analytically or numerically and combined effects of thermal radiation, variable viscosity, nanoparticles shape and volume fraction on the inherent irreversibility and thermal stability of water base nanofluid Couette flow containing copper nanoparticles were investigated.

The inherent irreversibility of a variable viscosity ethylene glycol/silver (EG/Ag) nanofluid single-phase Poiseuille flow in a vertical microchannel with convective cooling under the combined influence of buoyancy force, nonlinear thermal radiation, nanoparticles shape and volume fraction was investigated.

A modified Buongiorno model was proposed and utilized to examine the nanoparticles distribution pattern in a nanofluid flow through a microchannel filled with a porous medium. A more realistic modified Buongiorno's nanofluid model was proposed and utilized to examine the impact of nanoparticles injection and distribution on inherent irreversibility in a microchannel Poiseuille flow of nanofluid with variable properties.

#### 7.2. Conclusions

The theoretical model based on the first-law and second-law of thermodynamics was developed for the combined effects of nonlinear thermal radiation and variable viscosity on Couette and Poiseuille flow of nanofluid with variable properties. The nonlinear problem was numerically tackled by using the shooting method with the Runge-Kutta-Fehlberg integration scheme. Some of the pertinent results can be summarized as follows:

## Velocity Profile

- The Cu-water Couette flow velocity profiles shows an inflexion point when the values of  $Nr$  and  $\gamma$  increase.
- Velocity profiles diminished with rising values of  $\phi$ ,  $Bi$  and  $Nr$  but enhanced with increasing values of  $Gr$ ,  $Ec$ ,  $\lambda$ ,  $m$ .
- An increase in  $Ec$ ,  $Nt$ ,  $\lambda_1$ ,  $\lambda_2$  enhances the velocity near the moving upper plate but decreases the velocity near the lower fixed plate.

Meanwhile as  $Nb$  increases, the velocity declines near the moving plate but increases near the fixed plate. It is interesting to note that a turning point occurs in the velocity profiles at the microchannel centreline.

- Increase in  $Sc$  and  $\lambda$  lessen the velocity profiles but enhance the nanoparticles concentration profiles.

The flow rate of nanofluid (Cu-water) is lower than that of base fluid (water) in the microchannel. Velocity profiles is enhanced with a rise in  $Ec$ ,  $Nt$  and  $\lambda$  but lessened with an increase in  $Le$ ,  $Nb$  and  $\gamma$ .

## Temperature Profile

- As  $\phi$  and  $Ec$  ascend, the Cu-water temperature amplifies while the trend is opposite when  $Nr$  and  $\gamma$  increase.
- Cu-water temperature lessens with a rise in the value of nanoparticle shape parameter  $m$ .
- Thermal stability is enhanced with escalating values of  $\beta$ ,  $Nr$ ,  $m$  and  $\gamma$ , while an increase in  $\phi$  may facilitate the onset of thermal instability in Cu-water Couette flow.
- Temperature profiles rises with amplifying values of  $Gr$ ,  $Ec$ ,  $\lambda$ ,  $m$  but diminished with rising values of  $\phi$ ,  $Bi$  and  $Nr$ .
- Generally, the nanofluid temperature is highest along the microchannel centreline and minimum at the walls. The temperature drops with increasing values of  $Nt$ ,  $\lambda_1$ ,  $\lambda_2$  but rises with increasing values of  $Nb$ ,  $m$ ,  $Ec$  and  $Sc$ .
- The nanofluid (Cu-Water) temperature is lower than that of base fluid (water) in the microchannel. The temperature drops with increasing values of  $Nb$ ,  $Le$  and  $\gamma$  but rises with increasing values of  $Nt$ ,  $Ec$  and  $\lambda$ .



### Nanoparticles concentration profiles

- The nanoparticles concentration is lowest along the microchannel centreline and highest at the walls. Moreover, an increase in  $Sc$ ,  $m$ ,  $Nb$ ,  $\lambda_1$ ,  $\lambda_2$  enhances the nanoparticles concentration across the microchannel, while an increase in  $Ec$  and  $Nt$  lessens the concentration.
- Nanoparticles tend to aggregate more towards the microchannel centreline region as compared to the wall region.
- The nanoparticles concentration is highest along the microchannel centreline region but lowest at the walls. An increase in  $\gamma$ ,  $Le$  and  $Nb$  enhances the nanoparticles concentration across the microchannel, while an increase in  $\lambda$  and  $Nt$  lessens the concentration.

### Skin Friction, Nusselt Number, Sherwood number and Thermal Stability Conditions

- Increase in  $\lambda$ ,  $m$ ,  $Ec$  and  $Gr$  escalate the skin-friction and Nusselt number while increases in  $\phi$ ,  $Bi$ ,  $Nr$  lessen the skin-friction and Nusselt number.
- Critical Eckert number  $Ec^*$  exist such that for  $0 \leq Ec \leq Ec^*$  the flow is thermally stable and for  $Ec > Ec^*$  the flow is thermally unstable.
- The magnitude of  $Ec^*$  is enhanced with rising values of  $\phi$ ,  $Bi$  and  $Nr$ , but diminished with an increase in  $\lambda$ ,  $m$ ,  $Ec$  and  $Gr$ .
- It is noteworthy that the flow thermal stability is enhanced with increasing values of  $Nb$  and  $m$  while an increase in  $Nt$ ,  $\lambda_1$ ,  $\lambda_2$  and  $Sc$  expedite thermal instability in the flow field
- Skin friction diminishes with a rise in  $Sc$  and  $\lambda$ , but amplifies with an increase in  $A$  and  $Da$ .
- The skin friction, Nusselt number and Sherwood number diminish with an increasing values of  $Ec$ ,  $\lambda_1$  and  $\lambda_2$ . In addition, an increase in  $Nb$  and  $Ec$  boosts the Nusselt number while an increase in  $Nt$  lowers the Nusselt number.
- Nusselt number for nanofluid (Cu-water) is higher than that of base fluid (Water). The Nusselt number reduces with an increase in  $\gamma$  and  $Le$ , but increases with an increase in  $Ec$ ,  $\lambda$ ,  $Nb$  and  $Nt$ .

## Entropy Generation Rate and Bejan number

- The dominant effects of heat transfer irreversibility is manifest near the two plates region and enhanced with escalating values of  $\phi$  and  $Ec$  while dominance effect of fluid friction irreversibility is evident within the channel core region.
- Increase in  $\phi$ ,  $Nr$  and  $m$  enhance the dominant effects of fluid friction irreversibility, while an increase in  $\lambda$ ,  $Bi$ ,  $Ec$  and  $Gr$  boost dominance effects of heat transfer irreversibility
- Entropy production is more pronounced at the walls and less along the microchannel core region. However, an increase in  $Ec$ ,  $Nt$ ,  $m$ ,  $Sc$ , expedites entropy generation rate while an increase in  $Nb$ ,  $\lambda_1$ ,  $\lambda_2$  lessens the entropy production.
- Nanofluid generates more entropy as compared to base fluid. Entropy production is more pronounced at the walls and less along the microchannel core region. An increase in  $\gamma$ ,  $Le$ ,  $\lambda$ ,  $Nb$  and  $Ec$  expedites entropy generation rate while an increase in  $Nt$  lessens the entropy production.
- Generally, Bejan number is highest at the walls with dominant effect of heat transfer irreversibility and lowest along the microchannel core region with dominant effects of fluid friction and nanoparticles concentration irreversibility. An increase in  $Ec$ ,  $Nb$ ,  $m$ ,  $Sc$ , expedites domination of heat transfer irreversibility near the walls by increasing Bejan number, while an increase in  $Nt$ ,  $\lambda_1$ ,  $\lambda_2$  lessens the Bejan number and heightens fluid friction and nanoparticles concentration irreversibility effects.

### 7.3. Recommendations

Finally, using Cu-nanoparticles as additives to lubricants or coolant can greatly improve their tribological properties by reducing friction, wear and heat transfer enhancement.

It could therefore be concluded from the above results that the thermodynamic performance and thermal stability of EG/Ag nanofluid flow in a microchannel can be enhanced with appropriate regulation of the emerging thermophysical parameter values. This analysis would undoubtedly serve as a useful tool for obtaining the conditions needed for a design of such an integrated system in order to achieve optimal performance.

Finally, nanofluid provides technologically advanced heat transfer fluid. The aggregation of nanoparticles toward the microchannel centreline region boosts the heat and mass transfer rate

while ensuring the maintenance and control of skin friction. With the appropriate regulation of the emerging thermophysical parameters such as Brownian motion, thermophoresis, nanoparticles injection rate, Eckert number, Lewis number and viscosity variations parameter, the heat and mass transfer rate can further be enhanced and entropy generation rate minimized for optimum performance through the reduction of the skin friction and enhancement of the Sherwood number.

#### **7.4. Future Research Work**

In general, the future work may be application oriented as well as controllable. There may be mathematical stalemate to solve the governing equations also. However, some of the following future work may be proposed.

- Three-dimensional laminar flow of various non-Newtonian fluids (Jeffrey fluid, micropolar fluid, couple stress etc.,) through different surfaces (Stretching Sheet, Cone, Circular cylinders, and spheres).
- Diverse methods like spectral methods, finite difference method and finite element method could be used.
- Chapter two to six concerning fluids with hybrid nanofluids could further be modified.

## LIST OF REFERENCES

- [1] Choi, S.U.S.: Enhancing thermal conductivity of fluids with nanoparticles, in: D.A. Siginer, H.P. Wang (Eds.), developments and applications of non-Newtonian flows FED-vol. 231/MD-vol. 66, ASME, New York, 1995, pp. 99–105.
- [2] Choi, S.U.S.: Nanofluids: from vision to reality through research, *Journal of Heat Transfer*, vol. 131, no. 3, 2009, pp. 1–9.
- [3] Yu, W., France, D. M., Routbort, J. L. and Choi, S.U.S: Review and comparison of nanofluid thermal conductivity and heat transfer enhancements, *Heat Transfer Engineering*, vol. 29, no.5, 2008, pp. 432–460.
- [4] Tyler, T., Shenderova, O., Cunningham, G., Walsh, J., Drobnik, J. and McGuire, G.: Thermal transport properties of diamond-based nanofluids and nanocomposites, *Diamond and Related Materials*, vol. 15, no. 11-12, 2006, pp. 2078–2081.
- [5] Das, S.R., Choi, S.U.S. and Patel, H.E.: Heat transfer in nanofluids—a review. *Heat Transfer Engineering*, vol. 27, no. 10, 2006, pp. 3-19.
- [6] Liu, M., Lin, M. C., Huang, I., and Wang, C.: Enhancement of thermal conductivity with carbon nanotube for nanofluids, *International Communication on Heat Mass*, vol.32, no.9, 2005, pp. 1202-1210.
- [7] Choi, S. U. S., Zhang, Z. G. and Keblinski, P.: Nanofluids in encyclopedia of nanoscience and nanotechnology, H. S. Nalwa, Ed., vol. 6, 2004, pp. 757–737, American Scientific, Los Angeles, Calif, USA.
- [8] Granqvist, C. G., and Buhrman, R. A.: Log-normal size distributions from magnetization measurements on small superconducting Al particles, *Journal of Applied Physics*, vol.47,
- [9] Das, S.R., Choi, S.U.S. and Patel, H.E.: Heat transfer in nanofluids—a review. *Heat transfer engineering*, vol. 27, 2006, pp. 3-19.
- [10] Eastman, J.A., Choi, U.S., Li, S., Thompson, L.J. and Lee, S.: Enhanced thermal conductivity through the development of nanofluids. In *Nanophase and Nanocomposite Materials II*. Edited by Komarneni S, Parker JC, Wollenberger HJ. Pittsburg: Materials Research Society; 1997, pp.3-11.
- [11] Oztop, H.F., Abu-Nada, E.: Numerical study of natural convection in partially heated rectangular enclosures filled with nanofluids, *International Journal of Heat Fluid Flow*, vol.29, 2008, pp. 1326-1336.

- [12] Lee, S. and Choi, S. U. S.: Application of metallic nanoparticle suspensions in advanced cooling systems, in recent advances in solids/structures and application of metallic materials (ed. Shinpyo, L.), PVP-Vol. 342 /MD-Vol. 72, New York: ASME, 1996, pp.227-234.
- [13] Wang, X., Xu, X. and Choi, S. U. S.: Thermal conductivity of nanoparticle-fluid mixture, Journal of Thermophysics and Heat Transfer, vol.13, no.4, 1999, pp.474-480.
- [14] Murshed, S.M.S., Leong, K.C. and Yang, C.: A combined model for the effective thermal conductivity of nanofluids, Applied Thermal Engineering, vol 29, 2009, pp. 2477-2483.
- [15] Lee, S., Choi, U.S., Li, S. and Eastman, J.A.: Measuring thermal conductivity of fluids containing oxide nanoparticles, Journal of Heat Transfer 121, 1999, pp. 280–289.
- [16] Chopkar, M., Das, P. K., and Manna, I.: Synthesis and characterization of nanofluid for advanced heat transfer applications, Scripta Mater., vol.55, no.6, 2006, pp. 549-552.
- [17] Moghadassi, A.R., Hosseini, S.M., Henneke, D.E.: Effect of CuO nanoparticles in enhancing the thermal conductivities of monoethylene glycol and paraffin fluids, Industrial Engineering and Chemistry Research, vol.49, 2010, pp. 1900-1904.
- [18] Xie, H., Wang, J., Xi, T. and Liu, Y.: Thermal conductivity of suspensions containing nanosized SiC particles, International Journal Thermophysics, vol.23, no.2, 2002, pp. 571-580.
- [19] Murshed, S., Leong, K., and Yang, C.: Enhanced thermal conductivity of TiO<sub>2</sub>-Water based nanofluids, International Journal of Thermal Sciences, vol.44, no.4, 2005, pp. 367-373.
- [20] Zhu, H.T., Zhang, C.Y., Tang, Y.M. and Wang, J.X.: Novel synthesis and thermal conductivity of CuO nanofluid, Journal of Physical Chemistry, vol.111, 2007, pp. 1646-1652.
- [21] Zhu, D., Li, X., Wang, N., Wang, X., Gao, J. and Li, H.: Dispersion behavior and thermal conductivity characteristics of Al<sub>2</sub>O<sub>3</sub>-H<sub>2</sub>O nanofluids, Current Applied Physics, vol 9, 2009, pp. 131-139.
- [22] Hiegeister, R., Andra, W., Buske, N., Hergt, R., Hilger, I., Richter, U. and Kaiser, : applications of magnetite ferrofluids for hyperthermia, Journal of magnetism and Magnetic Materials, vol. 210, 1999, pp. 420-422.
- [23] Northrup, E. F.: Some newly observed manifestations of forces in the interior of an electrical conductor, Phys. Rev, vol.24, no. 6, 1907, pp.474.

- [24] Stefani, F., Gundrum, T. and Gerbeth, G.: Contactless inductive flow tomography *Phys. Rev. E* 70, 2002.
- [25] Donzelli, G., Cerbino, R. and Vailati, A.: Bistable heat transfer in a nanofluid, *Physical Review Letters*, vol. 102, no. 10, Article ID 104503, 2009, 4 pages.
- [26] Kim, S. J., Bang, I. C., Buongiorno, J. and Hu, L. W.: Study of pool boiling and critical heat flux enhancement in nanofluids, *Bulletin of the Polish Academy of Sciences Technical Sciences*, vol. 55, no. 2, 2007, pp. 211–216.
- [27] Kim, S. J. Bang, I. C. Buongiorno, J. and Hu, L. W.: Surface wettability change during pool boiling of nanofluids and its effect on critical heat flux,” *International Journal of Heat and Mass Transfer*, vol. 50, no. 19-20, pp. 4105–4116, 2007.
- [28] Buongiorno, J., Hu, L.W., Kim, S. J., Hannink, R. Truong, B. and Forrest, E.: Nanofluids for enhanced economics and safety of nuclear reactors: an evaluation of the potential features issues, and research gaps, *Nuclear Technology*, vol.162, no. 1, 2008, pp.80–91.
- [29] Wong, K.V. and Leon, O.D.: Applications of Nanofluids, current and future, *Advances in Mechanical Engineering Volume 2010*, Article ID 519659, 11pages, doi:10.1155/2010/519659.
- [30] Kao, M. J., Lo, C. H., Tsung, T. T., Wu Y. Y., Jwo, C. S. and Lin, H. M.: Copper-oxide brake nanofluid manufactured using arc- submerged nanoparticle synthesis system, *Journal of Alloys and Compounds*, vol. 434-435, 2007, pp. 672–674.
- [31] Kao, M. J., Chang, H., Wu, Y. Y., Tsung, T. T. and Lin, H. M.: Producing aluminum oxide brake nanofluids using plasma charging system, *Journal of the Chinese Society of Mechanical Engineers*, vol. 28, no. 2, 2007, pp. 123–131.
- [32] Vafaei, S., Borca-Tasciuc, T., Podowski, M.Z, Purkayastha, A., Ramanath, G., and Ajayan, P. M.: Effect of nanoparticles on sessile droplet contact angle, *Nanotechnology*, vol. 17, no. 10, 2006, pp.2523–2527.
- [33] Tsou, F.K., Sparrow, E.M. and Goldstein: R.J. Flow and heat transfer in the boundary layer on a continuous moving surface. *Int. J. Heat Mass Transfer*, vol.10, 1967, pp.219-235.
- [34] Li, Q. and Xuan, Y.: Experimental investigation on transport properties of nanofluids, in *Heat Transfer Science and Technology Higher Education Press*, 2000, pp.757-762.
- [35] Xuan, Y.M. and Li, Q.: Heat transfer enhancement of nanofluids, *International Journal of Heat Fluid Flow*, vol. 21, 2000, pp.58–64.
- [36] Jang, S.P. and Choi, S.U.S.: Role of Brownian motion in the enhanced thermal conductivity of nanofluids. *Applied Physics Letters*, vol.84, 2004, pp. 4316-4318.

- [37] Evans, W., Fish, J. and Keblinski, P.: Role of Brownian motion hydrodynamics on nanofluid thermal conductivity. *Applied Physics Letters*, vol.88, 2006, pp. 093116-1 0931161-3.
- [38] Chang, B.H and Mills, A.F: Natural convection of microparticle suspensions in thin enclosures. *International Journal of Heat Mass Transfer*. Vol.51, 2008, pp.1332-1341.
- [39] Putra, N., Roetzel, W. and Das, S.K.: Natural convection of nanofluids. *Heat Mass Transfer*, vol.39, 2003, pp.775–84.
- [40] Bernaz, L.,Bonnet, J.M. and Seiler, J.M.: Investigation of natural convection heat transfer to the cooled top boundary of a heated pool. *Nuclear Engineering and Design*, vol. 204, 2001, pp.413–427.
- [41] Khanafer, K., Vafai, K. and Lightstone, M.: Buoyancy-driven heat transfer enhancement in a two-dimensional enclosure utilizing nanofluids, *International Journal of Heat Mass Transfer*. Vol.46, 2003, pp.3639-3653.
- [42] Wen, D. and Ding, Y.: Experimental Investigation into Convective Heat Transfer of Nanofluids at the Entrance Region under Laminar Flow Conditions, *International Journal Heat Mass Transfer*, vol. 47, 2004, pp.5181–5188.
- [43] Rong,Y. J and Sheng,C. T.:Numerical research of nature convective heat transfer enhancement filled with nanofluids in rectangular enclosures, *International Journal*, vol.33, 2006, pp.727-736.
- [44] Ho, C.J.,Chen, M.W, Li, Z.W.:Numerical simulation of natural convection of nanofluid in a square enclosure: Effects due to uncertainties of viscosity and thermal conductivity, *International Journal*, vol.51, 2008, pp.4506–4516.
- [45] Xuan, Y. and Li, Q.: Investigation on convective heat transfer and flow features of Nanofluids. *ASME J HeatTransfer* vol.125, no.15, 2003, pp.1-5.
- [46] Pak, B. C. and Cho, Y. I.: Hydrodynamic and heat transfer study of dispersed fluids with submicron metallic oxide particles, *Experimental Heat Transfer*, vol.11, 1998, pp.151-170.
- [47] Tahery, A.A, Pesteei, S.M, Zehforoosh, A.: *International Journal of Chemical Engineering and Applications*, Vol. 1, no. 1, 2010.
- [48] Hakan, F. O. and Eiyad, A.:Numerical study of natural convection in partially heated rectangular enclosures filled with nanofluids, *International Journal*. Vol.29, 2008, pp.1326–1336.

- [49] Maïga, S.E.B, Palm, S.J, Nguyen, C.T., Roy, G. and Galanis, N.: Heat transfer enhancement by using nanofluids in forced convection flows, *International Journal. Heat and Fluid Flow*, vol.26, 2005, pp.530–546.
- [50] Peyghambarzadeh, S.M., Hashemabadi, S.H., Hoseini, S.M., and Seifi Jamnani, M.: Experimental study of heat transfer enhancement using water/ethylene glycol based nanofluids as a new coolant for car radiators, *International Communications in Heat and Mass Transfer*, vol.38, 2011, pp.1283–1290.
- [51] Assael, M.J., Metaxa, I.N, Kakosimos, K and Konstadinou, D.: Thermal conductivity of nanofluids – Experimental and Theoretical, Chemical Engineering Department, Aristotle University, 54124 Thessaloniki, Greece.
- [52] Anjali, S.P., and Andrews, J.: Laminar Boundary Layer Flow on a Nanofluid over a flat plate, *International Journal of Maths and Mechanics*, vol. 7, No. 6, 2011, pp. 52-71.
- [53] Popa, C., Polidori, G., Arfaoui, A. and Fohanno, S.: Heat and mass transfer in external boundary layer flows using nanofluids, *Heat and Mass Transfer – Modeling and Simulation*, Intech, vol. 5, 2011, pp. 95-116.
- [54] Aziz, A: A similarity solution for laminar thermal boundary layer over a flat plate with a convective surface boundary condition. *Commun Nonlinear Sci Numer Simul*, vol.14, 2009, pp.1064-1068.
- [55] Makinde, O.D. and Aziz, A.: MHD mixed convection from a vertical plate embedded in a porous medium with a convective boundary condition. *International Journal, Therm Sci*, vol.49, 2010 pp.1813-1820.
- [56] Ishak A: Similarity solutions for flow and heat transfer over a permeable surface with convective boundary condition. *Appl Math Comput*, vol. 217, 2010, pp.837-842.
- [57] Makinde, O.D. and Onyejekwe, O.: A numerical study of MHD generalized Couette flow and heat transfer with variable viscosity and electrical conductivity, *Journal of Magnetism and Magnetic Materials*, vol. 323, no.22, 2011, pp. 2757-2763.
- [58] Makinde, O.D., Iskander, T., Mabood, F, Khan, W.A. and Tshela, M.S.: MHD Couette-Poiseuille flow of variable viscosity nanofluids in a rotating permeable channel with hall effects, *Journal of Molecular Liquids*, vol.221, 2016, pp. 778-787.
- [59] Motsumi, T. and Makinde, O.D.: Effects of thermal radiation and viscous dissipation on boundary layer flow of nanofluids over a permeable moving at plate, *Physica Scripta*, vol.86, no.4, 2012, pp. 045003.
- [60] Makinde, O.D., Khan, W.A. and Aziz, A.: On inherent irreversibility in Sakiadis flow of nanofluids, *International Journal of Exergy*, vol.13, no.2, 2013, pp.159-174.



- [61] Mkwizu, M.H. and Makinde, O.D.: Entropy generation in a variable viscosity channel flow of nanofluids with convective cooling, *Comptes Rendus Mécanique*, vol.343, 2015, pp.38-56.
- [62] Olatundun A.T , Makinde O.D., Analysis of Blasius flow of hybrid nanofluids over a convectively heated surface. *Defect and Diffusion Forum*, 377 (2017) 29-41, 2017.
- [63] Khamliche, T., Khamliche, S. Doyle, T.B., Makinde, O.D. and M. Maaza.: Thermal conductivity enhancement of nano-silver particles dispersed ethylene glycol based nanofluids. *Materials Research Express*, 5(3), #035020, 2018.
- [64] Mahanthesh, B.,Gireesha, B.J., Gorla, R. S. R. and Makinde, O.D.: Magnetohydrodynamic three-dimensional flow of nanofluids with slip and thermal radiation over a nonlinear stretching sheet: a numerical study. *Neural Computing and Applications*, vol.30, no.5, 2018, pp.1557–1567.
- [65] Nayak, M.K. Hakeem, A.K.A. and Makinde, O.D.: Influence of Cattaneo-Christov heat flux model on mixed convection flow of third grade nanofluid over an inclined stretched Riga plate. *Defect and Diffusion Forum*, vol.387, 2018, pp.121–134.
- [66] Afridi, M.I. Qasim, M. and Makinde, O.D.: Minimization of entropy production in three dimensional dissipative flow of nanofluid with Graphene nanoparticles: A Numerical Study. *Defect and Diffusion Forum*, vol.387, 2018, pp.157–165.
- [67] Sharma, M.K. Manjeet, C. and Makinde, O.D.: Flow and heat Transfer in nanofluid Flow through a cylinder filled with foam porous medium under radial injection. *Defect and Diffusion Forum*, vol.387, 2018, pp.166–181.
- [68] Makinde, O.D.: Heat transfer in variable viscosity microchannel flow of EG-Water/Ag nanofluids with convective cooling. *Defect and Diffusion Forum*, vol.387, 2018, pp.182–193.
- [69] Ram, P. Joshi, V.K., Makinde, O.D. and Kumar, A.: Convective boundary layer flow of magnetic nanofluids under the influence of geothermal viscosity. *Defect and Diffusion Forum*, vol.387, 2018, pp.296–307.
- [70] Basha, H.T., Gunakala, S.R., Makinde, O.D. and Sivaraj, R.: Chemically reacting unsteady flow of nanofluid over a cone and plate with activation energy. *Defect and Diffusion Forum*, vol.387, 2018, pp.343–351.
- [71] Sarojamma, G., Lakshmi, R.V., Narayana, P.V.S. and Makinde, O.D.: Nonlinear radiative flow of a micropolar nanofluid through a vertical channel with porous collapsible walls. *Defect and Diffusion Forum*, vol.387, 2018, pp. 498–509.

- [72] Jagan, K., Sivasankaran, S. Bhuvanewari, M. Rajan, S. and Makinde, O.D.: Soret and Dufour effect on MHD Jeffrey nanofluid flow towards a stretching cylinder with triple stratification, radiation and slip. *Defect and Diffusion Forum*, vol.387, 2018, pp. 523–533.
- [73] Gangadhar, K., Ramana, K.V., Ibrahim, S.M. and Makinde, O.D.: Slip flow of an unsteady nanofluid past a stretching surface in a transverse magnetic field using SRM. *Defect and Diffusion Forum*, vol.387, 2018, pp.562–574.
- [74] Nayak, M.K., Bhatti, M.M. Makinde, O.D. and Akbar N.S.: Transient magneto-squeezing flow of NaCl-CNP nanofluid over a sensor surface inspired by temperature dependent viscosity. *Defect and Diffusion Forum*, vol.387, 2018, pp.600–614.
- [75] Basha, H.T., Makinde, O.D., Arora, A., Singh, A. and Sivaraj R.: Unsteady flow of chemically reacting nanofluid over a cone and plate with heat source/sink. *Defect and Diffusion Forum*, vol.387, 2018, pp.615–624.
- [76] Woods, L. C.: *Thermodynamics of Fluid Systems*, Oxford University Press, Oxford, 1975.
- [77] Batchelor G. K., *An introduction to fluid dynamics*. Cambridge, UK: Cambridge University Press, 1967.
- [78] Eegunjobi A. S., Makinde O.D., Tshela M.S., Franks O. Irreversibility analysis of unsteady Couette flow with variable viscosity. *Journal of Hydrodynamics*, 27(2),304–310, 2015.
- [79] Johns L. E., Narayanan R. Frictional heating in plane Couette flow. *Proc. Roy. Soc. A* 453, 1653–1670, 1997.
- [80] Yan F., Wang Z., Du Y., Su S., Zheng Y., Li Q. Research on rheological and flow behavior of lubricating grease in extremely cold weather. *Industrial Lubrication and Tribology*, 69(6), 1066-1073, 2017.
- [81] Leong K.Y., Saidur R., Kazi S. N., A. H. Mamun A. H. Performance investigation of an automotive car radiator operated with nanofluid-based coolants (nanofluid as a coolant in a radiator). *Applied Thermal Engineering*, 30(17/18), 2685-2692, 2010.
- [82] Khalil A.N.M, Ali M.A.M, Azmi A.I. Effect of Al<sub>2</sub>O<sub>3</sub> nanolubricant with SDBS on tool wear during turning process of AISI 1050 with minimal quantity lubricant. *Procedia Manufacturing*, 2, 130-134, 2015.
- [83] Elias M.M., Miqdad M., Mahbubu I. M., Saidur R., Kamalisarvestani M., Sohel M. R., Hepbasli A., Rahim N. A., Amalina M. A. Effect of nanoparticle shape on the heat transfer and thermodynamic performance of a shell and tube heat exchanger. *International Communications in Heat and Mass Transfer*, 44, 93–99, 2013.

- [84] Keblinski P., Phillpot S. R., Choi S. U.S, Eastman J. A. Mechanism of heat flow in suspensions of nano-sized particles (nanofluids). *Int. J. Heat Mass Transfer*, 42, 855-863, 2002.
- [85] Buongiorno J. Convective transport in nanofluids. *ASME J. Heat Transf.* 128, 240-250, 2006.
- [86] Makinde O. D. Effects of viscous dissipation and Newtonian heating on boundary layer flow of nanofluids over a flat plate. *International Journal of Numerical Methods for Heat and Fluid flow*, 23(8), 1291-1303, 2013.
- [87] Saidur R., Leong K. Y., Mohammad H. A. A review of applications and challenges of nanofluids. *Renewable and Sustainable energy Reviews*, 15, 1646-1668, 2011.
- [88] Namburu P. K., Kulkarni D. P., Dandekar A., Das D. K. Experimental investigation of viscosity and specific heat of silicon dioxide nanofluids. *Micro Nano Lett.* 2(3), 67-71, 2007.
- [89] Ali A. O., Makinde O. D. Modelling the effect of variable viscosity on unsteady Couette flow of nanofluids with convective cooling. *Journal of Applied Fluid Mechanics*, 8(4), 793-802, 2015.
- [90] Ali A. O., Makinde O.D., Nkansah-Gyekye Y. Numerical study of unsteady MHD Couette flow and heat transfer of nanofluids in a rotating system with convective cooling. *International Journal of Numerical Methods for Heat & Fluid Flow*, 26(5), 1567-1579, 2016.
- [91] Makinde O.D. Thermal decomposition of unsteady non-Newtonian MHD Couette flow with variable properties. *International Journal of Numerical Methods for Heat & Fluid Flow*, 25(2), 252-264, 2015.
- [92] Tyagi H. Radiative and combustion properties of nanoparticle-laden liquids PhD thesis, Arizona, USA: Arizona State University 2008.
- [93] **Rosseland S.** *Astrofysik and atom-theoretische grundlagen.* Berlin, Germany, Springer 41-44, 1931.
- [94] Makinde O. D., Animasaun I. L. Bioconvection in MHD nanofluid flow with nonlinear thermal radiation and quartic autocatalysis chemical reaction past an upper surface of a paraboloid of revolution. *International Journal of Thermal Sciences*, 109, 159-171, 2016.

- [95] Makinde O. D., Animasaun I. L. Thermophoresis and Brownian motion effects on MHD bioconvection of nanofluid with nonlinear thermal radiation and quartic chemical reaction past an upper horizontal surface of a paraboloid of revolution. *Journal of Molecular Liquids*, 221, 733-743, 2016.
- [96] Bejan A. Entropy generation minimization. Florida, USA: CRC Press, Boca Raton, 1996.
- [97] Ellahi R., Hassan M., Zeeshan A. Shape effects of nanosize particles in Cu-H<sub>2</sub>O nanofluid on entropy generation. *Int. J. Heat Mass Tran.*, 81, 449–456, 2015.
- [98] Abolbashari M. H., Freidoonimehr N., Nazari F., Rashidi M. M. Analytical modeling of entropy generation for Casson nanofluid flow induced by a stretching surface. *Adv. Powder Technol.*, 26, 542–552, 2015.
- [99] Makinde O. D., Eegunjobi A. S. MHD couple stress nanofluid flow in a permeable wall channel with entropy generation and nonlinear radiative heat. *Journal of Thermal Science and Technology*, 12(2), 17-00252-JTST0033(1-16), 2017.
- [100] Mkwizu M. H., Makinde O. D., Nkansah-Gyekye Y. Numerical investigation into entropy generation in a transient generalized Couette flow of nanofluids with convective cooling. *Sadhana - Academy Proceedings in Engineering Science*, 40(7), 2073–2093, 2015.
- [101] Das S., Jana R. N., Makinde O. D. MHD flow of Cu-Al<sub>2</sub>O<sub>3</sub>/Water hybrid nanofluid in porous channel. Analysis of entropy generation. *Defect and Diffusion Forum*, 377, 42-61, 2017.
- [102] Brinkman H. C. The viscosity of concentrated suspensions and solutions. *J. Chem. Phys.*, 20(4), 571-571, 1952.
- [103] Cebeci T., Bradshaw P. Physical and computational aspects of convective heat transfer. New York, USA: Springer, 1988.
- [104] P. X. Jiang, M. H. Fan, G. S. Si, Z. P. Ren, Thermal hydraulic performance of small scale microchannel and porous-media heat-exchangers, *Int. J. Heat Mass Transfer* 44 (2001) 1039–1051.
- [105] T. C. Hung, Y.-X. Huang, W. M. Yan, Thermal performance analysis of porous microchannel heat sinks with different configuration designs, *Int. J. Heat Mass Transfer* 66 (2013) 235–243.
- [106] T. C. Hung, W.-M. Yan, Thermal performance enhancement of microchannel heat sinks with sintered porous media, *Numer. Heat Transfer Part A: Appl.* 63 (2013) 666–686.

- [107] R. A. Wirtz, P. McKinley, Buoyancy effects on downwards laminar convection between parallel plates. *Fundamentals of forced and mixed convection*. ASME HTD 42 (1985) 105-112.
- [108] O. D. Makinde, P.O. Olanrewaju, Buoyancy effects on thermal boundary layer over a vertical plate with a convective surface boundary, *J. Fluids Eng.* 132 (2010) 044502-4.
- [109] O. D. Makinde, Similarity solution for natural convection from a moving vertical plate with internal heat generation and a convective boundary condition, *Therm. Sci.* 15 (2011) 137-143.
- [110] S. M. Peyghambarzadeh, S.H. Hashemabadi, A.R. Chabi, M. Salimi, Performance of water based CuO and Al<sub>2</sub>O<sub>3</sub> nanofluids in a Cu–Be alloy heat sink with rectangular microchannels, *Energy Convers. Manage.* 86 (2014) 28–38.
- [111] O.D. Makinde, F. Mabood, W.A. Khan, M.S. Tshehla, MHD flow of a variable viscosity nanofluid over a radially stretching convective surface with radiative heat, *Journal of Molecular Liquids*, 219 (2016) 624-630.
- [112] S. M., S.H. Hashemabadi, A.R. Chabi, M. Salimi, Performance of water based CuO and Al<sub>2</sub>O<sub>3</sub> nanofluids in a Cu–Be alloy heat sink with rectangular microchannels, *Energy Convers. Manage.* 86 (2014) 28–38.
- [113] M. G. Reddy, O. D. Makinde, Magnetohydrodynamic peristaltic transport of Jeffery nanofluid in an asymmetric channel. *Journal of Molecular Liquids*, 223 (2016) 1242-1248.
- [114] O. D. Makinde, K. G. Kumar, S. Manjunatha, B. J. Gireesha, Effect of nonlinear thermal radiation on MHD boundary layer flow and melting heat transfer of micro-polar fluid over a stretching surface with fluid particles suspension, *Defect and Diffusion Forum*, 378 (2017) 125-136.
- [115] W. A. Khan, O. D. Makinde, Z. H. Khan, Non-aligned MHD stagnation point flow of variable viscosity nanofluids past a stretching sheet with radiative heat. *International Journal of Heat and Mass Transfer*, 96 (2016) 525-534.
- [116] C. T. Nguyen, F. Desgranges, G. Roy, N. Galanis, T. Mare, S. Boucher, H. Angue Minsta, Temperature and particle-size dependent viscosity data for water based nanofluids – hysteresis phenomenon. *Int. J. Heat Fluid Flow* 28 (2007) 1492–1506.
- [117] I. Ullah, S. Shafie, O. D. Makinde, I. Khan: Unsteady MHD Falkner-Skan flow of Casson nanofluid with generative/destructive chemical reaction. *Chemical Engineering Science*, 172 (2017) 694–706.

- [118] M.I. Afridi, M. Qasim, O. D. Makinde, Second law analysis of boundary layer flow with variable fluid properties, *ASME - Journal of Heat Transfer*, 39(10) (2017) 104505.
- [119] S. Das, S. Chakraborty, R. N. Jana, O. D. Makinde, Entropy analysis of unsteady magneto-nanofluid flow past accelerating stretching sheet with convective boundary condition. *Applied Mathematics and Mechanics*, 36(12) 1593-1610.
- [120] O. Prakash, O. D. Makinde, MHD oscillatory Couette flow of dusty fluid in a channel filled with a porous medium with radiative heat and buoyancy force. *Latin American Applied Research*, 45(3) (2015) 185-191.
- [121] T. Chinyoka, O. D. Makinde, Numerical investigation of entropy generation in unsteady MHD generalized Couette flow with variable electrical conductivity. *The Scientific World Journal*, 2013 (2013) Article#364695 (11 pages).
- [122] O. D. Makinde, O. Franks, On MHD Unsteady reactive Couette flow with heat transfer and variable properties, *Central European Journal of Engineering*, 4(1) (2014) 54-63.
- [123] N. S. Kobo, O. D. Makinde, Second law analysis for a variable viscosity reactive Couette flow under Arrhenius kinetics, *Mathematical Problems in Engineering*, 2010 (2010) 278104(15pages).
- [124] G. S. Seth, S. Sarkar, O. D. Makinde, Combined free and forced convection Couette-Hartmann flow in a rotating channel with arbitrary conducting walls and Hall effects. *Journal of Mechanics*, 32 (5) (2016) 613-629.
- [125] S. Das, R.N. Jana, O.D. Makinde, Transient hydromagnetic reactive Couette flow and heat transfer in a rotating frame of reference. *Alexandria Engineering Journal*, 55(1) (2016) 635-644.
- [126] S. Das, S. Chakraborty, R.N. Jana, O.D. Makinde, Mixed convective Couette flow of reactive nanofluids between concentric vertical cylindrical pipes, *Journal of Nanofluids* 4 (4) (2015) 485-493.
- [127] R.L. Monaledi, O.D. Makinde, Entropy analysis of a radiating variable viscosity EG/Ag nanofluid flow in microchannels with buoyancy force and convective cooling, *Defect and Diffusion Forum*, 387 (2018) 273–285.
- [128] C. Richter, F. Kotz, N. Keller, T. M. Nargang, K. Sachsenheimer, D. Helmer, B. E. Rapp, An analytical solution to neumann-type mixed boundary poiseuille microfluidic flow in rectangular channel cross-sections (slip/no-slip) including a numerical technique to derive it. *Journal of Biomedical Science and Engineering*, 10, 205-219, 2017.
- [129] Y. Li, W. Van Roy, L. Lagae, P. M. Vereecken, Analysis of fully on-chip microfluidic electrochemical systems under laminar flow. *Electrochimica Acta*, 231, 200-208, 2017

- [130] T. M. Squires, S. R. Quake, Microfluidics: Fluid physics at the nanoliter scale. *Rev Mod Phys.*, 77, 977-1026, 2005.
- [131] N. T. Obot, Toward a better understanding of friction and heat/mass transfer in microchannel – A literatures review, *Microscale Thermophysical Engineering*, 6, 155-173, 2002.
- [132] C. Yang, D. Li, J. H. Masliyah, Modeling forced liquid convection in rectangular microchannels with electrokinetic effects, *International Journal of Heat and Mass Transfer*, 41, 4229-4249, 1998.
- [133] J. M. Koo, C. Kleinstreuer, Liquid flow in microchannels: Experimental observations and computational analyses of microfluidics effects. *J Micromech Microeng*, 13, 568-579, 2003.
- [134] M. Venkateswarlu, M. Prameela, O.D. Makinde, Influence of heat generation and viscous dissipation on hydromagnetic fully developed natural convection flow in a vertical microchannel. *Journal of Nanofluids*, 8 (7), 1506-1516, 2019.
- [135] M. Venkateswarlu, O.D. Makinde, D.V. Lakshmi, Influence of thermal radiation and heat generation on steady hydromagnetic flow in a vertical micro-porous-channel in presence of suction/injection, *Journal of Nanofluids*, 8 (5), 1010-1019, 2019.
- [136] C. Pang, J. W. Lee, Y. T. Kang, Review on combined heat and mass transfer characteristics in nanofluids, *Int. J. Therm. Sci.*, vol. 87, pp. 49–67, 2015.
- [137] P. Ganesan, I. Behroyan, S. He, S. Sivasankaran, S. C. Sandaran, Turbulent forced convection of Cu–Water nanofluid in a heated tube: improvement of the two-phase model, *Numer Heat Transf. A Appl.*, 69(4) 401–420, 2016.
- [138] O. D. Makinde, A. Aziz, Boundary layer flow of a nanofluid past a stretching sheet with a convective boundary condition. *International Journal of Thermal Sciences*, 50, 1326-1332, 2011.
- [139] P. Mayeli, H. Hesami, M. H. D. Faraji Moghaddam, Numerical investigation of the MHD forced convection and entropy generation in a straight duct with sinusoidal walls containing water–Al<sub>2</sub>O<sub>3</sub> nanofluid, *Numer. Heat Transf. A Appl.*, 71(12), 1235–1250, 2017.
- [140] M. Abbaszadeh, A. Ababaei, A. A. Abbasian Arani, A. Abbasi Sharifabadi, MHD forced convection and entropy generation of CuO-water nanofluid in a microchannel considering slip velocity and temperature jump, *J. Braz. Soc. Mech. Sci. Eng.*, 39(3), pp. 775 –790, 2017.



- [141] R. L. Monaledi, O. D. Makinde, Inherent irreversibility in Cu-H<sub>2</sub>O nanofluid Couette flow with variable viscosity and nonlinear radiative heat transfer. *International Journal of Fluid Mechanics Research*, 46(6), 525–543, 2019.
- [142] [https://www.google.com/url?sa=i&url=https%3A%2F%2Fen.wikipedia.org%2Fwiki%2FCouette\\_flow&psig=AOvVaw0Z8Hm9Rws8qCDLEhIhbjgj&ust=1603611170412000&source=images&cd=vfe&ved=0CAIQjRxqFwoTCICunefbzOwCFQAAAAAdAAAAABAD](https://www.google.com/url?sa=i&url=https%3A%2F%2Fen.wikipedia.org%2Fwiki%2FCouette_flow&psig=AOvVaw0Z8Hm9Rws8qCDLEhIhbjgj&ust=1603611170412000&source=images&cd=vfe&ved=0CAIQjRxqFwoTCICunefbzOwCFQAAAAAdAAAAABAD).
- [143] <https://www.google.com/url?sa=i&url=https%3A%2F%2Fwww.chegg.com%2Fhome-work-help%2Fconsider-steady-laminar-fully-developed-two-dimensional-pois-chapter-7-problem-97p-solution-9780077295462-exc&psig=AOvVaw2ZJSshn5IJxzdO2KQICWCa&ust=1603611412525000&source=images&cd=vfe&ved=0CAIQjRxqFwoTCMjHsqDczOwCFQAAAAAdAAAAABAI>.
- [144] [https://www.google.com/url?sa=i&url=https%3A%2F%2Fwww.sciencedirect.com%2Ftopics%2Fengineering%2Fmicrochannel&psig=AOvVaw189DmORiT3q6hbAFP\\_Q5o1&ust=1603611687994000&source=images&cd=vfe&ved=0CAIQjRxqFwoTCPiuz3dzOwCFQAAAAAdAAAAABAD](https://www.google.com/url?sa=i&url=https%3A%2F%2Fwww.sciencedirect.com%2Ftopics%2Fengineering%2Fmicrochannel&psig=AOvVaw189DmORiT3q6hbAFP_Q5o1&ust=1603611687994000&source=images&cd=vfe&ved=0CAIQjRxqFwoTCPiuz3dzOwCFQAAAAAdAAAAABAD).
- [145] <https://www.google.com/url?sa=i&url=https%3A%2F%2Fwww.machinedesign.com%2Flearning-resources%2Fwhats-the-difference-between%2Fdocument%2F21834474%2Fwhats-the-difference-between-conduction-convection-and-radiation&psig=AOvVaw2UCuncpDHPAb8XQpHx4EdV&ust=1603611765057000&source=images&cd=vfe&ved=0CAIQjRxqFwoTCIjaq8DdzOwCFQAAAAAdAAAAABAD>.
- [146] <https://www.google.com/url?sa=i&url=https%3A%2F%2Fwww.intechopen.com%2Fbooks%2Fnanofluid-heat-and-mass-transfer-in-engineering-problems%2Fmeasuring-nanofluid-thermal-diffusivity-and-thermal-effusivity-the-reliability-of-the-photopyroelect&psig=AOvVaw1iSca7TuKTgDFvulhhU9-X&ust=1603612077250000&source=images&cd=vfe&ved=0CAIQjRxqFwoTCLiw9XezOwCFQAAAAAdAAAAABAD>.



[147]

[https://www.google.com/imgres?imgurl=https%3A%2F%2Fpubs.rsc.org%2Fimage%2Farticle%2F2017%2FRA%2Fc6ra28243a%2Fc6ra28243a-f3\\_hi-res.gif&imgrefurl=https%3A%2F%2Fpubs.rsc.org%2Fen%2Fcontent%2Farticlehtml%2F2017%2FRA%2Fc6ra28243a&tbnid=ddEFwe5Ny1UsM&vet=12ahUKEwjV0rb938zsAhVRdRQKHRsmBZYQMygAegUIARCUAQ..i&docid=zaMIUD70GJPPIM&w=912&h=363&q=how%20nanofluids%20is%20formed&hl=en&ved=2ahUKEwjV0rb938zsAhVRdRQKHRsmBZYQMygAegUIARCUAQ](https://www.google.com/imgres?imgurl=https%3A%2F%2Fpubs.rsc.org%2Fimage%2Farticle%2F2017%2FRA%2Fc6ra28243a%2Fc6ra28243a-f3_hi-res.gif&imgrefurl=https%3A%2F%2Fpubs.rsc.org%2Fen%2Fcontent%2Farticlehtml%2F2017%2FRA%2Fc6ra28243a&tbnid=ddEFwe5Ny1UsM&vet=12ahUKEwjV0rb938zsAhVRdRQKHRsmBZYQMygAegUIARCUAQ..i&docid=zaMIUD70GJPPIM&w=912&h=363&q=how%20nanofluids%20is%20formed&hl=en&ved=2ahUKEwjV0rb938zsAhVRdRQKHRsmBZYQMygAegUIARCUAQ).

[148]

[https://www.google.com/imgres?imgurl=https%3A%2F%2Fmedia.springernature.com%2Fflw685%2Fspringer-static%2Fimage%2Fart%253A10.1007%252Fs10973-020-10056-8%2FMediaObjects%2F10973\\_2020\\_10056\\_Fig3\\_HTML.png&imgrefurl=https%3A%2F%2Flink.springer.com%2Farticle%2F10.1007%2Fs10973-020-10056-8&tbnid=cz1tRvH\\_gU9vyM&vet=12ahUKEwiwjKOF4szsAhWr2uAKHTqtDhsQMygAegUIARCBAQ..i&docid=Oe9MSKHVaH-9DM&w=685&h=488&itg=1&q=nanofluid%20copper&hl=en&ved=2ahUKEwiwjKOF4szsAhWr2uAKHTqtDhsQMygAegUIARCBAQ](https://www.google.com/imgres?imgurl=https%3A%2F%2Fmedia.springernature.com%2Fflw685%2Fspringer-static%2Fimage%2Fart%253A10.1007%252Fs10973-020-10056-8%2FMediaObjects%2F10973_2020_10056_Fig3_HTML.png&imgrefurl=https%3A%2F%2Flink.springer.com%2Farticle%2F10.1007%2Fs10973-020-10056-8&tbnid=cz1tRvH_gU9vyM&vet=12ahUKEwiwjKOF4szsAhWr2uAKHTqtDhsQMygAegUIARCBAQ..i&docid=Oe9MSKHVaH-9DM&w=685&h=488&itg=1&q=nanofluid%20copper&hl=en&ved=2ahUKEwiwjKOF4szsAhWr2uAKHTqtDhsQMygAegUIARCBAQ).

[149]

[https://www.google.com/url?sa=i&url=https%3A%2F%2Fwww.slideshare.net%2FEhsanBHaghighi%2Fphd-dissertation-for-share&psig=AOvVaw1ZQRX7nNS\\_1YXAmHCL5eQM&ust=1603612633932000&source=images&cd=vfe&ved=0CAIQjRxxqFwoTCMD02qHizOwCFQAAAAAdAAAABAQ](https://www.google.com/url?sa=i&url=https%3A%2F%2Fwww.slideshare.net%2FEhsanBHaghighi%2Fphd-dissertation-for-share&psig=AOvVaw1ZQRX7nNS_1YXAmHCL5eQM&ust=1603612633932000&source=images&cd=vfe&ved=0CAIQjRxxqFwoTCMD02qHizOwCFQAAAAAdAAAABAQ).

[150]

[https://www.google.com/imgres?imgurl=https%3A%2F%2Fimage.slidesharecdn.com%2Fnanotechnologyandfluidflowmechanics13bch04313bch0622-150502093409-conversion-gate01%2F95%2Fnanotechnology-and-fluid-flow-mechanics-16-638.jpg%3Fcb%3D1430563804&imgrefurl=https%3A%2F%2Fwww.slideshare.net%2Fvedant\\_09%2Fnanotechnology-and-fluid-flow-mechanics&tbnid=NkHMufxz\\_baM&vet=12ahUKEwjbn9XJ4szsAhUU9OAKHYQJBSIQMygGegUIARCpAQ..i&docid=jvTXuvExuRoQZM&w=638&h=479&q=Applications%20of%20nanofluids&hl=en&ved=2ahUKEwjbn9XJ4szsAhUU9OAKHYQJBSIQMygGegUIARCpAQ](https://www.google.com/imgres?imgurl=https%3A%2F%2Fimage.slidesharecdn.com%2Fnanotechnologyandfluidflowmechanics13bch04313bch0622-150502093409-conversion-gate01%2F95%2Fnanotechnology-and-fluid-flow-mechanics-16-638.jpg%3Fcb%3D1430563804&imgrefurl=https%3A%2F%2Fwww.slideshare.net%2Fvedant_09%2Fnanotechnology-and-fluid-flow-mechanics&tbnid=NkHMufxz_baM&vet=12ahUKEwjbn9XJ4szsAhUU9OAKHYQJBSIQMygGegUIARCpAQ..i&docid=jvTXuvExuRoQZM&w=638&h=479&q=Applications%20of%20nanofluids&hl=en&ved=2ahUKEwjbn9XJ4szsAhUU9OAKHYQJBSIQMygGegUIARCpAQ).

[151]

[https://www.google.com/imgres?imgurl=https%3A%2F%2Fi.ytimg.com%2Fvi%2F2mQyFA1S1tE%2Fmaxresdefault.jpg&imgrefurl=https%3A%2F%2Fwww.youtube.com%2Fwatch%3Fv%3D2mQyFA1S1tE&tbnid=4F\\_KjkGDuMzSnM&vet=12ahUKEwi6loO48zsAhXeBWMBHbibD7oQMygTegUIARDfAQ..i&docid=YNGOX8Qy8IHZ7M&w=1280&h=720&q=military%20tank%20firining&hl=en&ved=2ahUKEwi6loO48zsAhXeBWMBHbibD7oQMygTegUIARDfAQ.](https://www.google.com/imgres?imgurl=https%3A%2F%2Fi.ytimg.com%2Fvi%2F2mQyFA1S1tE%2Fmaxresdefault.jpg&imgrefurl=https%3A%2F%2Fwww.youtube.com%2Fwatch%3Fv%3D2mQyFA1S1tE&tbnid=4F_KjkGDuMzSnM&vet=12ahUKEwi6loO48zsAhXeBWMBHbibD7oQMygTegUIARDfAQ..i&docid=YNGOX8Qy8IHZ7M&w=1280&h=720&q=military%20tank%20firining&hl=en&ved=2ahUKEwi6loO48zsAhXeBWMBHbibD7oQMygTegUIARDfAQ)

[152]

[https://www.google.com/imgres?imgurl=https%3A%2F%2Fi.ytimg.com%2Fvi%2FiUVWhzIEngU%2Fmaxresdefault.jpg&imgrefurl=https%3A%2F%2Fwww.youtube.com%2Fwatch%3Fv%3DiUVWhzIEngU&tbnid=nOWfKhZfcNhkSM&vet=12ahUKEwiEuJKq48zsAhUwAWMBHRfmC-QQMygCegUIARCoAQ..i&docid=pcJvpiBsMw3YBM&w=1280&h=720&q=discover%20bleed%20cooling%20system&hl=en&ved=2ahUKEwiEuJKq48zsAhUwAWMBHRfmC-QQMygCegUIARCoAQ.](https://www.google.com/imgres?imgurl=https%3A%2F%2Fi.ytimg.com%2Fvi%2FiUVWhzIEngU%2Fmaxresdefault.jpg&imgrefurl=https%3A%2F%2Fwww.youtube.com%2Fwatch%3Fv%3DiUVWhzIEngU&tbnid=nOWfKhZfcNhkSM&vet=12ahUKEwiEuJKq48zsAhUwAWMBHRfmC-QQMygCegUIARCoAQ..i&docid=pcJvpiBsMw3YBM&w=1280&h=720&q=discover%20bleed%20cooling%20system&hl=en&ved=2ahUKEwiEuJKq48zsAhUwAWMBHRfmC-QQMygCegUIARCoAQ)

[153]

[https://www.google.com/imgres?imgurl=https%3A%2F%2Fwww.dailymaverick.co.za%2Fwp-content%2Fuploads%2FGreg-SeritiReview-option-2-1600x904.jpg&imgrefurl=https%3A%2F%2Fwww.dailymaverick.co.za%2Farticle%2F2020-05-05-covid-19-makes-sas-maritime-strategy-more-complex-and-urgent%2F&tbnid=sfN7xRzeBxaRM&vet=12ahUKEwig9bDe48zsAhVFwOAKHXpiDIgQMygSegUIARDOAQ..i&docid=K-XXpf8IGAMaSM&w=1600&h=904&q=Sa%20navy%20ships&hl=en&ved=2ahUKEwig9bDe48zsAhVFwOAKHXpiDIgQMygSegUIARDOAQ.](https://www.google.com/imgres?imgurl=https%3A%2F%2Fwww.dailymaverick.co.za%2Fwp-content%2Fuploads%2FGreg-SeritiReview-option-2-1600x904.jpg&imgrefurl=https%3A%2F%2Fwww.dailymaverick.co.za%2Farticle%2F2020-05-05-covid-19-makes-sas-maritime-strategy-more-complex-and-urgent%2F&tbnid=sfN7xRzeBxaRM&vet=12ahUKEwig9bDe48zsAhVFwOAKHXpiDIgQMygSegUIARDOAQ..i&docid=K-XXpf8IGAMaSM&w=1600&h=904&q=Sa%20navy%20ships&hl=en&ved=2ahUKEwig9bDe48zsAhVFwOAKHXpiDIgQMygSegUIARDOAQ)